570622

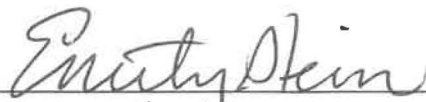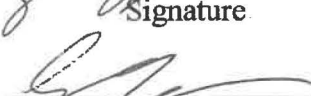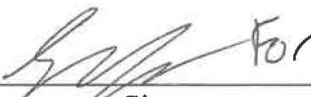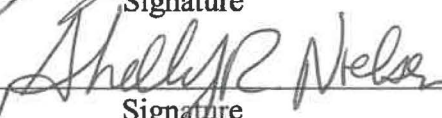# SANDIA NATIONAL LABORATORIES
WASTE ISOLATION PILOT PLANT

Update to the PFLOTRAN-BRAGFLO Benchmark: Comparison of Test Cases and Simulations on the 2-D Flared Grid

Revision 1

Author:	Emily R. Stein	_Emily Stein_	10/29/2018
	Print	Signature	Date
Author:	Jennifer M. Frederick	_For_	11/1/2018
	Print	Signature	Date
Author:	Glenn E. Hammond	_For_	11/1/2018
	Print	Signature	Date
Author:	James C. Bethune		10/31/2018
	Print	Signature	Date
Technical Review:	S. David Sevougian	_For_	10/31/2018
	Print	Signature	Date
QA Review	Shelly Nielsen	_Shelly R Nielsen_	10-31-18
	Print	Signature	Date
Management Review:	Sean Dunagan		10/31/2018
	Print	Signature	Date

WIPP:4.4.1.3:PA:QA-L:508062

Acknowledgments

Table of Contents

Information Only

List of Appendices

List of Figures

Information Only

List of Tables

Executive Summary

The proposed addition of new waste panels to the Waste Isolation Pilot Plant (WIPP) challenges the modeling assumptions inherent in the two-dimensional (2-D) flared grid used in performance assessment (PA) calculations of brine and gas flow in and around the repository, and requires development of a new 3-D model for use in PA. Because a 3-D grid that adequately represents the WIPP repository and its surroundings is expected to be considerably larger than the current 2-D flared grid, replacement of BRAGFLO with a two-phase flow simulator capable of running in a high-performance computing environment is essential. PFLOTRAN, a massively-parallel simulator of subsurface multiphase flow and reactive transport sponsored by the Department of Energy (DOE), has been adopted and its capabilities have been extended to include simulation of two-phase, immiscible flow (as in the current WIPP PA) and associated WIPP-specific process models such as gas generation, creep closure, and fracture.

PFLOTRAN development and testing has been ongoing since 2014 (Zeitler et al. 2017). In FY 2018, the focus has been on ensuring and demonstrating that implementations of two-phase immiscible flow and all WIPP-specific process models in PFLOTRAN are consistent with implementations in BRAGFLO, and that flow simulations run with PFLOTRAN mimic the results obtained with BRAGFLO for the WIPP PA. Previously existing and newly developed zero-, one-, and two-dimensional test cases were used to verify correct implementation of two-phase flow and WIPP-specific process models in PFLOTRAN by comparing PFLOTRAN results to BRAGFLO results. A PA-scale benchmark comparison of the two codes was executed using the 2-D flared grid and inputs from the 1800 simulations performed for the 2014 Compliance Recertification Application (CRA). The PFLOTRAN-BRAGFLO benchmark was used to verify that PFLOTRAN performs robustly across the full input parameter space sampled in PA and to quantify the effect, if any, of transitioning to PFLOTRAN on the results of WIPP PA flow calculations.

The WIPP-specific process models incorporated in PFLOTRAN are gas generation and brine consumption/generation; creep closure in portions of the underground excavation that contain waste; fracturing in the disturbed rock zone (DRZ) and marker beds; pore compressibility; the Klinkenberg correction for gas permeability; characteristic curves (relative permeability and capillary pressure as functions of saturation); the Redlich-Kwong-Soave equation of state for gas; and material changes associated with borehole intrusion and with evolution of the DRZ, panel closures, and the borehole. Initially, these process models were coupled to PFLOTRAN's GENERAL mode, which simulates two-phase, miscible flow plus energy conservation (heat transport).

Testing in FY 2017 made clear that (1) calculations on the 2-D flared grid (particularly those involving borehole intrusion) challenged Newton solver convergence in PFLOTRAN's GENERAL mode, and that (2) PFLOTRAN and BRAGFLO solutions on the 2-D flared grid were not yet sufficiently close to demonstrate with confidence that WIPP-specific process models were correctly implemented and coupled in PFLOTRAN. Both of these problems were addressed over the course of FY 2018 by more precisely implementing BRAGFLO's solver tolerances, time step and iteration controls, and method of discretizing the governing equations in PFLOTRAN's two-phase, immiscible flow mode; by tightly coupling the constitutive relationships described by process models into the system of flow equations; and by refactoring individual process models to ensure numerical implementation consistent with numerical implementation in BRAGFLO.

FY 2018 test case results demonstrate uniformly good agreement between PFLOTRAN and BRAGFLO solutions with relative differences in porosity, liquid and gas pressure, liquid and gas saturation, and liquid and gas density generally less than 1%. Rates of MgO hydration and gas generation calculated when using the gas and brine source/sink model agree to within 1% as well. The comparison is improved relative to results of the same test cases in FY 2017, when calculated brine pressures in test cases including creep closure differed by up to 20%, and MgO hydration rates differed by > 25%.

PFLOTRAN and BRAGFLO outputs were compared for 1800 simulations whose input parameters duplicated those used for the three replicates of sampled parameters and six scenarios in the 2014 CRA WIPP PA calculations. A comparison was made of volume-weighted averages of liquid pressure and liquid saturation for each of nine regions in the excavated volume (waste area, operations area, etc.), and of liquid mass flow at eight locations, including the intersection of the borehole and the Culebra. Comparison of standard uncertainty analysis metrics, e.g., mean, median, etc., displayed in the form of box plots, showed no statistically meaningful differences between PFLOTRAN results and BRAGFLO results. The uncertainty metrics and quantiles effectively overlie each other.

The good agreement on both small test problems and on the full set of PA flow simulations indicates correct implementation of two-phase, immiscible flow and associated WIPP-specific process models in PFLOTRAN. Additionally, robust simulation over the full input parameter space sampled in PA has been demonstrated. In the future, these simulations can support formal verification of PFLOTRAN for quality assurance, and the PFLOTRAN-BRAGFLO 2-D flared grid benchmark will provide a new (PFLOTRAN) baseline for WIPP PA flow calculations, against which further changes to conceptual and numerical models may be compared during the transition to a 3-D WIPP PA.

Acronyms

CRA   Compliance Recertification Application

DOE   Department of Energy

DRZ   Disturbed Rock Zone

EOS   Equation of State

FY   Fiscal Year

PA   Performance Assessment

PFD   PFLOTRAN Development

QA   Quality Assurance

RKS   Redlich-Kwong-Soave (equation of state)

WIPP   Waste Isolation Pilot Plant

Repository Regions

EXP   Experimental Area

MPCS Middle Panel Closure System

NPCS North Panel Closure System

NROR North Rest of Repository

SPCS South Panel Closure System

SROR South Rest of REpository

OPS   Operations Area

SHAFT   Shaft (3 cells at repository horizon)

WAS_AREA Waste Area

This page intentionally left blank.

1 Introduction

Revision 1 was made to correct formatting errors in section 8, and contains no updates to technical content.

The proposed addition of new waste panels to the Waste Isolation Pilot Plant (WIPP) challenges the modeling assumptions inherent in the two-dimensional (2-D) flared grid used in performance assessment (PA) calculations of brine and gas flow in and around the repository (US DOE 1996; US DOE 2014), and requires development of a new 3-D model for use in PA. The 2-D flared grid represents a vertical cross section running the length of the repository and extending beyond the north and south land withdrawal boundaries. It approximates radial concentric flow toward and away from the repository by increasing the length of the third dimension (the horizontal dimension perpendicular to the symmetry axis) as a function of distance from the repository (SNL1992; Voss 1984). Proposed new waste panels would be placed off the symmetry axis of the current repository, invalidating the premise of 2-D radial concentric flow.

The DOE has tasked Sandia with developing the tools necessary to run PA calculations that can simulate a 3-D model domain. At the core of this task is the development of an efficient 3-D flow simulator that incorporates WIPP-specific process models to replace BRAGFLO. Although BRAGFLO can calculate solutions in 3-D, it cannot leverage high performance computing, a necessary capability for efficient execution of the large problems expected to result from a 3-D representation of the expanded WIPP repository. In 2013, the DOE and Sandia decided to adopt the massively-parallel, open-source, multiphase flow and reactive transport code PFLOTRAN (https://pa.sandia.gov; https://www.pflotran.org; Lichtner et al. 2018; Hammond and Frederick 2017; Hammond et al. 2014; Hammond et al. 2011), and to incorporate WIPP-specific process models such as gas generation, creep closure, and fracture into it.

In addition to the ability to run in parallel on a supercomputer, the advantages of PFLOTRAN include its binary output format and its multiphase and reactive transport capabilities. PFLOTRAN uses the HDF5 binary output format, a modern file format that allows efficient reading and writing of large datasets. Python and other software libraries are readily available for manipulating HDF5 files during pre- and post-processing. PFLOTRAN has the ability to simulate miscible, two-phase flow coupled with the energy equation, a capability that may be desired in the future by the DOE. Because of its reactive transport capability, PFLOTRAN can replace both BRAGFLO and the transport codes PANEL and NUTS, simplifying WIPP PA run control, eliminating the need for data storage between flow and transport codes, and improving the coupling between the flow and transport calculations.

Development and testing of PFLOTRAN for use as the flow simulator in WIPP PA is one part of a multi-year project (Zeitler et al. 2017), the ultimate goal of which is to integrate a new 3-D repository conceptual model into WIPP PA for use in the 2024 Compliance Recertification Application (CRA). The scope of the project includes replacing BRAGFLO, PANEL, and NUTS with PFLOTRAN; migrating to new computer hardware and a Linux operating system; and developing a new run control system. It requires rigorous quality assurance (QA) of all new software and a peer review of the new conceptual model.

Development and testing of PFLOTRAN for WIPP PA has been ongoing since FY2014. Work has included evaluating test cases that were initially developed for the BRAGFLO and NUTS codes; development of new test cases; implementation of WIPP-specific process models in

PFLOTRAN; development of a two-phase immiscible flow mode in PFLOTRAN (WIPP_FLOW mode); development of prePFLOTRAN, a collection of python scripts that queries the online parameter database (http://tgw.sandia.gov) and writes PFLOTRAN input decks; and execution of a full PFLOTRAN-BRAGFLO benchmark, comparing PFLOTRAN and BRAGFLO outputs across 1800 simulations that essentially duplicate those performed for the 2014 CRA WIPP PA calculations. The objectives of the tasks listed above are to:

1. Demonstrate that all WIPP-specific process models are correctly implemented in PFLOTRAN.

2. Develop test cases and simulations that will support formal verification of PFLOTRAN.

3. Quantify the differences between PFLOTRAN and BRAGFLO solutions, and demonstrate that by itself, the adoption of PFLOTRAN has negligible influence on the results of flow calculations used in WIPP PA.

4. Create a set of PFLOTRAN simulation results, which can be used to quantify the effects of future improvements to the model domain (i.e. 3-D grid), new process and constitutive model implementations, and/or different numerical solutions of the flow equations.

At the end of FY 2017, sufficient code development and testing had been done that process model implementation and test case development were nearly complete (Zeitler et al. 2017). However, two problems were discovered in the initial comparison of PFLOTRAN to BRAGFLO using the 2-D flared grid and inputs from the 2014 CRA:

1. After borehole intrusion, PFLOTRAN was unable to calculate a solution.

2. Without borehole intrusion, PFLOTRAN calculated pressures and saturations in the model domain in some locations in the model domain that differed from those calculated by BRAGFLO by several tens of percent. These differences were too large to be confident that all WIPP-specific process models were correctly coupled into the system of flow equations.

Because of the WIPP-specific process models (including the material change that represents borehole intrusion), WIPP PA simulations present unique numerical challenges. In FY 2018, code development focused on overcoming these challenges, and on ensuring implementation details in both codes were sufficiently well understood that differences between PFLOTRAN and BRAGFLO results could also be understood.

This report describes the development of WIPP_FLOW mode in PFLOTRAN and improvements to process model implementation, presents updated results for previous test cases and results for new test cases, and presents the results of the full (1800 simulation) PFLOTRAN-BRAGFLO 2-D flared grid benchmark (also called the PFLOTRAN development (PFD) analysis). Two companion reports are expected to be completed in FY 2018 – the first documenting development of PFLOTRAN for WIPP PA transport simulations and comparison of results to NUTS, and the second documenting the progress made toward development of an initial 3-D model domain for benchmarking against the 2-D flared grid.

2   PFLOTRAN Development and Testing Approach

2.1   Implementation of WIPP_FLOW Mode and WIPP Process Models

Prior to FY 2017, an effort was made to simulate the WIPP PA calculation using the GENERAL (multi-phase) flow mode within PFLOTRAN. The benefit of using PFLOTRAN's GENERAL mode was that (1) it considers miscible, two-phase flow with two fluid components (air, water) and two fluid phases (gas, liquid), (2) it is anisothermal (it simulates heat convection and conduction through an energy conservation equation), and (3) it already exists, eliminating the need to develop a new flow mode. However, as the 2-D flared benchmark progressed, it became clear that the simulations (1) challenged Newton solver convergence in PFLOTRAN's GENERAL mode, and (2) did not yet allow for the confident demonstration that WIPP-specific process models were correctly implemented and coupled in PFLOTRAN. Both of these problems were addressed over the course of FY 2018 by more precisely implementing BRAGFLO's solver tolerances, time step and iteration controls, and method of discretizing the governing equations into WIPP_FLOW mode; and by tightly coupling all process models into the system of flow equations. Section 3 further explains the reasoning behind the transition from GENERAL mode to WIPP_FLOW mode. Section 4 describes the code development required to achieve the level of agreement between PFLOTRAN and BRAGFLO demonstrated in this report.

Currently, PFLOTRAN's WIPP_FLOW mode duplicates BRAGFLO's numerical implementation of two-phase immiscible flow (including use of ALPHA and ELEVATION terms – see Section 4.4), and incorporates all of the WIPP-specific process models found in BRAGFLO. The WIPP-specific process models for which development work occurred in FY 2017 and FY 2018 include:

- Waste area gas generation/brine consumption chemistry
- Waste area creep closure
- Fracturing of marker beds and disturbed rock zone (DRZ)
- Compressibility of pore space
- Klinkenberg effect on gas permeability
- WIPP-PA capillary pressure and relative permeability functions
- Redlich-Kwong-Soave equation of state for the gas phase
- Radionuclide source term

The process model for simulating instantaneous material changes associated with borehole intrusion (and with evolution of panel closures and shaft materials) was implemented prior to FY 2017. Testing of all of these except (1) capillary and relative permeability functions and (2) the radionuclide source term is addressed in this report. Testing of the capillary pressure and relative permeability functions (also called characteristic curves) is fully documented on the PFLOTRAN website at: https://www.documentation.pflotran.org/qa_tests/pc_sat_rel_perm.html. Development and testing of the radionuclide source term will be documented in the FY 2018 transport milestone report.

WIPP_FLOW mode was used for all simulations presented in this report, and is expected to be carried forward in the development of the 3-D WIPP PA.

2.2   WIPP Process Model Testing (Single-Cell)

A set of single-cell tests developed for debugging purposes in FY 2017 (Zeitler et al. 2017) exercises all of the newly added or updated WIPP-specific process models in PFLOTRAN. The tests presented in Section 5 demonstrate the performance of individual process models in isolation, or in simple combination, on single-cell domains. The advantage of single-cell tests is that inter-cell flow is eliminated and thus the differences due to individual process models can be better isolated. Process models are tested simultaneously because discrepancies for separate process model tests are not necessarily indicative of the resulting discrepancies when multiple process models are tested in combination. The WIPP-specific process models exercised in the single-cell tests include: waste area gas generation/brine consumption chemistry, waste area creep closure, compressibility of pore space, fracturing of marker beds and DRZ, Klinkenberg effect on gas permeability, and the Redlich-Kwong-Soave equation of state.

2.3   WIPP Process Model Testing (Multi-Cell)

A set of multi-cell tests developed in FY 2017 (Zeitler et al. 2017) exercises all of the newly added or updated WIPP-specific process models in PFLOTRAN in isolation, or in simple combination, on multi-cell domains (Section 6). These multi-cell domains are much smaller and less complicated than the full 2-D flared grid, and serve to uncover potential issues when inter-cell flow occurs. Process models were tested simultaneously because discrepancies for separate process model tests are not necessarily indicative of the resulting discrepancies when multiple process models are tested in combination. The WIPP-specific process models exercised in the multi-cell tests are the same as for the single-cell tests: waste area gas generation/brine consumption chemistry, waste area creep closure, compressibility of pore space, fracturing of marker beds and DRZ, Klinkenberg effect on gas permeability, and the Redlich-Kwong-Soave equation of state.

2.4   Miniature Flared Grid Testing

Two miniature 2-D flared grid tests developed for this report verify the functionality of the ALPHA and ELEVATION parameters. ALPHA is a term used to incorporate unequal areas of adjacent cell faces in a flared grid into the harmonic average of transmissibility between cells (Peaceman 1977; Camphouse 2012a). ELEVATION is a term used to adjust the pressure at a cell center for elevation differences due to dipping formations (Camphouse 2012a). The miniature flared grid tests are also designed to test the simulation of borehole intrusion. Borehole intrusions are simulated using abrupt changes in material properties. These present a numerical challenge that has not been addressed in other test problems. Additionally the 2-D flared grid test problems exercise the same WIPP-specific process models exercised in the single- and multi-cell tests: waste area gas generation/brine consumption chemistry, waste area creep closure, compressibility of pore space, fracturing of marker beds and DRZ, Klinkenberg effect on gas permeability, the Redlich-Kwong-Soave equation of state. The two flared grid tests contain 5×3 grid cells and 5×11 grid cells, thus they are much smaller than the full-scale WIPP PA 2-D flared grid, and simpler to debug.

2.5 PFLOTRAN-BRAGFLO 2-D Flared Grid Benchmark

The PFLOTRAN-BRAGFLO 2-D flared grid benchmark compares PFLOTRAN and BRAGFLO outputs from 1800 simulations that essentially duplicated the BRAGFLO simulations performed for the 2014 CRA WIPP PA calculations. Parameters are stored in the online parameter database at http://tgw.sandia.gov under the analysis name PFD, which stands for PFLOTRAN development. Completing the suite of 1800 PA simulations ensures that PFLOTRAN is tested on a complex problem relevant to PA, using all WIPP-specific process models and over the full range of parameter values sampled in PA. The objectives of the comparison are: 1) to quantify the differences between the outputs of the two codes; 2) to demonstrate on a simulation by simulation basis that the differences between the solutions fall below acceptable thresholds; and 3) to explain any differences that exceed the thresholds. The benchmark includes a detailed comparison of a single simulation – Replicate 1, Scenario 2, Vector 001 (R1S2V001) – which updates and replaces the single vector comparisons in the FY 2017 milestone report (Zeitler et al. 2017).

3 Motivation for Developing WIPP_FLOW Mode

Prior to FY 2017, an effort was made to simulate the WIPP PA calculation using the GENERAL (multiphase) flow mode within PFLOTRAN. The benefit of using PFLOTRAN's GENERAL mode was that (1) it considers miscible, two-phase flow with two fluid components (air, water) and two fluid phases (gas, liquid), (2) it is anisothermal (heat convection and conduction through an energy conservation equation), and (3) it already exists, eliminating the need to develop a new flow mode.

With GENERAL mode, there are three governing conservation equations (two mass and one energy; Lichtner et al. 2018):

$$\frac{\partial\left(\phi\left[s_l\rho_l X_w^l + s_g\rho_g X_w^g\right]\right)}{\partial t} = -\nabla\cdot\left(\rho_l X_w^l \boldsymbol{q}_l + \rho_g X_w^g \boldsymbol{q}_g + \boldsymbol{J}_w^l + \boldsymbol{J}_w^g\right) + q_w$$

$$\frac{\partial\left(\phi\left[s_l\rho_l X_a^l + s_g\rho_g X_a^g\right]\right)}{\partial t} = -\nabla\cdot\left(\rho_l X_a^l \boldsymbol{q}_l + \rho_g X_a^g \boldsymbol{q}_g + \boldsymbol{J}_a^l + \boldsymbol{J}_a^g\right) + q_a$$

$$\frac{\partial\left(\phi\left[s_l\rho_l U_l + s_g\rho_g U_g\right] + [1-\phi]C_p^{\text{rock}}\rho_{\text{rock}}T\right)}{\partial t} = -\nabla\cdot\left(\rho_l H_l \boldsymbol{q}_l + \rho_g H_w \boldsymbol{q}_g - \kappa_{\text{eff}}\nabla T\right) + q_e$$

where

$$\boldsymbol{q}_\alpha = -\frac{kk_{r\alpha}}{\mu_\alpha}\nabla(p_\alpha - W_a\rho_\alpha \boldsymbol{g}z)\ (\alpha = l, g)$$

$$\boldsymbol{J}_a^l = -\tau\phi s_l D_l \rho_l \nabla X_a^l$$

$$\boldsymbol{J}_a^g = -\tau\phi s_g D_g^0\left(\frac{T+T_K}{T_K}\right)^\theta \frac{p_0}{p_g}\rho_g\nabla X_a^g$$

$$\boldsymbol{J}_w^l = -\boldsymbol{J}_a^l$$

$$\boldsymbol{J}_w^g = -\boldsymbol{J}_a^g,$$

and

ϕ = porosity [-]
s_l = liquid phase saturation [-]
s_g = gas phase saturation [-]
ρ_l = liquid phase density [kmol/m^3]
ρ_g = gas phase density [kmol/m^3]
X_w^l = water mole fraction in liquid phase [-]
X_a^l = air mole fraction in liquid phase [-]
X_w^g = water mole fraction in gas phase [-]
X_a^g = air mole fraction in gas phase [-]
$\boldsymbol{q}_l$ = liquid phase Darcy flux [m/s]
$\boldsymbol{q}_g$ = gas phase Darcy flux [m/s]
$\boldsymbol{J}_w^l$ = diffusion of water in liquid phase [kmol/m^2-s]

$\boldsymbol{J}_a^l$ = diffusion of air in liquid phase [kmol/m^2-s]
$\boldsymbol{J}_w^g$ = diffusion of water in gas phase [kmol/m^2-s]
$\boldsymbol{J}_a^g$ = diffusion of air in gas phase [kmol/m^2-s]
q_l = liquid source term [kmol/m^3-s]
q_g = gas source term [kmol/m^3-s]
q_e = energy source term [W/m^3]
U_l = liquid phase internal energy [J/m^3]
U_g = gas phase internal energy [J/m^3]
H_l = liquid phase enthalpy [J/m^3]
H_g = gas phase enthalpy [J/m^3]
C_p^{rock} = rock heat capacity [J/kg-K]

ρ_{rock} = rock density [kg/m^3]

T = temperature [C]

κ_{eff} = rock thermal conductivity [W/K-m]

k = intrinsic permeability [m^2]

α = fluid phase [l, g]

$k_{r\alpha}$ = phase relative permeability [-]

μ_α = phase viscosity [Pa-s]

p_α = phase pressure [Pa]

ρ_α = phase density [kmol/m^3]

W_α = molecular weight [kg/kmol]

$\boldsymbol{g}$ = gravity vector [m^2/s]

z = vertical distance [m]

τ = tortuosity [-]

D_l = liquid phase diffusion coefficient [m^2/s]

D_g^0 = gas phase diffusion coefficient at p_0 and T_K [m^2/s]

p_0 = gas phase reference pressure [Pa]

T_K = 273.15 degrees [K]

θ = temperature exponent

Each grid cell has three primary dependent variables, depending on the thermodynamic state of the cell. Fluid phases are permitted to mix. Air (or any gaseous component) dissolves into the liquid phase, and water evaporates into the gas phase as water vapor. This miscibility can complicate the calculation of fluid constitutive relations such as phase density, enthalpy and viscosity since component mixtures must be accommodated. For instance, gas-phase water vapor density differs from air density, and both are a function of pressure and temperature. Although strategies exist for calculating constitutive relations for miscible phases, the mixture approach is more complicated than considering single-component phases.

Fluid phase appearance/disappearance is also allowed in GENERAL mode with the primary dependent variables depending upon the thermodynamic state of the system. For instance, for a single-phase liquid state, the primary dependent variables are liquid pressure, dissolved air mole fraction in the liquid phase, and temperature. For a two-phase state, the primary dependent variables are gas pressure, gas saturation and temperature.

In the effort to apply GENERAL mode to simulating the WIPP PA calculation, it became evident that poor Newton solver convergence hindered GENERAL mode performance, expressed through restrictions on time step size that greatly slowed simulation progress. Phase appearance/disappearance, miscibility, and the use of a numerical Jacobian were believed to be the primary culprits. Early in FY 2017, deactivation of miscibility was added as an option forcing a persistent two-phase state, and the analytical derivatives to the anisothermal multiphase flow equation were derived and encoded in PFLOTRAN. However, these steps failed to resolve the convergence issues. As a result, the decision was made to abandon GENERAL mode in favor of an immiscible, isothermal flow mode similar to what is implemented in BRAGFLO.

The development of WIPP_FLOW mode started in May of FY 2017. WIPP_FLOW mode is isothermal. WIPP_FLOW mode mimics the solution of GENERAL mode's mass conservation equations with the exception that the thermodynamic state of the system is always two-phase and the phases are immiscible. The governing equations for WIPP_FLOW mode simplify greatly to

$$\frac{\partial(\phi s_l \rho_l)}{\partial t} = -\nabla \cdot (\rho_l \boldsymbol{q}_l) + q_w$$

$$\frac{\partial(\phi s_g \rho_g)}{\partial t} = -\nabla \cdot (\rho_g \boldsymbol{q}_g) + q_a$$

where

$$\boldsymbol{q}_\alpha = -\frac{k k_{r\alpha}}{\mu_\alpha} \nabla(p_\alpha - W_a \rho_\alpha \boldsymbol{g} z) \ (\alpha = l, g).$$

By August of FY 2017, a prototype of WIPP_FLOW that implemented the governing equations for two-phase, immiscible flow was available for comparison against BRAGFLO. At that point, all of BRAGFLO's process models as described in BRAGFLO documentation (Camphouse 2012a;b) (the BRAGFLO source code had not been examined in detail) were implemented within PFLOTRAN and sequentially or fully coupled to WIPP_FLOW. However, two problems were discovered in the initial comparison of PFLOTRAN to BRAGFLO using the 2-D flared grid (Zeitler et al. 2017). At borehole intrusion, PFLOTRAN was unable to calculate a solution and cut the time step size until the simulation failed. Without borehole intrusion, PFLOTRAN calculated pressures and saturations in the model domain that differed from those calculated by BRAGFLO by several tens of percent. These differences were too large to be confident that all WIPP-specific process models were correctly coupled into the system of flow equations.

To overcome the simulation failures due to time step reduction, and to demonstrate with confidence that WIPP-specific process models implemented in PFLOTRAN are functioning as intended across the sampled input space, additional code development was needed. Therefore, in FY 2018, the numerical implementation of two-phase immiscible flow in WIPP_FLOW mode was completely refactored (i.e., rewritten) to more precisely match the implementation in BRAGFLO. Refactoring included but was not limited to changes to the approach for discretizing the flux equations, to the set of criteria used to determine Newton solver convergence and associated tolerances, and to the controls on time step size. It also included full coupling of all process models, and the addition of ALPHA and ELEVATION.

4 Features Implemented or Refactored in the Development of WIPP_FLOW18

This section documents the specific code modifications made in WIPP_FLOW and in associated WIPP-specific process models during the refactoring of WIPP_FLOW mode. In this section, WIPP_FLOW17 refers to the version of WIPP_FLOW mode developed in FY 2017 and documented in the previous milestone report (Zeitler et al. 2017). WIPP_FLOW18 refers to the version developed in FY 2018 and documented in this milestone report.

4.1 Negative Gas Pressures

In both PFLOTRAN and BRAGFLO, gas pressure is measured as absolute pressure. A perfect vacuum has an absolute pressure of zero, and thus, absolute gas pressure cannot physically drop below zero.

In WIPP_FLOW17, the time step was immediately cut during Newton iteration when the gas pressure at any grid cell dropped below zero:

$$P_g < 0,$$

because negative absolute gas pressure is nonphysical. Negative gas pressures occur when the change in gas pressure over a Newton iteration is large and negative, and the gas pressure from the previous solution is small – there is overshoot during Newton iteration.

In WIPP PA simulations run with BRAGFLO on the 2-D flared grid, negative gas pressures occasionally occur in localized regions of the model domain, particularly in the initial phase of a simulation (-5 to 0 yr), and typically resolve to positive pressures at some later time in the simulation. Given the current conceptualization and parameterization, allowing gas pressure to go negative in WIPP PA simulations is necessary to avoid reducing the time step so much that a solution cannot be obtained.

The rejection of negative gas pressures in WIPP_FLOW17 played a significant role in preventing PFLOTRAN simulations on the 2-D flared grid from running to completion (i.e. to 10,000 years). Therefore, this restriction was removed from WIPP_FLOW18. Allowing negative gas pressures is consistent with how BRAGFLO is used in WIPP PA calculations and is necessary to complete the 2-D flared grid benchmark simulations. Because BRAGFLO and PFLOTRAN's WIPP_FLOW18 truncate gas pressure within the gas density equation of state (Section 4.9), the negative gas pressure has minimal impact on the governing mass conservation equation.

4.2 Fixed (Non-Changing) Upwind Direction During Time Step

Within WIPP_FLOW17 flux calculations, the mobility term (defined as fluid phase relative permeability divided by fluid phase viscosity) is upwinded based on the direction of the pressure gradient. This pressure gradient factors in deviations of fluid pressure from hydrostatic in each grid cell and the hydrostatic pressure gradient induced by a difference in cell elevation. Of the two cells on either side of the face across which the fluid flux is to be calculated, the cell with the higher pressure is considered the "upwind cell", because fluid will flow out of the cell with the higher pressure toward the cell with lower pressure. The mobility term for the upwind cell is employed in the flux calculation.

Within most PFLOTRAN flow modes, the direction of upwinding can change between Newton iterations if the latest solution reversed the direction of the pressure gradient, or during a Newton iteration (Jacobian evaluation) if the pressure perturbations calculated with numerical derivatives reverse the pressure gradient (e.g. if the pressure of a cell is minutely below that of the other, but then perturbed minutely above, the upwind cell changes). If the upwind cell changes and the difference in relative permeability and/or viscosity between the cells is large, the calculated flux can change significantly. Repeated changes in upwind direction can cause significant oscillation within the Newton solver and hinder solver convergence.

In BRAGFLO, the user can choose when the upwind direction is re-evaluated. Re-evaluation can occur after a specified number of Newton iterations (anywhere from 1 to N) or the upwind direction can be fixed throughout the time step. In BRAGFLO simulations for WIPP PA, the upwind direction is fixed throughout each time step, thus eliminating oscillations in the solution due to changes in upwind direction during iteration. The same choices were implemented in WIPP_FLOW18, and the option to fix the upwind direction throughout a time step was used in the 2-D benchmark simulations.

Another difference between most PFLOTRAN flow modes and BRAGFLO is that BRAGFLO upwinds only the relative permeability, and not the viscosity. Instead, viscosity is included in the inverse-distance-weighted harmonic average of transmissibility (the product of area, intrinsic permeability, and fluid density divided by fluid viscosity) at the interface. This approach was also implemented in WIPP_FLOW18. Because the WIPP PA calculation specifies constant viscosity for both the liquid and gas phases, this removal of viscosity from the upwinded term by itself does not affect simulation results.

4.3   Conversion of Residual Vector and Jacobian Matrix Units

The infinity norms (maximum absolute value in the vector) of the liquid and gas phase residual vectors are used in determining Newton solver convergence. WIPP_FLOW18 (like other flow modes in PFLOTRAN) has units of kilomole per second (kmol/s) for the residual vector whereas BRAGLO's units are kg/m³ bulk. The option of converting the units to kg/m3 bulk was added to WIPP_FLOW18. To convert from PFLOTRAN to BRAGFLO units, the residual and Jacobian must be scaled by the formula (molecular) weight of the fluid component (W_α), the time step size (Δt) and the inverse of the cell volume (V)

$$Res(BRAGFLO) = Res(PFLOTRAN) \times \frac{W_\alpha \times \Delta t}{V}$$

This option (which did not exist in WIPP_FLOW17) was employed in the test case comparisons and the 2-D flared grid benchmark in this report.

4.4   Implementation of ALPHA and ELEVATION for Fluid Flux Calculations

There are two parameters (ALPHA and ELEVATION) used in the BRAGFLO fluid flux calculation that were not originally coded into PFLOTRAN and are not found in other DOE multiphase subsurface simulators (e.g., TOUGH2, FEHM, STOMP) discretized with the finite volume method. The following subsections describe these quantities and how they are implemented in both BRAGFLO and WIPP_FLOW18.

4.4.1 *ALPHA or α*

The WIPP PA 2-D flared grid has non-uniform grid spacing in the dimension orthogonal to the 2-D domain. The width of the cell in the orthogonal direction (BRAGFLO's Z-dimension and PFLOTRAN's Y-dimension) is represented by the parameter α (Figure 4.4-1).
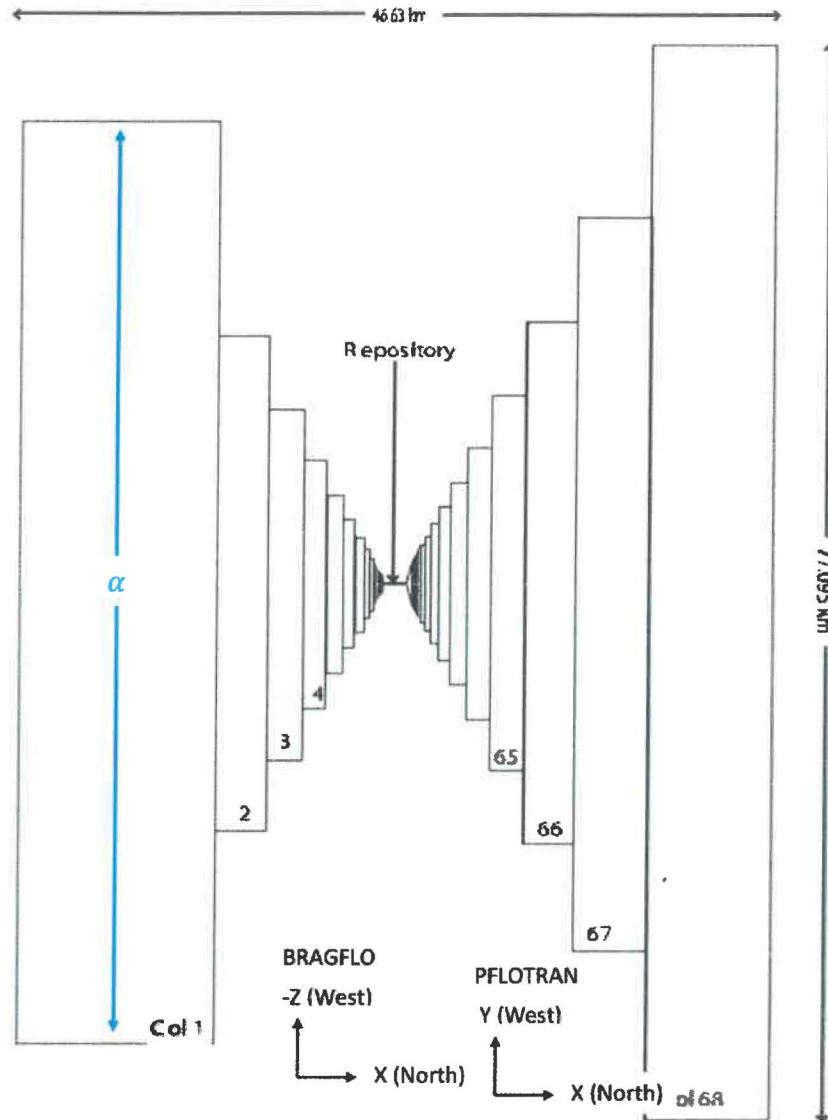
Figure 4.4-1 In the WIPP PA 2-D flared grid (DOE 2014) α is the width orthogonal to the 2-D grid. BRAGFLO and PFLOTRAN coordinate axes for the horizontal plane are shown.

Conceptually α is intended to be defined in such a way that the width of each cell increases smoothly as a function of the "radius" of the flared grid (SNL 1992). In practice, the implementation of α presents a challenge: When calculating the fluid flux between two grid cells, an interfacial area must be specified between the two grid cells. For Cartesian grids, this interfacial area is based on the dimensions of the shared face between two grid cells. However, in the case of a 2-D flared grid this interfacial area, and cell width α, as shown in Figure 4.4-1, varies in the

X direction. Use of the overlapping, intersectional area between the two faces (i.e., the cross-sectional area of the smaller grid cell) as the interfacial area normal to X is one approach, and the approach implemented in WIPP_FLOW17.

BRAGFLO employs an alternate approach that incorporates α into the harmonic average of transmissibility. For fluxes in the X direction, the harmonically-averaged transmissibility can be calculated as follows:

$$\frac{1}{\Delta x_{ave}}\left(\frac{Ak\rho}{\mu}\right)_{ave} = \frac{\left(\frac{\alpha\Delta zk\rho}{\mu}\right)_1 \left(\frac{\alpha\Delta zk\rho}{\mu}\right)_2}{\frac{\Delta x_1}{2}\left(\frac{\alpha\Delta zk\rho}{\mu}\right)_2 + \frac{\Delta x_2}{2}\left(\frac{\alpha\Delta zk\rho}{\mu}\right)_1}$$

where

$(\xi)_1$ = value of quantity ξ for cell 1 on one side of face

$(\xi)_2$ = value of quantity ξ for cell 2 on the other side of face

A = area [m^2]

Δx_1 = width of cell 1 in horizontal (X) dimension [m]

Δx_2 = width of cell 2 in horizontal (X) dimension [m]

Δx_{ave} = average cell width $((x_1 + x_2)/2)$ in horizontal (X) dimension [m]

α = grid cell width orthogonal to 2D domain [m]

Δz = grid cell width in vertical (BRAGFLO Y or PFLOTRAN Z) dimension [m]

k = intrinsic permeability [m^2]

ρ = fluid density [kg/m^3]

μ = fluid viscosity [Pa-s]

$(\xi)_{ave}$ = inverse distance weighted harmonic average of quantity ξ.

Note that $\alpha\Delta z$ is the cross-sectional area of the cell normal to the X direction. The complete fluid flux equation in units of kg/s is as follows:

$$q = -k_{r,up}\left(\frac{Ak\rho}{\mu}\right)_{ave}\frac{(P_2 - P_1 + \delta z\rho g)}{\Delta x_{ave}}$$

where

q = mass flux [kg/s]

$k_{r,up}$ = upwind relative permeability

P = pressure [Pa]

δz change in elevation between cell centers $(z_2 - z_1)$.

Therefore, through α, the cross-sectional area is incorporated in the flux calculation by including it in the harmonic average of transmissibility. This approach is implemented in WIPP_FLOW18

as the default option, and is used in the flared grid simulations (test cases and benchmark) in this report. WIPP_FLOW18 also supports intersectional cross-sectional area, but it is not the default option.

4.4.2 ELEVATION

As part of the WIPP PA calculation, BRAGFLO reads in the elevation of each grid cell center instead of calculating the elevations implicitly through the discretization (grid coordinates). The elevation term allows a head gradient to be imposed on the system through a modification to cell elevation. Implementation in the fluid flux equation takes the form:

$$q = -k_{r,up}\left(\frac{Ak\rho}{\mu}\right)_{ave} \frac{(P_2 - P_1 + (elev_2 - elev_1)\rho g)}{\Delta x_{ave}}$$

where

$elev$ = elevation of the cell center prescribed through an elevation dataset.

Here the δz in the previous section is replaced by the differencing of prescribed cell center elevations. This BRAGFLO capability did not exist in WIPP_FLOW17, but was implemented in WIPP_FLOW18.

4.5   Gas Generation and Brine Consumption/Generation

The gas generation process model calculates brine and gas source/sink terms as a function of the waste composition within a grid cell. During FY 2017, this capability was implemented within PFLOTRAN as a separate WIPP_SOURCE_SINK process model that was sequentially coupled to WIPP_FLOW17. The sequential coupling meant that the WIPP_SOURCE_SINK process model was evaluated after WIPP_FLOW17 completed its flow calculation. Sequential coupling facilitated implementation and Newton solver convergence. However, it also introduced operator splitting error that was largely a function of time step size.

To eliminate the operator splitting error, the WIPP_SOURCE_SINK process model was fully coupled into WIPP_FLOW18, i.e., WIPP_SOURCE_SINK is called and brine and gas source/sink terms are updated during each evaluation of the residual in WIPP_FLOW18.

Additional updates in WIPP_FLOW18 included mimicking BRAGFLO's order of operations for the evaluations of the gas generation equations in the process model, using BRAGFLO units for species mass (kg) rather than PFLOTRAN units (mol) in rate smoothing and tapering operations, and including additional smoothing algorithms that appeared in BRAGFLO source code but were not included in the BRAGFLO User Manual (Camphouse 2012a) or Design Document (Camphouse 2012b). Rate smoothing introduces a dependence on the current inventory of reactants. Rate tapering decreases reaction rate, if necessary, so that reactant inventory goes to zero at the end of a time step rather than during a time step.

Documentation for the current implementation of the gas generation and brine consumption/generation model can be found at: https://www.documentation.pflotran.org/theory_guide/wipp_source_sink.html.

4.6 Creep Closure Shutdown

BRAGFLO simulates creep closure within each cell containing a creep closure material (WAS_AREA or REPOSIT) until either (1) a prescribed shutdown time is reached or (2) a threshold shutdown pressure is surpassed. That shutdown time and shutdown pressure are implemented in BRAGFLO was discovered by analyzing the source code; neither is discussed in BRAGFLO documentation. In FY 2018, additional analysis of the BRAGFLO source code revealed that shutdown due to liquid pressure in excess of the threshold during Newton iteration is temporary; creep closure is re-enabled if the liquid pressure falls below the threshold shutdown pressure during successive iterations. When creep closure is shutdown during an iteration, soil compressibility is used to calculate porosity. At the end of the time step, if liquid pressure still exceeds the shutdown pressure, creep closure is turned off in that cell for the remainder of the simulation. BRAGFLO also truncates the creep-closure porosity to a minimum creep-closure porosity.

In WIPP_FLOW17, creep closure shutdown was permanent if the threshold pressure was exceeded during iteration, and truncation of creep-closure porosity to a minimum value was not implemented. Limits on creep closure in WIPP_FLOW18 are like those in BRAGFLO. Creep closure terminates once the shutdown time or threshold shutdown pressure has been exceeded at the end of a time step. During Newton iteration, creep closure may shutdown temporarily, triggering the use of soil compressibility as an alternative update to porosity. While creep closure is active, WIPP_FLOW18 truncates the creep-closure porosity to a minimum creep-closure porosity.

4.7 Truncation of Negative Gas Pressure in Klinkenberg Correction

Klinkenberg correction modifies the intrinsic permeability for the gas phase using the formula

$$k_g = k_l \left(1 + \frac{b k_l^{\,a}}{p_g}\right)$$

where k_l and k_g are the intrinsic permeabilities for the liquid and gas phases, p_g is the gas pressure, and a and b are material-specific parameters. Note that as gas pressure approaches zero, the equation becomes infinite. In WIPP_FLOW17, it was assumed that gas pressure must be greater than zero. However, BRAGFLO allows for zero or negative gas pressures (Section 4.1) and includes a conditional to prevent infinite Klinkenberg correction:

$$k_g = \begin{cases} k_l \left(1 + \frac{b k_l^{\,a}}{p_g}\right) & p_g > 0 \\ k_l & p_g \leq 0 \end{cases}.$$

WIPP_FLOW18 incorporates this conditional. Note that this conditional introduces a discontinuity at $p_g = 0$.

4.8 Redlich-Kwong-Soave Equation of State

The Redlich-Kwong-Soave (RKS) equation of state (EOS), used to calculate gas density, was modified in PFLOTRAN to use effective critical properties for H_2 gas. In addition, the calculation method was changed to use an analytical solution to the cubic equation rather than an iterative

root-finding solution. The iterative root-finding solution failed at high pressures (>100 MPa). This problem is solved in BRAGFLO by linearly extrapolating to calculate gas density at pressures greater than 100 MPa. WIPP_FLOW17 and WIPP_FLOW18 use the analytical solution, which is robust over all pressures (Zeitler et al. 2017).

4.9   Truncation of Gas Pressure in RKS EOS

WIPP_FLOW17 assumed gas pressure to be constrained to greater than zero, and thus, the division by gas pressure in the Redlich-Kwong-Soave equation of state for gas component density was not an issue. Because BRAGFLO allows negative gas pressures (Section 4.1), it truncates gas pressure at a minimum of 0.1 Pa within the RKS EOS. This approach was introduced into the WIPP_FLOW18 RKS EOS.

4.10   Cell-Centered Boundary Conditions

BRAGFLO implements Dirichlet pressure boundary conditions at the center of boundary cells. The pressure is held constant by zeroing the row in the residual corresponding to the update for liquid pressure in the Newton solution. The off-diagonal entries in the same row of the Jacobian are zeroed and the diagonal entry is scaled as follows:

$$J_{i,i_{\text{Dirichlet}}}^{\text{scaled}} = J_{i,i_{\text{Dirichlet}}} \times 10^8 + 10^8.$$

WIPP_FLOW17 implements Dirichlet pressure (and saturation) boundary conditions at the face of the cell where the pressure would naturally be applied in the problem domain. Therefore, the difference in location where the Dirichlet condition is applied is half the grid spacing in the direction of the vector connecting the face and cell center.

In the current WIPP PA calculation (DOE 2014), the separation between the cell center and face at the boundary can be up to ~6.1 km. This difference in distance to the boundary condition can result in differences in the solution. BRAGFLO's approach to cell-centered boundary conditions was implemented as a non-default option in WIPP_FLOW18, and used for the 2-D flared grid benchmark simulations.

4.11   Characteristic Curves

Characteristic curves define the relationships between capillary pressure and liquid (and/or gas) saturation and between relative permeability and liquid (and/or gas) saturation. The necessary WIPP-specific characteristic curves were implemented in PFLOTRAN prior to FY 2017, and all of them were carefully reviewed in FY 2017 (particularly with regard to logic statements) to ensure that the implementations matched implementations in BRAGFLO (Zeitler et al. 2017).

During a second review of the characteristic curves that occurred in July 2018, an error in the calculation of effective liquid saturation ($S_{e_{21}}$) in the KRP12 capillary pressure curve was found. The simulations presented in this report were run with an executable of PFLOTRAN that includes the erroneous form of the equation for KRP12 $S_{e_{21}}$. The erroneous equation is,

$$S_{e_{21}} = \max\left[\min\left[\frac{S_w - S_{min} - S_{eff\,min}}{1 - S_{min} - S_{eff\,min}}, 1\right], S_{eff\,min}\right]$$

The correct form of the equation is,

$$S_{e_{21}} = \max\left[\min\left[\frac{S_w - (S_{min} - S_{eff\,min})}{1 - (S_{min} - S_{eff\,min})}, 1\right], S_{eff\,min}\right]$$

where the only difference is the set of parentheses that should surround the $S_{min} - S_{eff\,min}$ term in both the numerator and denominator. This error does not impact the 2-D flared grid PA comparison (Section 8) because $S_{e_{21}}$ is only used in the calculation of capillary pressure, which is forced to zero in the regions of the model domain where KRP12 is used (i.e., the waste area and the north and south rest of repository). This error has been fixed, although the fix did not occur before the full PA comparison was performed.

Documentation for and results of testing the implementation of the characteristic curves can be found at: https://www.documentation.pflotran.org/qa_tests/pc_sat_rel_perm.html.

4.12 Pressure and Saturation Perturbations for Calculation of Numerical Derivatives in the Jacobian Matrix

Both BRAGFLO and PFLOTRAN employ Newton's method to solve the nonlinear system of equations governing fluid flow. Newton's method involves iteratively calculating a residual function (evaluating each governing equation at each grid cell)

$$f(x) = 0,$$

and an update to the residual (as a function of the residual and its derivative) that drives the residual function closer to zero with each iteration

$$x_{n+1} = x_n - \frac{f(x_n)}{f'(x_n)}.$$

For a system of equations, Newton's method takes the form

$$f(x_n) = 0$$

$$J\delta x = f(x_n)$$

$$x_{n+1} = x_n - \delta x$$

The Jacobian J is composed of the partial derivatives of the residual with respect to the primary dependent variables in the problem. These partial derivatives can be calculated analytically (derived through calculus) or numerically through perturbation. Analytical Jacobians can be problematic when discontinuities exist in the constitutive relations (e.g. relative permeability, capillary pressure) employed within the residual calculation, which is common for WIPP PA. Therefore, a numerical Jacobian has been the preferred approach. A numerical Jacobian is calculated by differencing the residual function evaluated with perturbed and non-perturbed primary dependent variables and dividing by the perturbation

$$J = \frac{f(x+\Delta x) - f(x)}{\Delta x}.$$

The choice of perturbation (Δx) can impact the solution. In WIPP_FLOW17, the perturbed values for primary dependent variables liquid pressure (p) and gas saturation (s) were

$$p_{pert} = p + 10^{-8} \times p + 10^{-10}$$

$$s_{pert} = \begin{cases} s - 10^{-8} & if \ s > 0.5 \\ s + 10^{-8} & if \ s \leq 0.5 \end{cases}$$

In WIPP_FLOW18, the perturbation of primary dependent variables was refactored to match the implementation within BRAGFLO

$$p_{pert} = p + max(10^{-8} \times p, 10^{-2})$$

$$s_{pert} = \begin{cases} s - max(10^{-8} \times s, 10^{-10}) & if \ 1 - s - s_{rl} < 0 \ and \ s + max(10^{-8} \times s, 10^{-10}) > 1 \\ s + max(10^{-8} \times s, 10^{-10}) & if \ 1 - s - s_{rl} < 0 \ and \ s + max(10^{-8} \times s, 10^{-10}) \leq 1 \\ s + max(10^{-8} \times s, 10^{-10}) & if \ 1 - s - s_{rl} \geq 0 \ and \ s - max(10^{-8} \times s, 10^{-10}) < 0 \\ s - max(10^{-8} \times s, 10^{-10}) & if \ 1 - s - s_{rl} \geq 0 \ and \ s - max(10^{-8} \times s, 10^{-10}) \geq 0 \end{cases}$$

Here, p_{pert} is the perturbed pressure in Pascal, s_{pert} is the perturbed saturation, and s_{rl} is the liquid residual saturation. The values 10^{-2} and 10^{-10} are the minimum liquid pressure and gas saturation perturbations (HMIN(2) and HMIN(1) in BRAGFLO, respectively). The value 10^{-8} is the relative perturbation value for both liquid pressure and gas saturation (DH(2) and DH(1) in BRAGFLO).

4.13 Refactor of Residual Evaluation for Convergence Check

The FTOLNORM convergence criteria in BRAGFLO is a hybrid metric based on the infinity norm of the residual (R) and scaled residual (R_{scaled}) for each phase (i):

$$\left\| min(R_i, R_{scaled,i}) \right\|_{\infty} < FTOLNORM_i.$$

The scaled residual is calculated by dividing the residual by the accumulation term (a_i) for each phase (i):

$$R_{scaled} = \frac{R_i}{a_i}.$$

Here, the accumulation term [kg water/m^3 bulk] is calculated as

$$a_i = \phi s_i \rho_i,$$

where

ϕ = porosity [m^3 pore/m^3 bulk]

s_i = phase saturation [m^3 fluid/m^3 pore]

ρ_i = phase density [kg fluid/m^3 fluid].

WIPP_FLOW17 calculated this infinity norm prior to the update of the accumulation term. In other words, the accumulation term (a) is from the previous Newton iteration. BRAGFLO uses the current or updated accumulation term.

WIPP_FLOW18 has been refactored to use the updated accumulation term and matches BRAGFLO's implementation.

4.14 Refactor of Calculation of Maximum Change in Gas Saturation for Time Step Update

When calculating the maximum change in gas saturation over a time step, BRAGFLO uses the parameter TSWITCH (GAS_SAT_GOV_SWITCH_ABS_TO_REL in PFLOTRAN) to switch between checking absolute and relative changes in gas saturation. When the gas saturation at a grid cell is less than TSWITCH, the check is on absolute change in gas saturation otherwise the check is on relative change

$$\text{max change} = \left\| \begin{bmatrix} \left| s_g^{k+1} - s_g^k \right| & s_g \leq TSWITCH \\ \left| \dfrac{s_g^{k+1} - s_g^k}{s_g^{k+1}} \right| & s_g > TSWITCH \end{bmatrix} \right\|_\infty.$$

This implementation prevents calculating a near-infinite maximum (relative) change in gas saturation as gas saturations approach zero.

WIPP_FLOW17 calculated all maximum changes as absolute

$$\text{max change} = \left\| |x^{k+1} - x^k| \right\|_\infty,$$

where x is liquid pressure (p_l) or gas saturation (s_g). The implementation in WIPP_FLOW18 matches that of BRAGFLO with the conditional on TSWITCH for gas saturation.

4.15 Scaling of Jacobian Matrix

Considering a single grid cell problem, BRAGFLO and PFLOTRAN solve the following linear system of equations during Newton iteration

$$\begin{bmatrix} \dfrac{\partial R_l}{\partial p_l} & \dfrac{\partial R_l}{\partial s_g} \\ \dfrac{\partial R_g}{\partial p_l} & \dfrac{\partial R_g}{\partial s_g} \end{bmatrix} \begin{bmatrix} \Delta p_l \\ \Delta s_g \end{bmatrix} = \begin{bmatrix} R_l \\ R_g \end{bmatrix},$$

where

R_l = liquid phase residual
R_g = gas phase residual
p_l = liquid pressure
s_g = gas saturation.

The two by two Jacobian matrix stores the derivatives of the residuals with respect to the primary dependent variables (p_l and s_g).

BRAGFLO scales this linear system using an input parameter P_SCALE (default = 10^7) as follows:

Prior to solution,

1. Scale columns for derivatives with respect to liquid pressure $\left(\dfrac{\partial R_i}{\partial p_l} \right)$ by P_SCALE.

2. Scale each matrix row and corresponding residual entry on the right-hand-side by the reciprocal of the infinity norm of the row entries of the matrix (absolute value of the largest entry in the matrix row).

After solution,

1. Scale all updates for liquid pressure (Δp_l) by P_SCALE.

Such scaling did not exist in WIPP_FLOW17, but has been implemented as an option in WIPP_FLOW18, and is used in the 2-D flared grid benchmark simulations.

4.16 Truncation of Gas Saturation

After the Newton update, BRAGFLO employs the following guidelines in accepting and/or truncating the solution for gas saturation.

$$-TOL_{\text{loose}} > s_g \text{ or } s_g > 1 + TOL_{\text{loose}} \qquad \text{Reject solution and cut time step}$$
$$-TOL_{\text{loose}} \leq s_g \leq 1 + TOL_{\text{loose}} \qquad \text{Truncate to [0,1] and force iteration}$$
$$-TOL_{\text{tight}} < s_g < 1 + TOL_{\text{tight}} \qquad \text{Truncate to [0,1] and accept solution}$$

The solution is rejected and the time step is cut, if the updated gas saturation at any grid cell is outside the bounds $[-TOL_{\text{loose}}, 1 + TOL_{\text{loose}}]$. Within these bounds, the solution is truncated and an additional Newton iteration is forced, if the (non-truncated) updated gas saturation at any grid cell is outside the bounds $[-TOL_{\text{tight}}, 1 + TOL_{\text{tight}}]$. Otherwise, the solution is accepted if the Newton solver has converged. This capability existed in WIPP_FLOW17 and continues to be used in WIPP_FLOW18.

4.17 Criteria for Solution Convergence and Acceptance

This section describes the criteria employed to determine whether the Newton solution has converged and whether the converged solution is acceptable. It discusses both the criteria that existed in WIPP_FLOW17 and those added to WIPP_FLOW18.

4.17.1 Features that Existed in WIPP_FLOW17 and Continue to be Used in WIPP_FLOW18

4.17.1.1 Bounds Checking for Gas Saturation

Section 4.16 describes truncation that occurs when the updated solution for gas saturation lies outside the bounds of TOL_{loose} or TOL_{tight}. These two bounds also dictate whether a converged solution is acceptable.

4.17.1.1.1 Time Step Reduction through TOL_{loose}

If the updated solution for gas saturation within a grid cell lies outside the bounds of TOL_{loose}, as described in Section 4.16, the calculation of the current time step is rejected or discontinued, the time step is reduced in size, and calculation using the new, reduced time step is initiated. (TOL_{loose} is GAS_SAT_THRESH_FORCE_TS_CUT in the PFLOTRAN input deck and DEPLIMIT(1) in BRAGFLO.)

4.17.1.1.2 Force Newton Iteration through TOL_{tight}

If the updated solution for gas saturation within a grid cell lies outside the bounds of TOL_{tight}, as described in Section 4.16, the gas saturation in that grid cell is truncated to lie between [0,1] and an additional Newton iteration is required prior to declaring convergence. (TOL_{tight} is

GAS_SAT_THRESH_FORCE_EXTRA_NI in the PFLOTRAN input deck and SATLIMIT in BRAGFLO.)

4.17.1.1.3 Solution Acceptance

A converged solution is accepted if gas saturation (s_g) for all cells is within the bounds $\left[-TOL_{\text{tight}}, 1 + TOL_{\text{tight}}\right]$.

Accepted if:

$$-TOL_{\text{tight}} < s_g < 1 + TOL_{\text{tight}}$$

4.17.1.2 Relative Change in Liquid Pressure (Over Newton Iteration)

Convergence is declared when the infinity norm of the relative change in liquid pressure is less than MAX_ALLOW_REL_LIQ_PRES_CHANG_NI (EPSNORM(2) in BRAGFLO).

Converged when:

$$\left\|\frac{\left|\Delta p_l^{\text{Newton Iteration}}\right|}{|p_l|}\right\|_\infty < MAX\_ALLOW\_REL\_LIQ\_PRES\_CHANG\_NI$$

4.17.1.3 Absolute Change in Gas Saturation (Over Newton Iteration)

Convergence is declared when the infinity norm of the absolute change of gas saturation is less than the MAX_ALLOW_REL_GAS_SAT_CHANGE_NI. (The converged solution is accepted if the criteria described in Section 4.17.1.1 are met.)

Converged when:

$$\left\|\Delta s_g^{\text{Newton Iteration}}\right\|_\infty < MAX\_ALLOW\_REL\_GAS\_SAT\_CHANGE\_NI$$

In BRAGFLO, the same comparison was formulated in log space using EPSNORM(1)

$$-\log_{10}\left\|\Delta s_g^{\text{Newton Iteration}}\right\|_\infty < \text{EPSNORM}(1)$$

4.17.1.4 Minimum Liquid Pressure Check

Time step size is cut when the minimum liquid pressure drops below MIN_LIQ_PRES_FORCE_TS_CUT (DEPLIMIT(2) in BRAGFLO).

Cut time step when:

$$p_{l,i} < \text{ MIN\_LIQ\_PRES\_FORCE\_TS\_CUT } \forall i$$

4.17.2 Features Added or Refactored within WIPP_FLOW18

4.17.2.1 Scaled Residual with Post-Update Accumulation Term

Section 4.10 describes how the residual at each grid cell is scaled by the cell's accumulation term. In WIPP_FLOW17, the accumulation term used to scale the residual was evaluated based on the solution from the previous Newton iteration. This approach was inconsistent with the implementation in BRAGFLO. The algorithm has been refactored in WIPP_FLOW18 to use the accumulation term that is consistent with the most up-to-date residual calculation.

Convergence is declared when the infinity norm of the scaled residual is less than the LIQUID_RESIDUAL_INFINITY_TOL or GAS_RESIDUAL_INFINITY_TOL (FTOLNORM(2) and FTOLNORM(1), respectively, in BRAGFLO).

$$\left\|\frac{R_i}{a_i}\right\|_\infty < i\_\text{RESIDUAL\_INFINITY\_TOL} \text{ for phase } i$$

4.17.2.2 Absolute Change in Liquid Pressure (Over Time Step)

Once the Newton solver has converged based on Newton iteration convergence criteria, the time step will be rejected and recalculated with a smaller time step size if the maximum absolute change in liquid pressure (infinity norm on the change in liquid pressure) is greater than MAX_ALLOW_LIQ_PRES_CHANGE_TS (DDEPMAX(2) in BRAGFLO).

Not accepted if:

$$\left\|\Delta p_l^\text{Timestep}\right\|_\infty > \text{MAX\_ALLOW\_LIQ\_PRES\_CHANGE\_TS}$$

4.17.2.3 Absolute Change in Gas Saturation (Over Time Step)

Once the Newton solver has converged based on Newton iteration convergence criteria, the time step will be rejected and recalculated with a smaller time step size if the maximum absolute change in gas saturation (infinity norm on the change in gas saturation) is greater than MAX_ALLOW_GAS_SAT_CHANGE_TS (DDEPMAX(1) in BRAGFLO).

Not accepted if:

$$\left\|\Delta s_g^\text{Timestep}\right\|_\infty > \text{MAX\_ALLOW\_GAS\_SAT\_CHANGE\_TS}$$

4.18 Time Step Ramping

WIPP_FLOW17 used the default PFLOTRAN controls on time step ramping. In BRAGFLO and in WIPP_FLOW18, time step size is ramped (adjusted between time steps) on the basis of the following criteria:

$$\Delta t^{k+1}$$

$$= max\left(\Delta t_{min}, \min\left(\Delta t_{max}, \sigma_{growth}\Delta t^k, min\left(\frac{2\Delta s_{g,gov}}{\Delta s_{g,gov} + \left\|\Delta s_g^k\right\|_\infty}, \frac{2\Delta p_{l,gov}}{\Delta p_{l,gov} + \left\|\Delta p_l^k\right\|_\infty}\right)\Delta t^k\right)\right)$$

where:

Δt^k = time step size for previous time step

Δt^{k+1} = time step size for new time step

Δt_{min} = minimum time step size (DELTMIN in BRAGFLO)

Δt_{max} = maximum time step size (DELTMAX in BRAGFLO)

σ_{growth} = maximum time step growth scaling factor (DTIMEMAX in BRAGFLO)

$\Delta s_{g,gov}$ = gas saturation governor (DELTADEPNORM(1) in BRAGFLO)

$\Delta p_{l,gov}$ = liquid pressure governor (DELTADEPNORM(2) in BRAGFLO)

This algorithm truncates the time step to lie between Δt_{min} and Δt_{max}. It allows the time step to grow at a maximum rate of $\sigma_{growth}\Delta t^k$ when the maximum changes in liquid pressure and gas

saturation are below the governing thresholds. It decreases the time step size when maximum changes are above the thresholds.

Note that the maximum change in gas saturation (Δs_g^k) is calculated as a relative or absolute change above and below GAS_SAT_GOV_SWITCH_ABS_TO_REL (TSWITCH in BRAGFLO), respectively (see Section 4.14).

The parameters discussed in Sections 4.12 through 4.18 are summarized in Table 4.18-1. Also listed are parameters controlling the maximum number of Newton iterations (ITMAX in BRAGFLO), the maximum consecutive number of time step reductions (IRESETMAX in BRAGFLO), and the factor by which time step is reduced when it is reduced (DELTFACTOR in BRAGFLO). Later sections of this report refer to the parameters in Table 4.18-1 collectively as "solution control" parameters.

Table 4.18-1. Parameters controlling Newton solver convergence, acceptance of solution, time stepping, and iteration.

BRAGFLO Variable[a]	BRAGFLO Label[b]	PFLOTRAN Keyword[c]	PFLOTRAN Block[d]
FTOLNORM(2)	FTOL_PRES	LIQUID_RESIDUAL_INFINITY_TOL	OPTIONS
FTOLNORM(1)	FTOL_SAT	GAS_RESIDUAL_INFINITY_TOL	OPTIONS
EPSNORM(2)	EPS_PRES	MAX_ALLOW_REL_LIQ_PRES_CHANG_NI	OPTIONS
EPSNORM(1)	EPS_SAT	MAX_ALLOW_REL_GAS_SAT_CHANGE_NI	OPTIONS
DH(1)	DHSAT_REL	REL_GAS_SATURATION_PERTURBATION	OPTIONS
DH(2)	DHPRES_REL	REL_LIQ_PRESSURE_PERTURBATION	OPTIONS
HMIN(1)	DHSAT_MIN	MIN_GAS_SATURATION_PERTURBATION	OPTIONS
HMIN(2)	DHPRES_MIN	MIN_LIQ_PRESSURE_PERTURBATION	OPTIONS
SATLIMIT	SATLIMIT	GAS_SAT_THRESH_FORCE_EXTRA_NI	OPTIONS
DEPLIMIT(1)	DSATLIM	GAS_SAT_THRESH_FORCE_TS_CUT	OPTIONS
DDEPMAX(1)	DSAT_MAX	MAX_ALLOW_GAS_SAT_CHANGE_TS	OPTIONS
DELTADEPNORM(1)	SATNORM	GAS_SAT_CHANGE_TS_GOVERNOR	OPTIONS
TSWITCH	TSWITCH	GAS_SAT_GOV_SWITCH_ABS_TO_REL	OPTIONS
DEPLIMIT(2)	DPRELIM	MIN_LIQ_PRES_FORCE_TS_CUT	OPTIONS
DDEPMAX(2)	DPRES_MAX	MAX_ALLOW_LIQ_PRES_CHANGE_TS	OPTIONS
DELTADEPNORM(2)	PRESNORM	LIQ_PRES_CHANGE_TS_GOVERNOR	OPTIONS
P_SCALE	P_SCALE	JACOBIAN_PRESSURE_DERIV_SCALE	OPTIONS
ITMAX	ITMAX	MAXIMUM_NUMBER_OF_ITERATIONS	NEWTON_SOLVER
IRESETMAX	IMAX	MAXIMUM_CONSECUTIVE_TS_CUTS	TIMESTEPPER
DELTFACTOR	DT_REDU	TIMESTEP_REDUCTION_FACTOR	TIMESTEPPER
DTIMEMAX	DT_INCR	TIMESTEP_MAXIMUM_GROWTH_FACTOR	TIMESTEPPER
DELTMAX	DT_MAX	MAXIMUM_TIMESTEP_SIZE	TIME
DELTMIN	DELTMIN	MINIMUM_TIMESTEP_SIZE	OPTIONS

[a] Variable name in BRAGFLO User's Manual (Camphouse 2012a).

[b] Likely label in BRAGFLO input deck (comment only, not required).

[c] Required keyword in input deck.

[d] Required block in input deck.

5   WIPP Process Model Testing (Single-Cell)

Several single cell tests were developed as part of the debugging effort for the BRAGFLO-PFLOTRAN comparison. The advantage of single-cell tests is that intercell flow is eliminated and thus the differences due to individual process models can be better isolated. This section discusses the design of and results from the individual process model test cases on single-cell domains.

The suite of single-cell test cases was developed and designed to exercise individual process models in isolation, or in combination. Each single-cell test case includes a PFLOTRAN input deck and a corresponding BRAGFLO input deck that implements the identical simulation. A single plotting script that automatically plots all test case results is executed as the final step. Parameters used for each test are representative of those employed in WIPP PA.

5.1   Calculation Details

All BRAGFLO results were produced on the Linux cluster head node (jt.sandia.gov) using the BRAGFLO executable stored at:

- /Archive/pflotran_bragflo_comparison_20180928/executables/bragflo-jt

All PFLOTRAN results were produced on the Linux cluster head node (jt.sandia.gov) using the PFLOTRAN executable stored at:

- /Archive/pflotran_bragflo_comparison_20180928/executables/pflotran-071318

All test input decks, plotting scripts, and results are located on the Linux cluster in the folder:

- /Archive/pflotran_bragflo_comparison_20180928/pflotran-bragflo-test-cases-stripped

Table 5.1-1 shows the values of the solution control parameters used in each single-cell test case. In the first column ("BRAGFLO"), the BRAGFLO solution control parameter name is given. In the second column ("PFLOTRAN"), the equivalent PFLOTRAN solution control parameter name is given. In the third column ("BLOCK"), the PFLOTRAN input deck block where the solution control keyword is placed is listed. The fourth and fifth columns ("VALUE", "UNIT") show the values and corresponding units of the solution control parameter used.

Table 5.1-1 Solution control parameter values for single-cell test runs.

BRAGFLO	PFLOTRAN	BLOCK	VALUE	UNIT
FTOLNORM(2)	LIQUID_RESIDUAL_INFINITY_TOL	OPTIONS	1.0d-6	kg/m3
FTOLNORM(1)	GAS_RESIDUAL_INFINITY_TOL	OPTIONS	1.0d-6	kg/m3
EPSNORM(2)	MAX_ALLOW_REL_LIQ_PRES_CHANG_NI	OPTIONS	1.0d-5	-
EPSNORM(1)	MAX_ALLOW_REL_GAS_SAT_CHANGE_NI	OPTIONS	1.0d-5	-
DH(1)	REL_GAS_SATURATION_PERTURBATION	OPTIONS	1.0d-8	-
DH(2)	REL_LIQ_PRESSURE_PERTURBATION	OPTIONS	1.0d-8	-
HMIN(1)	MIN_GAS_SATURATION_PERTURBATION	OPTIONS	1.0d-10	-
HMIN(2)	MIN_LIQ_PRESSURE_PERTURBATION	OPTIONS	1.0d-2	Pa
DTIMEMAX	TIMESTEP_MAXIMUM_GROWTH_FACTOR	TIMESTEPPER	1.25d0	-
SATLIMIT	GAS_SAT_THRESH_FORCE_EXTRA_NI	OPTIONS	1.0d-3	-
DEPLIMIT(1)	GAS_SAT_THRESH_FORCE_TS_CUT	OPTIONS	2.0d-1	-
DDEPMAX(1)	MAX_ALLOW_GAS_SAT_CHANGE_TS	OPTIONS	1.0d0	-
DELTADEPNORM(1)	GAS_SAT_CHANGE_TS_GOVERNOR	OPTIONS	3.0d-1	-
TSWITCH	GAS_SAT_GOV_SWITCH_ABS_TO_REL	OPTIONS	1.0d0	-
DEPLIMIT(2)	MIN_LIQ_PRES_FORCE_TS_CUT	OPTIONS	-1.0d8	Pa
DDEPMAX(2)	MAX_ALLOW_LIQ_PRES_CHANGE_TS	OPTIONS	1.0d7	Pa
DELTADEPNORM(2)	LIQ_PRES_CHANGE_TS_GOVERNOR	OPTIONS	5.0d5	Pa
P_SCALE	JACOBIAN_PRESSURE_DERIV_SCALE	OPTIONS	1.0d7	Pa
ITMAX	MAXIMUM_NUMBER_OF_ITERATIONS	NEWTON_SOLVER	8	-
IRESETMAX	MAXIMUM_CONSECUTIVE_TS_CUT	TIMESTEPPER	40	-
DELTFACTOR	TIMESTEP_REDUCTION_FACTOR	TIMESTEPPER	5.0d-1	-
DELTMAX	MAXIMUM_TIMESTEP_SIZE	TIME	1.73448d9	sec
DELTMIN	MINIMUM_TIMESTEP_SIZE	OPTIONS	8.64d-4	sec

Percent differences are calculated according to,

$$\% = 100 \times abs\left[\frac{X_{BF} - X_{PF}}{X_{BF}}\right]$$

where X_{BF} is the BRAGFLO solution, and X_{PF} is the PFLOTRAN solution. Because the two codes may take slightly different time steps, the PFLOTRAN solution is interpolated at the BRAGFLO output times. This may introduce slight differences in the comparison if differences in time step exist. In the above calculation, it is possible for division by zero to occur if the BRAGFLO solution happens to be zero. To avoid division by zero, values (of both solutions) are truncated to $\varepsilon = 10^{-20}$ if $0 \leq value < \varepsilon$ and truncated to $-\varepsilon$ if $-\varepsilon < value < 0$. The absolute value of the resulting percent difference is taken, and therefore the percent differences seen in the following plots will always be positive, regardless of whether the original PFLOTRAN solution was larger or smaller than the BRAGFLO solution. This last step was chosen so that a log scaling of the percent difference could be plotted.

In the following plots, the percent difference on the vertical axis is displayed linearly between 0 and 1, and on a log scale above 1. This scaling was chosen to magnify the difference when the difference is small (less than 1%) and so that the entire range between 0 and 100 could be displayed (which would not be possible/practical if the vertical axis was entirely log scaled).

5.2   Test Group #1: Gas Generation/Brine Consumption Chemistry

5.2.1 Purpose and Setup

Three test cases are presented that compare the gas generation and brine consumption chemistry process models between BRAGFLO and PFLOTRAN. These cases use reactant concentrations and reaction rate constants pulled from the PFD Analysis Replicate 1, Scenario 2, Vector 1. The process models used in PFLOTRAN include: KRP12, WIPP_SOURCE_SINK.

The first test case ("SATHIGH")[1] demonstrates a scenario when the initial brine saturation is high (0.98). The second test case ("SATMID")[2] demonstrates a scenario when the initial brine saturation is in the middle (0.50). Finally, the third test case ("SATLOW")[3] demonstrates a scenario when the initial brine saturation is very low (0.075). In this third test case ("SATLOW"), brine is consumed in the simulation until it decreases to the minimum saturation required for chemistry to occur, 0.015.

5.2.2 Results

5.2.2.1 High Initial Liquid Saturation (0.98)
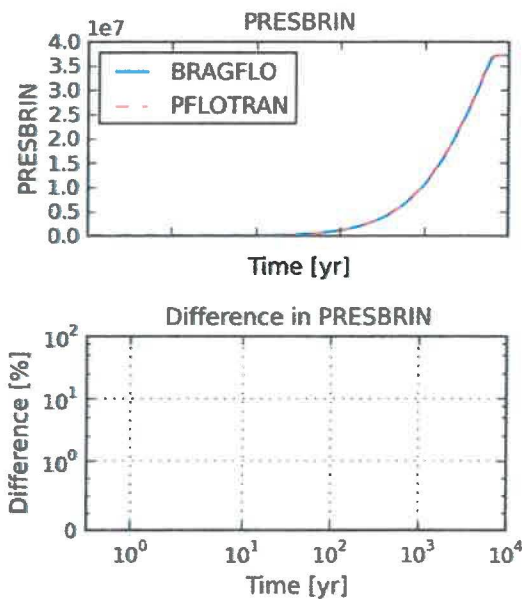
Figure 5.2-1 Test case "SATHIGH" brine pressure [Pa].
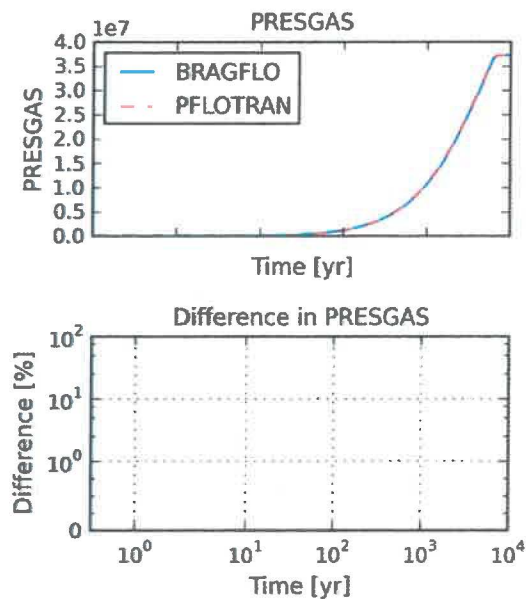
Figure 5.2-2 Test case "SATHIGH" gas pressure [Pa].

[1] The "SATHIGH" test case refers to the verification test located at pflotran-bragflo-test-cases-stripped/tests_single_cell/case060200/pf_case060210_0d_gas_generation_hisat.in.
[2] The "MIDHIGH" test case refers to the verification test located at pflotran-bragflo-test-cases-stripped/tests_single_cell/case060200/pf_case060200_0d_gas_generation_midsat.in.
[3] The "LOWHIGH" test case refers to the verification test located at pflotran-bragflo-test-cases-stripped/tests_single_cell/case060200/pf_case060220_0d_gas_generation_superlowsat.in.
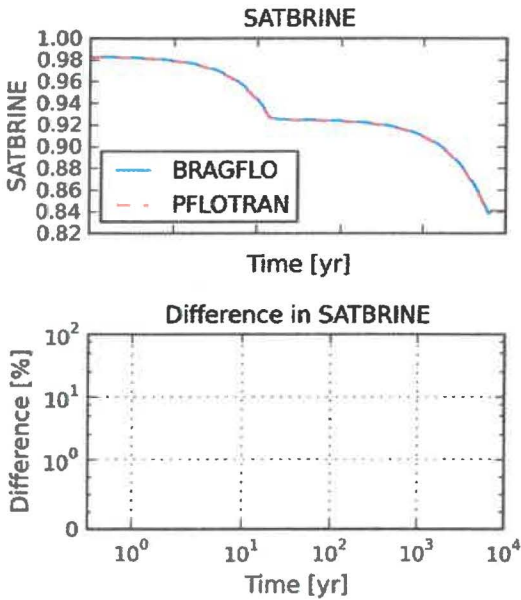
Figure 5.2-3 Test case "SATHIGH" brine saturation.

Figure 5.2-4 Test case "SATHIGH" gas saturation.

Figure 5.2-5 Test case "SATHIGH" gas generation rate [mol-H_2/m^3/sec].

Figure 5.2-6 Test case "SATHIGH" brine generation rate [mol-H_2O/m^3/sec].
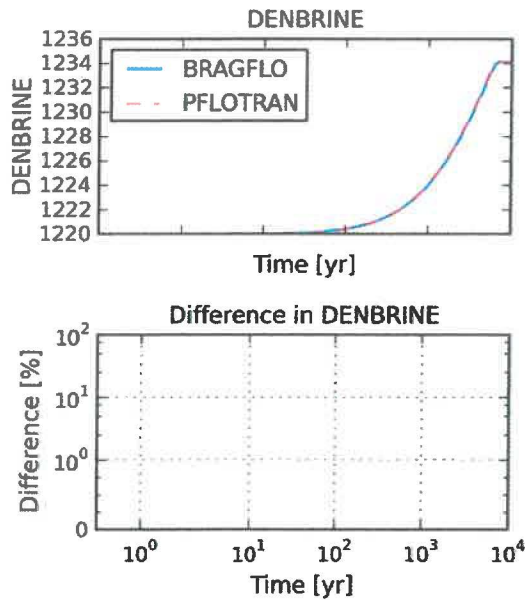
Figure 5.2-7 Test case "SATHIGH" brine density [kg/m³].

Figure 5.2-9 Test case "SATHIGH" gas density [kg/m³].

Figure 5.2-8 Test case "SATHIGH" MgO hydration rate [mol-MgO/m³/sec].
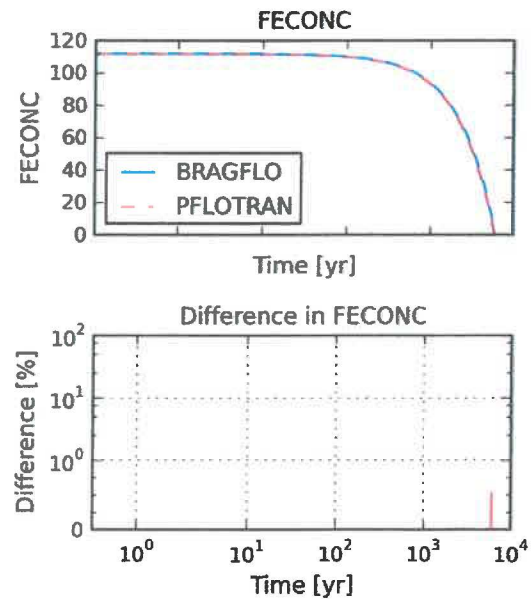
Figure 5.2-10 Test case "SATHIGH" iron concentration [mol-Fe/m³].

5.2.2.2 Mid Initial Liquid Saturation (0.50)
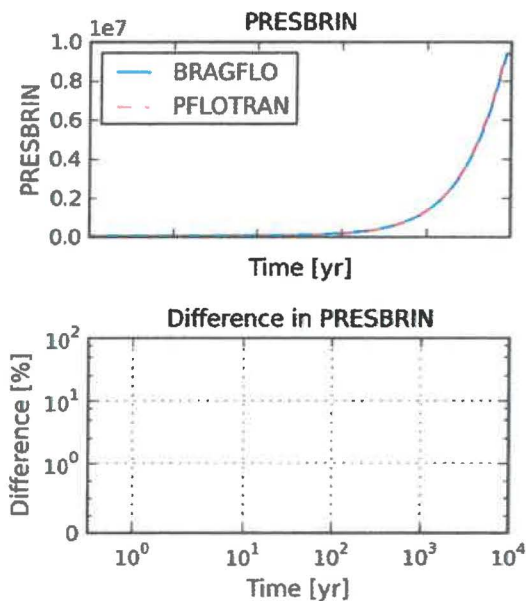
Figure 5.2-11 Test case "SATMID" brine pressure [Pa].
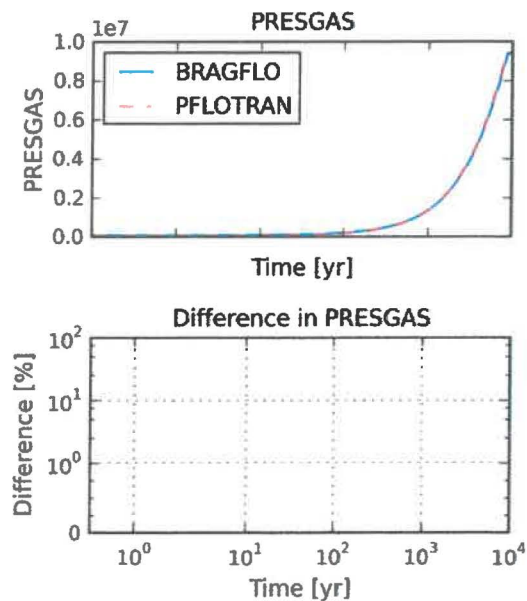
Figure 5.2-12 Test case "SATMID" gas pressure [Pa].
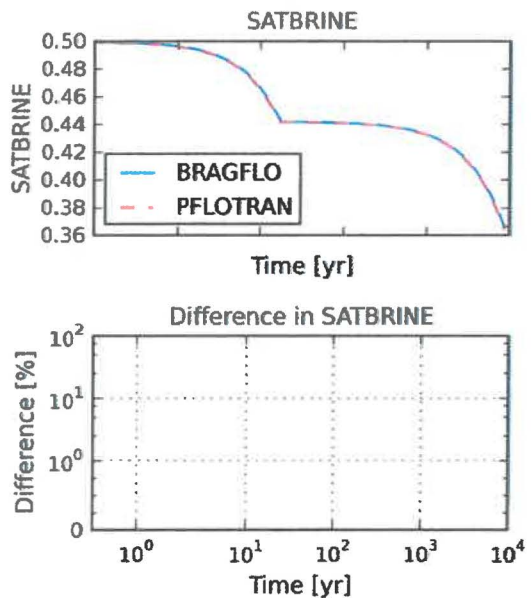
Figure 5.2-13 Test case "SATMID" brine saturation.
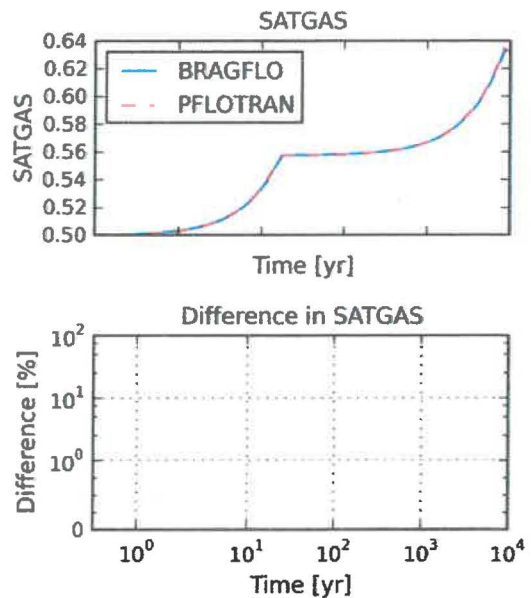
Figure 5.2-14 Test case "SATMID" gas saturation.
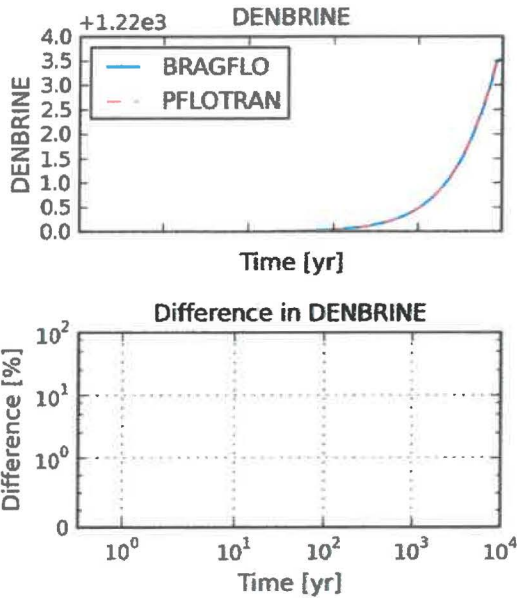
Figure 5.2-15 Test case "SATMID" brine density [kg/m^3].
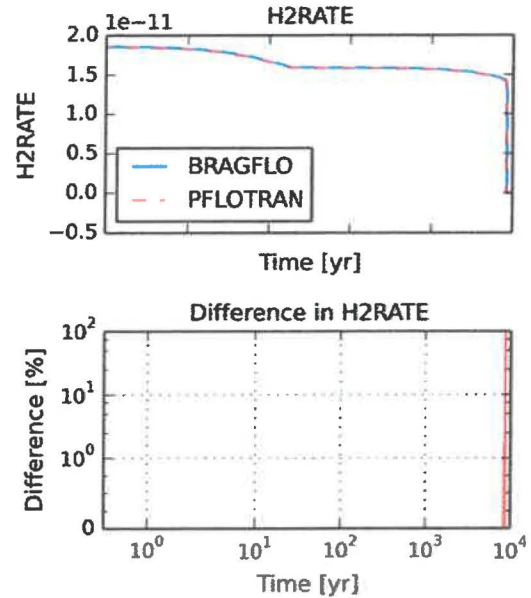
Figure 5.2-17 Test case "SATMID" gas generation rate [mol-H$_2$/m^3/sec].
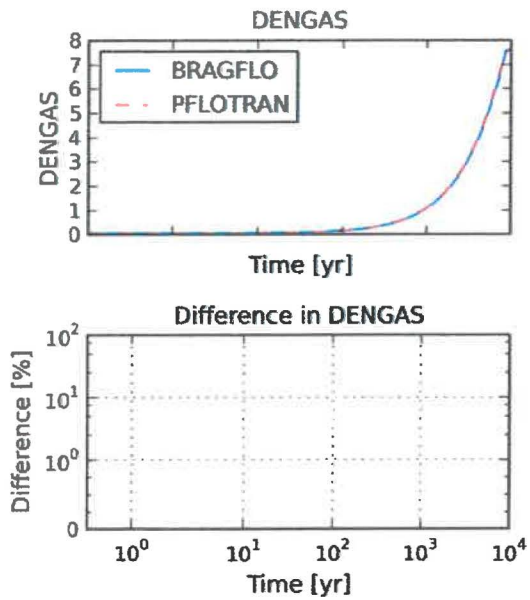
Figure 5.2-16 Test case "SATMID" gas density [kg/m^3].
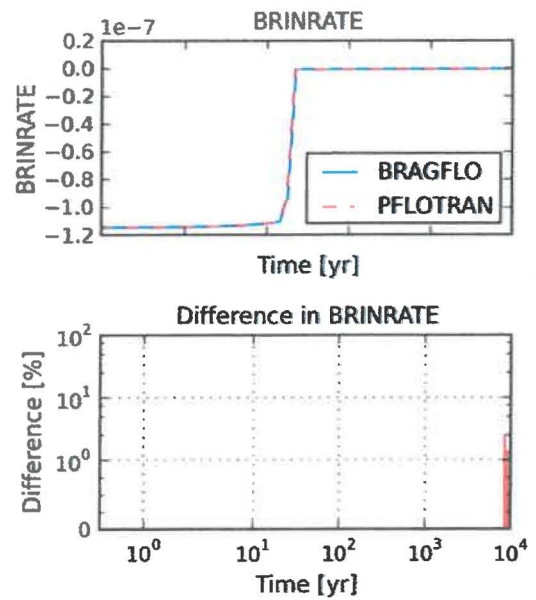
Figure 5.2-18 Test case "SATMID" brine generation rate [mol-H$_2$O/m^3/sec].
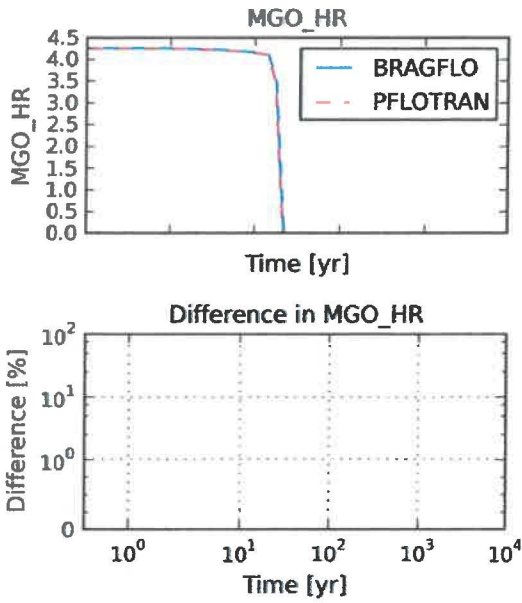
Figure 5.2-19 Test case "SATMID" MgO hydration rate [mol-MgO/m^3/sec].
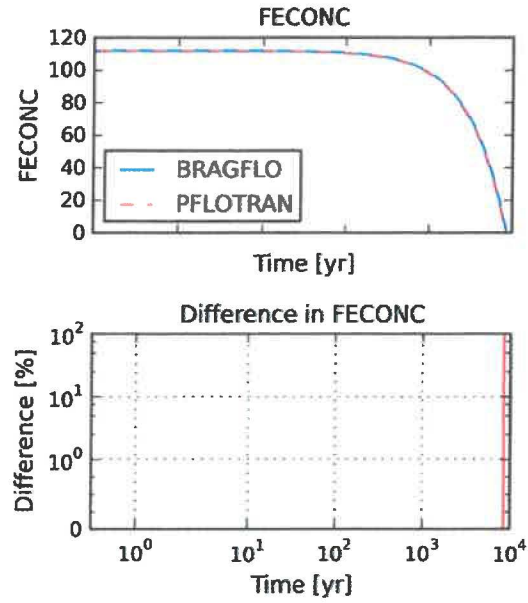
Figure 5.2-20 Test case "SATMID" iron concentration [mol-Fe/m^3].

5.2.2.3 Low Initial Liquid Saturation (0.075)
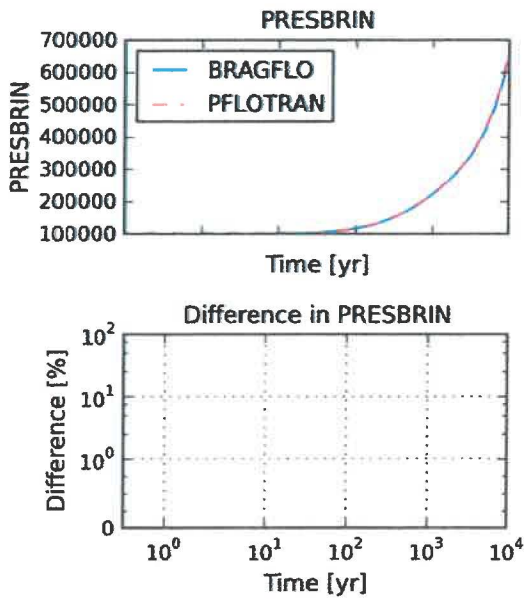
Figure 5.2-21 Test case "SATLOW" brine pressure [Pa].
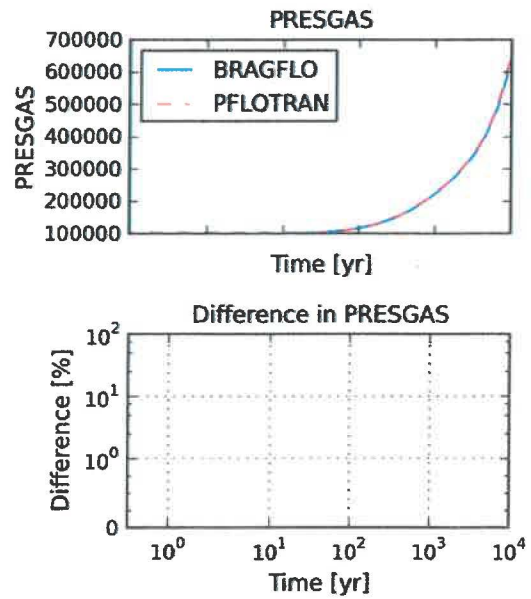
Figure 5.2-22 Test case "SATLOW" gas pressure [Pa].
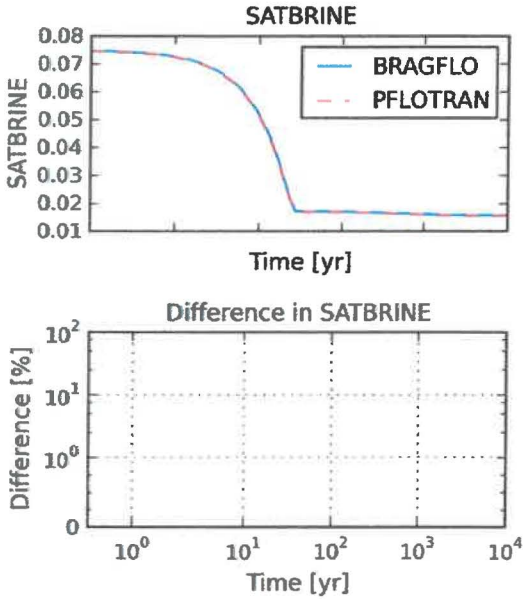
Figure 5.2-23   Test case "SATLOW" brine saturation.
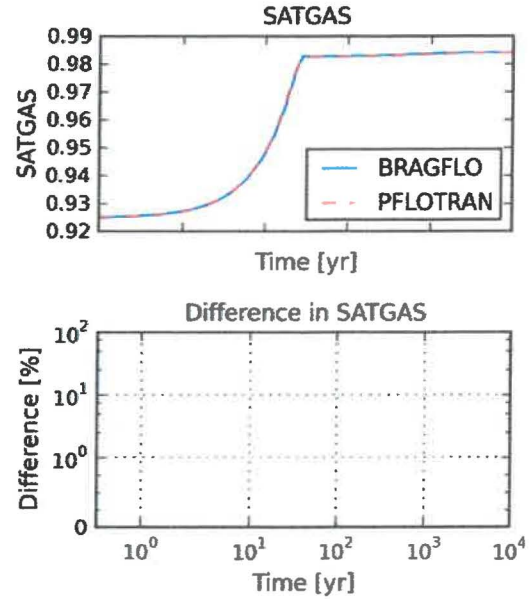
Figure 5.2-24   Test case "SATLOW" gas saturation.
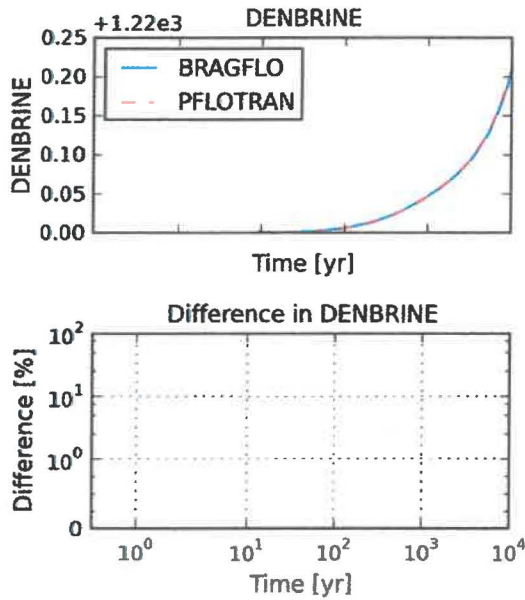
Figure 5.2-25 Test case "SATLOW" brine density [kg/m³].
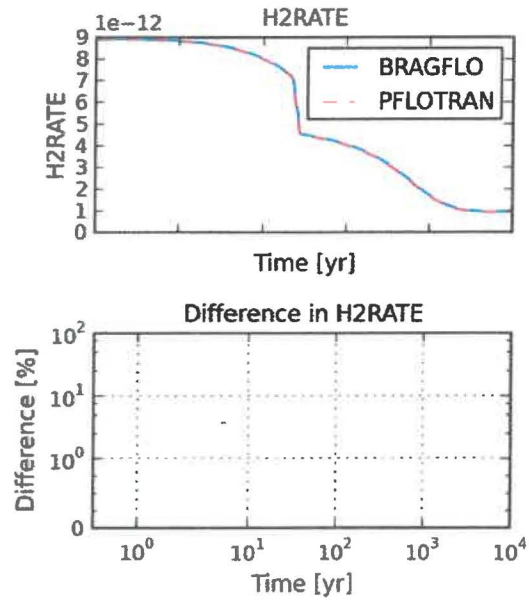
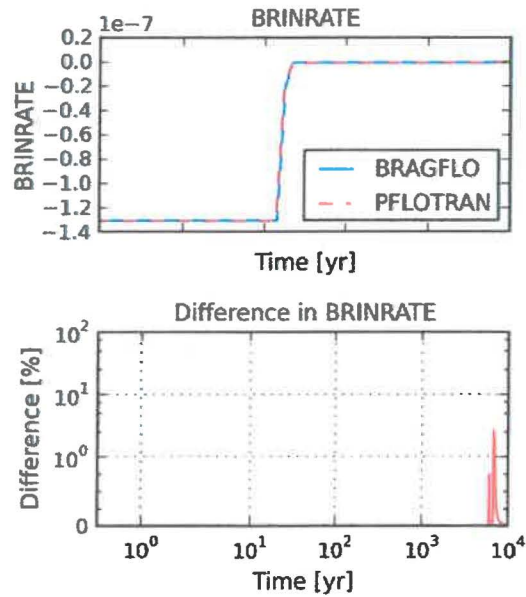Figure 5.2-27 Test case "SATLOW" gas generation rate [mol-H₂/m³/sec].
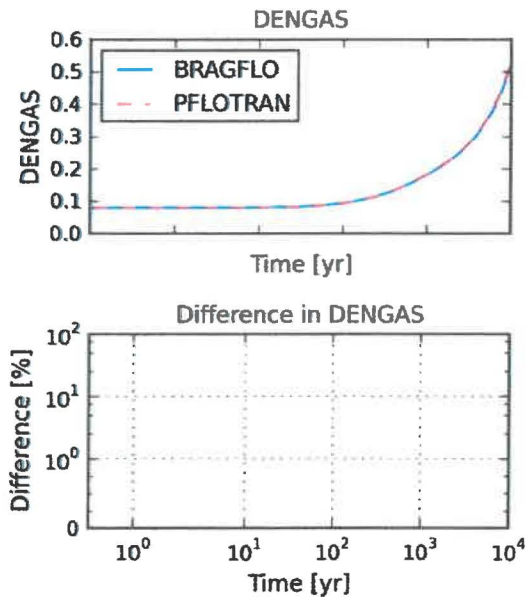
Figure 5.2-26 Test case "SATLOW" gas density [kg/m³].

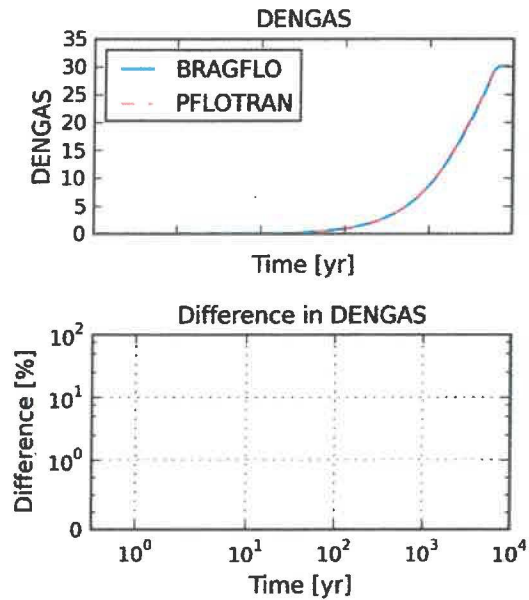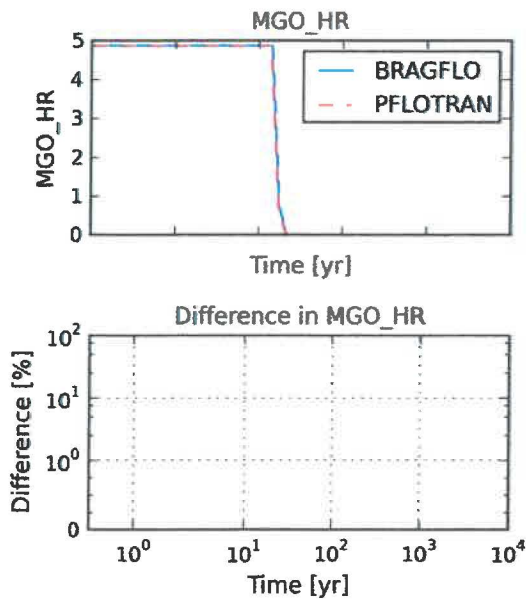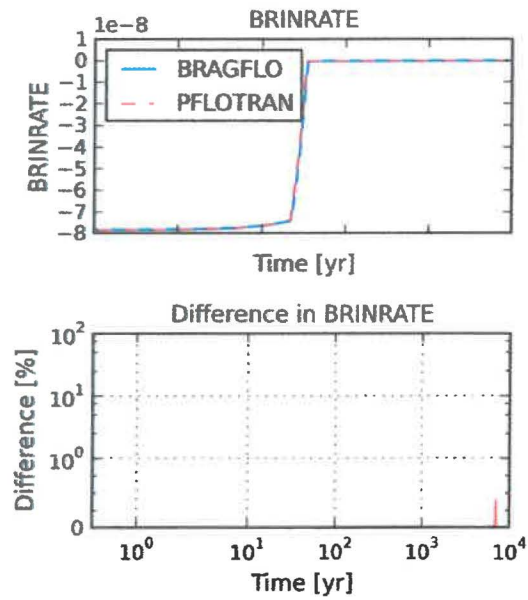Figure 5.2-28 Test case "SATLOW" brine generation rate [mol-H₂O/m³/sec].
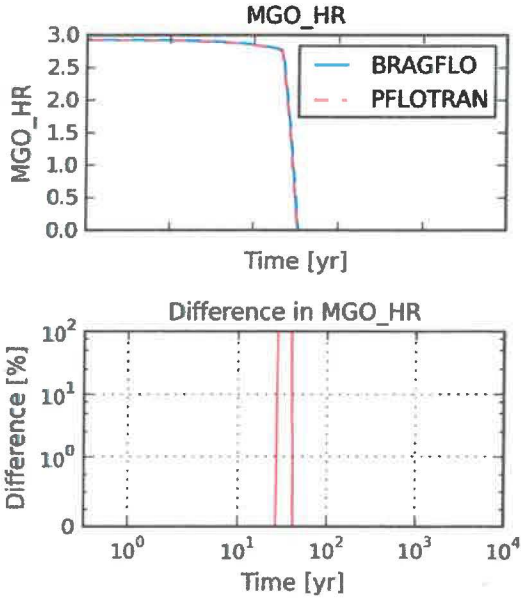
Figure 5.2-29 Test case "SATLOW" MgO hydration rate [mol-MgO/m³/sec].
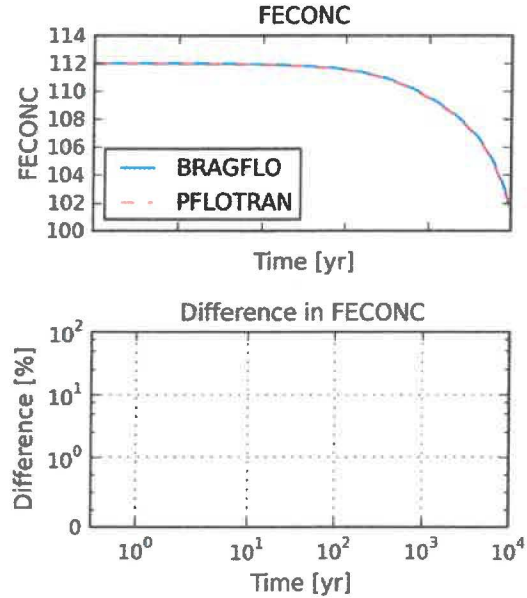
Figure 5.2-30 Test case "SATLOW" iron concentration [mol-Fe/m³].

5.2.3 Conclusions

In the majority of the plots presented, the difference between BRAGFLO and PFLOTRAN is essentially zero, meaning that the gas generation/brine consumption chemistry process models compare well. This represents a substantial improvement in the comparison since FY 2017 (Zeitler et al. 2017), when differences in MgO hydration exceeded 25% because hydration rate was lagging in time in PFLOTRAN relative to BRAGFLO. In test cases "SATHIGH" and "SATMID," there is a difference between BRAGFLO and PFLOTRAN when the gas generation rate drops to zero (see Figure 5.2-5 and Figure 5.2-17), due to slight differences in time stepping. However, this difference does not affect the remaining part of the simulation, and therefore can be ignored. Additionally, the difference in MgO hydration rate for test case "SATLOW" spikes to over 100% when the hydration rate drops to zero. Similarly, this difference can be ignored because it occurs when the rate drops to zero where the relative difference calculation can produce irrelevantly large difference values.

5.3 Test Group #2: Waste Area Creep Closure

5.3.1 Purpose and Setup

Three test cases are presented that compare waste area creep closure between BRAGFLO and PFLOTRAN. In the first test case ("CREEP1")[4], the cell mass balance is kept static (no gas is injected or produced) while creep is allowed to occur. In the second test case ("CREEP2")[5], gas is injected at a constant rate (2.302670×10^{-6} kg/s) while creep is allowed to occur. In the third test case ("CREEP3")[6], gas is produced via the gas generation/brine consumption chemistry process model rather than being injected, and creep is allowed to occur. In the third test case, reactant concentrations and rate constants are pulled from the PFD analysis, Replicate 1, Scenario 2, Vector 1. The process models used in PFLOTRAN include: KRP12, CREEP_CLOSURE, WIPP_SOURCE_SINK.

5.3.2 Results

In all three test cases, porosity vs. time compares well between BRAGFLO and PFLOTRAN (see Figure 5.3-7, Figure 5.3-14, and Figure 5.3-21). However, because no flow into or out of the cell can occur, small differences in porosity can cause significant differences in pressure. The creep closure process model includes logic to turn off creep closure permanently if a certain maximum threshold pressure is reached (in this case 50 MPa), which causes the plateau in pressure in the figures. The result of this logic, and the precise value of porosity when creep closure shutoff occurs, is very sensitive to time step size. In the test cases presented, the difference in brine and gas pressure between BRAGFLO and PFLOTRAN rises temporarily to a maximum of ~7.5% for the first test case when creep closure turns off. The difference then drops about an order of magnitude to 1.0% or less for the remaining portion of the simulation while the pressure remains constant (see, for example, Figure 5.3-2).

---

[4] The "CREEP1" test case refers to the verification test located at pflotran-bragflo-test-cases-stripped/tests_single_cell/case060300/pf_case060300_0d_creep_static.in.

[5] The "CREEP2" test case refers to the verification test located at pflotran-bragflo-test-cases-stripped/tests_single_cell/case060300/pf_case060310_0d_gas_injection.in.

[6] The "CREEP3" test case refers to the verification test located at pflotran-bragflo-test-cases-stripped/tests_single_cell/case060300/pf_case060320_0d_gas_generation.in.

5.3.2.1 Static Creep Closure
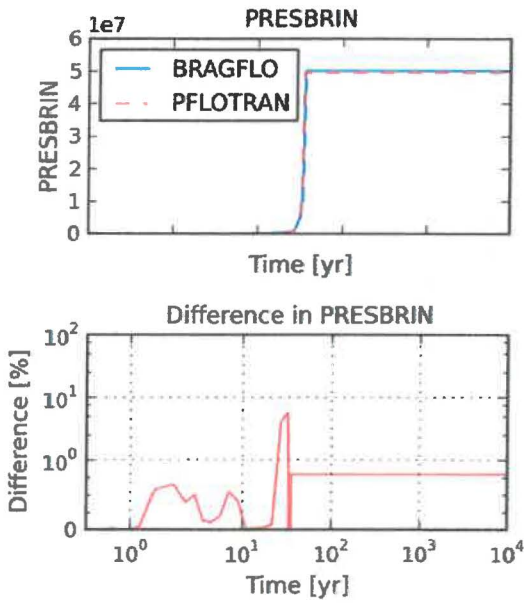
Figure 5.3-1 Test case "CREEP1" brine pressure [Pa].
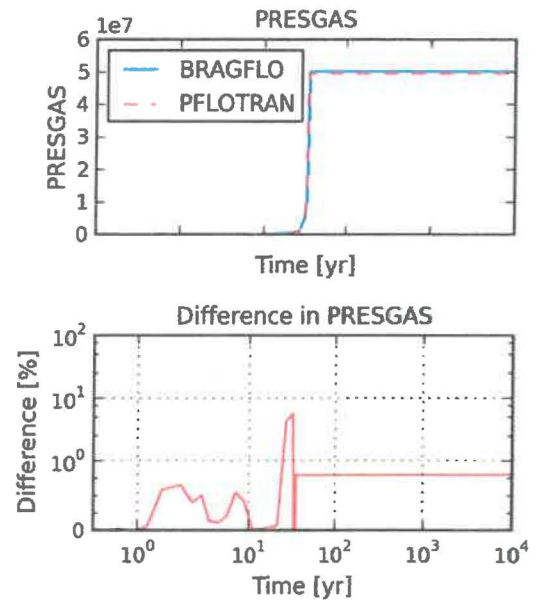
Figure 5.3-2 Test case "CREEP1" gas pressure [Pa].

Figure 5.3-3 Test case "CREEP1" brine saturation.
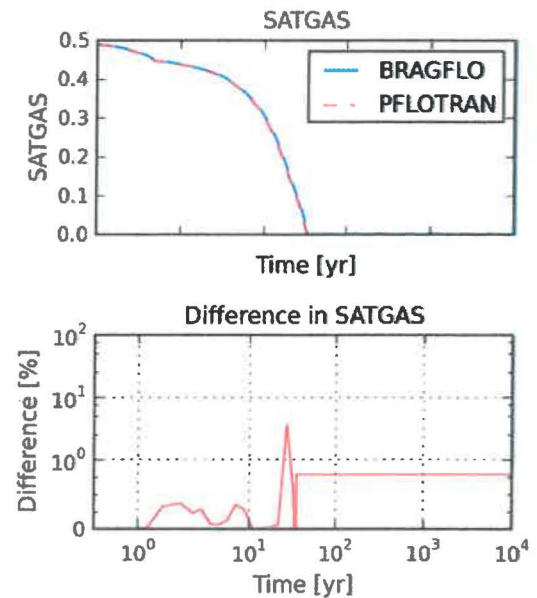
Figure 5.3-4 Test case "CREEP1" gas saturation.
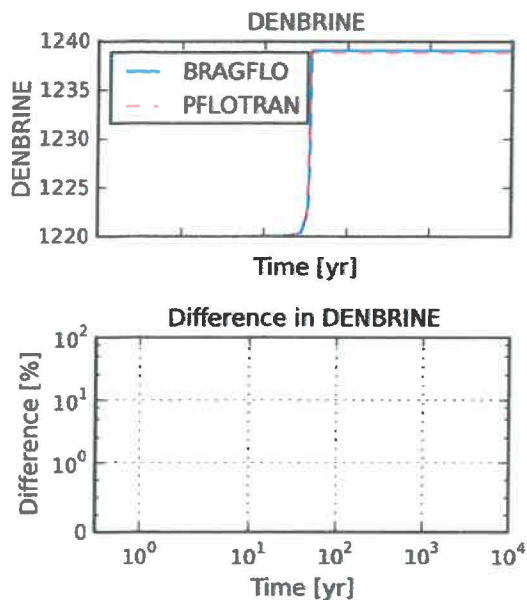
Figure 5.3-5 Test case "CREEP1" brine density [kg/m^3].
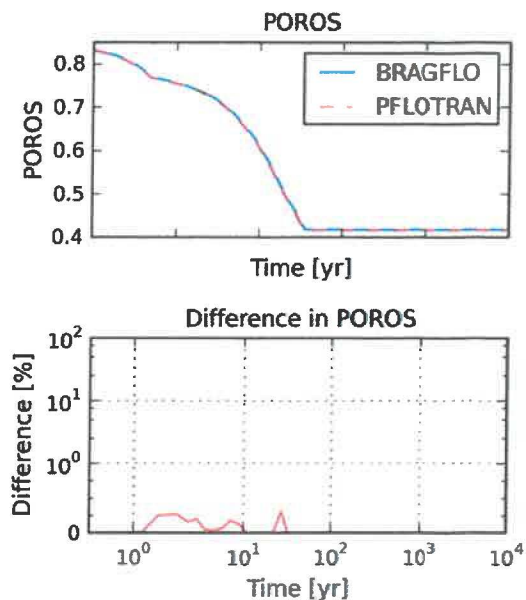
Figure 5.3-7 Test case "CREEP1" porosity.
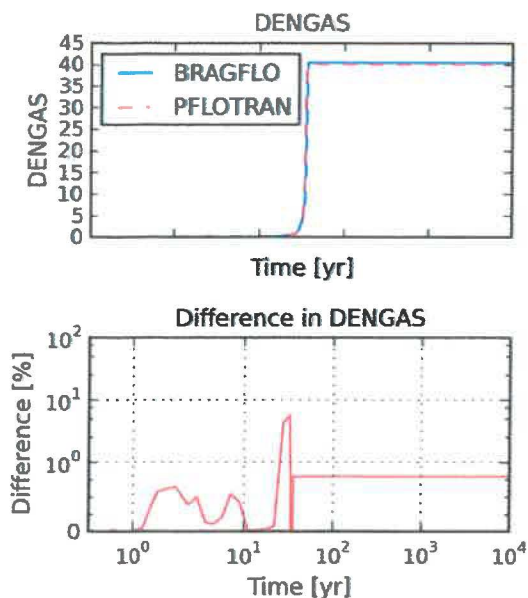
Figure 5.3-6 Test case "CREEP1" gas density [kg/m^3].

Information Only

5.3.2.2 *Creep Closure with Gas Injection*
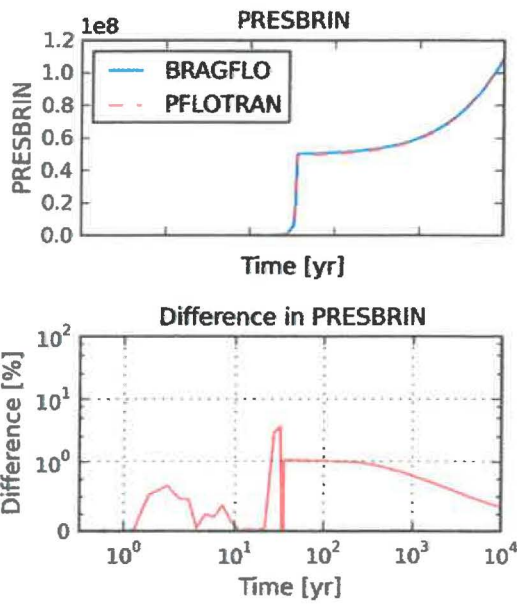
Figure 5.3-8 Test case "CREEP2" brine pressure [Pa].
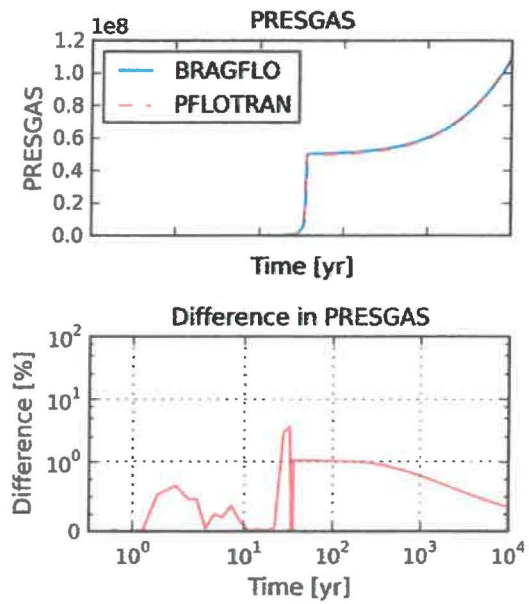
Figure 5.3-9 Test case "CREEP2" gas pressure [Pa].
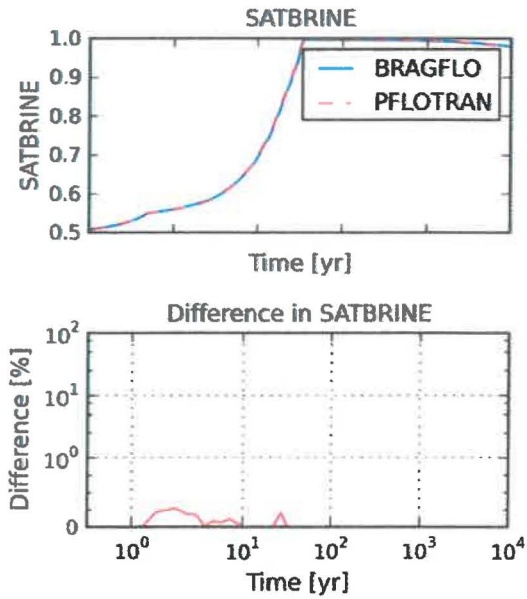
Figure 5.3-10 Test case "CREEP2" brine saturation.
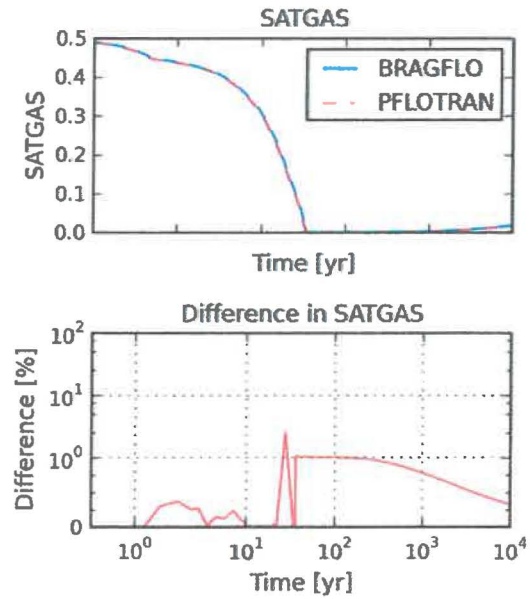
Figure 5.3-11 Test case "CREEP2" gas saturation.
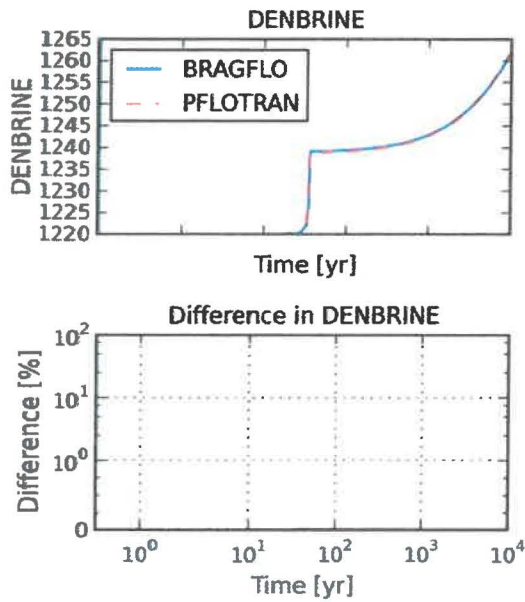
Figure 5.3-12 Test case "CREEP2" brine density [kg/m³].
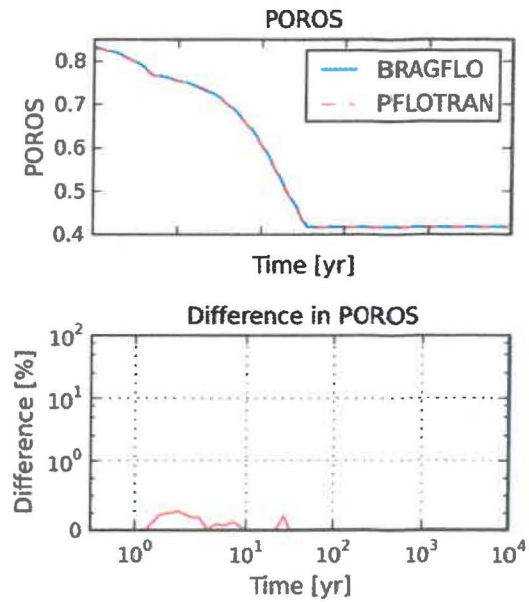
Figure 5.3-14 Test case "CREEP2" porosity.
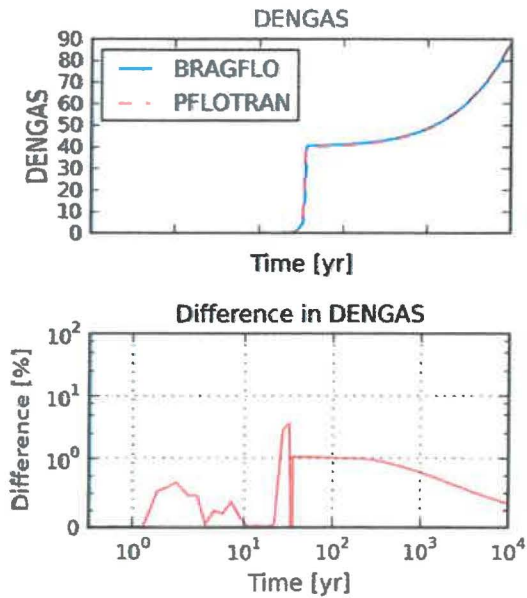
Figure 5.3-13 Test case "CREEP2" gas density [kg/m³].

5.3.2.3   *Creep Closure with Gas Production*
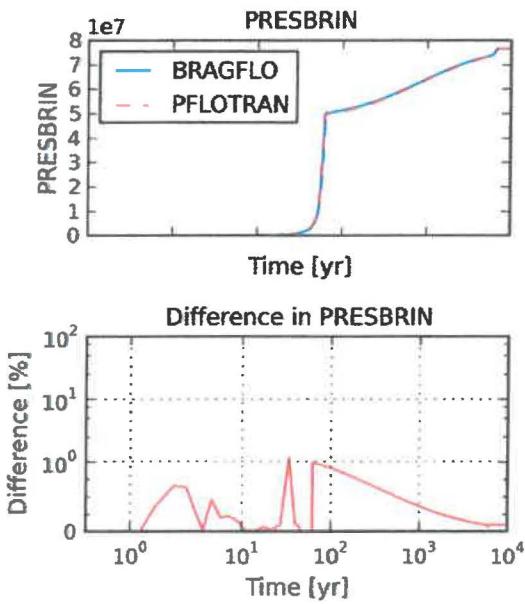
Figure 5.3-15 Test case "CREEP3" brine pressure [Pa].
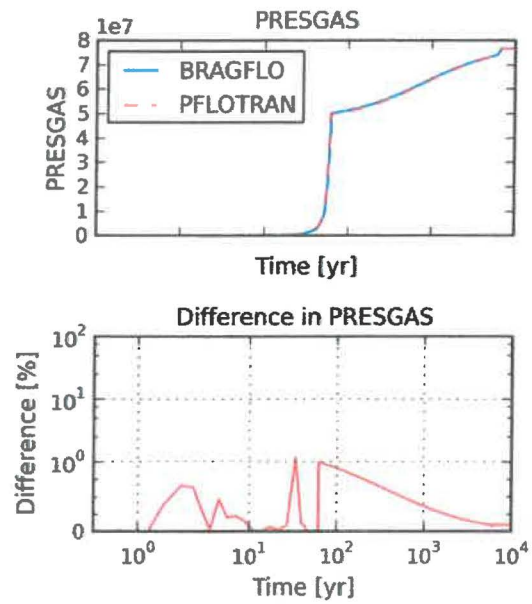
Figure 5.3-16 Test case "CREEP3" gas pressure [Pa].
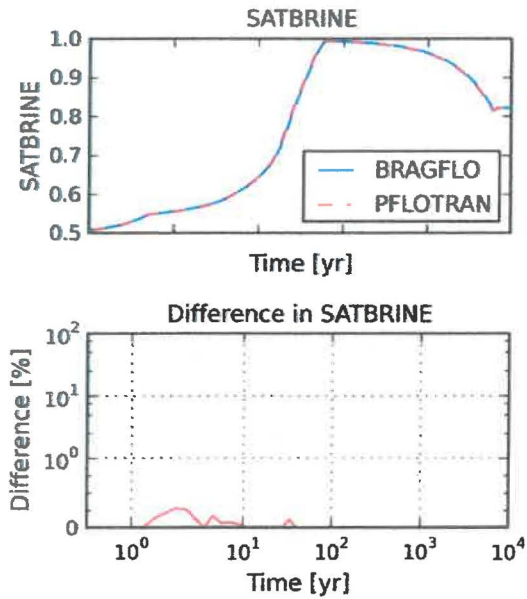
Figure 5.3-17 Test case "CREEP3" brine saturation.
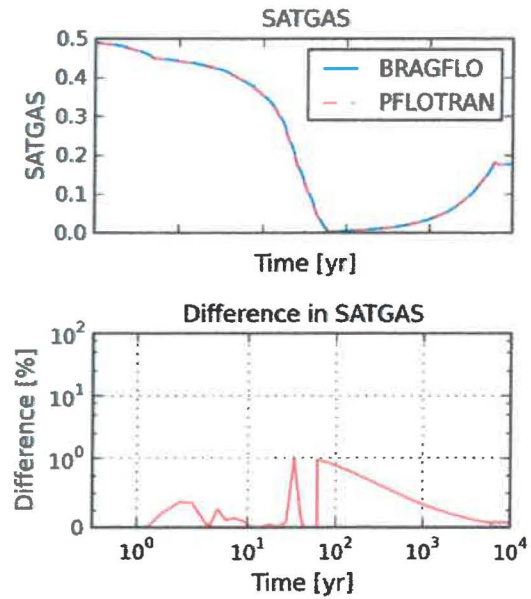
Figure 5.3-18 Test case "CREEP3" gas saturation.
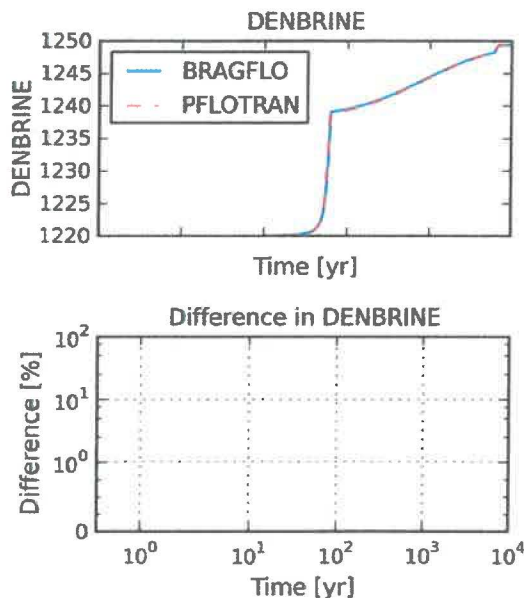
Figure 5.3-19 Test case "CREEP3" brine density [kg/m^3].

Figure 5.3-21 Test case "CREEP3" porosity.

Figure 5.3-20 Test case "CREEP3" gas density [kg/m^3].
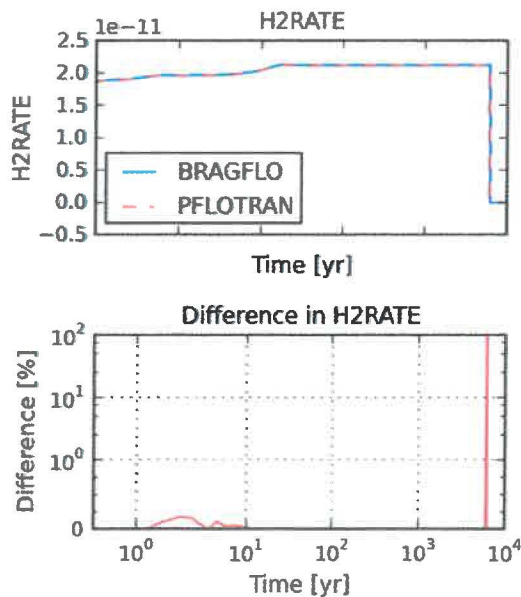
Figure 5.3-22 Test case "CREEP3" gas generation rate [mol-H$_2$/m^3/sec].

Information Only
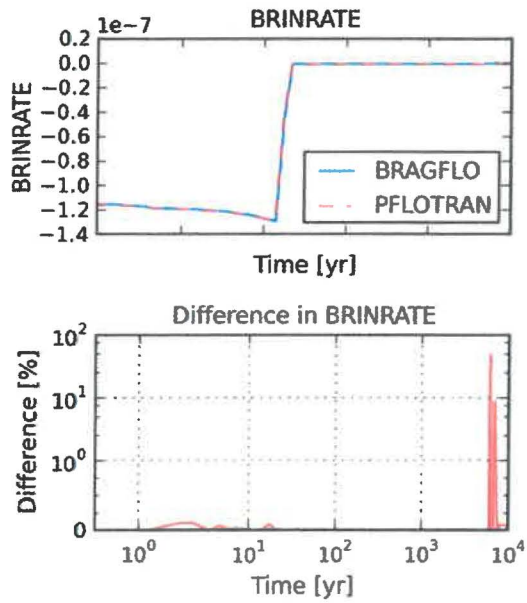
Figure 5.3-23. Test case "CREEP3" brine generation rate [mol-H_2O/m^3/sec].

5.3.3 Conclusions

The waste area creep closure process model test cases demonstrate that the creep closure process models are comparable between BRAGFLO and PFLOTRAN. When creep closure and the gas generation/brine consumption chemistry process models are used together, the differences between BRAGFLO and PFLOTRAN are the smallest of the three cases presented (less than 1%). As in the gas generation test cases summarized in Section 5.2.3, there is a spike in relative difference in gas generation rate when the gas generation rate drops to zero (see Figure 5.3-22, for example), however this difference does not affect the remaining part of the simulation, and can be ignored. The comparison improved relative to the FY 2017 comparison, in which differences in brine pressure of up to 20% occurred (Zeitler et al. 2017). The improvement may be attributed to full coupling of the gas generation and creep closure process models, other updates to the gas generation and creep closure process models, and/or the implementation and use of solution control parameters identical to those implemented in BRAGFLO.

5.4   Test Group #3: Pore Space Compressibility

5.4.1 Purpose and Setup

One test case ("COMP")[7] is presented to compare the pore space compressibility models between BRAGFLO and PFLOTRAN. This test case uses Marker Bed 138 material properties consistent with PFD Replicate 1, Vector 1 parameter values, but with the fracture model disabled. The process models used in PFLOTRAN include: SOIL_COMPRESSIBILITY, KRP4. In this test case, gas is injected at a constant rate, causing pressure to increase in the grid cell over time.

5.4.2 Results

---

[7] The "COMP" test case refers to the verification test located at pflotran-bragflo-test-cases-stripped/tests_single_cell/case060400/pf_case060400_0d_porecomp_gas_injection.in.
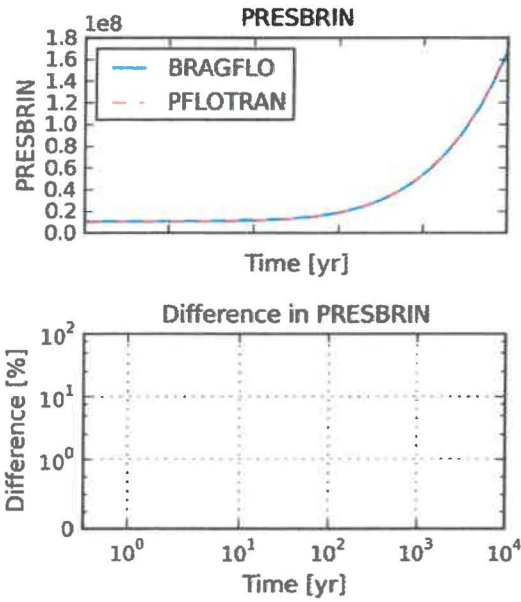
Figure 5.4-1 Test case "COMP" brine pressure [Pa].
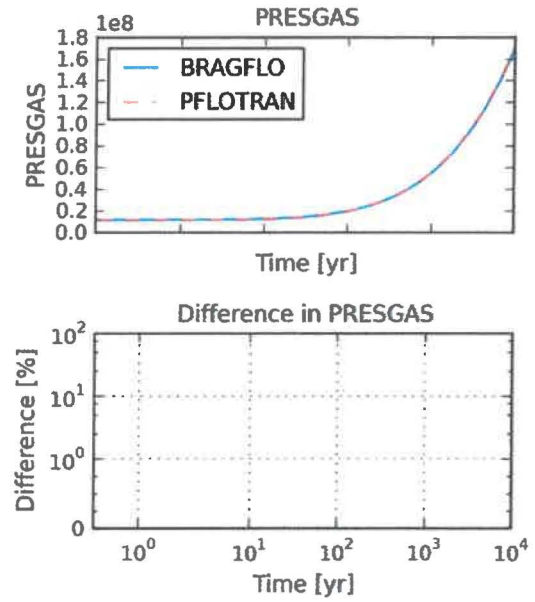
Figure 5.4-2 Test case "COMP" gas pressure [Pa].
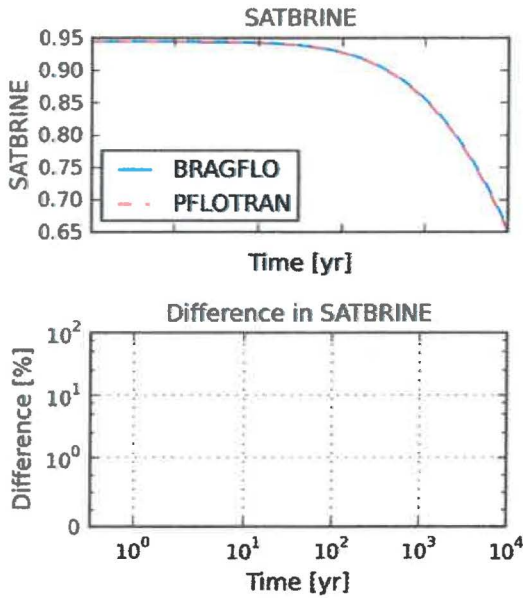
Figure 5.4-3 Test case "COMP" brine saturation.
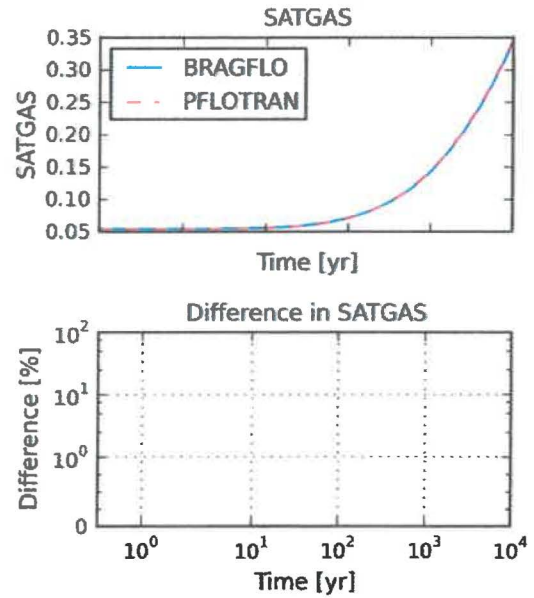
Figure 5.4-4 Test case "COMP" gas saturation.
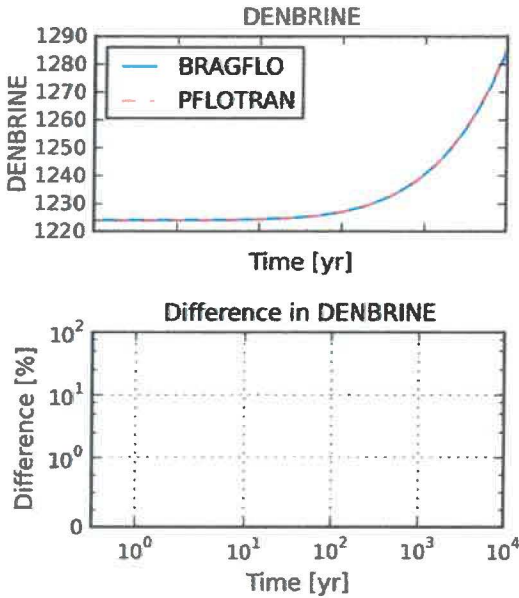
Figure 5.4-5 Test case "COMP" brine density [kg/m³].
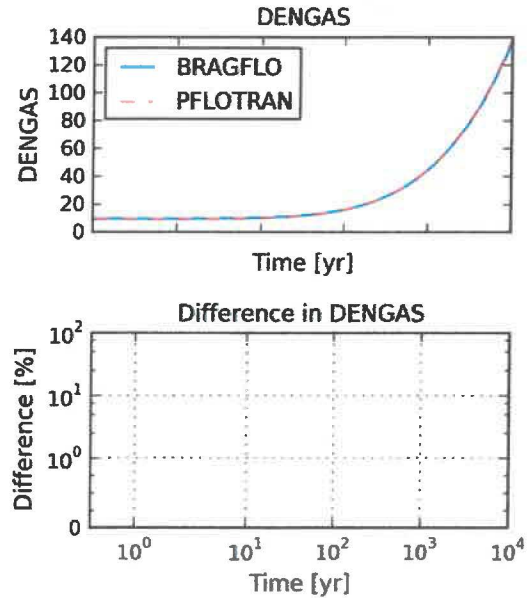
Figure 5.4-6 Test case "COMP" gas density [kg/m³].
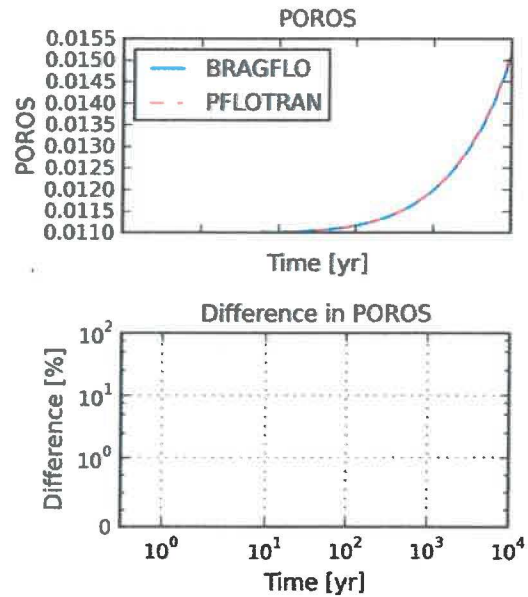
Figure 5.4-7 Test case "COMP" porosity.

5.4.3 Conclusions

The pore space compressibility process models in BRAGFLO and PFLOTRAN are comparable and produce identical results.

5.5   Test Group #4: Fracturing of Marker Beds

5.5.1 Purpose and Setup

One test case ("FRAC")[8] is presented to compare the marker bed fracturing models between BRAGFLO and PFLOTRAN. This test case uses Marker Bed 138 material properties consistent with PFD Replicate 1, Vector 1 parameter values. The process models used in PFLOTRAN include: FRACTURE, KRP4. In this test case, gas is injected at a constant rate (2.302670×10^{-6} kg/s), causing pressure to increase in the grid cell over time.

5.5.2 Results
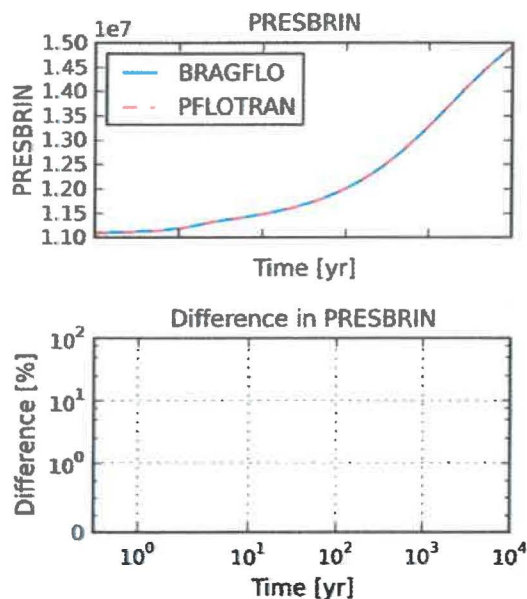
Figure 5.5-1 Test case "FRAC" brine pressure [Pa].
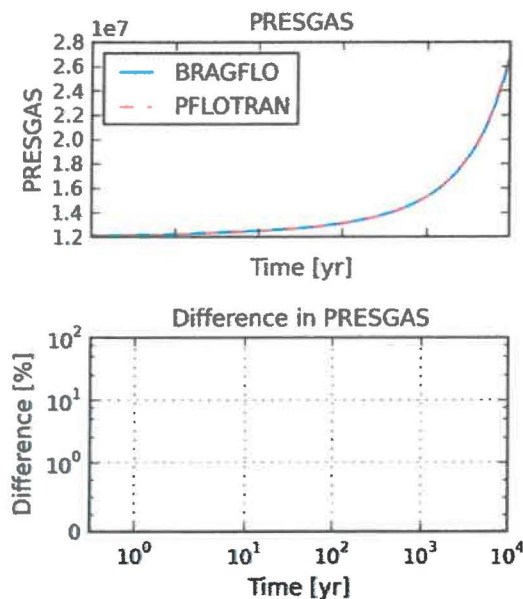
Figure 5.5-2 Test case "FRAC" gas pressure [Pa].

---

[8] The "FRAC" test case refers to the verification test located at pflotran-bragflo-test-cases-stripped/tests_single_cell/case060500/pf_case060500_0d_fracture_gas_injection.in.
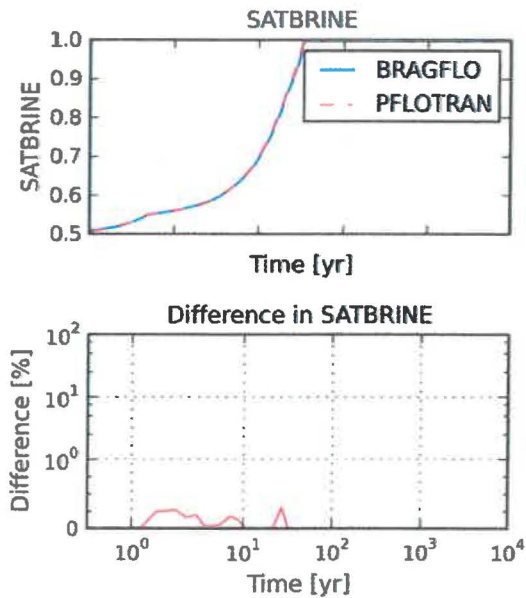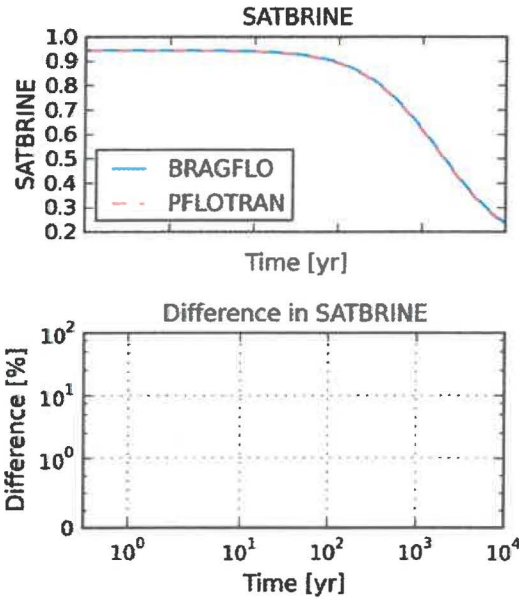
Figure 5.5-3 Test case "FRAC" brine saturation.
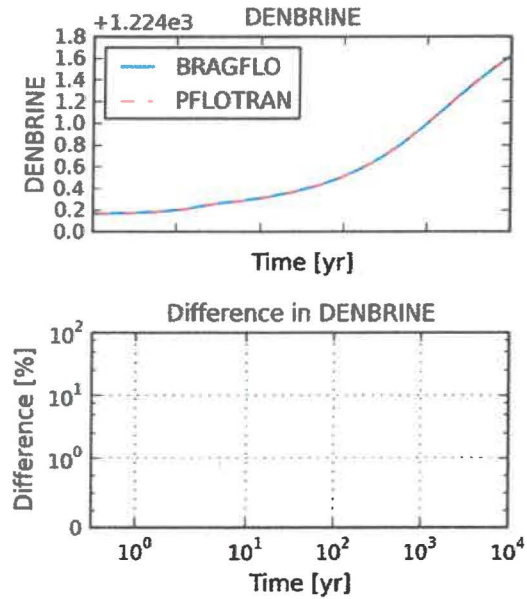
Figure 5.5-5 Test case "FRAC" brine density [kg/m^3].
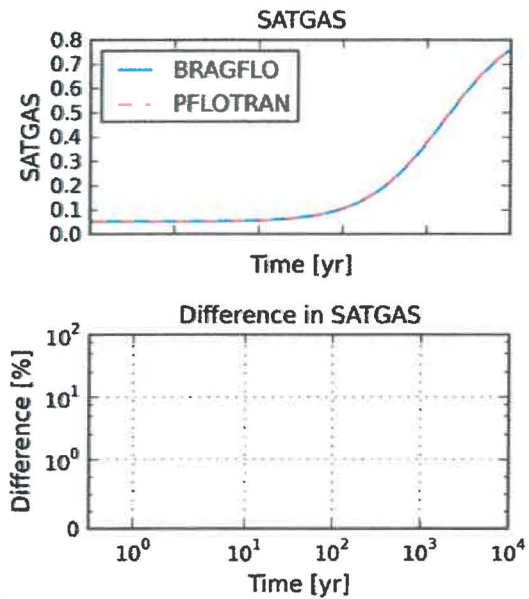
Figure 5.5-4 Test case "FRAC" gas saturation.
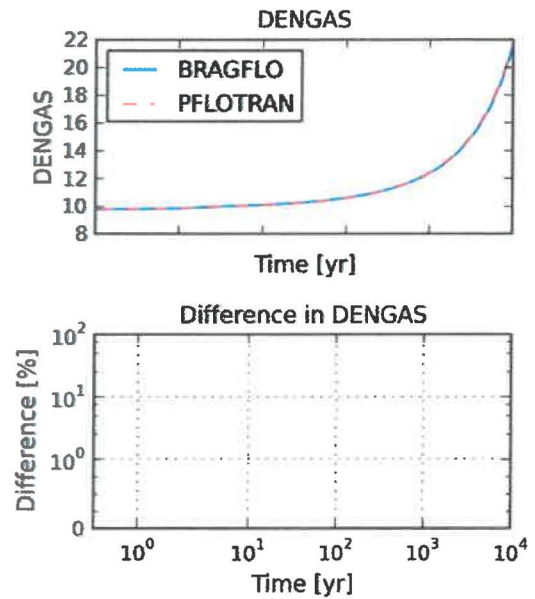
Figure 5.5-6 Test case "FRAC" gas density [kg/m^3].
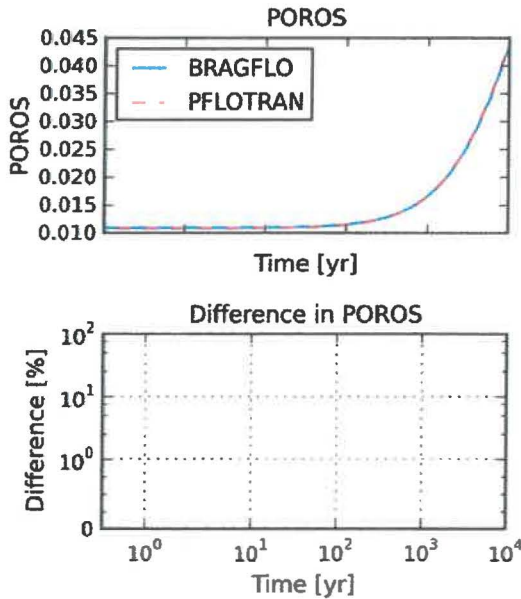
Figure 5.5-7 Test case "FRAC" porosity.

5.5.3 Conclusions

The marker bed fracturing process models in BRAGFLO and PFLOTRAN are comparable and produce identical results.

5.6 Test Group #5: Klinkenberg Effect on Permeability to Gas

5.6.1 Purpose and Setup

One test case ("KLINK")[9] is presented to compare the Klinkenberg permeability-to-gas models between BRAGFLO and PFLOTRAN. This test case uses Marker Bed 138 material properties consistent with PFD Replicate 1, Vector 1 parameter values, but with the fracture model disabled. The process models used in PFLOTRAN include: KLINKENBERG, KRP4. In this test case, gas is injected at a constant rate (2.302670×10^{-6} kg/s), causing pressure to increase in the grid cell over time.

5.6.2 Results

---

[9] The "KLINK" test case refers to the verification test located at pflotran-bragflo-test-cases-stripped/tests_single_cell/case060600/pf_case060600_0d_klinkenberg_gas_injection.in.
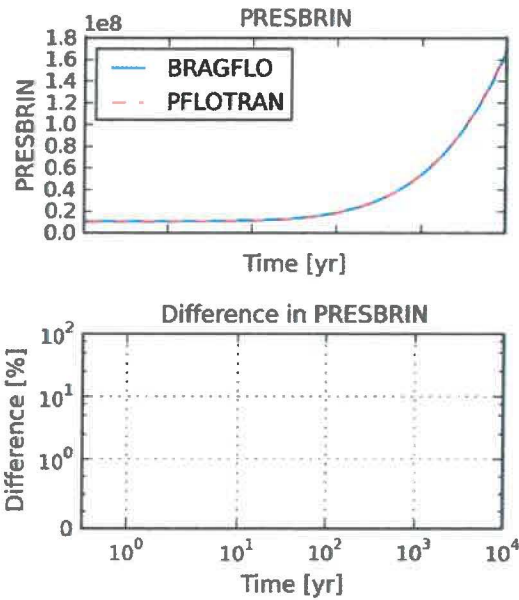
Figure 5.6-1 Test case "KLINK" brine pressure [Pa].
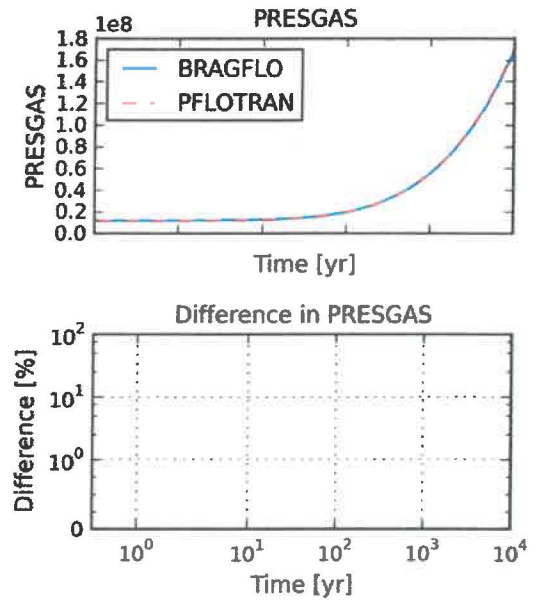
Figure 5.6-2 Test case "KLINK" gas pressure [Pa].
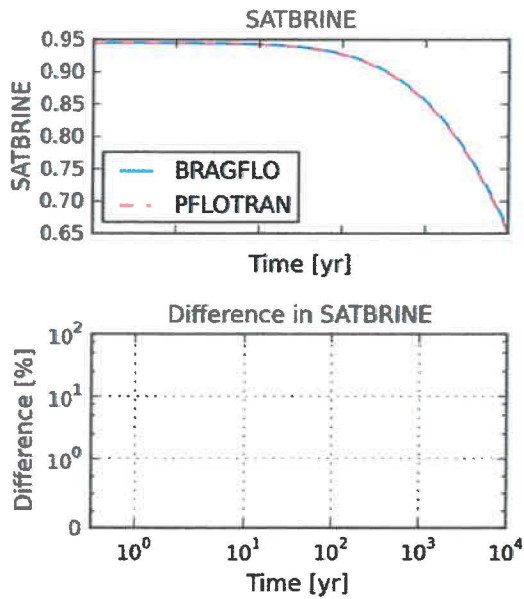
Figure 5.6-3 Test case "KLINK" brine saturation.
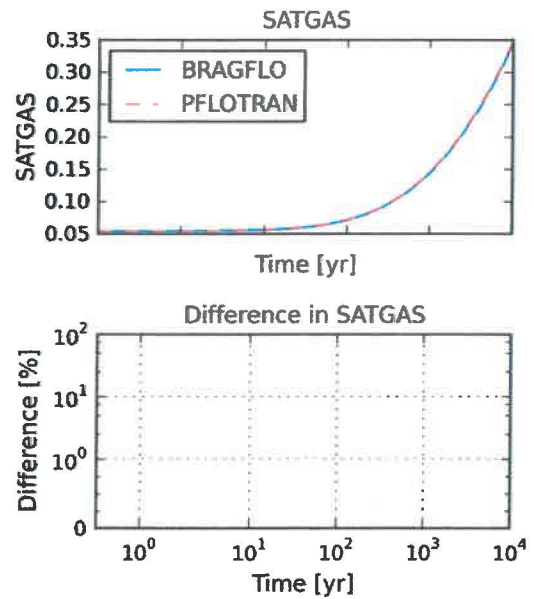
Figure 5.6-4 Test case "KLINK" gas saturation.
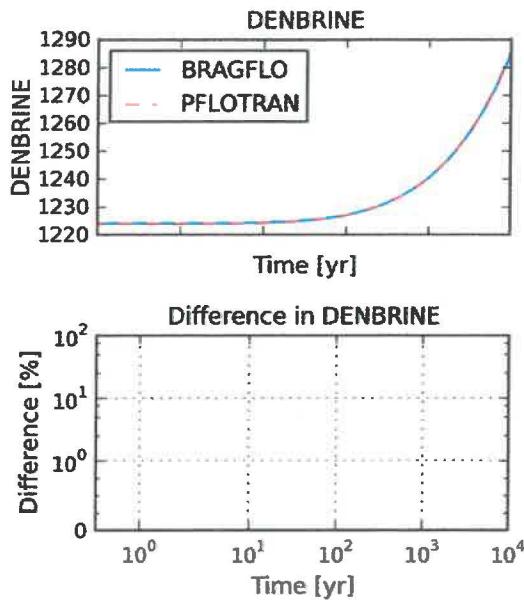
Figure 5.6-5 Test case "KLINK" brine density [kg/m^3].
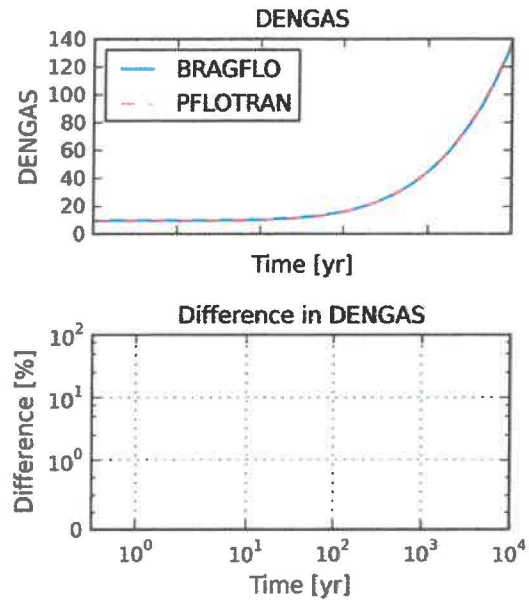
Figure 5.6-6 Test case "KLINK" gas density [kg/m^3].
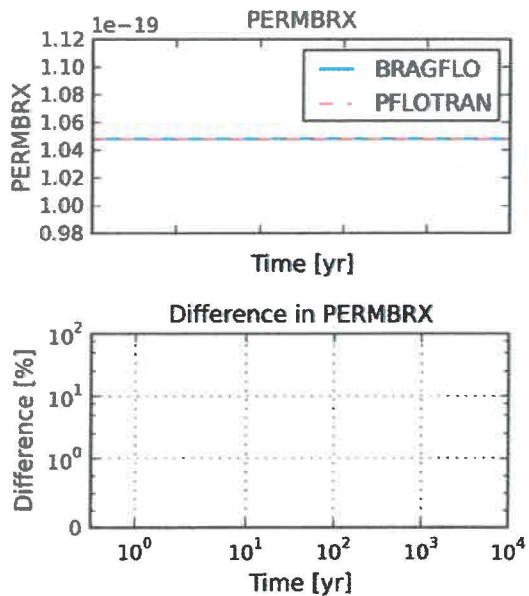
Figure 5.6-7 Test case "KLINK" x-permeability to brine [m^2].
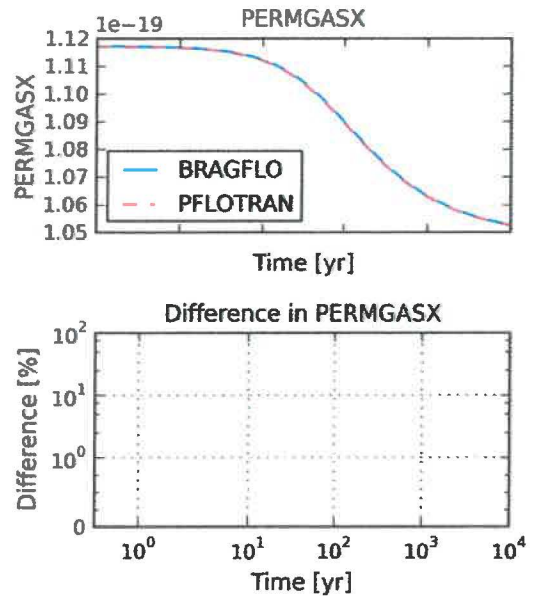
Figure 5.6-8 Test case "KLINK" x-permeability to gas [m^2].

5.6.3 Conclusions

The Klinkenberg permeability-to-gas effect process models in BRAGFLO and PFLOTRAN produce identical results.

5.7   Test Group #6: Redlich-Kwong-Soave Equation of State

5.7.1 Purpose and Setup

One test case ("RKS")[10] is presented to compare the Redlich-Kwong-Soave (RKS) equation of state (EOS) model between BRAGFLO and PFLOTRAN. The RKS EOS is used to calculate gas density, given pressure. This test case uses waste area material properties (without creep closure) consistent with PFD Replicate 1, Vector 1 parameter values. The process models used in PFLOTRAN include: RKS, KRP12. In this test case, gas is injected at a constant rate (1×10^{-4} kg/s), causing pressure to increase in the grid cell over time.

5.7.2 Results

BRAGFLO and PFLOTRAN calculate similar results when the pressure is less than 100 MPa. By design, BRAGFLO linearly extrapolates gas density for pressures above 100 MPa based on the last two data points, while PFLOTRAN (also by design) continues to calculate gas density using the cubic root solution to the EOS (see also Section 4.8). Because PA simulations do not return pressures in excess of 100 MPa, this difference will have little to no impact on the PFLOTRAN-BRAGFLO comparisons for typical PA scenarios.

---

[10] The "RKS" test case refers to the verification test located at pflotran-bragflo-test-cases-stripped/tests_single_cell/case060700/pf_case060700_0d_rks_calc_gas_injection.in.
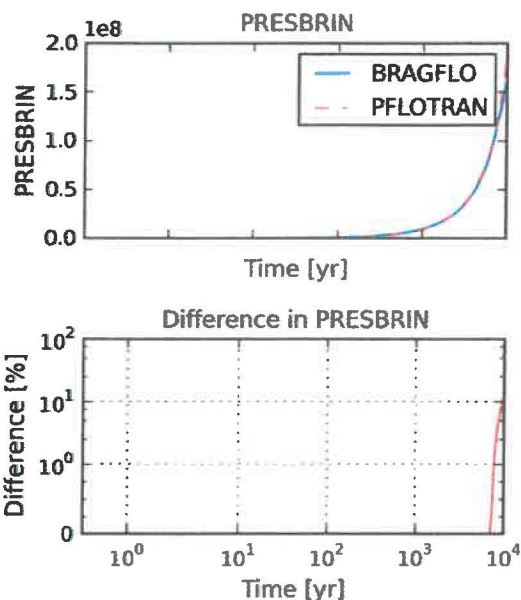
Figure 5.7-1 Test case "RKS" brine pressure [Pa].
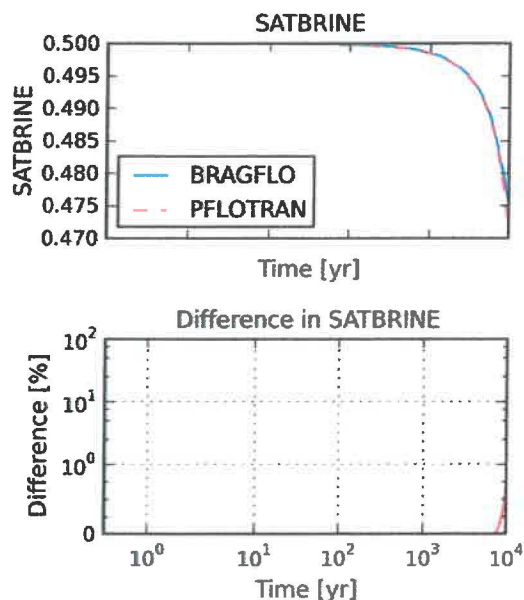
Figure 5.7-3 Test case "RKS" brine saturation.
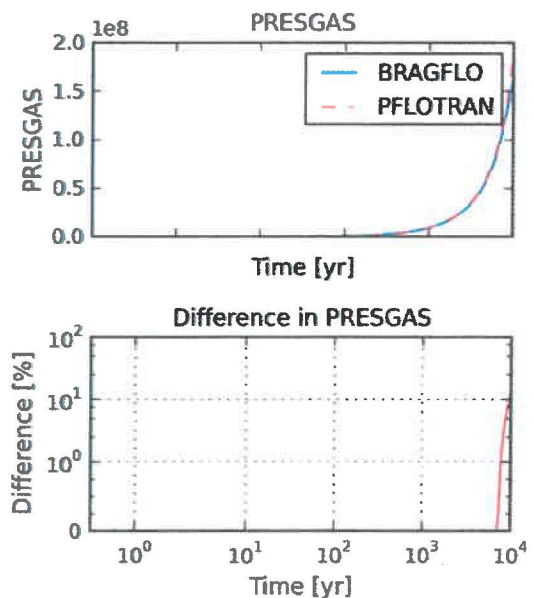
Figure 5.7-2 Test case "RKS" gas pressure [Pa].
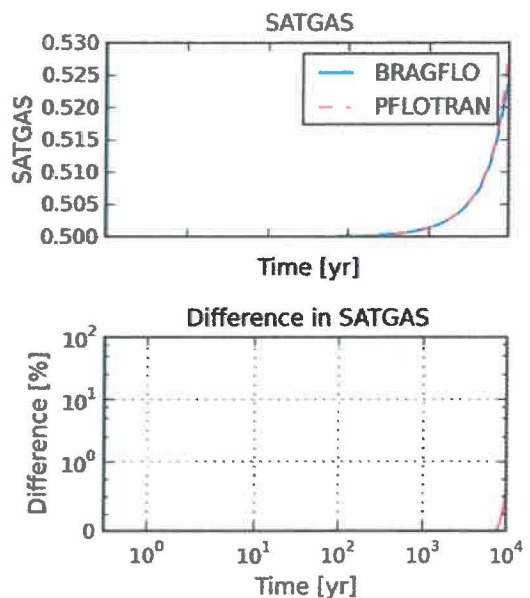
Figure 5.7-4 Test case "RKS" gas saturation.

Information Only
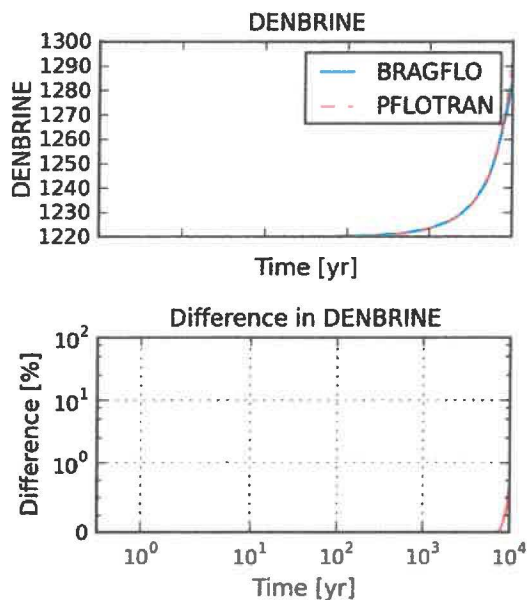
Figure 5.7-5 Test case "RKS" brine density [kg/m³].
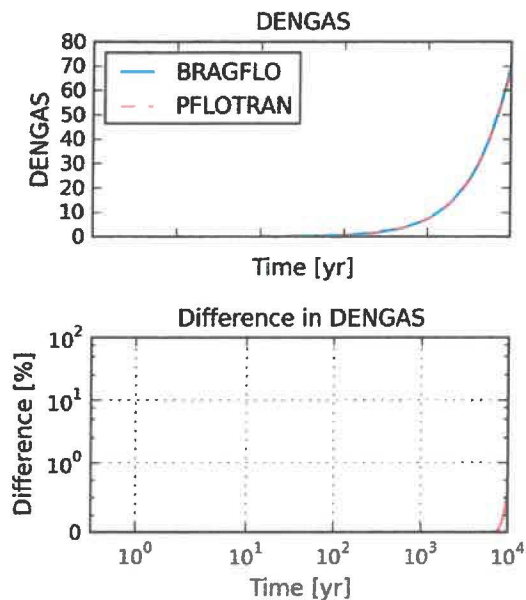
Figure 5.7-6 Test case "RKS" gas density [kg/m³].

5.7.3 Conclusions

The Redlich-Kwong-Soave equation of state models compare favorably between BRAGFLO and PFLOTRAN. No difference is observed between the EOS models when pressures are below 100 MPa. Due to the differences in how BRAGFLO and PFLOTRAN calculate gas density when pressures are above 100 MPa, a maximum difference of ~10% is seen in brine and gas pressures (Figure 5.7-1 and Figure 5.7-2) because of a ~1% difference in the gas density (Figure 5.7-6). Because PA simulations (i.e., PFD analysis on the 2-D flared grid) do not return pressures in excess of 100 MPa, this difference has little to no impact on the PFLOTRAN-BRAGFLO comparison in Section 8.

6   WIPP Process Model Testing (Multi-Cell)

A suite of multi-cell test cases was developed and designed to exercise individual process models in isolation, or in simple combination. Multiple process models were tested simultaneously because discrepancies for separate process model tests are not necessarily indicative of the resulting discrepancies when multiple process models are tested in combination.

Each multi-cell test case includes a PFLOTRAN input deck and a corresponding BRAGFLO input deck that implements the identical simulation. A single plotting script that automatically plots all test case results is executed as the final step. The plotting routine creates two plots per variable of interest: the value of the variable at a specific grid cell, and the average value of the variable over the multi-cell domain. Because outputs were saved at user-specified times rather than at every time step (as in the single-cell tests), calculation of differences does not require time interpolation and differences are plotted at the user-specified output times rather than as continuous lines. Parameters used for each test are representative of those employed in WIPP PA.

6.1   Calculation Details

All BRAGFLO results were produced on the Linux cluster head node (jt.sandia.gov) using the BRAGFLO executable stored at:

- /Archive/pflotran_bragflo_comparison_20180928/executables/bragflo-jt

All PFLOTRAN results were produced on the Linux cluster head node (jt.sandia.gov) using the PFLOTRAN executable stored at:

- /Archive/pflotran_bragflo_comparison_20180928/executables/pflotran-071318

All test input decks, plotting scripts, and results are located on the Linux cluster in the folder:

- /Archive/pflotran_bragflo_comparison_20180928/pflotran-bragflo-test-cases-stripped

Table 6.1-1 shows the values of the solution control parameters used in each multi-cell test case. In the first column ("BRAGFLO"), the BRAGFLO solution control parameter name is given. In the second column ("PFLOTRAN"), the equivalent PFLOTRAN solution control parameter name is given. In the third column ("BLOCK"), the PFLOTRAN input deck block where the solution control keyword is placed is listed. The fourth and fifth columns ("VALUE", "UNIT") show the values and corresponding units of the solution control parameter used.

Percent differences are calculated and plotted as described in Section 5.1.

Table 6.1-1 Solution control parameter values for multi-cell test runs.

BRAGFLO	PFLOTRAN	BLOCK	VALUE	UNIT
FTOLNORM(2)	LIQUID_RESIDUAL_INFINITY_TOL	OPTIONS	1.0d-2	kg/m3
FTOLNORM(1)	GAS_RESIDUAL_INFINITY_TOL	OPTIONS	1.0d-2	kg/m3
EPSNORM(2)	MAX_ALLOW_REL_LIQ_PRES_CHANG_NI	OPTIONS	1.0d-2	-
EPSNORM(1)	MAX_ALLOW_REL_GAS_SAT_CHANGE_NI	OPTIONS	1.0d-3	-
DH(1)	REL_GAS_SATURATION_PERTURBATION	OPTIONS	1.0d-8	-
DH(2)	REL_LIQ_PRESSURE_PERTURBATION	OPTIONS	1.0d-8	-
HMIN(1)	MIN_GAS_SATURATION_PERTURBATION	OPTIONS	1.0d-10	-
HMIN(2)	MIN_LIQ_PRESSURE_PERTURBATION	OPTIONS	1.0d-2	Pa
DTIMEMAX	TIMESTEP_MAXIMUM_GROWTH_FACTOR	TIMESTEPPER	1.25d0	-
SATLIMIT	GAS_SAT_THRESH_FORCE_EXTRA_NI	OPTIONS	1.0d-3	-
DEPLIMIT(1)	GAS_SAT_THRESH_FORCE_TS_CUT	OPTIONS	2.0d-1	-
DDEPMAX(1)	MAX_ALLOW_GAS_SAT_CHANGE_TS	OPTIONS	1.0d0	-
DELTADEPNORM(1)	GAS_SAT_CHANGE_TS_GOVERNOR	OPTIONS	3.0d-1	-
TSWITCH	GAS_SAT_GOV_SWITCH_ABS_TO_REL	OPTIONS	1.0d0	-
DEPLIMIT(2)	MIN_LIQ_PRES_FORCE_TS_CUT	OPTIONS	-1.0d8	Pa
DDEPMAX(2)	MAX_ALLOW_LIQ_PRES_CHANGE_TS	OPTIONS	1.0d7	Pa
DELTADEPNORM(2)	LIQ_PRES_CHANGE_TS_GOVERNOR	OPTIONS	5.0d5	Pa
P_SCALE	JACOBIAN_PRESSURE_DERIV_SCALE	OPTIONS	1.0d7	Pa
ITMAX	MAXIMUM_NUMBER_OF_ITERATIONS	NEWTON_SOLVER	8	-
IRESETMAX	MAXIMUM_CONSECUTIVE_TS_CUT	TIMESTEPPER	40	-
DELTFACTOR	TIMESTEP_REDUCTION_FACTOR	TIMESTEPPER	5.0d-1	-
DELTMAX	MAXIMUM_TIMESTEP_SIZE	TIME	1.73448d9	sec
DELTMIN	MINIMUM_TIMESTEP_SIZE	OPTIONS	8.64d-4	sec

6.2   Test Group #1: 2D Gas Generation/Brine Consumption Chemistry

6.2.1 Purpose and Setup

Three test cases are presented that compare the gas generation and brine consumption chemistry process models between BRAGFLO and PFLOTRAN. Each case uses reactant concentrations and reaction rate constants pulled from the PFD Analysis Replicate 1, Scenario 2, Vector 1 in the waste area cells. The process models used in PFLOTRAN include: KRP4, WIPP_SOURCE_SINK, RKS.

The three test cases consist of a 2-D vertical cross section containing a waste region that generates gas and that varies in size among the tests. Material properties are homogeneous throughout the 10.5-m by 21-m domain. The model domain is initialized to gravity/capillary equilibrium at much higher pressure (~4 MPa) than the atmosphere, with the bottom of the domain fully saturated (0.99999). All boundaries have no-flow boundary conditions. The simulation duration was specified as 10,000 yr. A representative sample of the problem domain is provided in Figure 6.2-1 for the "6A" baseline case.
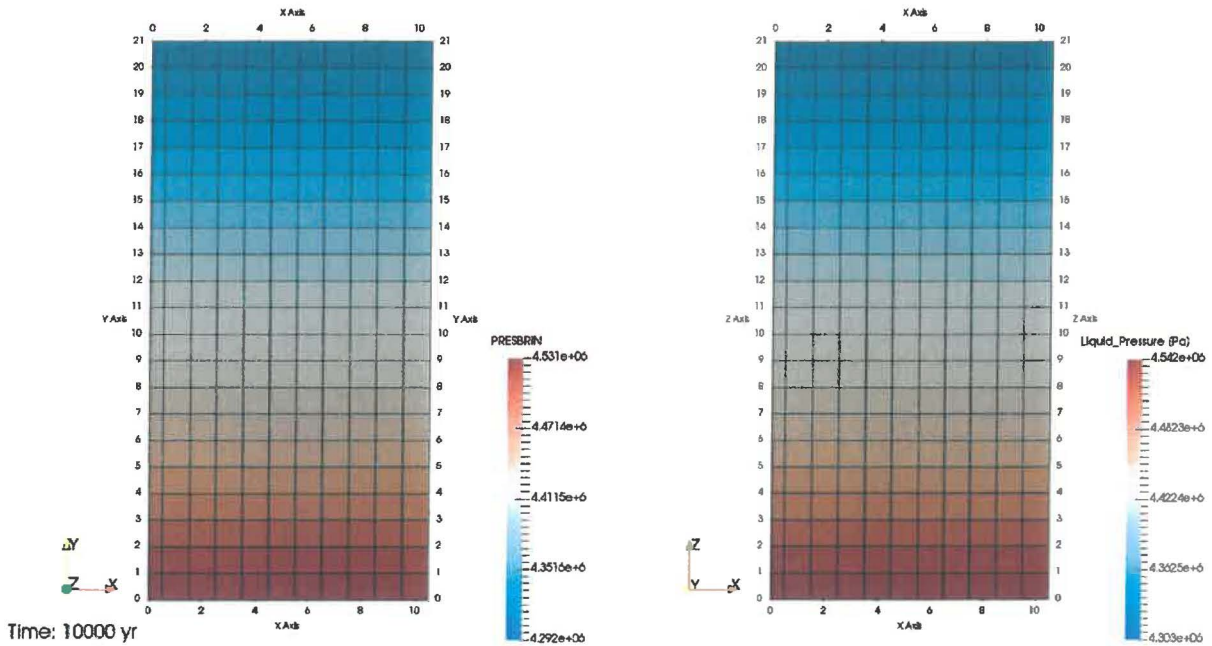
Figure 6.2-1 – Test Case "6a" Model Domain (BRAGFLO left, PFLOTRAN right). Cell (1,11) is marked with an "X."

In the first test case ("6A")[11] a single grid cell (1,11) generates gas. In the second test case ("6A_MIDGEN")[12] gas generation occurs in the 9 cells surrounding and including cell (1,11). Finally, in the third test case ("6A_ALLGEN")[13] gas generation occurs in every cell in the domain.

---

[11] The "6A" test case refers to the verification test located at pflotran-bragflo-test-cases-stripped/tests_multi_cell/6a/pf_6a.in.

[12] The "6A_MIDGEN" test case refers to the verification test located at pflotran-bragflo-test-cases-stripped/tests_multi_cell/6a/pf_6a_midgen.in.

[13] The "6A_ALLGEN" test case refers to the verification test located at pflotran-bragflo-test-cases-stripped/tests_multi_cell/6a/pf_6a_allgen.in.

6.2.2 Results

6.2.2.1 Test Case "6A"
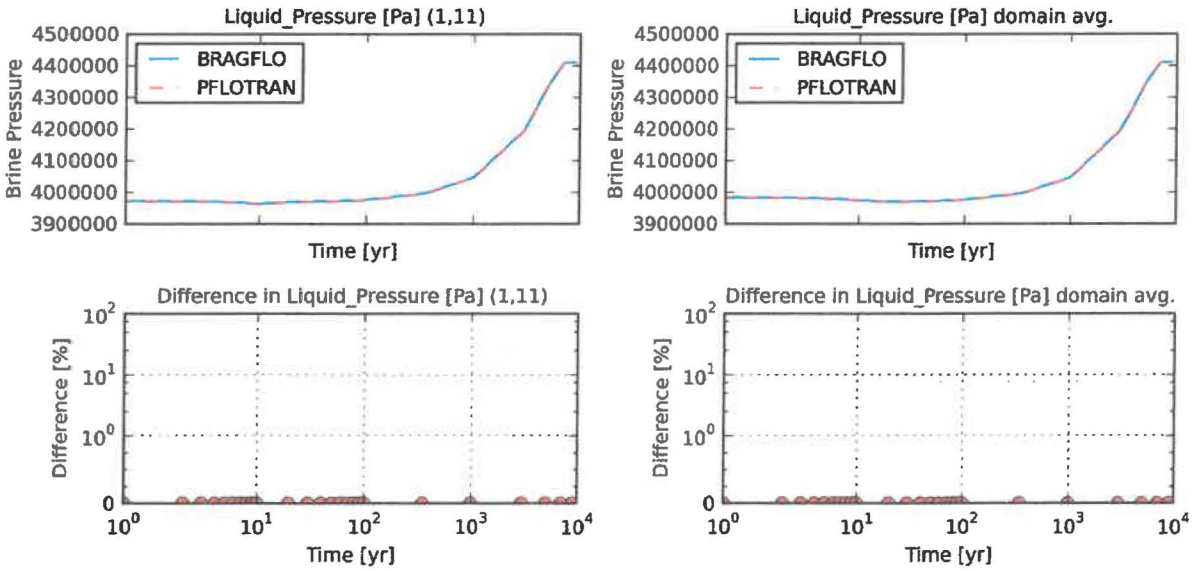
Figure 6.2-2 Test case "6A" brine pressure [Pa] at cell (1,11) and domain average.

Figure 6.2-3 Test case "6A" gas pressure [Pa] at cell (1,11) and domain average.

Figure 6.2-4 Test case "6A" brine saturation at cell (1,11) and domain average.

Figure 6.2-5 Test case "6A" gas saturation at cell (1,11) and domain average.

Figure 6.2-6 Test case "6A" brine density [kg/m³] at cell (1,11) and domain average.

Figure 6.2-7 Test case "6A" gas density [kg/m³] at cell (1,11) and domain average.
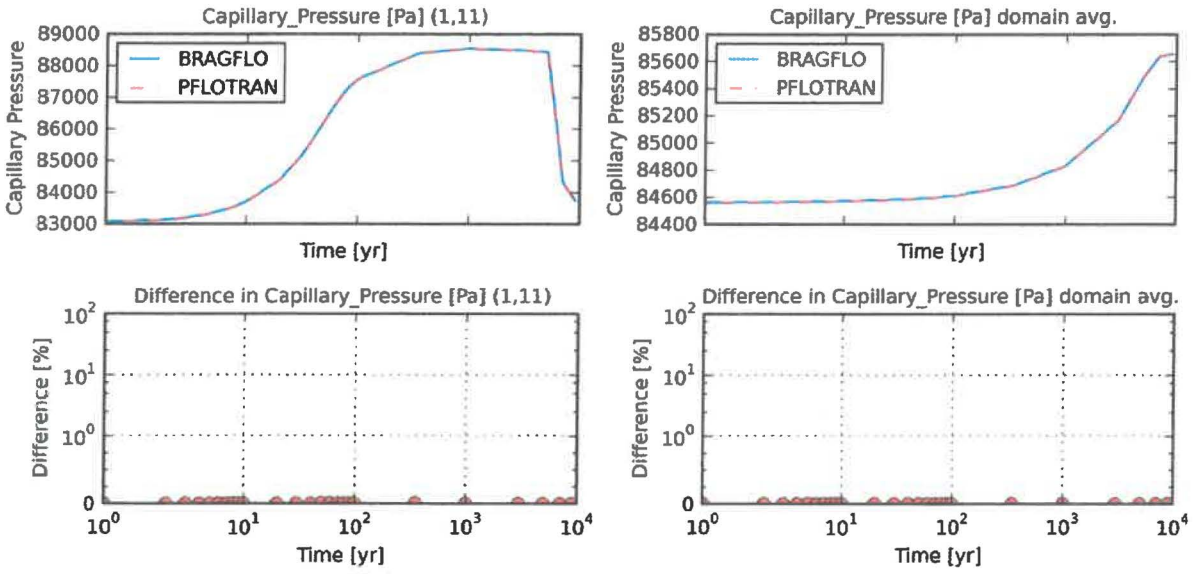
Figure 6.2-8 Test case "6A" capillary pressure [Pa] at cell (1,11) and domain average.
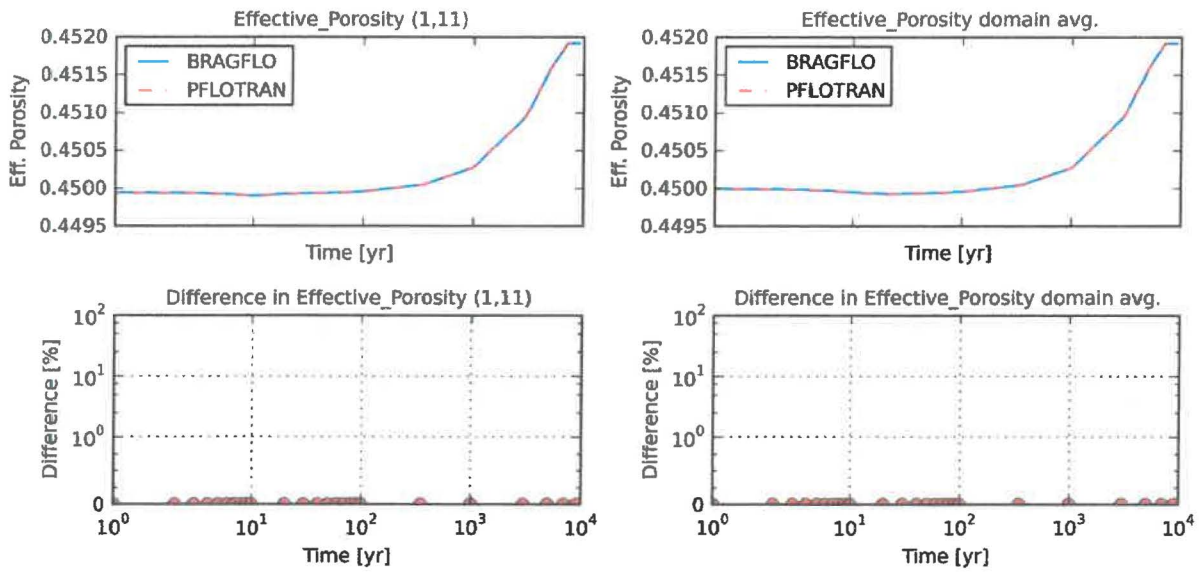
Figure 6.2-9 Test case "6A" porosity at cell (1,11) and domain average.

6.2.2.2 Test Case "6A_MIDGEN"
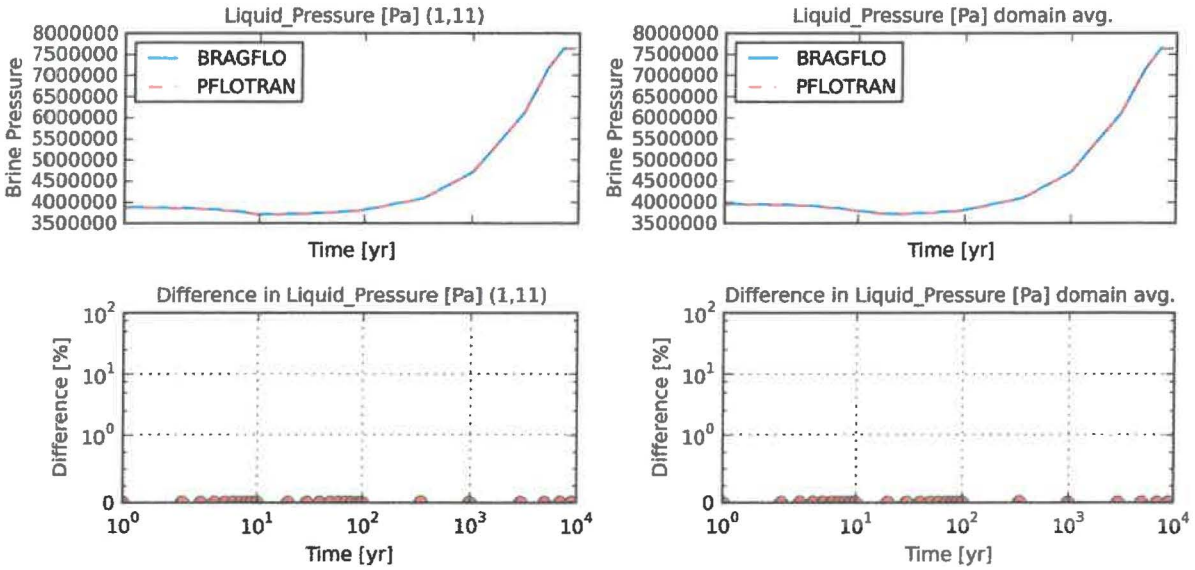
Figure 6.2-10 Test case "6A_MIDGEN" brine pressure [Pa] at cell (1,11) and domain average.
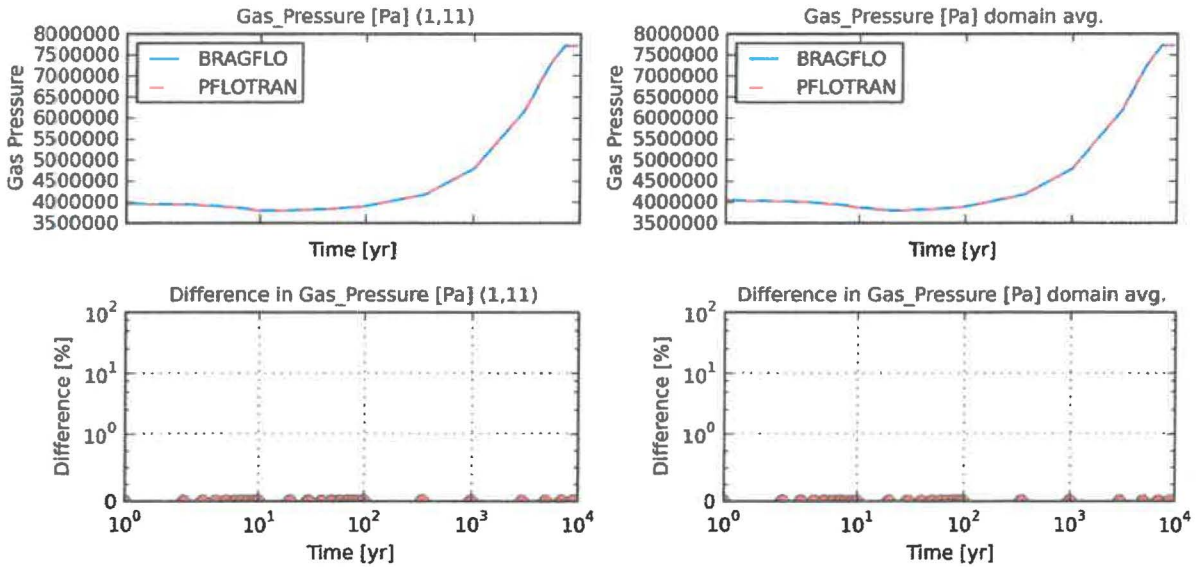
Figure 6.2-11 Test case "6A_MIDGEN" gas pressure [Pa] at cell (1,11) and domain average.

Figure 6.2-12 Test case "6A_MIDGEN" brine saturation at cell (1,11) and domain average.
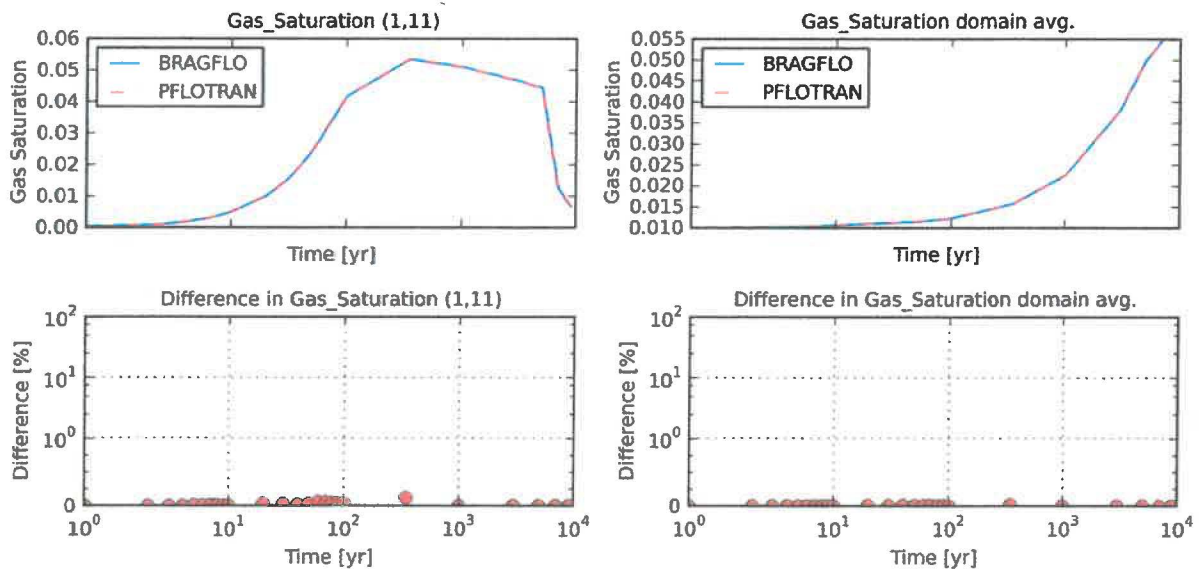
Figure 6.2-13 Test case "6A_MIDGEN" gas saturation at cell (1,11) and domain average.
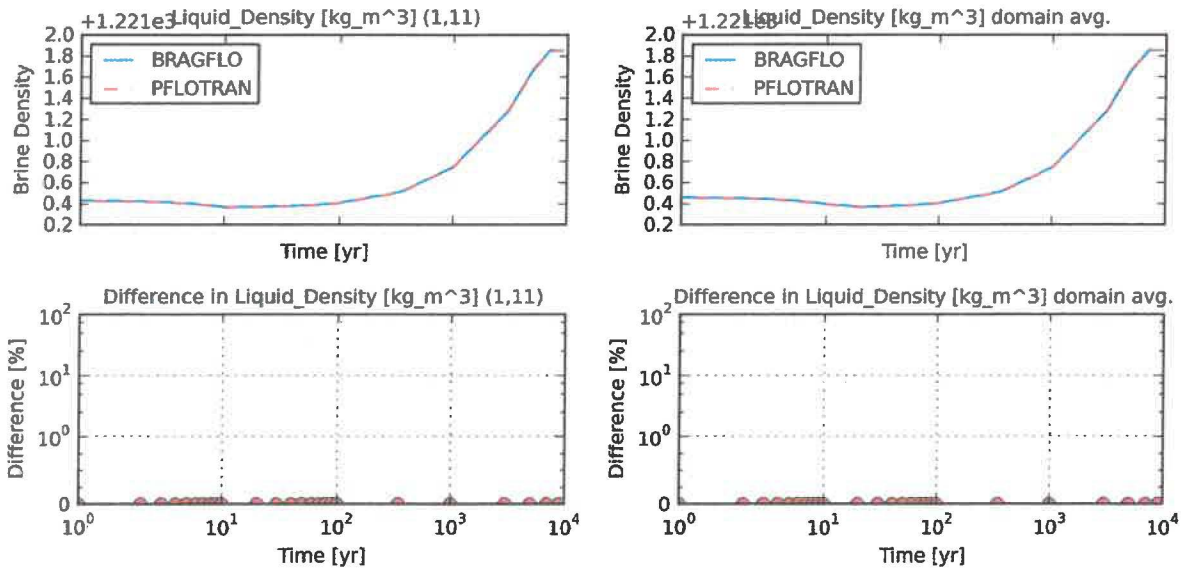
Figure 6.2-14 Test case "6A_MIDGEN" brine density [kg/m^3] at cell (1,11) and domain average.
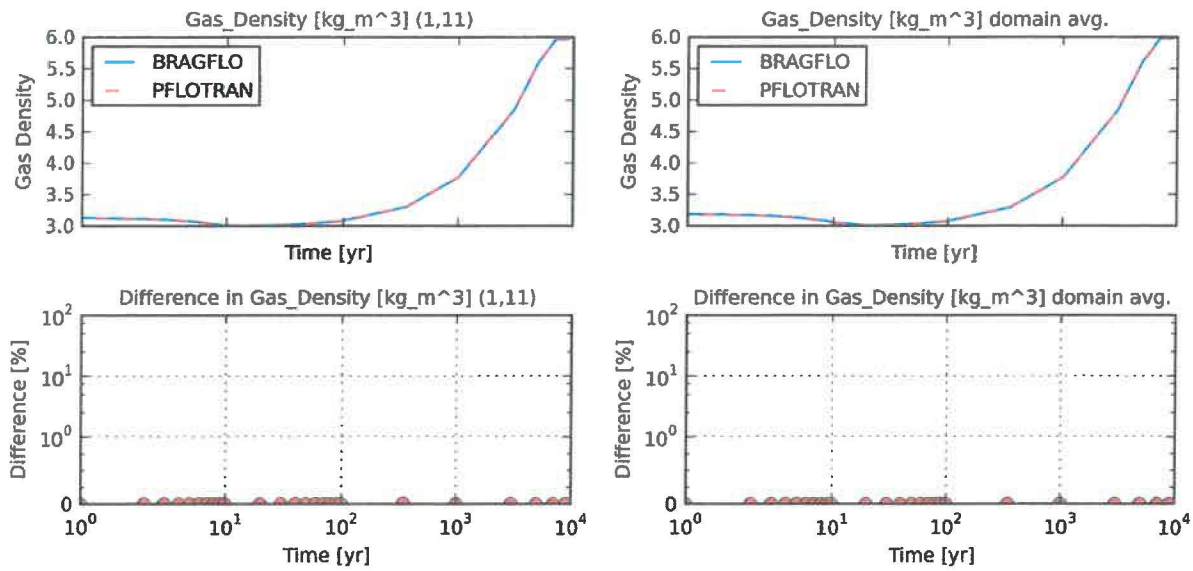
Figure 6.2-15 Test case "6A_MIDGEN" gas density [kg/m^3] at cell (1,11) and domain average.
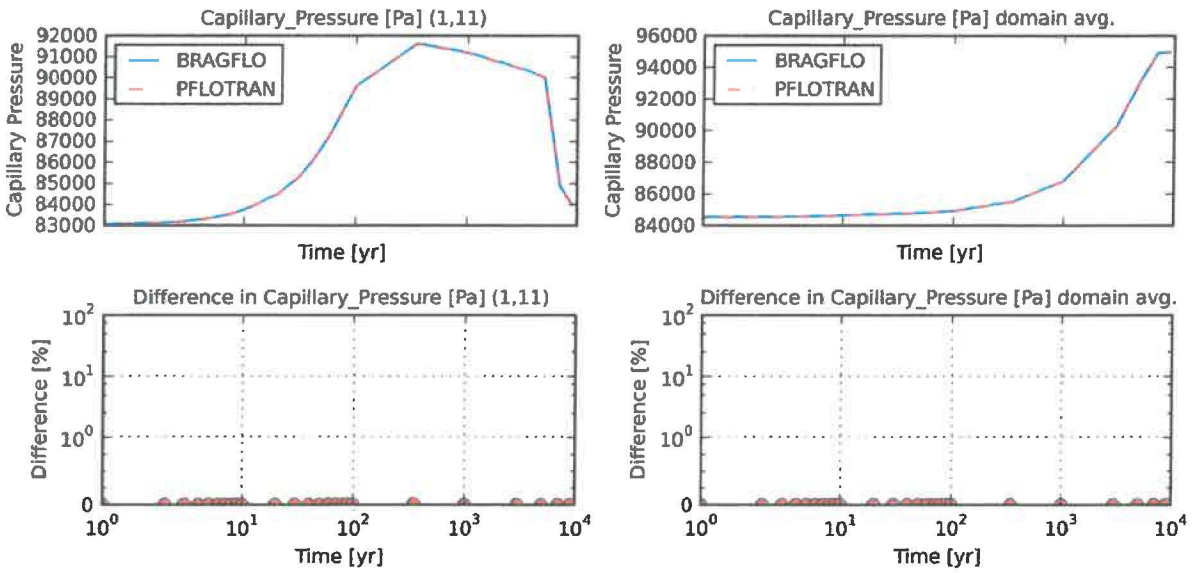
Figure 6.2-16 Test case "6A_MIDGEN" capillary pressure [Pa] at cell (1,11) and domain average.
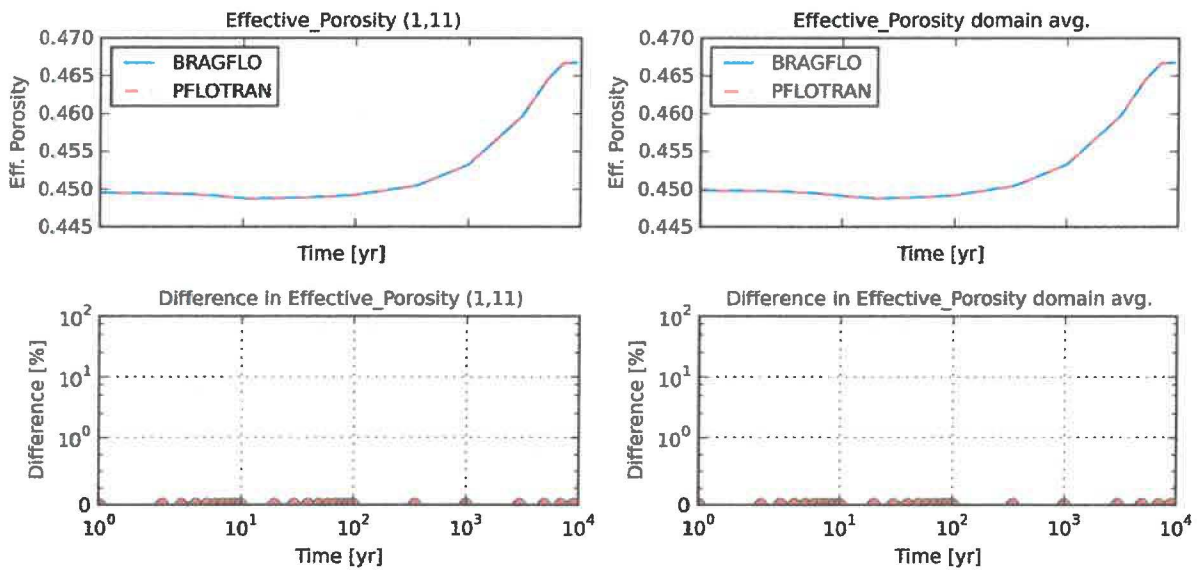
Figure 6.2-17 Test case "6A_MIDGEN" porosity at cell (1,11) and domain average.

Information Only

6.2.2.3 Test Case "6A_ALLGEN"
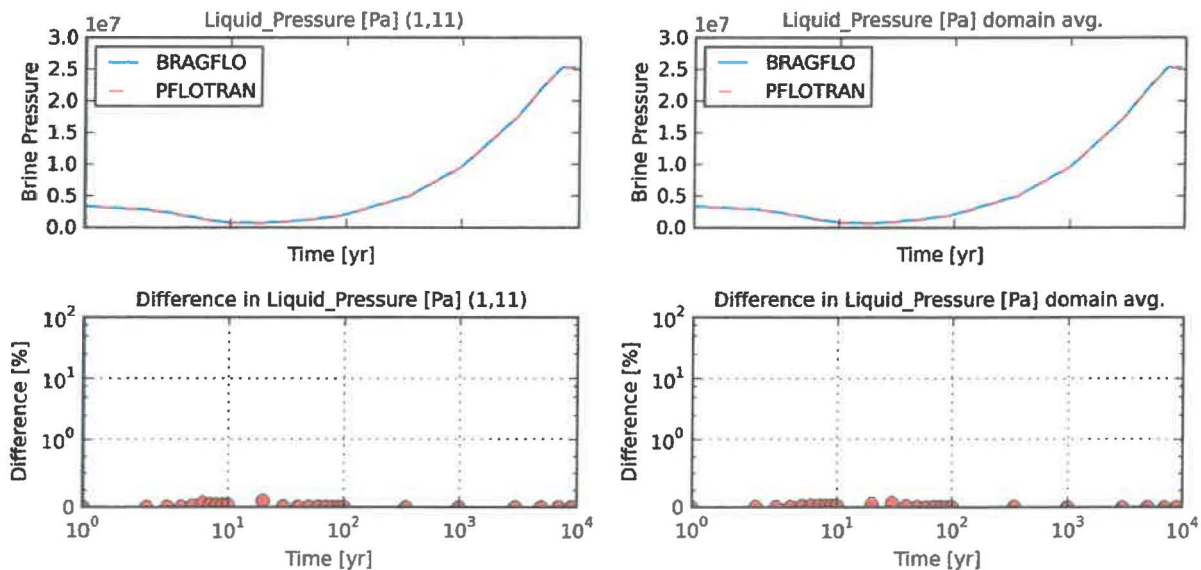
Figure 6.2-18 Test case "6A_ALLGEN" brine pressure [Pa] at cell (1,11) and domain average.
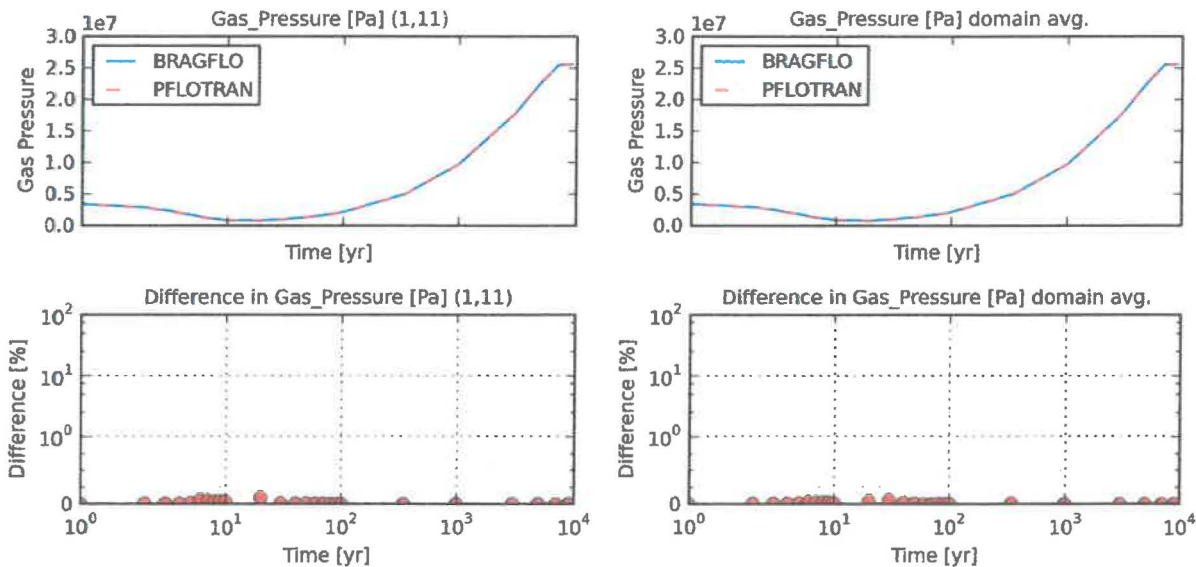
Figure 6.2-19 Test case "6A_ALLGEN" gas pressure [Pa] at cell (1,11) and domain average.
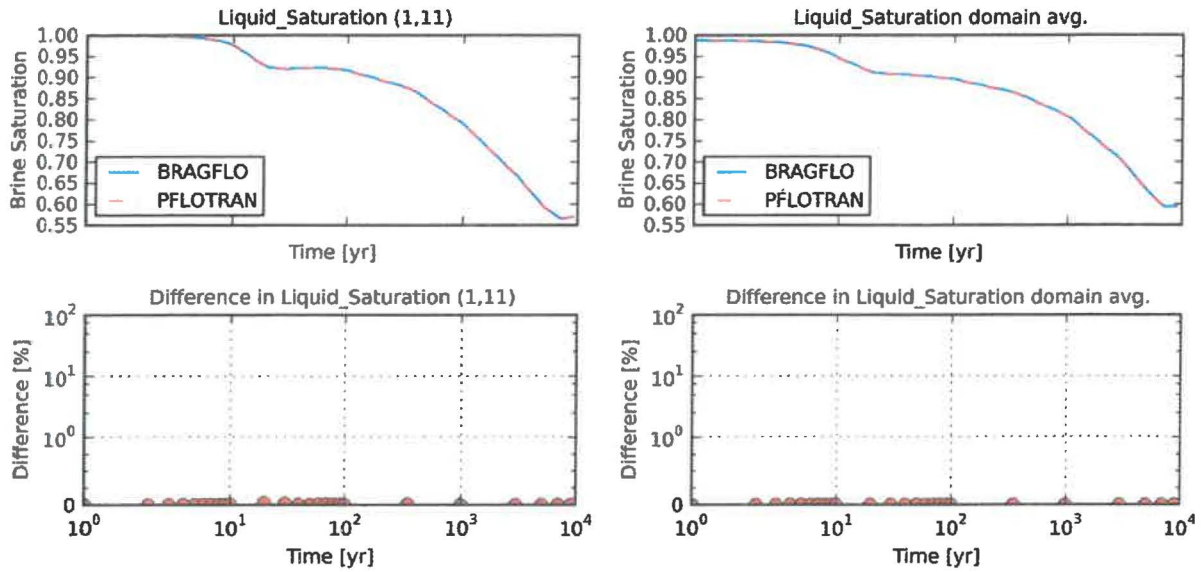
Figure 6.2-20 Test case "6A_ALLGEN" brine saturation at cell (1,11) and domain average.
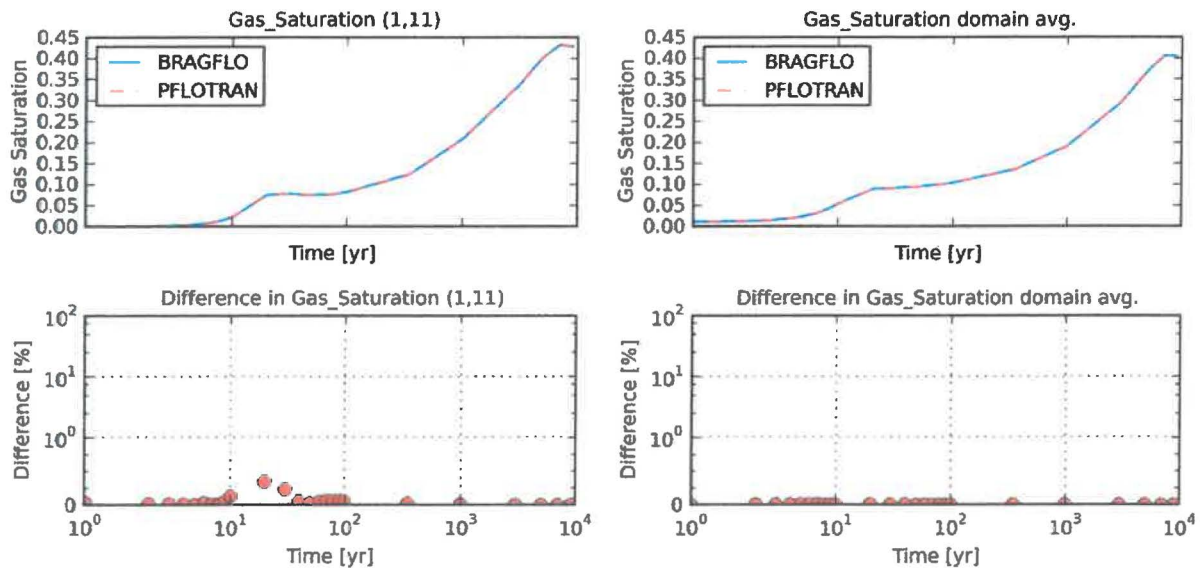
Figure 6.2-21 Test case "6A_ALLGEN" gas saturation at cell (1,11) and domain average.
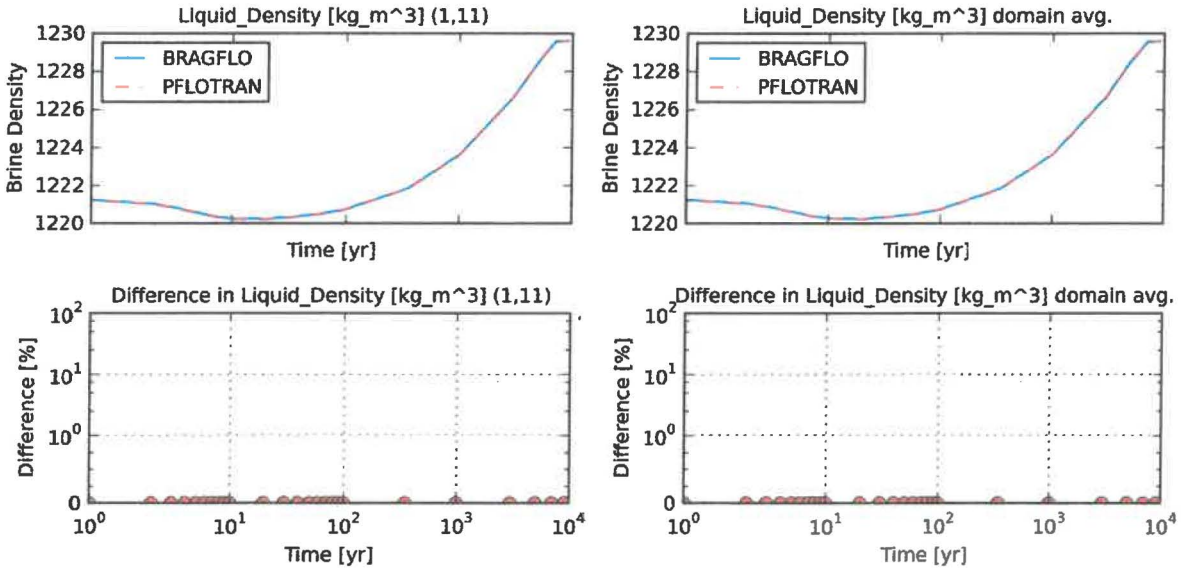
Figure 6.2-22 Test case "6A_ALLGEN" brine density [kg/m^3] at cell (1,11) and domain average.
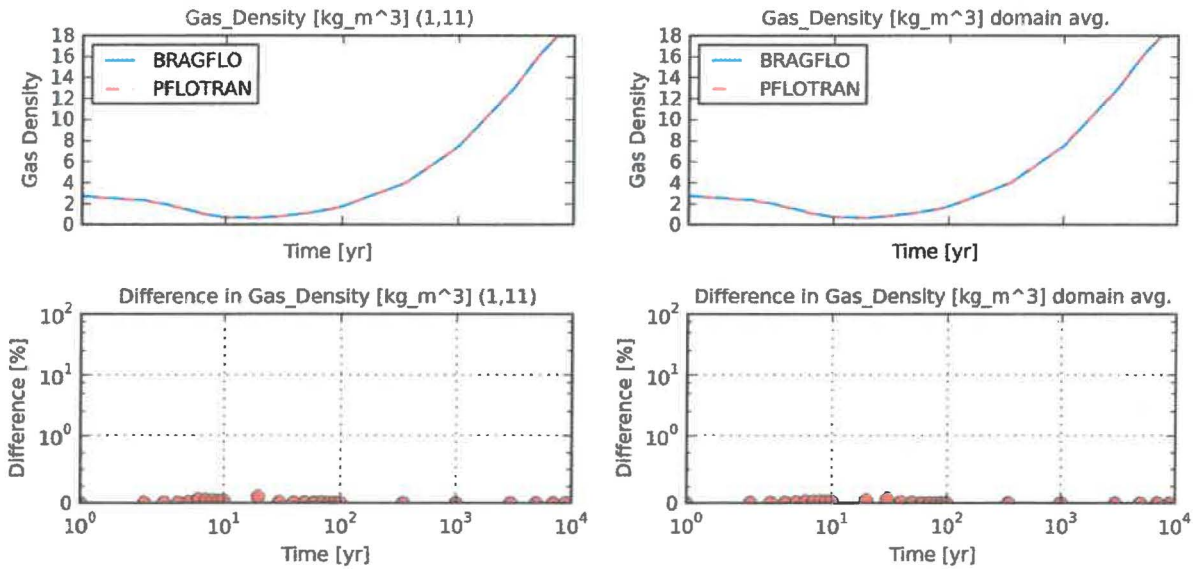
Figure 6.2-23 Test case "6A_ALLGEN" gas density [kg/m^3] at cell (1,11) and domain average.
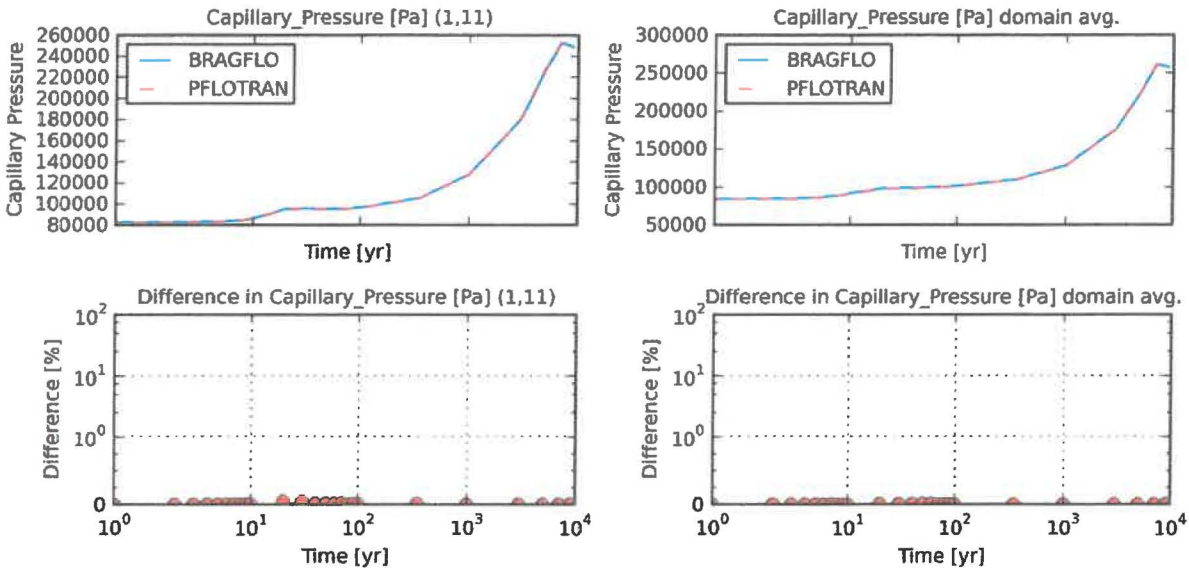
Figure 6.2-24 Test case "6A_ALLGEN" capillary pressure [Pa] at cell (1,11) and domain average.
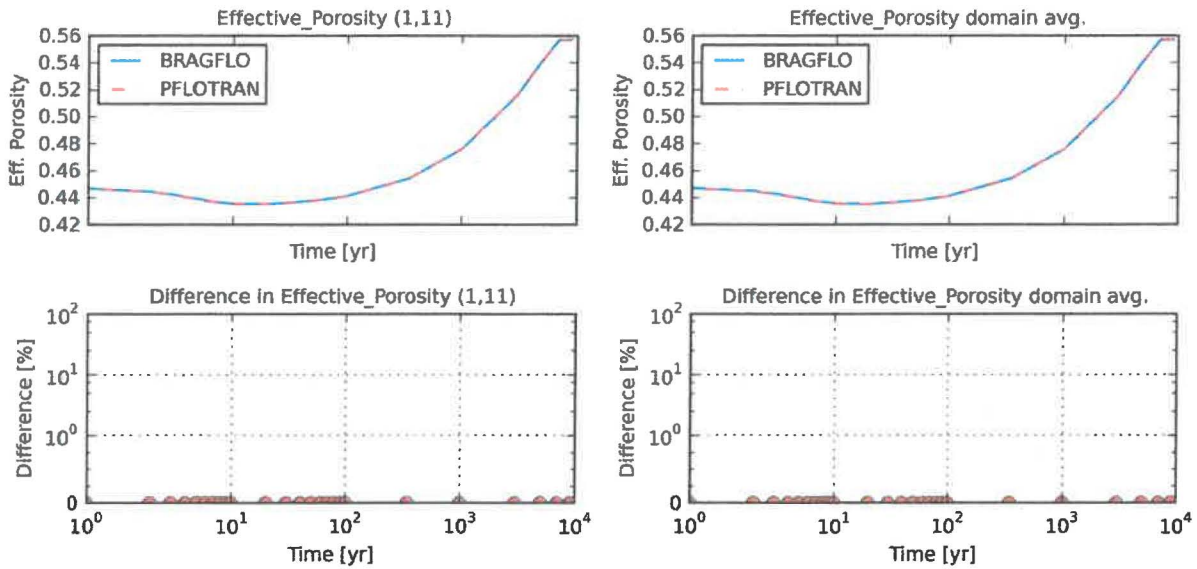
Figure 6.2-25 Test case "6A_ALLGEN" porosity at cell (1,11) and domain average.

6.2.3 Conclusions

In these test cases, gas generation ceases at approximately 8000 yr, at which time gas pressure levels off in the domain. Both BRAGFLO and PFLOTRAN predict the same behavior, and the gas generation/brine consumption chemistry process models produce nearly identical results in the multi-cell domain throughout each of the 10,000 yr simulations. Less than 0.30% difference is observed in all plots (Figure 6.2-1 through Figure 6.2-25) regardless of the number of cells included in the waste area and generating gas. Relative to the FY 2017 results the comparison is

improved, especially for the "6A_ALLGEN" case, which had more than 30% relative difference in brine pressure (Zeitler et al. 2017). This test case exemplifies the impact that: (1) full coupling, (2) identical order of calculations and smoothing for species reaction rates, and (3) identical solution controls, have on the comparison of gas generation rates between the two simulators.

6.3   Test Group #2: 2-D Creep Closure

6.3.1 Purpose and Setup

Three test cases are presented that compare the creep closure process models between BRAGFLO and PFLOTRAN. The process models used in PFLOTRAN include: CREEP_CLOSURE, KRP4, WIPP_SOURCE_SINK, RKS.

These three test cases consist of a 2-D domain subject to creep closure simulated using a porosity-surface developed for WIPP PA that relates porosity to liquid pressure and time after closure. The 50-m × 3.96-m domain consists of 15 cells (5 × 3 grid) with homogeneous material properties. Initial liquid pressure is 1.28039×10^5 Pa and initial liquid saturation is 0.065 throughout the model domain for two of the test case and 0.65 for one of the test cases. All boundaries have no-flow boundary conditions. The simulation duration was specified as 10,000 yr. A representative sample of the problem domain is provided in Figure 6.3-1 for the "6B" baseline case.
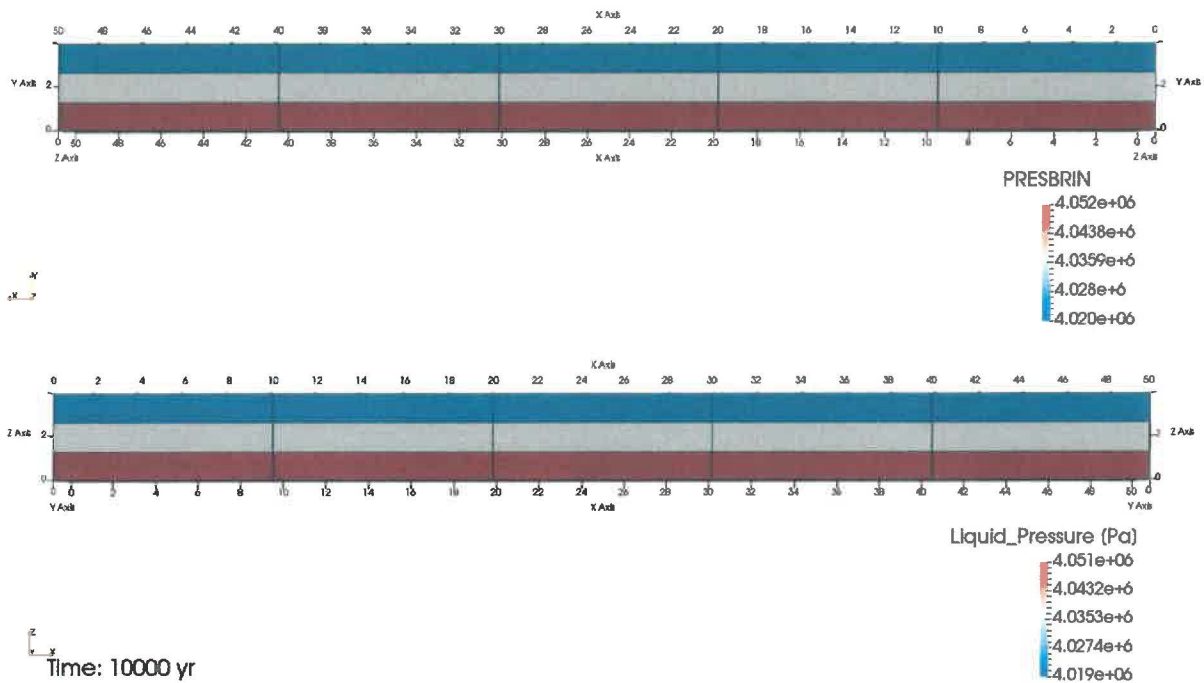
Figure 6.3-1 Test Case "6B" Model Domain (BRAGFLO top, PFLOTRAN bottom).

In the first test case ("6B")[14] creep closure acts alone without a source of gas. In the second test case ("6B_WGAS")[15] gas generation in the center cell of the domain is simulated with the WIPP_SOURCE_SINK model while creep closure is allowed to occur. In the second test case,

---

[14] The "6B" test case refers to the verification test located at pflotran-bragflo-test-cases-stripped/tests_multi_cell/6b/pf_6b.in.

[15] The "6B_WGAS" test case refers to the verification test located at pflotran-bragflo-test-cases-stripped/tests_multi_cell/6b/pf_6b_wgas.in.

reactant concentrations and rate constants are pulled from the PFD analysis, Replicate 1, Scenario 2, Vector 1, and the initial liquid saturation is 0.65 to provide enough water for gas generation to occur. Finally, in the third test case ("6A_WINJ")[16] gas is injected into the center cell of the domain at a constant rate (10^{-9} kg/s) while creep closure is allowed to occur.

6.3.2 Results

6.3.2.1 Test Case "6B"
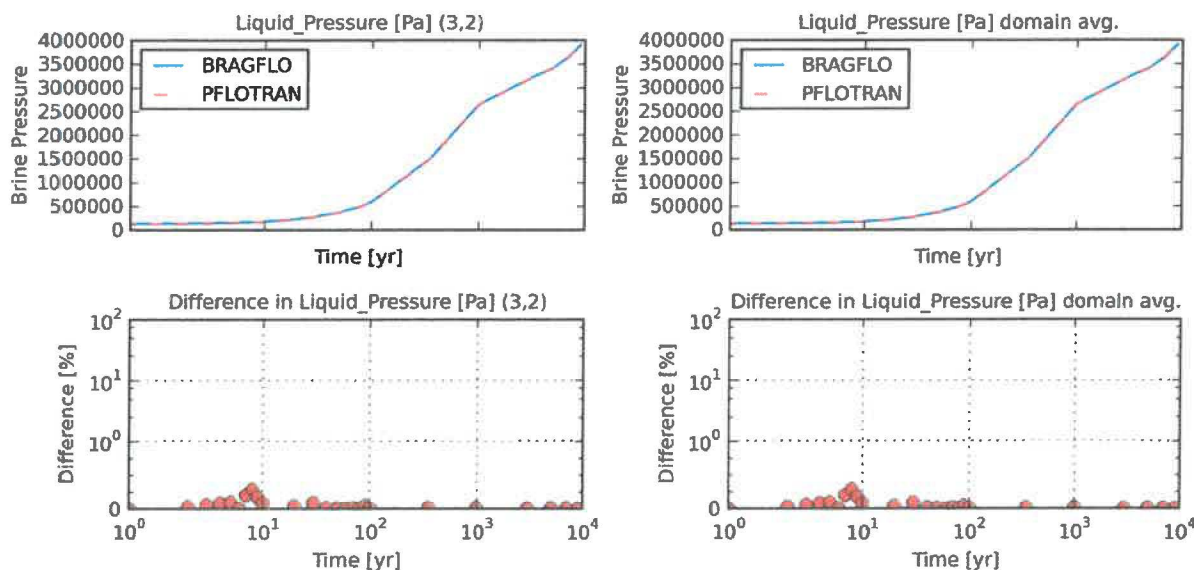
Figure 6.3-2 Test case "6B" brine pressure [Pa] at cell (3,2) and domain average.

---

[16] The "6B_WINJ" test case refers to the verification test located at pflotran-bragflo-test-cases-stripped/tests_multi_cell/6b/pf_6b_winj.in.
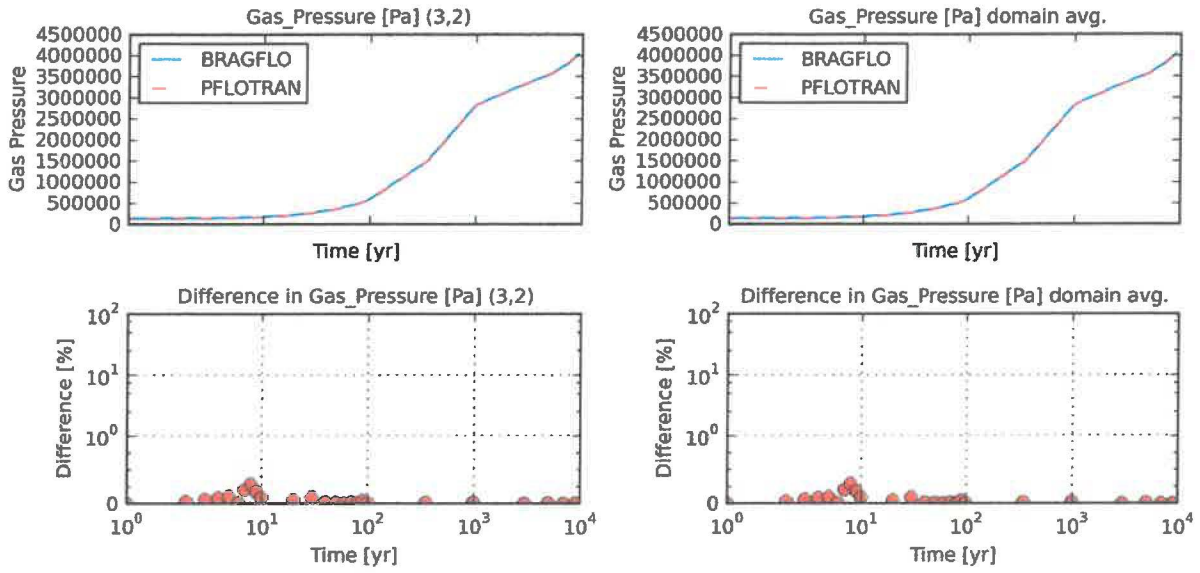
Figure 6.3-3 Test case "6B" gas pressure [Pa] at cell (3,2) and domain average.

Figure 6.3-4 Test case "6B" brine saturation at cell (3,2) and domain average.

Figure 6.3-5 Test case "6B" gas saturation at cell (3,2) and domain average.
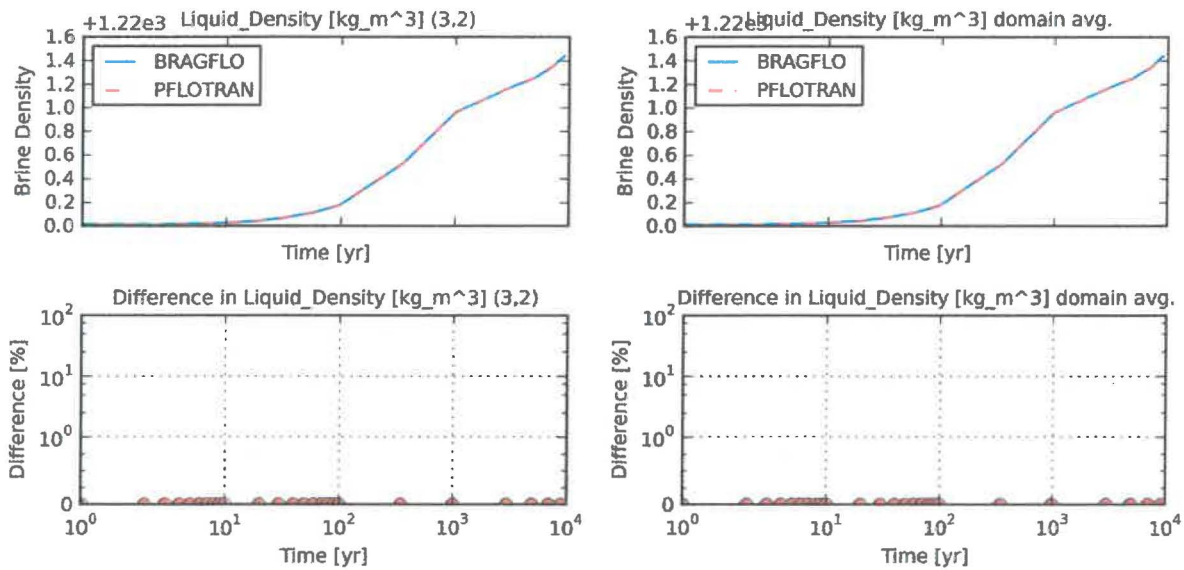
Figure 6.3-6 Test case "6B" brine density [kg/m³] at cell (3,2) and domain average.
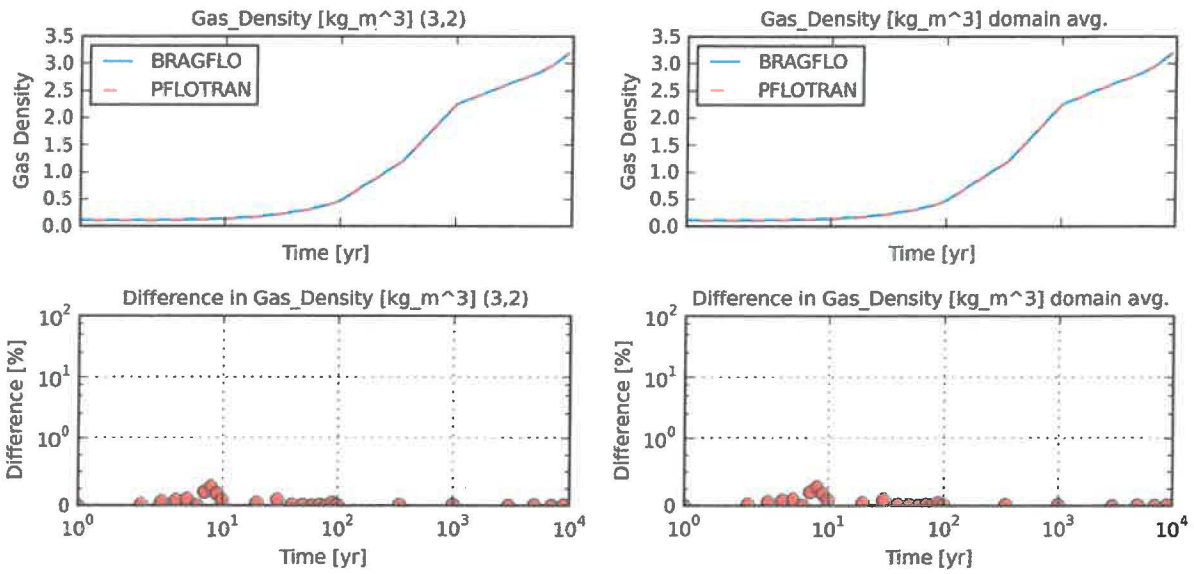
Figure 6.3-7 Test case "6B" gas density [kg/m^3] at cell (3,2) and domain average.
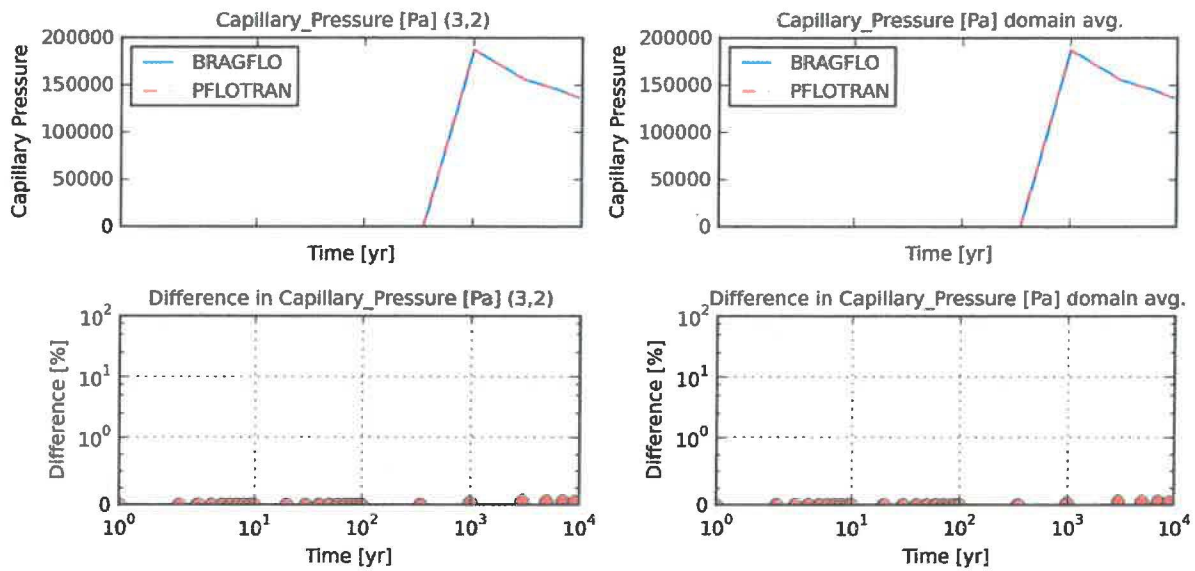
Figure 6.3-8 Test case "6B" capillary pressure [Pa] at cell (3,2) and domain average.
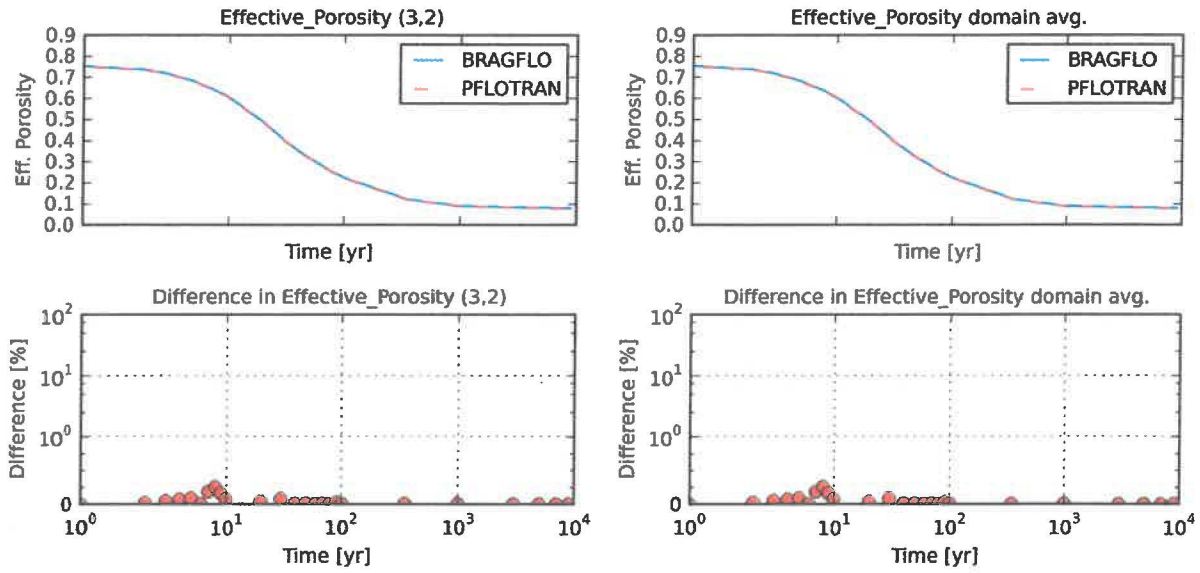
Figure 6.3-9 Test case "6B" porosity at cell (3,2) and domain average.

6.3.2.2 Test Case "6B_WGAS"
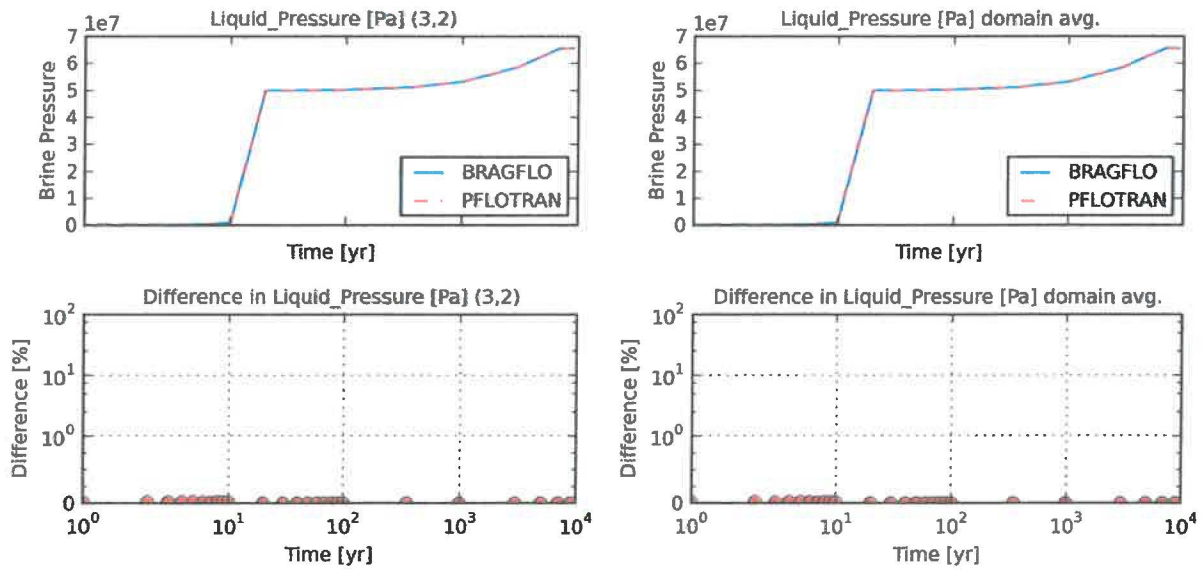
Figure 6.3-10 Test case "6B_WGAS" brine pressure [Pa] at cell (3,2) and domain average.
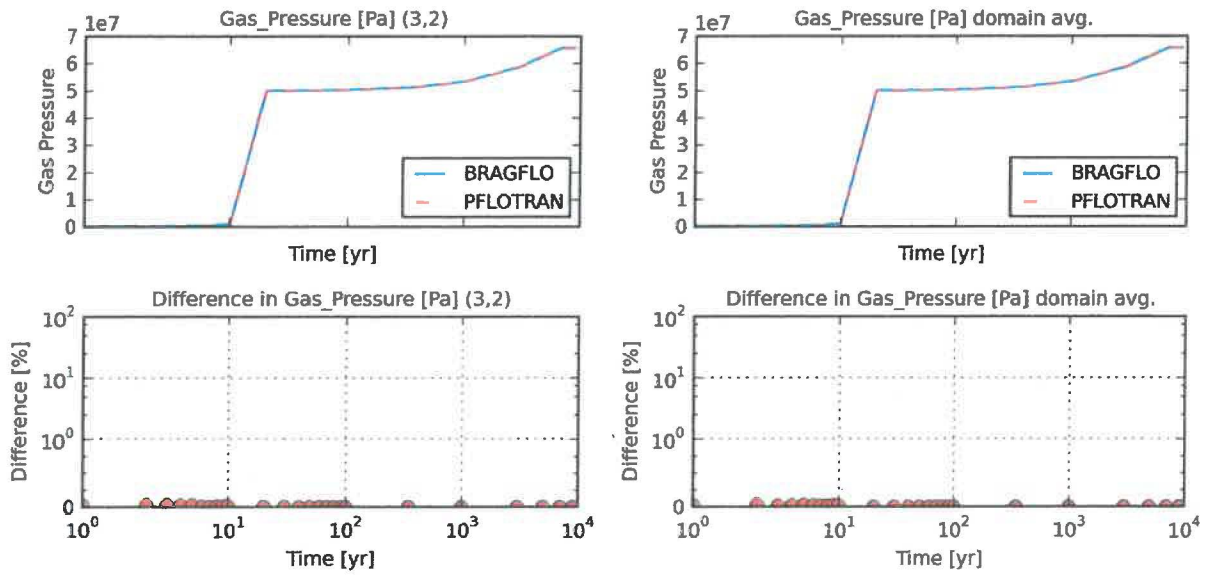
Figure 6.3-11 Test case "6B_WGAS" gas pressure [Pa] at cell (3,2) and domain average.
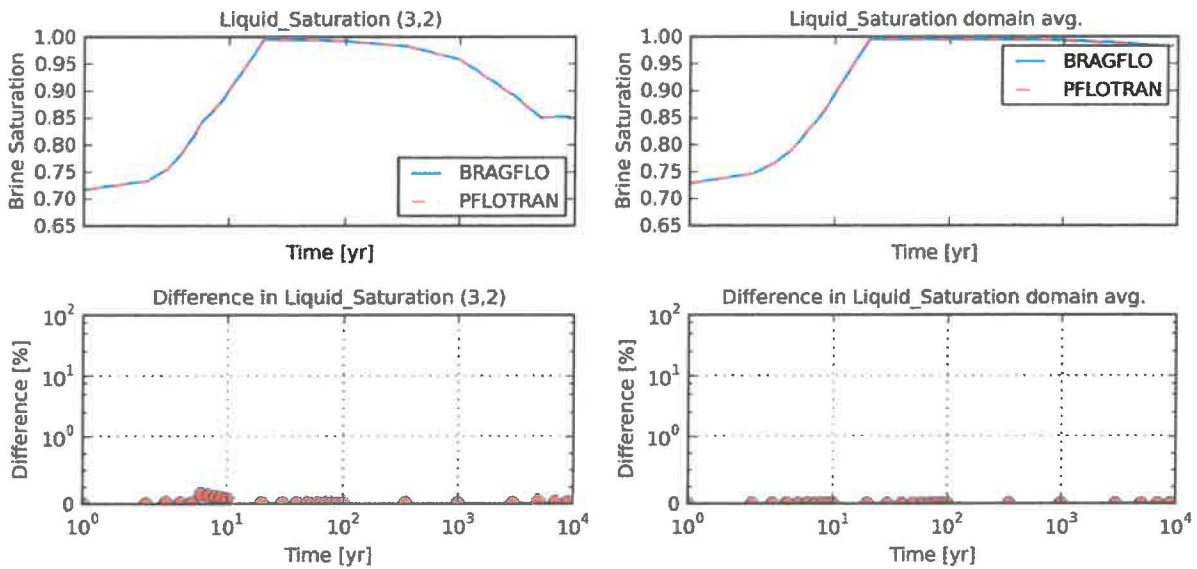
Figure 6.3-12 Test case "6B_WGAS" brine saturation at cell (3,2) and domain average.
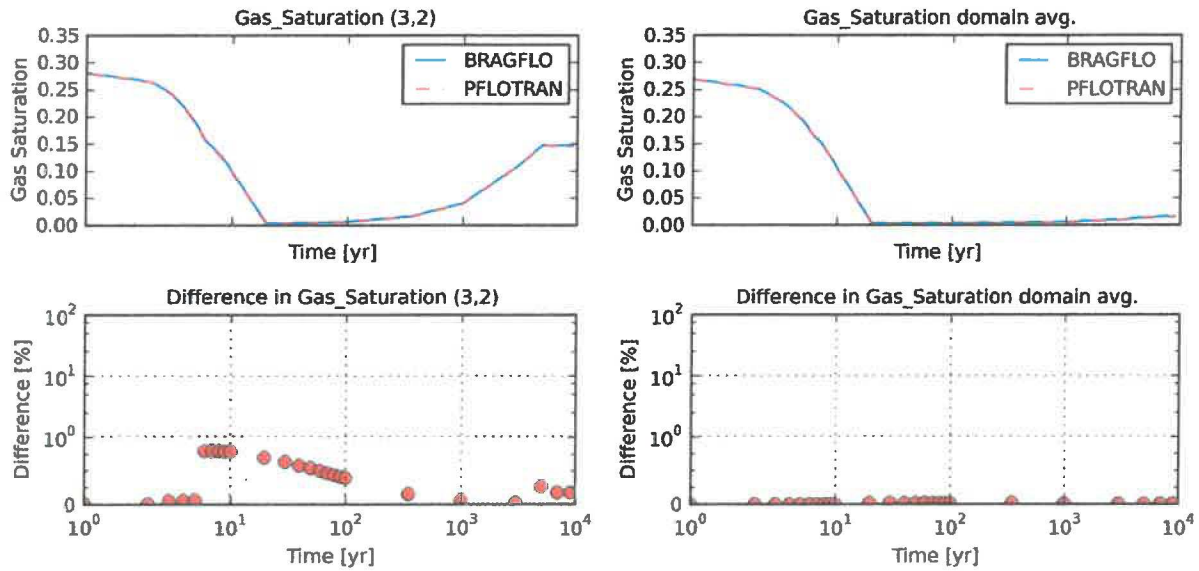
Figure 6.3-13 Test case "6B_WGAS" gas saturation at cell (3,2) and domain average.
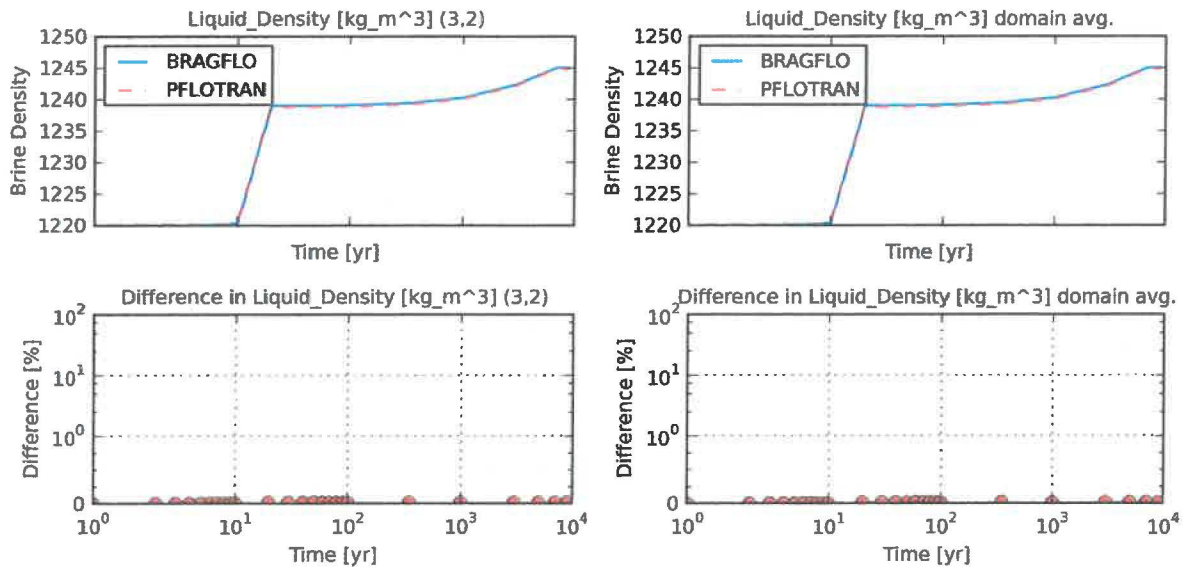
Figure 6.3-14 Test case "6B_WGAS" brine density [kg/m³] at cell (3,2) and domain average.
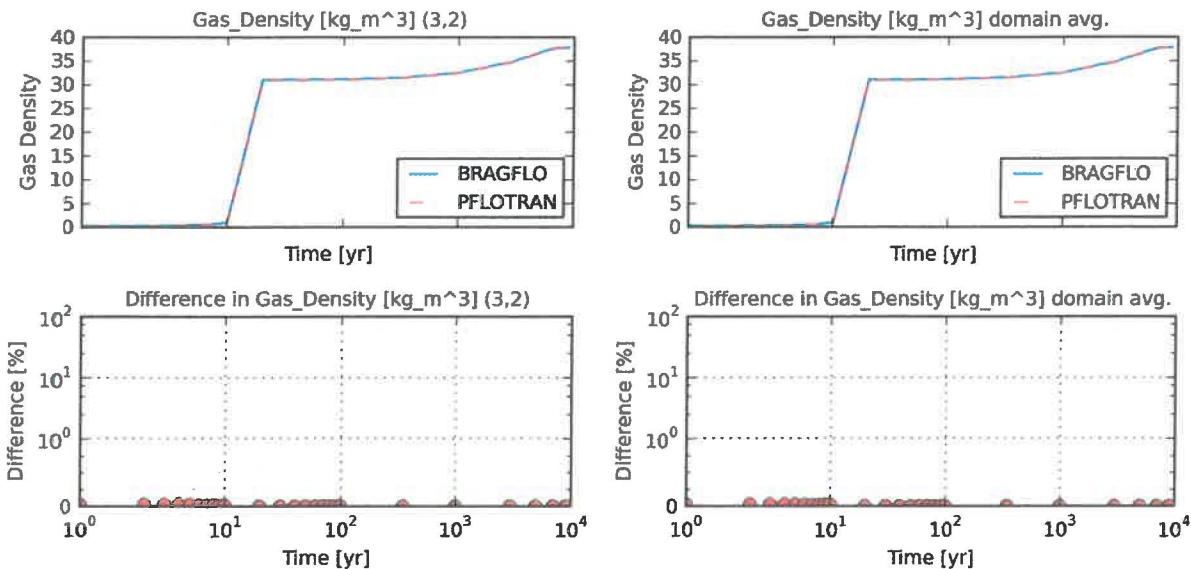
Figure 6.3-15 Test case "6B_WGAS" gas density [kg/m3] at cell (3,2) and domain average.
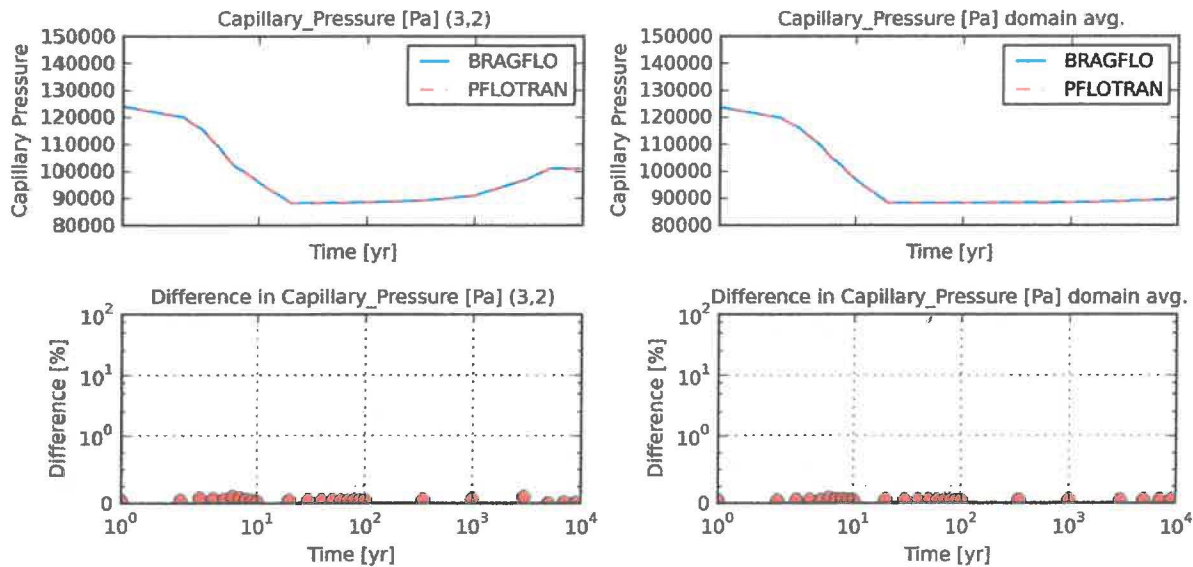
Figure 6.3-16 Test case "6B_WGAS" capillary pressure [Pa] at cell (3,2) and domain average.
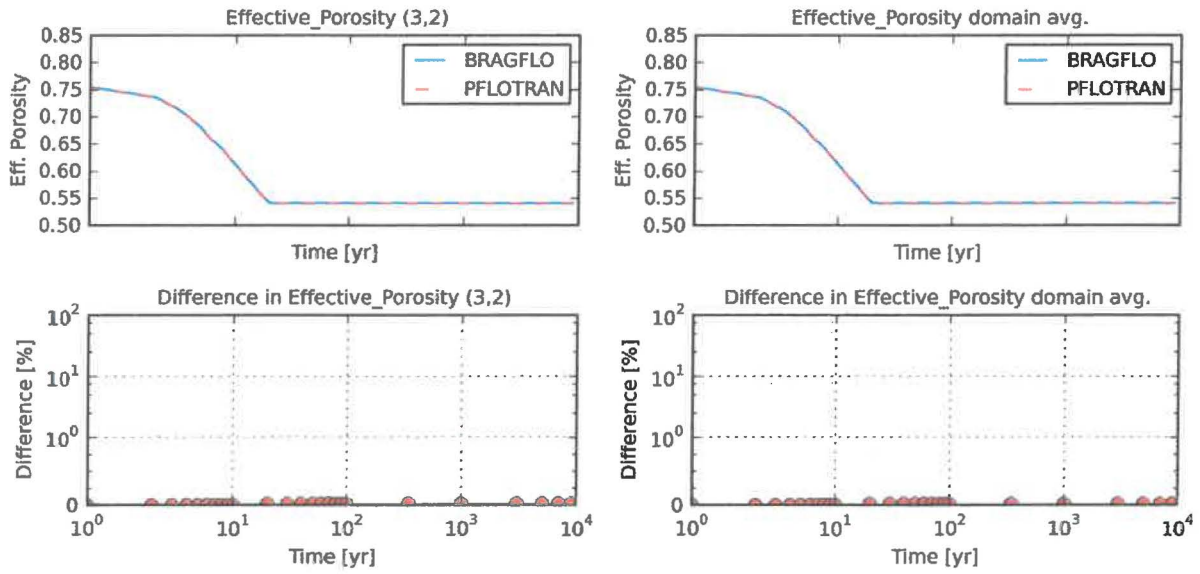
Figure 6.3-17 Test case "6B_WGAS" porosity at cell (3,2) and domain average.

6.3.2.3   Test Case "6B_WINJ"
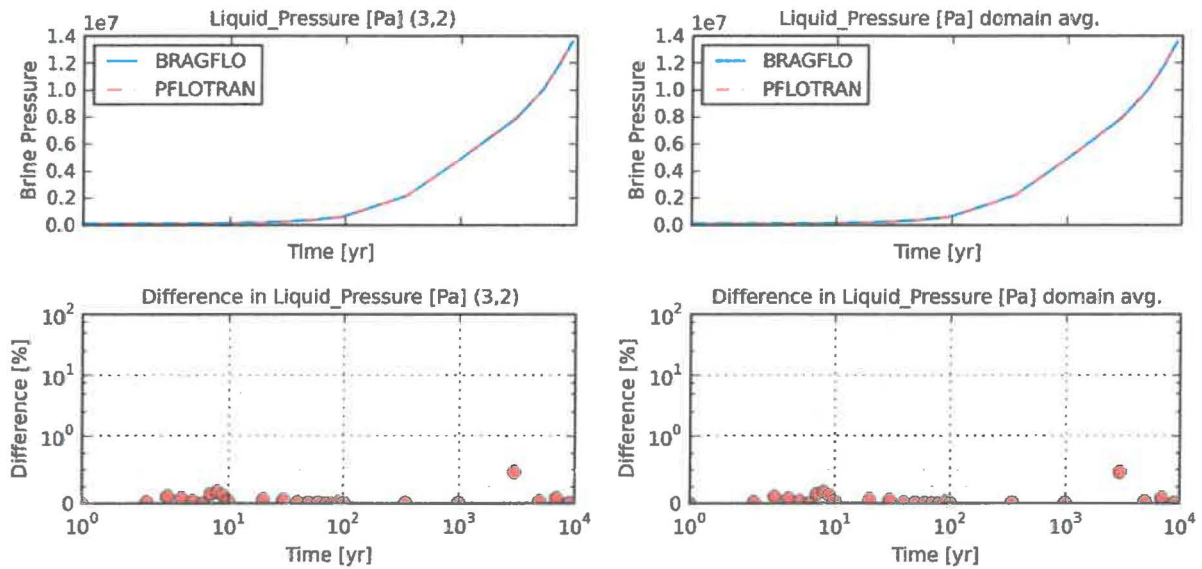
Figure 6.3-18 Test case "6B_WINJ" brine pressure [Pa] at cell (3,2) and domain average.
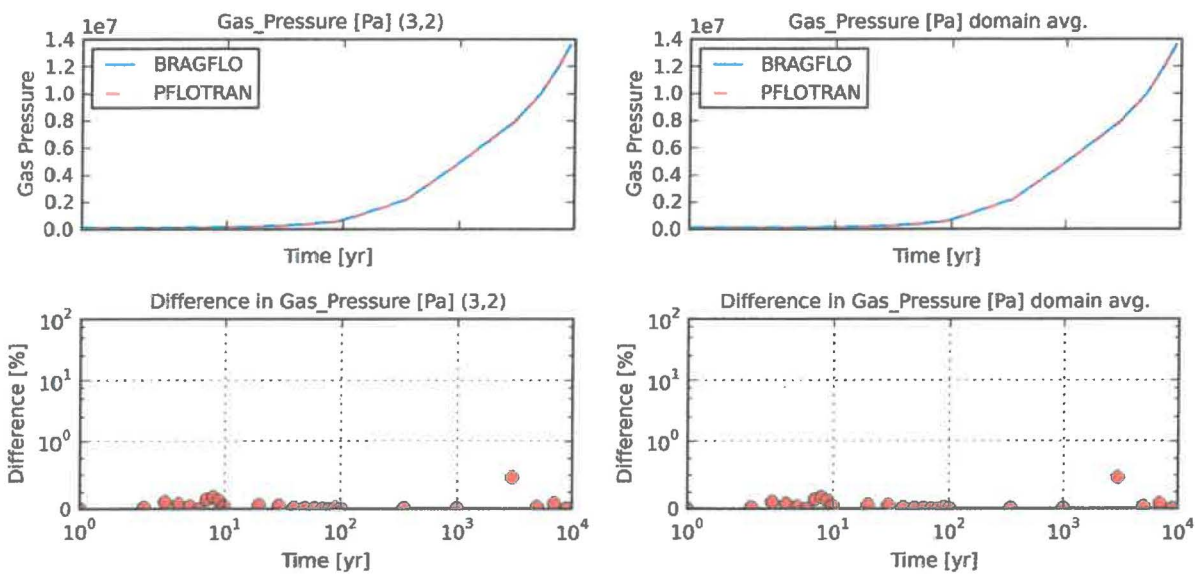
Figure 6.3-19 Test case "6B_WINJ" gas pressure [Pa] at cell (3,2) and domain average.
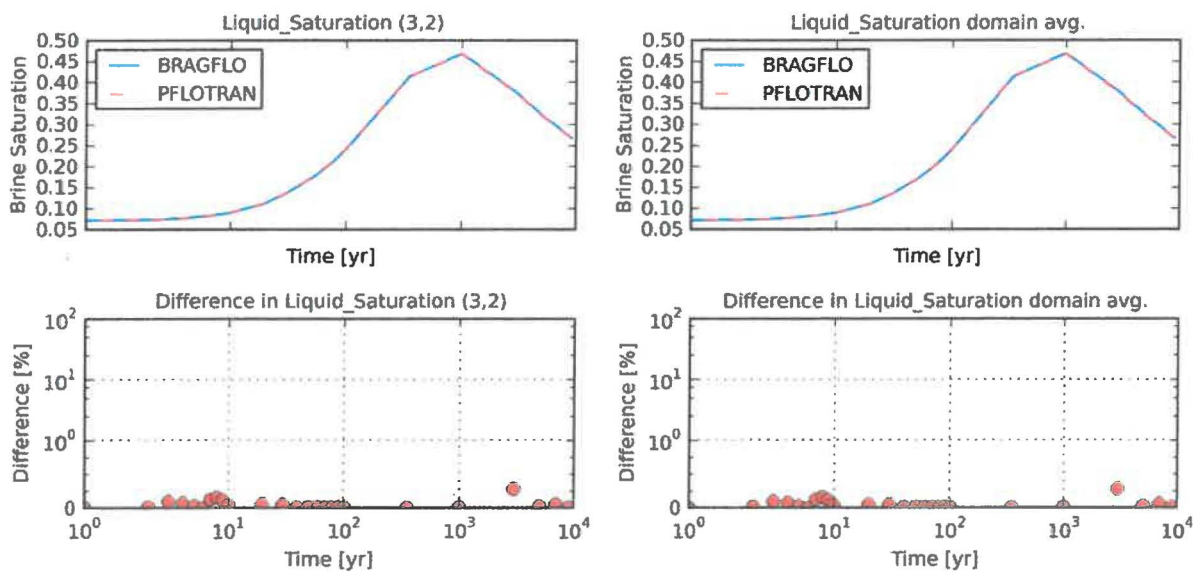
Figure 6.3-20 Test case "6B_WINJ" brine saturation at cell (3,2) and domain average.
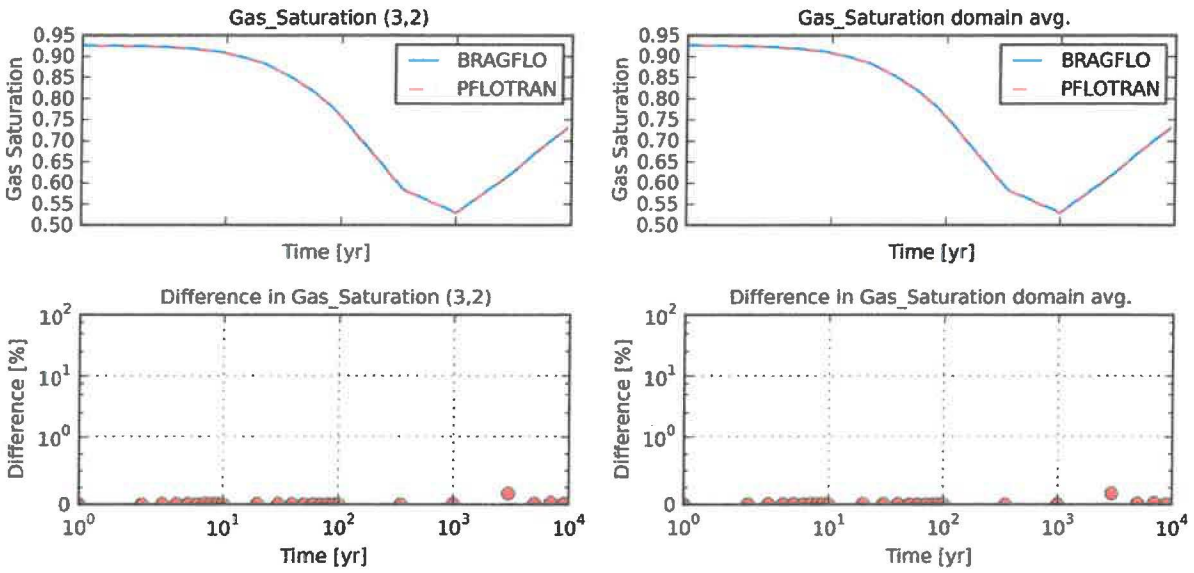
Figure 6.3-21 Test case "6B_WINJ" gas saturation at cell (3,2) and domain average.
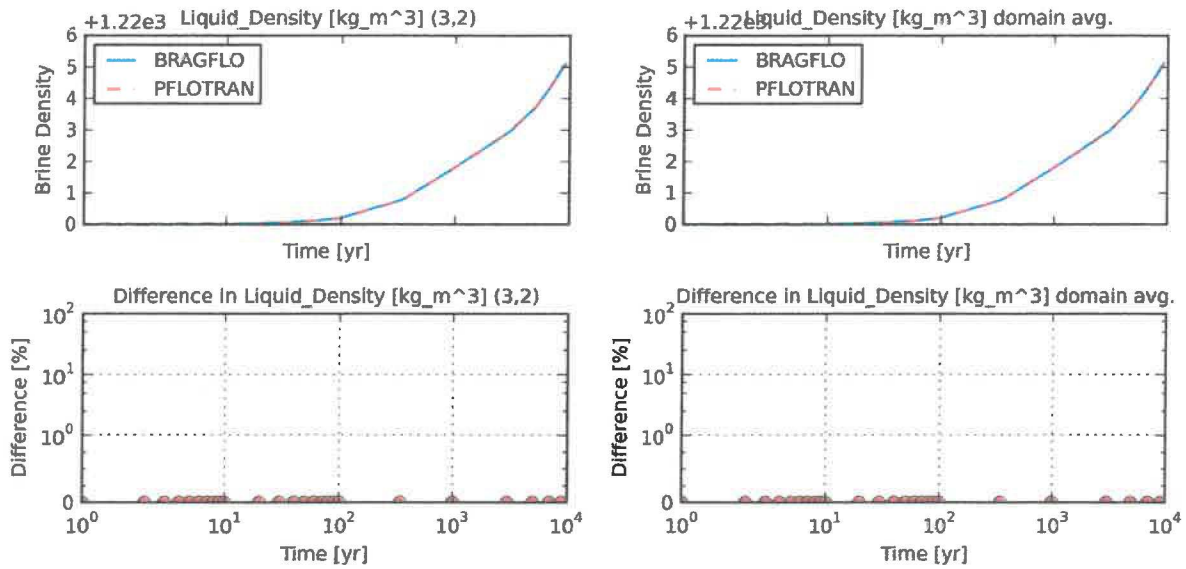
Figure 6.3-22 Test case "6B_WINJ" brine density [kg/m^3] at cell (3,2) and domain average.
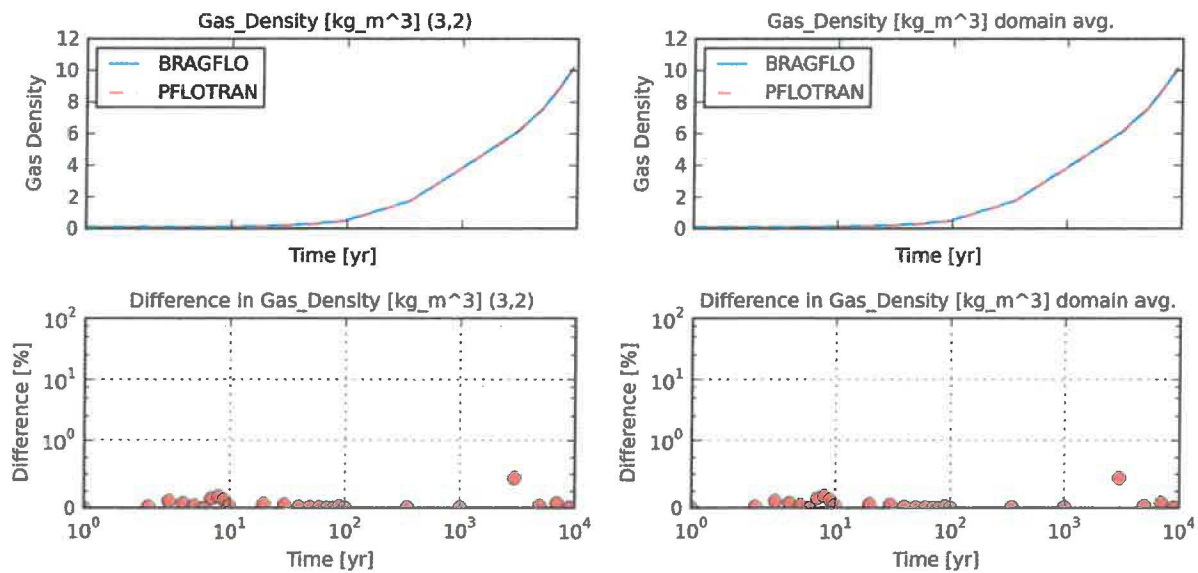
Figure 6.3-23 Test case "6B_WINJ" gas density [kg/m^3] at cell (3,2) and domain average.
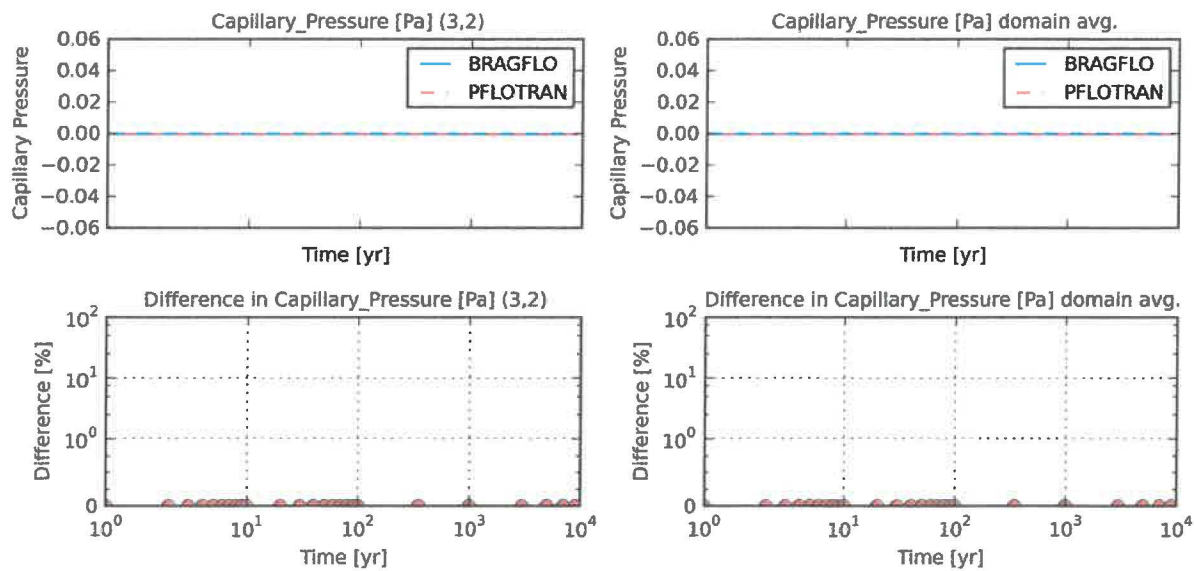
Figure 6.3-24 Test case "6B_WINJ" capillary pressure [Pa] at cell (3,2) and domain average.
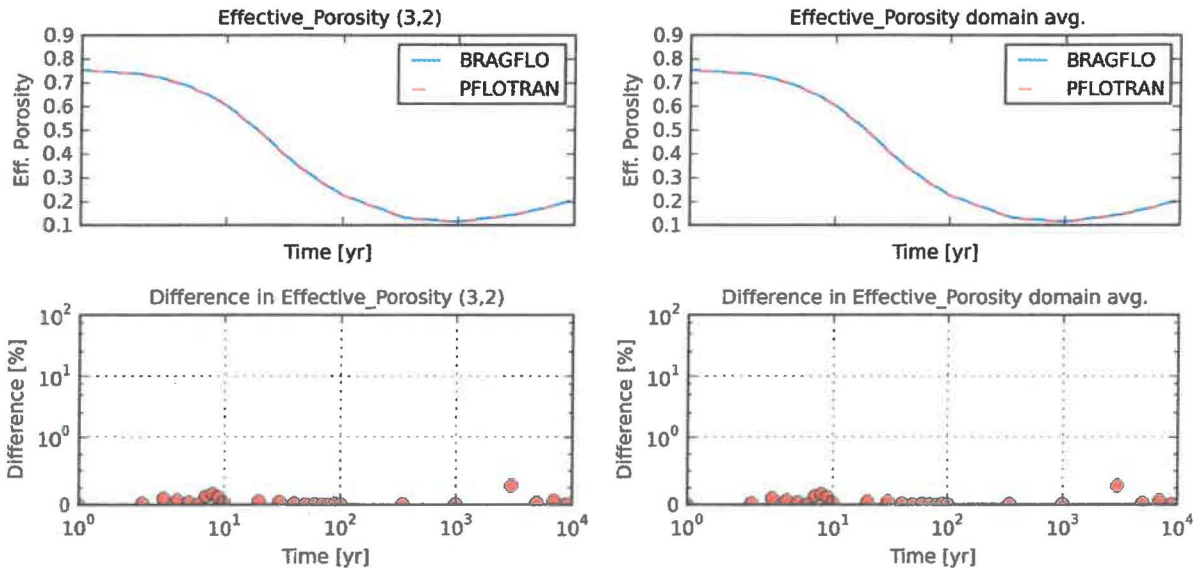
Figure 6.3-25 Test case "6B_WINJ" porosity at cell (3,2) and domain average.

6.3.3 Conclusions

The creep closure process model compares well between BRAGFLO and PFLOTRAN. When creep closure acts alone, in concert with gas generation/brine consumption, or with gas injection, the results compare well (< 1.0% difference).

6.4   Test Group #3: 1-D Fracture

6.4.1 Purpose and Setup

One test case is presented that compares marker bed fracturing models between BRAGFLO and PFLOTRAN, and the effect on pressure and saturation resulting from the dynamically varying porosity and permeability introduced by fracturing. This test case uses Marker Bed 138 material properties from the PFD Analysis Replicate 1, Vector 1. The process models used in PFLOTRAN include: WIPP-FRACTURE, KRP4, RKS.

This test case consists of a one-dimensional domain subject to (elastic) fracturing driven by liquid injection in the 3rd cell from the left at a rate of 1.0×10^{-7} kg/s for 5,000 years followed by liquid extraction from the same cell at a rate of 5.0×10^{-8} kg/s for the following 5,000 years. The 100-m $\times$ 10-m domain consists of 10 cells (10 $\times$ 1 grid). Initial conditions are 1 MPa liquid pressure in the left 5 cells and 2 MPa liquid pressure in the right 5 cells, with a liquid saturation of 1 throughout the model domain. All boundaries have no-flow boundary conditions. Fracturing is initiated in a grid cell when pressure climbs to 0.2 MPa above the initial pressure. No further fracturing occurs at pressures greater than 4.0 MPa above the initial pressure. A representative sample of the problem domain is provided in Figure 6.4-1 for the "6C"[17] case.
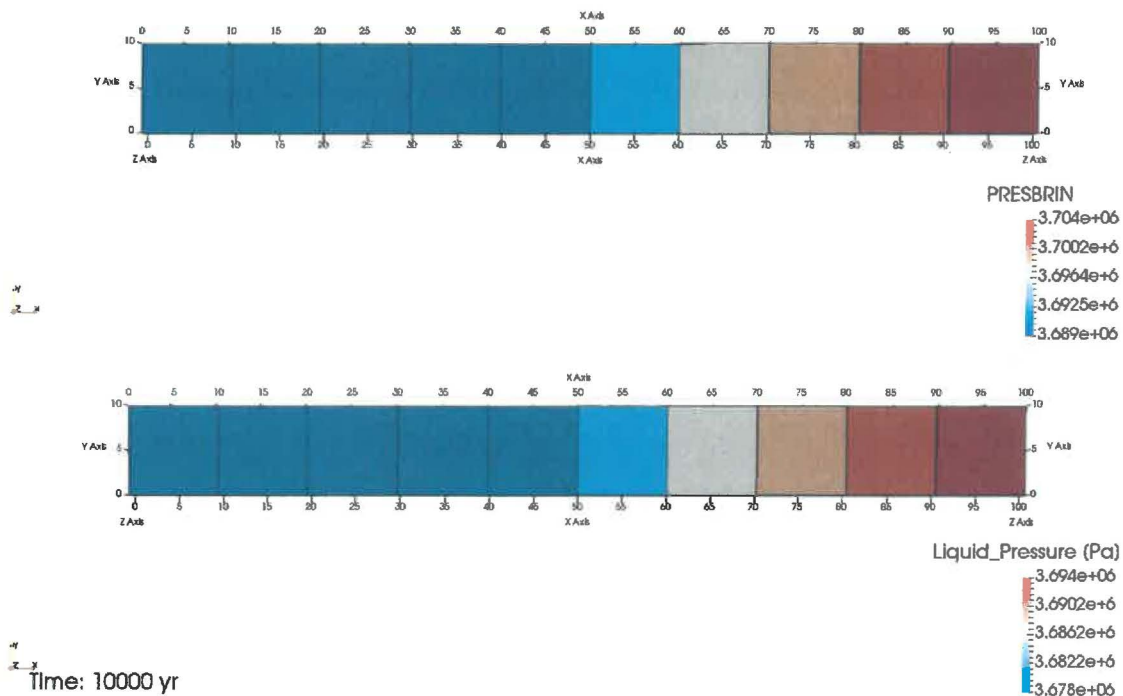
Figure 6.4-1 Test Case "6C" Model Domain (BRAGFLO top, PFLOTRAN bottom).

---

[17] The "6C" test case refers to the verification test located at pflotran-bragflo-test-cases-stripped/tests_multi_cell/6c/pf_6c.in.

6.4.2   Results

6.4.2.1   Test Case "6C"

Figure 6.4-2 Test case "6C" brine pressure [Pa] at cell (3,1) and domain average.

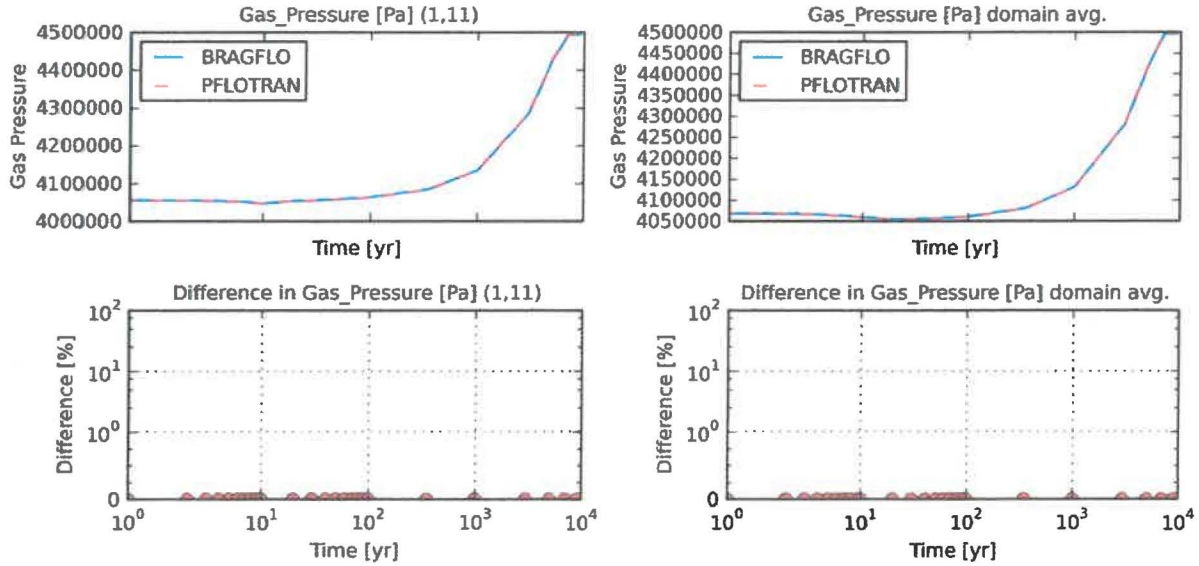

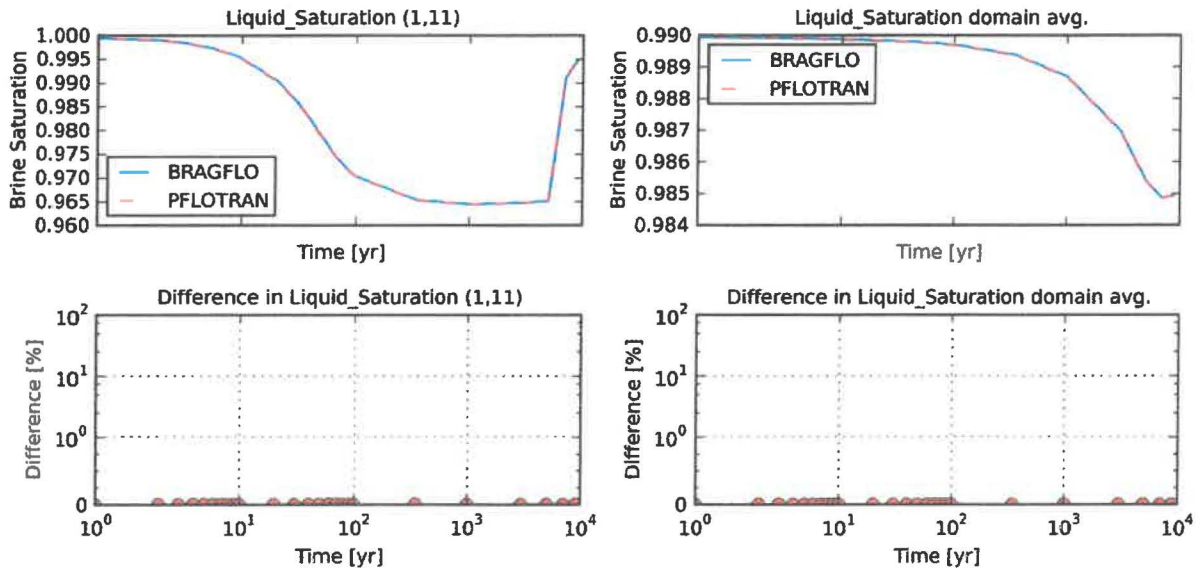Figure 6.4-3 Test case "6C" gas pressure [Pa] at cell (3,1) and domain average.
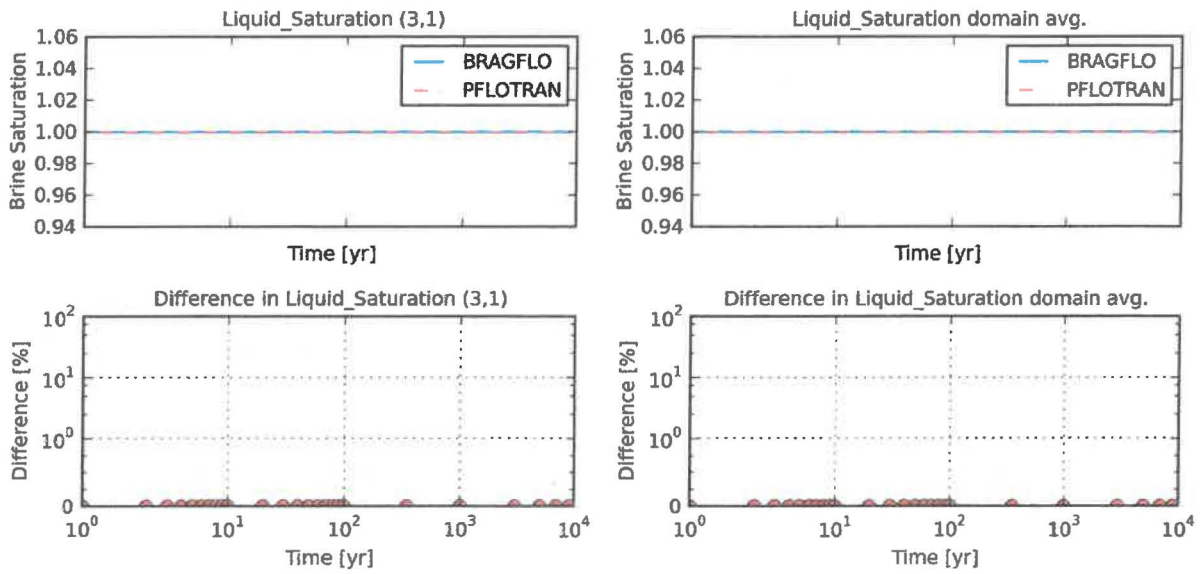
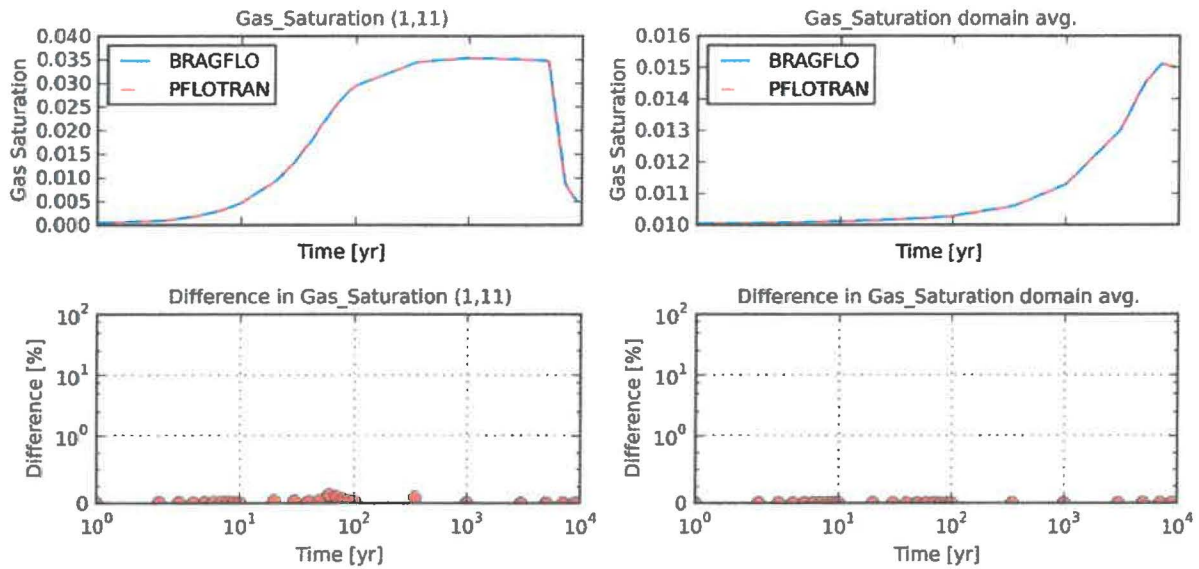Figure 6.4-4 Test case "6C" brine saturation at cell (3,1) and domain average.
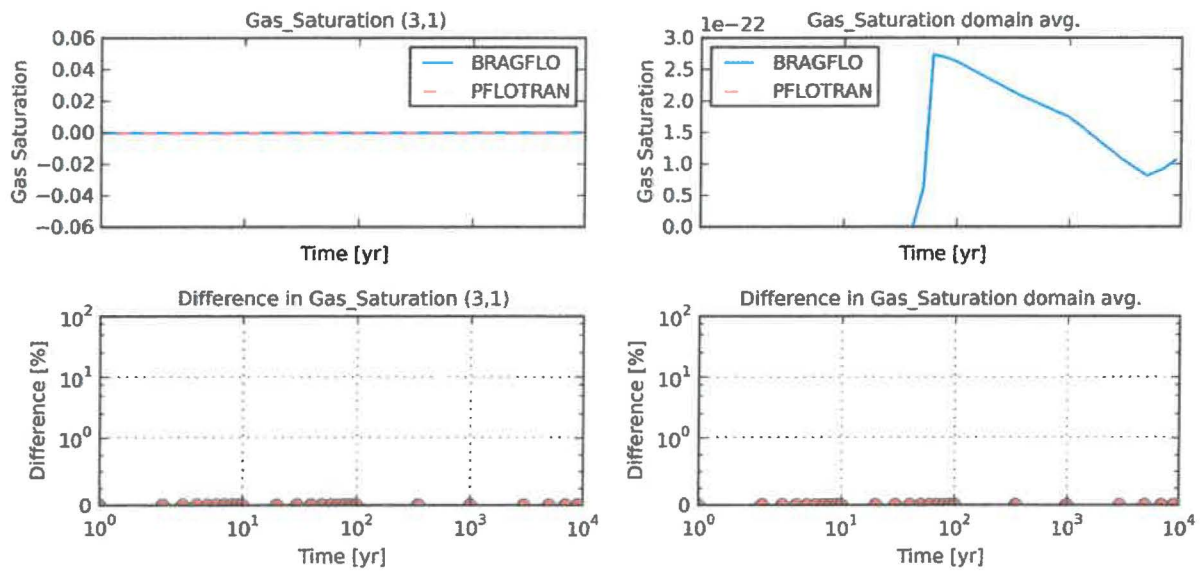
Figure 6.4-5 Test case "6C" gas saturation at cell (3,1) and domain average.
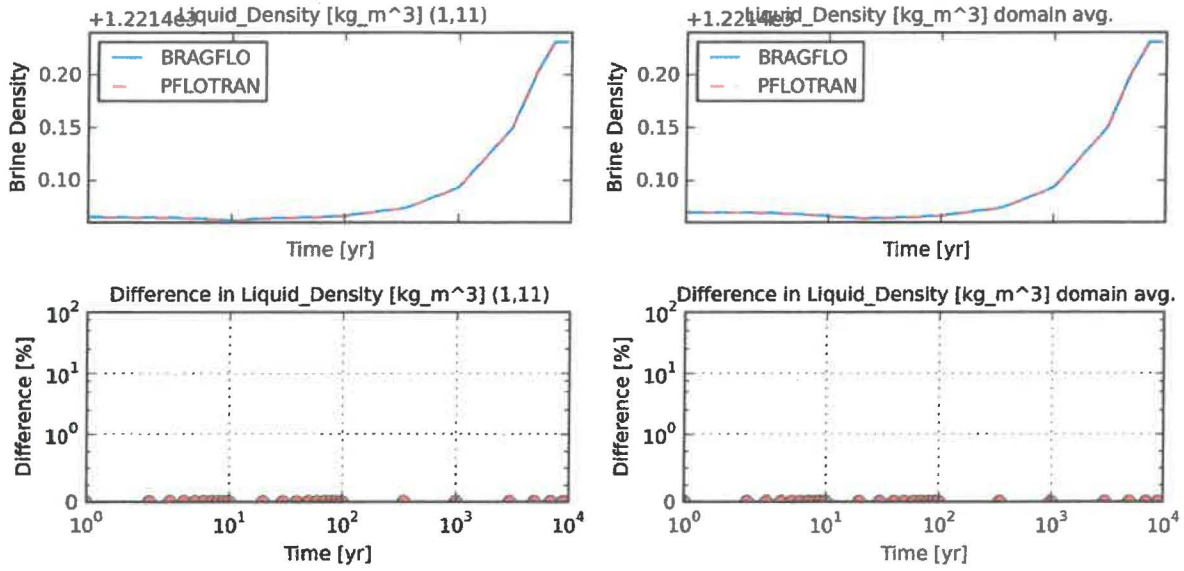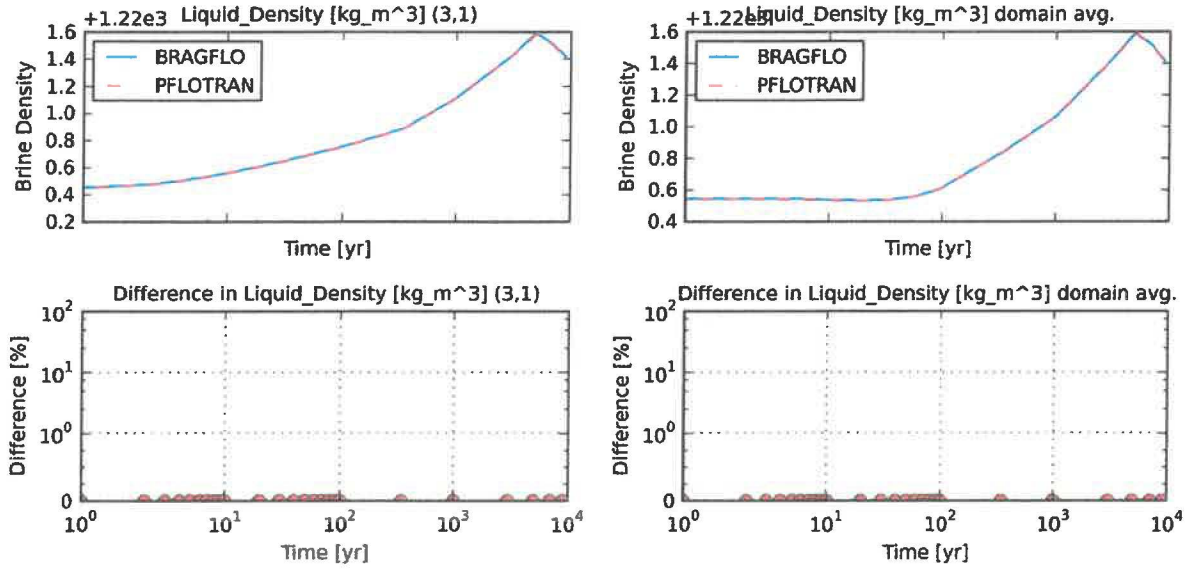
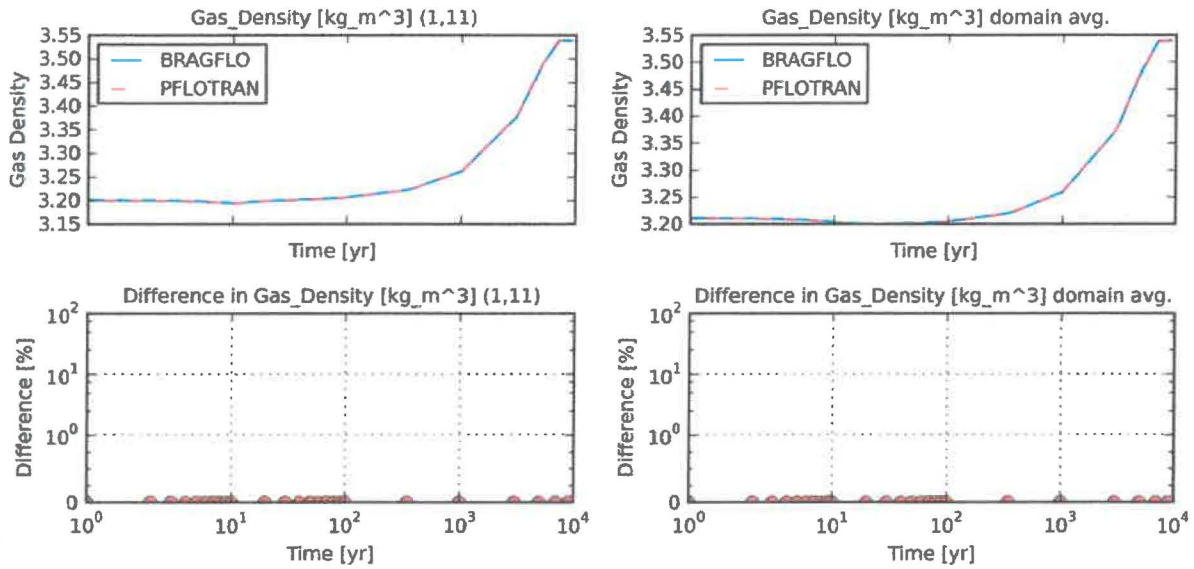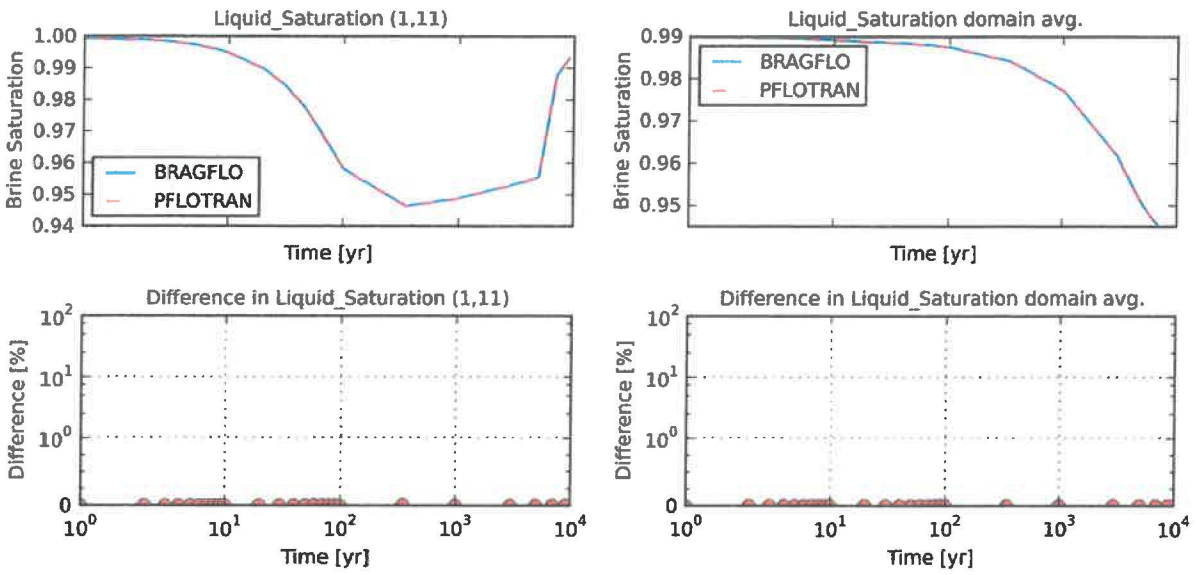Figure 6.4-6 Test case "6C" brine density [kg/m³] at cell (3,1) and domain average.
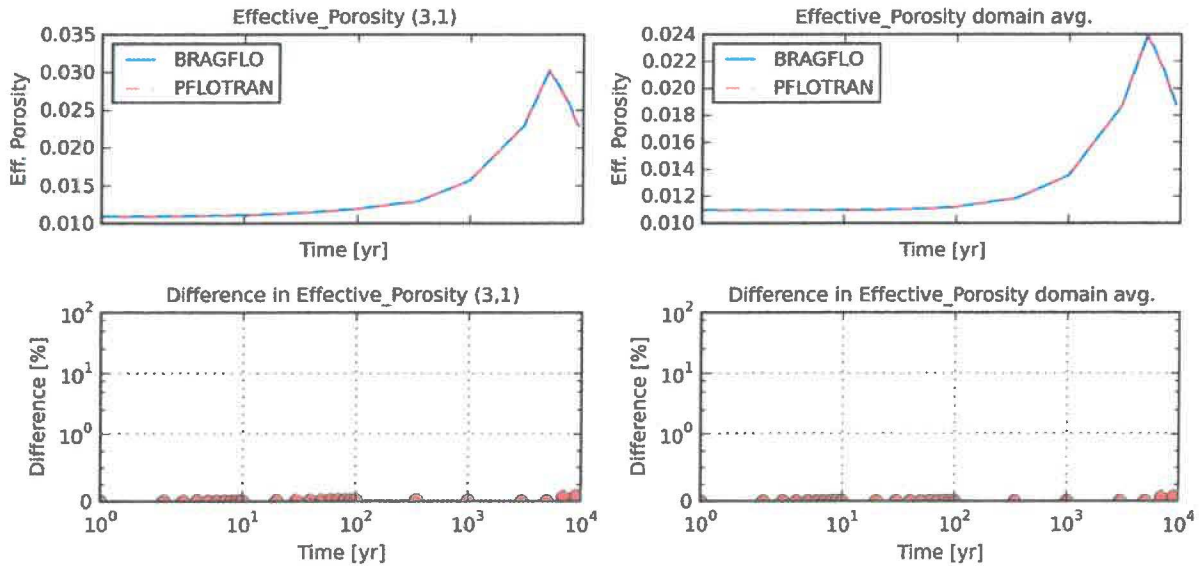
Figure 6.4-7 Test case "6C" porosity at cell (3,1) and domain average.

6.4.3 Conclusions

Due to the injection and then extraction of brine that raises and lowers pressure, fracture induces an increase and then decrease in porosity with time, as expected. The marker bed fracture process models between BRAGFLO and PFLOTRAN compare well, with a maximum difference of ~0.25%.

7 *Miniature Flared Grid Testing*

Two multi-cell tests were developed to test the implementation of ALPHA and ELEVATION in PFLOTRAN. These test problems use 2-D flared grids similar to that used in the current WIPP PA, in which cells adjacent to each other in the X direction do not share faces of equal area and may have unequal elevations due to dipping strata. Unequal areas at cell connections are accounted for using grid cell ALPHA parameters in the harmonic average of "transmissibility" (Section 4.4.1). Horizontal differences in elevation are accounted for with a correction to the pressure gradient using grid cell ELEVATION parameters (Section 4.4.2).

The first of the two miniature 2-D flared grid tests is a 5 cell × 3 cell ("5×3") problem with a 1° dip that demonstrates correct implementation of ALPHA and ELEVATION in PFLOTRAN, and demonstrates the functionality of all WIPP PA process models (except material changes) on a flared grid. The second of the two miniature flared grid tests is a 5 cell × 11 cell ("5×11") problem (with no dip) that simulates a borehole intrusion. In addition to providing additional demonstration that ALPHA is correctly implemented in PFLOTRAN, the 5×11 problem verifies that PFLOTRAN calculates the same solution that BRAGFLO does given the numerical challenges associated with abrupt material changes on a flared grid.

Each miniature 2-D flared grid test case includes a PFLOTRAN input deck and a corresponding BRAGFLO input deck that implements the identical simulation. A plotting script that automatically plots each of the test case results is executed as the final step. Parameters used for each test are representative of those employed in WIPP PA, taken from the PFD (see Section 8) parameter set.

7.1 Calculation Details

All BRAGFLO results were produced on the Linux cluster head node (jt.sandia.gov) using the BRAGFLO executable stored at:
- /Archive/pflotran_bragflo_comparison_20170929/executables/bragflo-jt

All PFLOTRAN results were produced on the Linux cluster head node (jt.sandia.gov) using the PFLOTRAN executable stored at:
- /Archive/pflotran_bragflo_comparison_20170929/executables/pflotran-071318

All test input decks, plotting scripts, and results are located on the Linux cluster in the folder:
- /Archive/pflotran_bragflo_comparison_20170929/pflotran-bragflo-test-cases-stripped

Table 7.1-1 shows the values of the solution control parameters used in the miniature flared grid test cases. In the first column ("BRAGFLO"), the BRAGFLO solution control parameter name is given. In the second column ("PFLOTRAN"), the equivalent PFLOTRAN solution control parameter name is given. In the third column ("BLOCK"), the PFLOTRAN input deck block where the solution control keyword is placed is listed. The fourth and fifth columns ("VALUE", "UNIT") show the values and corresponding units of the solution control parameter used.

Percent differences are calculated and plotted as described in Section 5.1.

Table 7.1-1 Solution control parameter values for miniature 2-D flared grid test cases.

BRAGFLO	PFLOTRAN	BLOCK	VALUE	UNIT
FTOLNORM(2)	LIQUID_RESIDUAL_INFINITY_TOL	OPTIONS	1.0d-2	kg/m3

FTOLNORM(1)	GAS_RESIDUAL_INFINITY_TOL	OPTIONS	1.0d-2	kg/m3
EPSNORM(2)	MAX_ALLOW_REL_LIQ_PRES_CHANG_NI	OPTIONS	1.0d-2	-
EPSNORM(1)	MAX_ALLOW_REL_GAS_SAT_CHANGE_NI	OPTIONS	1.0d-3	-
DH(1)	REL_GAS_SATURATION_PERTURBATION	OPTIONS	1.0d-8	-
DH(2)	REL_LIQ_PRESSURE_PERTURBATION	OPTIONS	1.0d-8	-
HMIN(1)	MIN_GAS_SATURATION_PERTURBATION	OPTIONS	1.0d-10	-
HMIN(2)	MIN_LIQ_PRESSURE_PERTURBATION	OPTIONS	1.0d-2	Pa
DTIMEMAX	TIMESTEP_MAXIMUM_GROWTH_FACTOR	TIMESTEPPER	1.25d0	-
SATLIMIT	GAS_SAT_THRESH_FORCE_EXTRA_NI	OPTIONS	1.0d-3	-
DEPLIMIT(1)	GAS_SAT_THRESH_FORCE_TS_CUT	OPTIONS	2.0d-1	-
DDEPMAX(1)	MAX_ALLOW_GAS_SAT_CHANGE_TS	OPTIONS	1.0d0	-
DELTADEPNORM(1)	GAS_SAT_CHANGE_TS_GOVERNOR	OPTIONS	3.0d-1	-
TSWITCH	GAS_SAT_GOV_SWITCH_ABS_TO_REL	OPTIONS	1.0d0	-
DEPLIMIT(2)	MIN_LIQ_PRES_FORCE_TS_CUT	OPTIONS	-1.0d8	Pa
DDEPMAX(2)	MAX_ALLOW_LIQ_PRES_CHANGE_TS	OPTIONS	1.0d7	Pa
DELTADEPNORM(2)	LIQ_PRES_CHANGE_TS_GOVERNOR	OPTIONS	5.0d5	Pa
P_SCALE	JACOBIAN_PRESSURE_DERIV_SCALE	OPTIONS	1.0d7	Pa
ITMAX	MAXIMUM_NUMBER_OF_ITERATIONS	NEWTON_SOLVER	8	-
IRESETMAX	MAXIMUM_CONSECUTIVE_TS_CUT	TIMESTEPPER	40	-
DELTFACTOR	TIMESTEP_REDUCTION_FACTOR	TIMESTEPPER	5.0d-1	-
DELTMAX	MAXIMUM_TIMESTEP_SIZE	TIME	1.73448d9	sec
DELTMIN	MINIMUM_TIMESTEP_SIZE	OPTIONS	8.64d-4	sec

7.2   Test Group #1: 5×3 Flared Grid

7.2.1 Purpose and Setup

This test consists of a miniature 2-D flared grid that contains 5 grid cells in the horizontal X-direction, and 3 grid cells in the vertical Z-direction ("5×3")[18]. Its purpose is to ensure that the implementation of ELEVATION and ALPHA in PFLOTRAN produces the same result as the implementation in BRAGFLO. Other process models included in this test case are: WIPP-FRACTURE, CREEP_CLOSURE, WIPP_SOURCE_SINK, RKS EOS, KLINKENBERG_EFFECT, and the KRP characteristic curves corresponding to the materials listed in the next paragraph.

In this miniature 2-D flared grid domain, two waste areas are separated by a panel closure. Above and below the waste areas and the panel closure, is a DRZ; undisturbed host rock (the Salado formation) is to the right and left (Figure 7.2-1). The materials used include: S_HALITE, DRZ_1, DRZ_PC_1, PCS_T1, WAS_AREA. Material properties are identical to those used in Replicate 1, Vector 1 in the PFD Analysis.

---

[18] The "5x3" test case refers to the verification test located at pflotran-bragflo-test-cases-stripped/tests_multi_cell/flared_5x3/pf_flared_allpm.in.
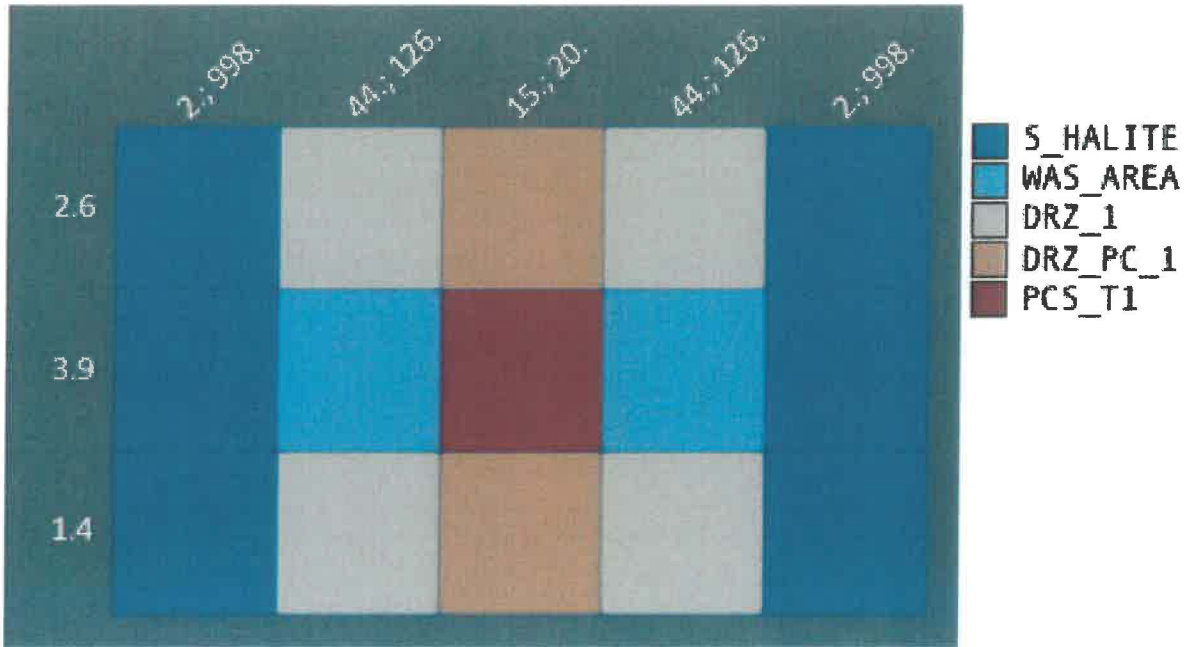
Figure 7.2-1 Equal area representation of the 5×3 miniature 2-D flared grid test case. Labels indicate grid cell dimensions – vertical dimensions (Z) are labeled down the side; X followed by Y dimensions are labeled across the top.

A 1° dip (downward to the left) is implemented over the entire domain using grid cell ELEVATION terms. All boundary conditions are no flow. Initial pressure is 4×10^7 Pa in the Salado and DRZ (materials S_HALITE, DRZ_1, and DRZ_PC_1), 128039 Pa in the waste areas (material WAS_AREA), and 101325 Pa in the panel closure (material PCS_T1). Initial gas saturation is 0.0 in the Salado and DRZ, 0.985 in the waste areas, and 0.434 in the panel closure. Creep closure and gas generation occur in the waste areas. Fracturing occurs in the DRZ (materials DRZ_1 and DRZ_PC_1). The following plots show the evolution of pressure, saturation, density, and porosity in waste area grid cell (2,2) and the domain average.

7.2.2 Results
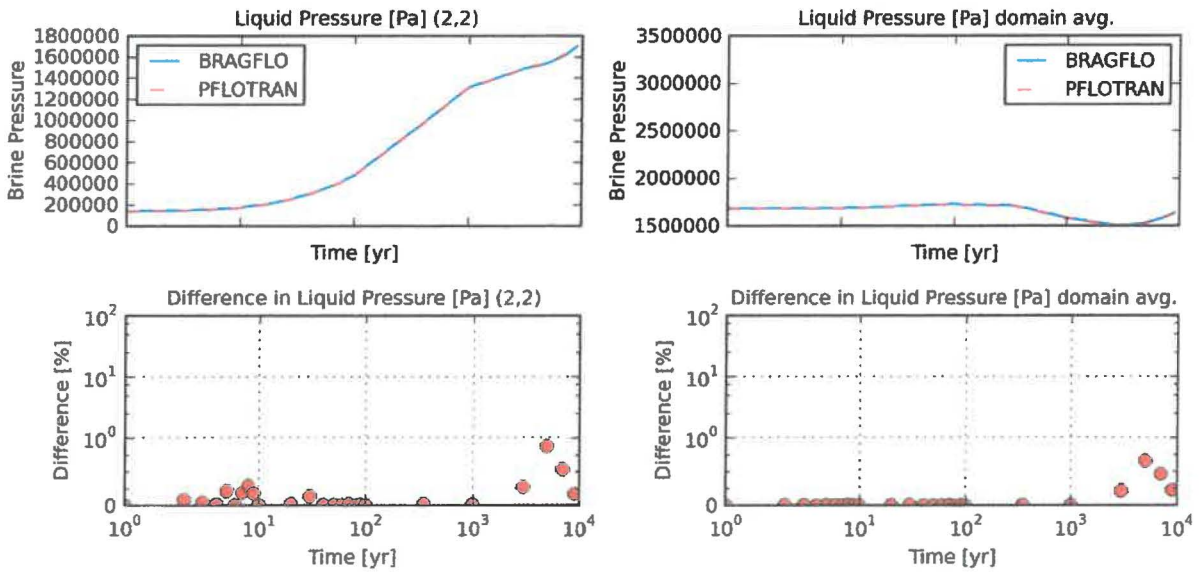
Figure 7.2-2 Test case "5×3" brine pressure [Pa] at cell (2,2) and domain average.
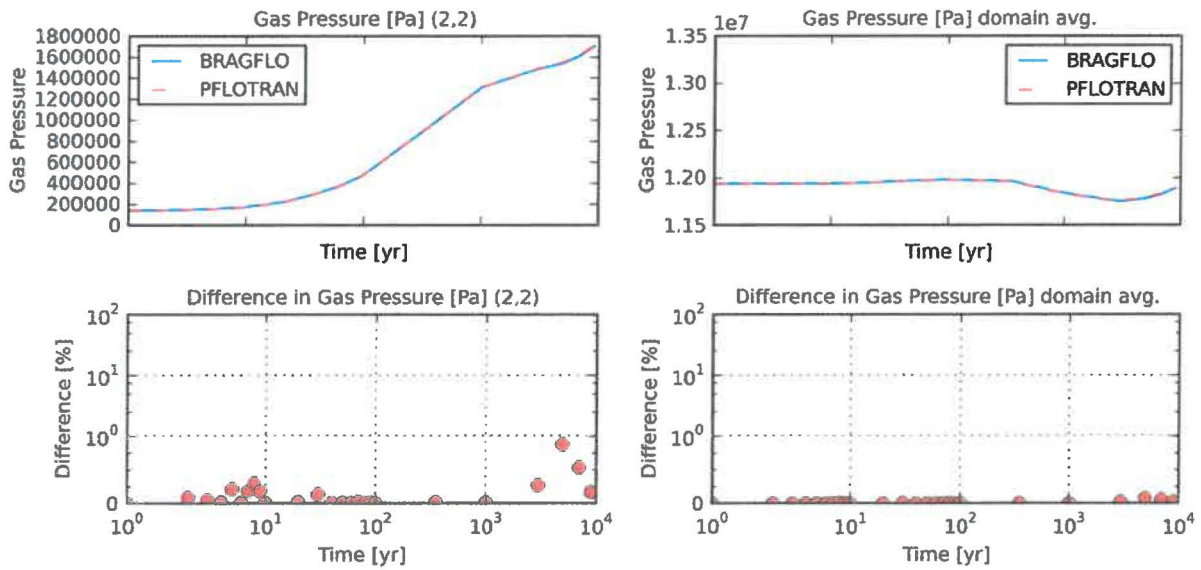
Figure 7.2-3 Test case "5×3" gas pressure [Pa] at cell (2,2) and domain average.
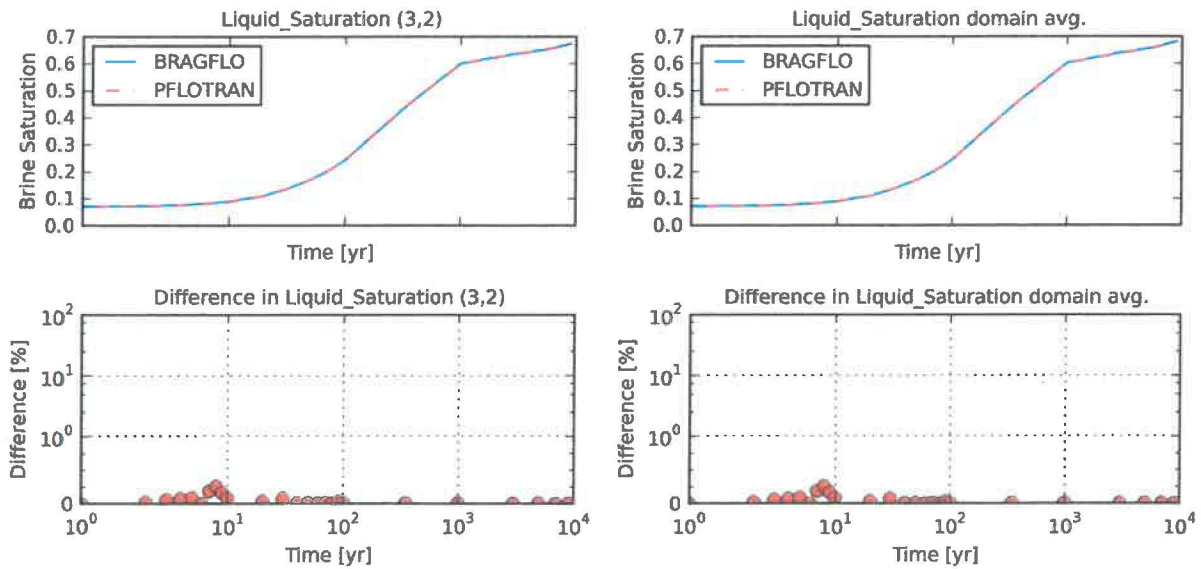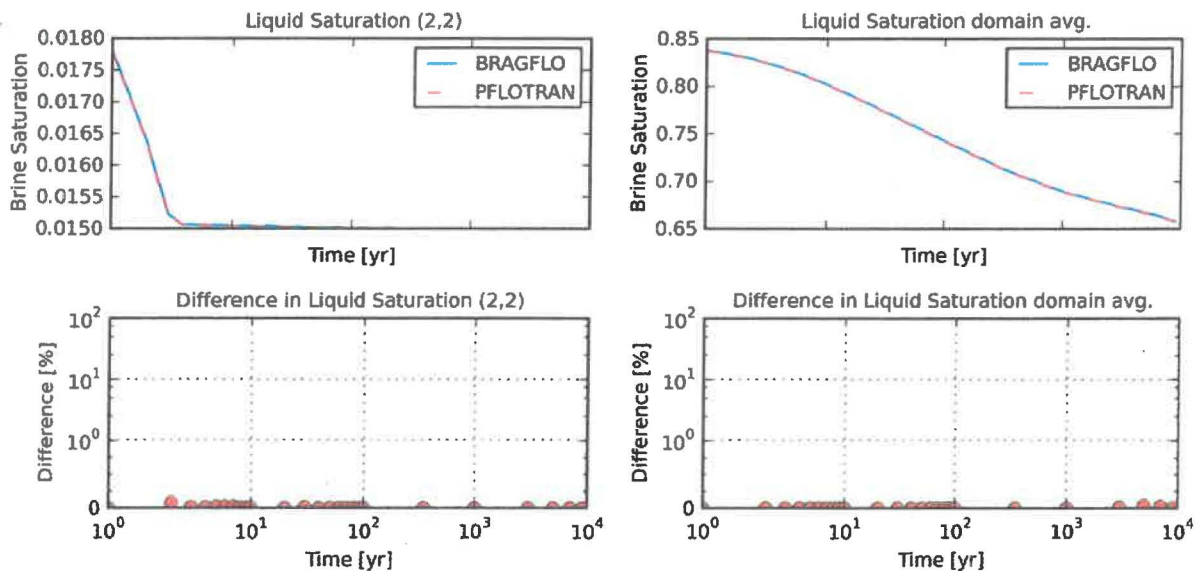
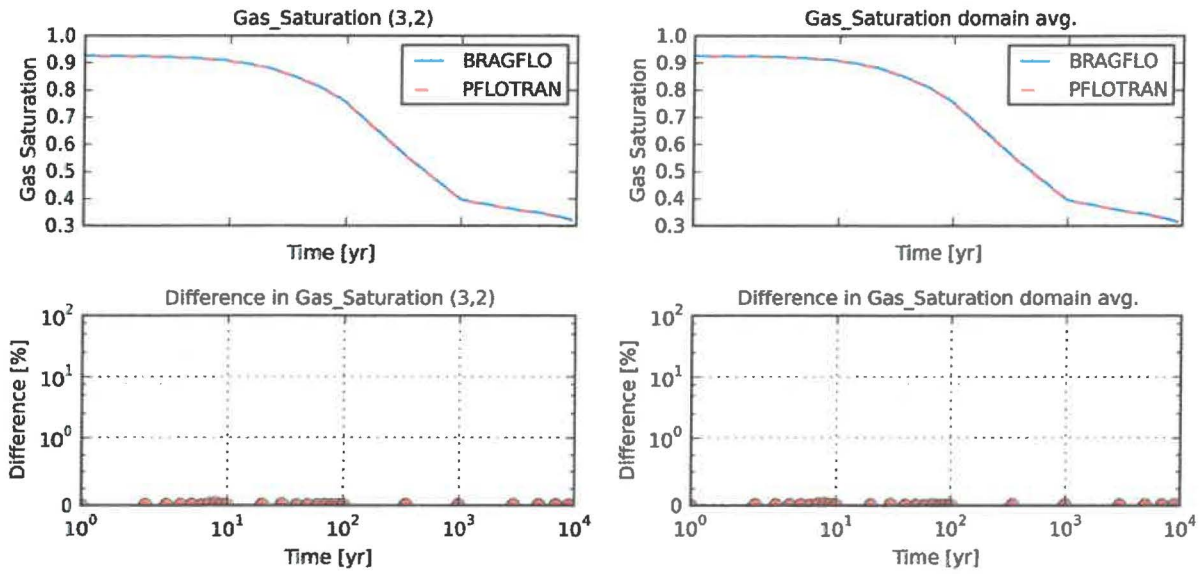Figure 7.2-4 Test case "5×3" brine saturation at cell (2,2) and domain average.
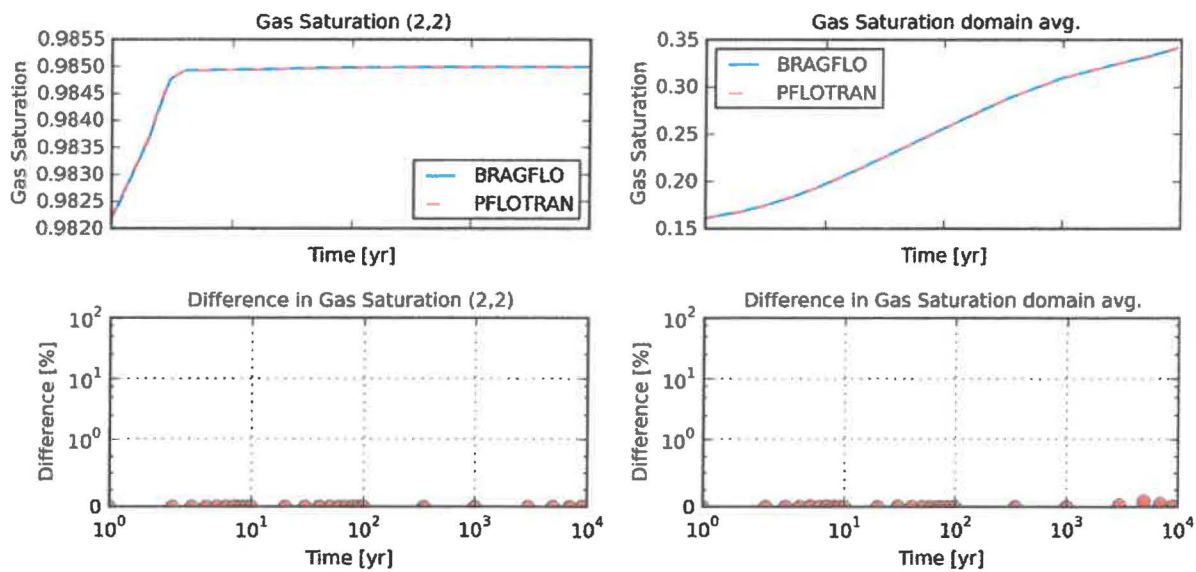
Figure 7.2-5 Test case "5×3" gas saturation at cell (2,2) and domain average.
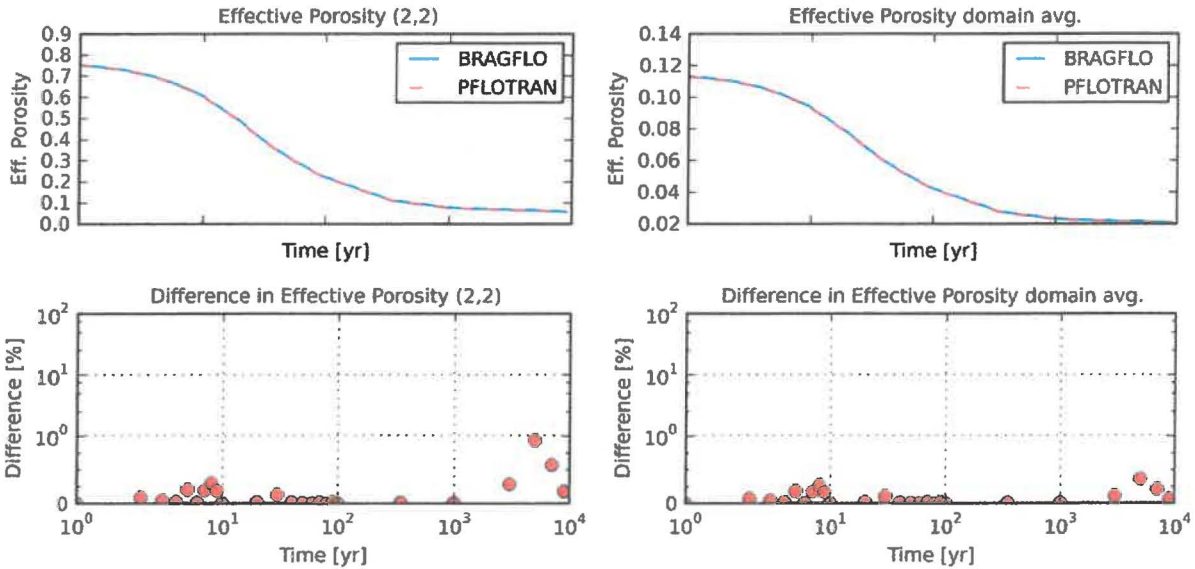
Figure 7.2-6 Test case "5×3" porosity at cell (2,2) and domain average.
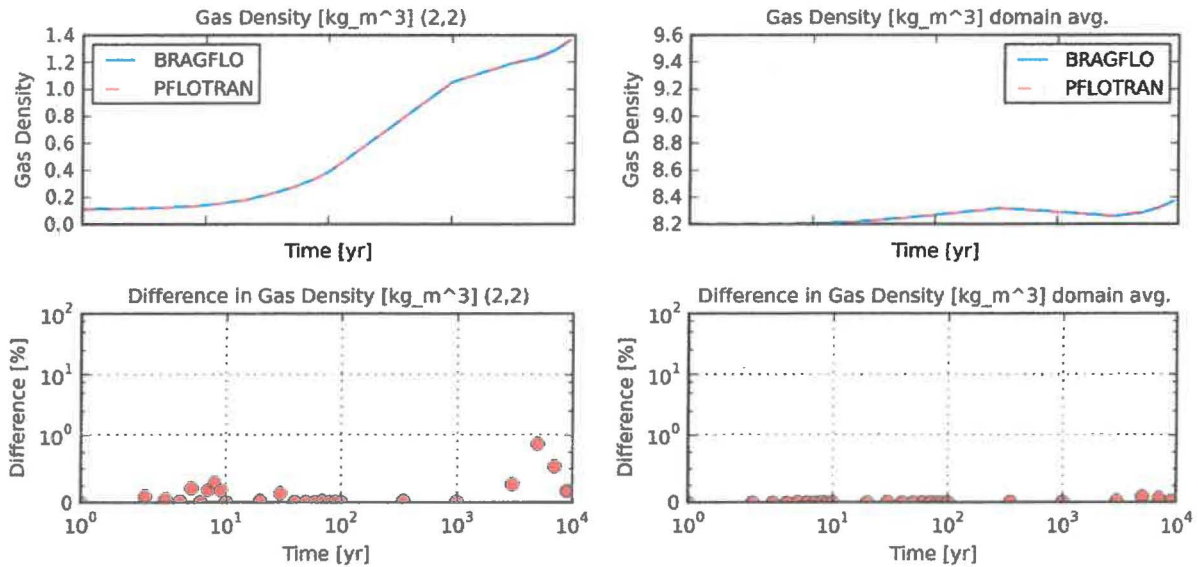
Figure 7.2-7 Test case "5×3" gas density [kg/m³] at cell (3,8) and domain average.

7.2.3 Conclusion

The "5×3" miniature 2-D flared grid test case shows that ALPHA and ELEVATION are properly implemented in PFLOTRAN. The maximum difference in results occurs toward the end of the simulation, when porosity relative differences in porosity, brine and gas pressure, and gas density are near 1%.

7.3   Test Group #2: 5×11 Flared Grid

7.3.1 Purpose and Setup

This second test consists of a miniature 2-D flared grid that contains 5 grid cells in the horizontal X-direction, and 11 grid cells in the vertical Z-direction ("5×11")[19]. Its purpose is to ensure that the implementation of step changes in material properties and the subsequent behavior of the solution in PFLOTRAN match the material property changes and code behavior in BRAGFLO. The 5×11 test case examines the numerically challenging material property changes associated with borehole intrusion. Other process models included in this test case are: ALPHA, ELEVATION (with dip of 0°) WIPP-FRACTURE, CREEP_CLOSURE, WIPP_SOURCE_SINK, RKS EOS, KLINKENBERG_EFFECT, and the KRP characteristic curves corresponding to the materials listed in the next paragraph.

In the 5×11 miniature 2-D flared grid domain, a waste area with DRZ above and below is surrounded by the Salado formation. The Castile formation underlies the Salado, and an overpressured brine reservoir within the Castile lies beneath the waste area. Above the Salado, the Los Medanos (Unnamed), Culebra, and Santa Rosa formations top off the domain (Figure 7.3-1). The materials used include: CASTILER, IMPERM_Z, S_HALITE, WAS_AREA, DRZ_1, UNNAMED, CULEBRA, and SANTAROS. Borehole intrusion, borehole degradation, and closure of the lower borehole due to salt creep are simulated with material changes. The borehole intrusion event occurs at 350 years, at which time materials in the center column of the grid are replaced with open borehole material (BH_OPEN) extending from the surface to the brine pocket except in the Los Medanos and the Santa Rosa, where the borehole is assumed to be plugged with concrete plugs (CONC_PLG). At 550 years, the borehole is assumed degraded, and both the open borehole and the concrete plugs are replaced with material BH_SAND. Finally, at 1550 years, material in the lower borehole is replaced with material BH_CREEP. Material properties are identical to those used in Replicate 1, Vector 1, in the PFD Analysis parameter set.

---

[19] The "5x11" test case refers to the verification test located at pflotran-bragflo-test-cases-stripped/tests_multi_cell/flared_5x11/pf_intrusion.in.
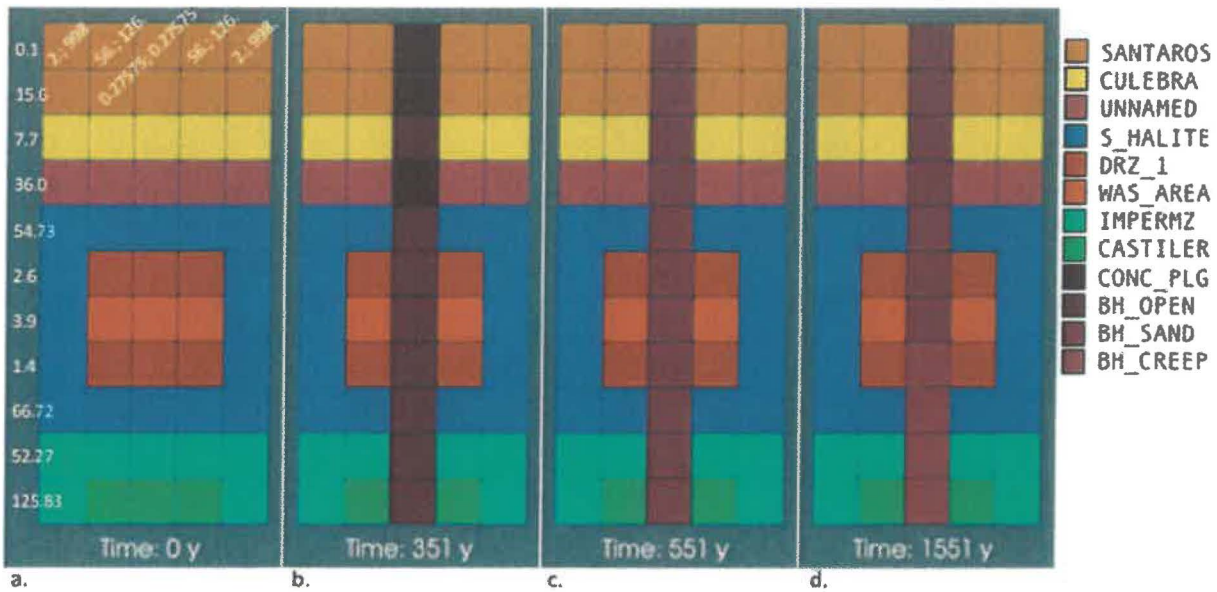
Figure 7.3-1 Equal area representations of the 5×11 miniature 2-D flared grid test case. Initial materials are shown (a.) as well as the material changes that occur at borehole intrusion (b.), due to borehole degradation (c.), and due to borehole creep (d.). Grid cell dimensions (m) are indicated in a. – vertical dimensions (Z) are listed down the side; X followed by Y dimensions are listed across the top.

Although the PFLOTRAN simulation uses grid cell ELEVATION terms to specify the elevation of each grid cell, no dip is implemented. Boundary conditions at the bottom and sides are no flow. A Dirichlet (constant) liquid pressure boundary condition of 101325 Pa is applied at the top of the domain. Gas saturation is also held constant at the top of the domain at 0.91637. In PFLOTRAN, Dirichlet boundary conditions are held at the cell surface. In BRAGFLO, Dirichlet boundary conditions are held at the center of the cell, hence the need for very thin cells at the top of the domain. Initial conditions include: liquid pressure of 101325 Pa and gas saturation of 0.91367 in the Santa Rosa; hydrostatic pressure and zero gas saturation in the Culebra, Los Medanos, Salado, DRZ, and Castile; liquid pressure of 128039 Pa and gas saturation of 0.985 in the waste area; and liquid pressure of 1.3312×10^7 Pa and zero gas saturation in the brine reservoir. Creep closure and gas generation occur in the waste areas. Fracture occurs in the DRZ. The following plots show the evolution of pressure, saturation, density, and porosity in the Los Medanos layer central grid cell (3,8) and the domain average. The grid cell (3,8) was chosen because it had the largest relative difference in the domain.

7.3.2 Results
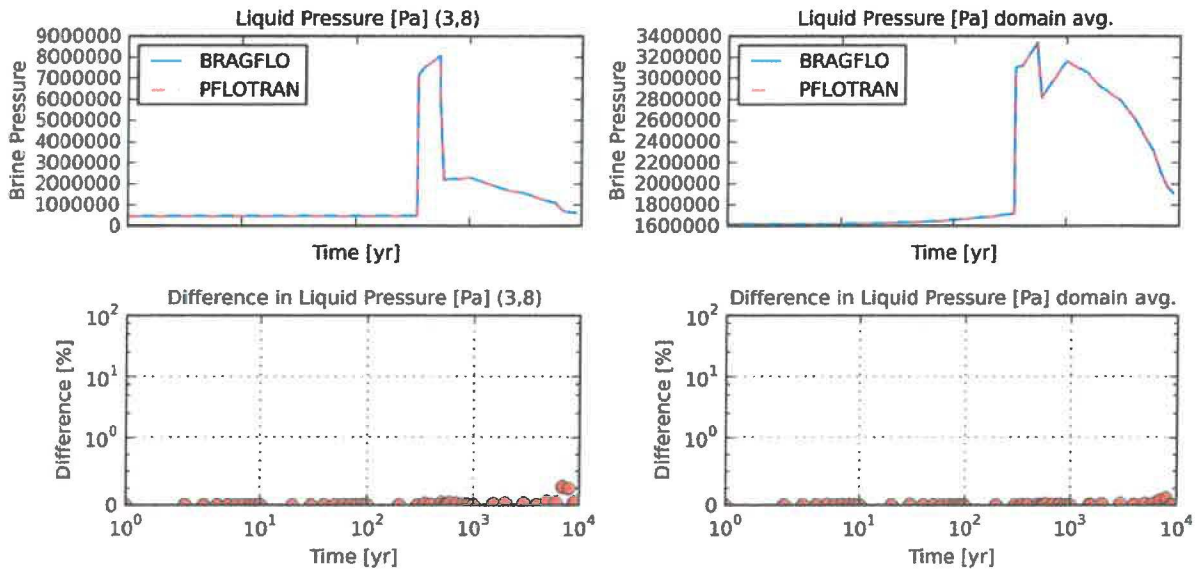
Figure 7.3-2 Test case "5x11" brine pressure [Pa] at cell (3,8) and domain average.
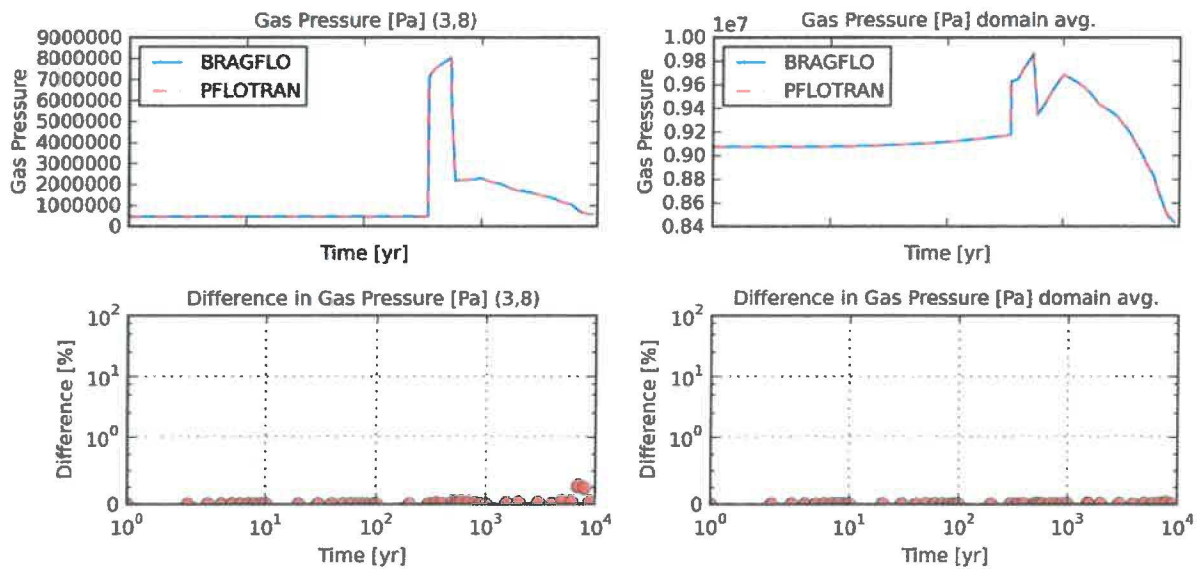
Figure 7.3-3 Test case "5x11" gas pressure [Pa] at cell (3,8) and domain average.

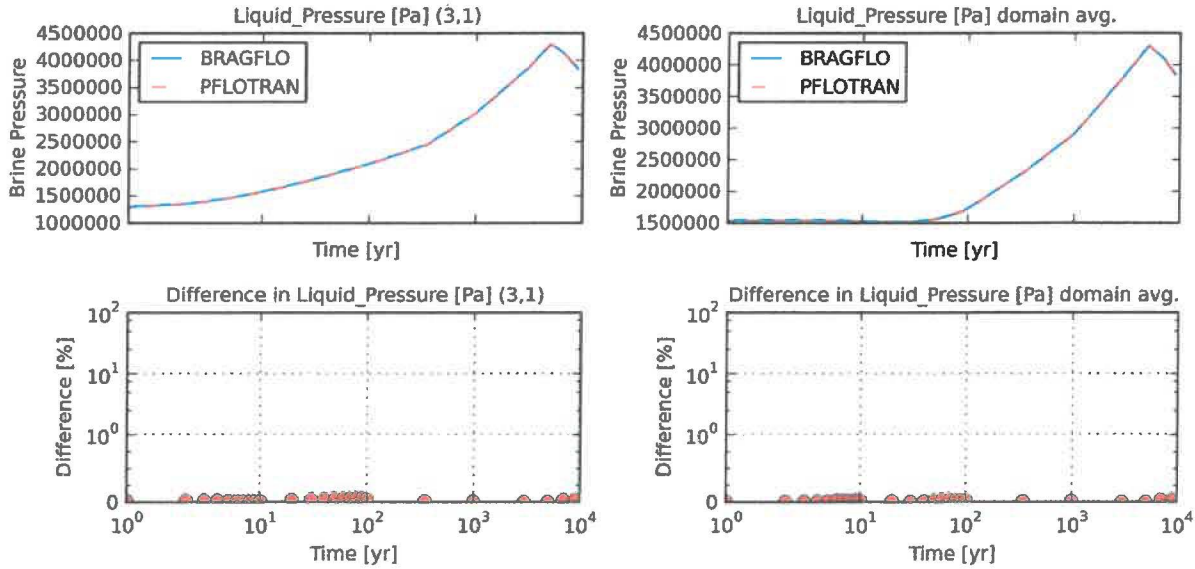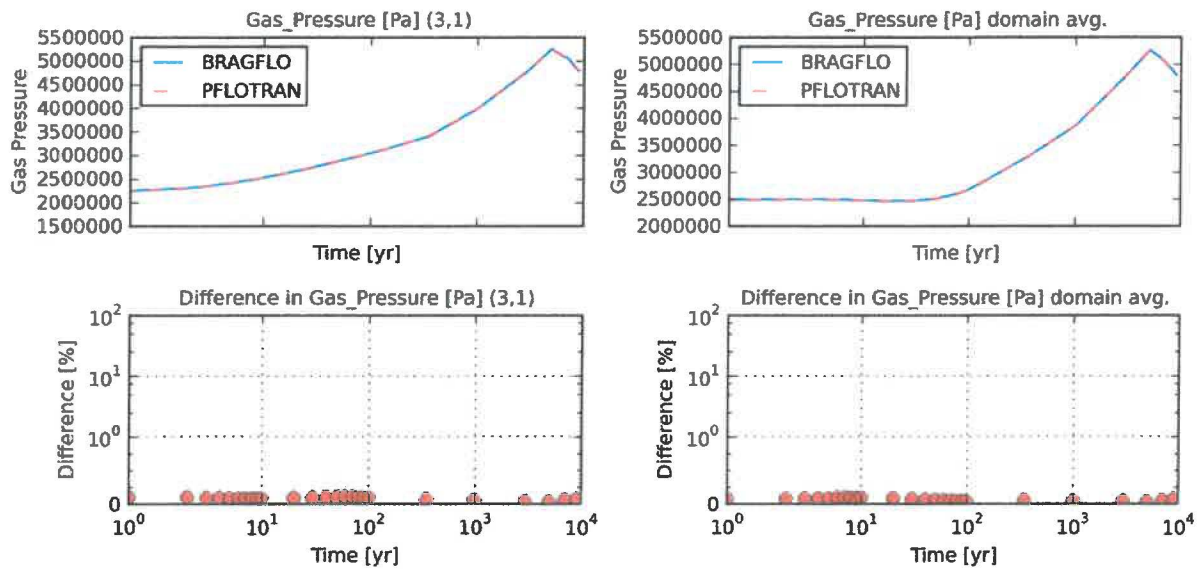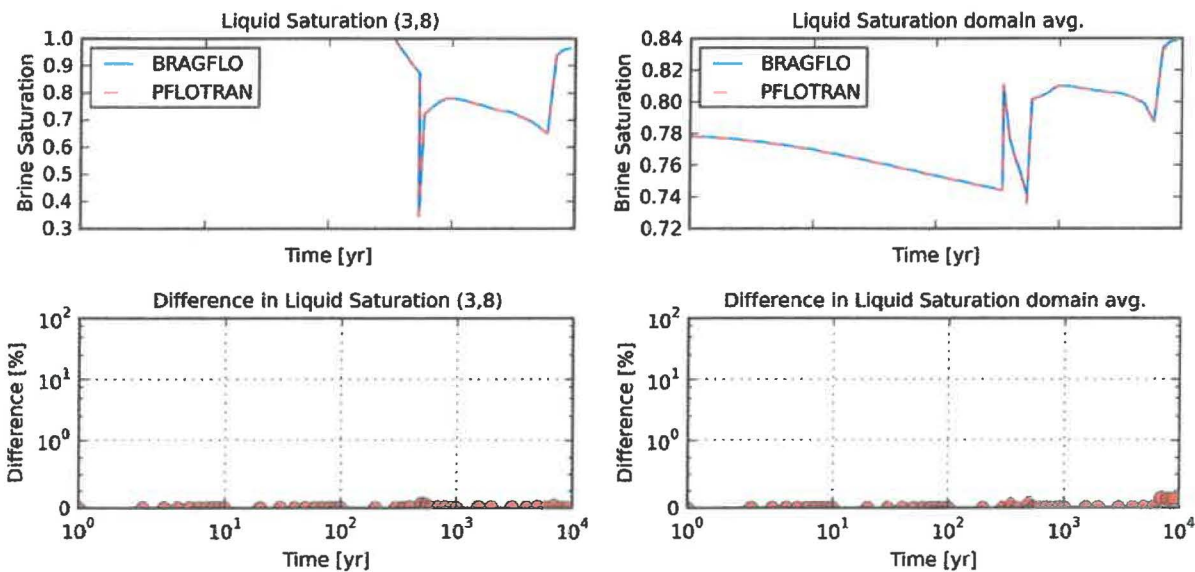Figure 7.3-4 Test case "5x11" brine saturation at cell (3,8) and domain average.
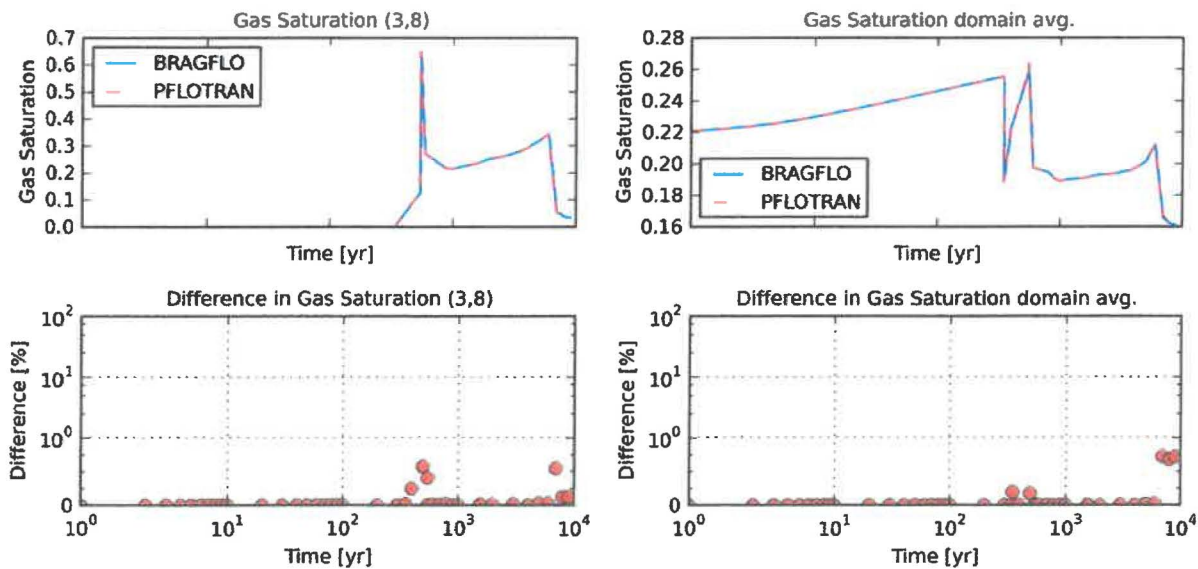
Figure 7.3-5 Test case "5×11" gas saturation at cell (3,8) and domain average.
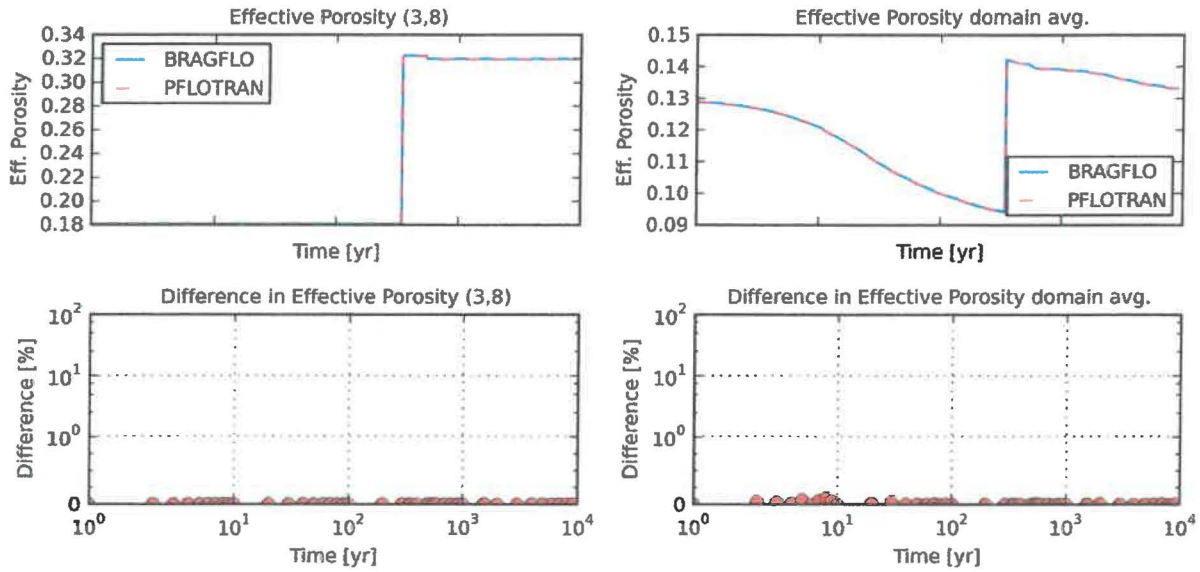
Figure 7.3-6 Test case "5×11" porosity at cell (3,8) and domain average.
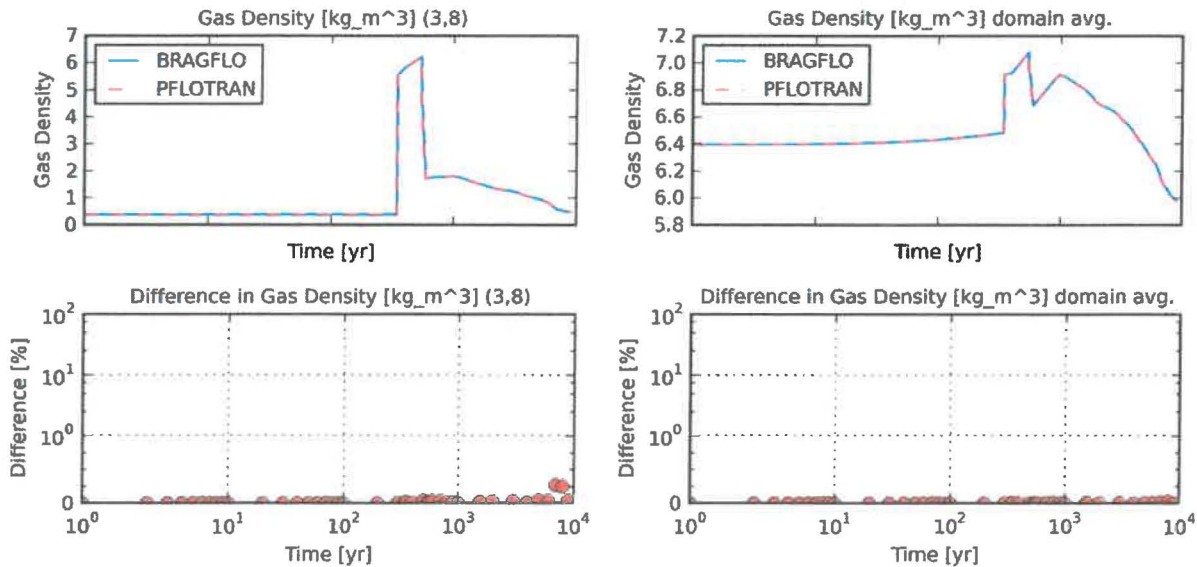
Figure 7.3-7 Test case "5×11" gas density [kg/m^3] at cell (3,8) and domain average.

7.3.3 Conclusion

The "5×11" miniature 2-D flared grid test case shows that the process of borehole intrusion, which includes computationally challenging material property changes, is properly handled in PFLOTRAN. The maximum difference in results is ~0.75%, which occurs in gas saturation, when gas saturation values are at a minimum.

8   PFLOTRAN-BRAGFLO 2-D Flared Grid Benchmark

8.1   Introduction

For the 2-D flared grid benchmark (also called the PFD analysis), PFLOTRAN and BRAGFLO outputs were compared for 1800 simulations whose input parameters duplicated those used for the three replicates of sampled parameters and six scenarios in the 2014 CRA WIPP PA calculations. Completing the suite of 1800 PA simulations ensured that PFLOTRAN was tested on a complex problem relevant to PA, using all WIPP-specific process models and over the full range of parameter values sampled in PA. The objectives of the comparison were: 1) to quantify the differences between the outputs of the two codes; 2) to demonstrate on a simulation by simulation basis that the differences between the solutions fall below acceptable thresholds; and 3) to explain any differences that exceed the thresholds.

The comparison was made twice, once using the standard PA value (10^{-2}) for the liquid residual infinity tolerance (FTOLNORM(2)), the gas residual infinity tolerance (FTOLNORM(1)), and the maximum allowable relative change in liquid pressure over a Newton iteration (EPSNORM(2)); and a second time tightening these tolerances to values of 10^{-4}. All other convergence criteria and parameters controlling time-stepping and iteration behavior were identical in the two comparisons and equal to those used in the 2014 CRA PA calculations. The PFD analysis differs from the 2014 CRA PA calculations in a few details, including: (1) the timing of saved output, (2) the use of the PFLOTRAN default value for the seconds per year conversion factor, (3) the grid, which is that used for the CRA_SEN4 analysis and contains a correction to the length of the north panel closure (Zeitler et al. 2017), and (4) the use of KRP11 rather than KRP5 in the open borehole (Zeitler et al. 2017).

Differences in liquid pressure and liquid saturation were assessed using volume-weighted average quantities from each region of the excavated volume (e.g., waste area, operations area, etc.). Differences in liquid mass flow were assessed at the intersections of the marker beds with the land withdrawal boundaries and at the intersections of the borehole and the shaft with the Culebra.

The remainder of Section 8 discusses:

- Calculation details (Section 8.2)
- Model setup, conceptual release pathways, and the six simulated scenarios (Section 8.3)
- Outputs used in the comparison (Section 8.4)
- Aggregate results (uncertainty distributions) by scenario and replicate (Section 8.5)
- Comparison of results for a typical simulation (Section 8.6)
- Comparison of results simulation by simulation (Section 8.7)

Discussion and comparison of results focuses on the simulations run with standard (10^{-2}) tolerances. Appendices E-K provide additional plots of the 10^{-2} tolerance comparison. The effect of tightening the tolerances is discussed in Appendix C, and detailed analyses of differences are presented in Appendix D. The full list of appendices is:

- Appendix A: Description of prePFLOTRAN Use and Functionality
- Appendix B: Supplemental Aggregate (Box Plot) Results
- Appendix C: Comparison with Tight Tolerances
- Appendix D: Analysis of Differences

- Appendix E: WAS_AREA Liquid Pressure
- Appendix F: OPS Liquid Pressure
- Appendix G: WAS_AREA Liquid Saturation
- Appendix H: OPS Liquid Saturation
- Appendix I: Borehole/Culebra Liquid Flow
- Appendix J: Shaft/Culebra Liquid Flow
- Appendix K: Anhydrite AB/South Land Withdrawal Boundary Liquid Flow
- Appendix L: Post-Processing and Plotting Scripts

8.2 Calculation Details

All BRAGFLO results were produced on the Solaris cluster head node (santana.sandia.gov) using the BRAGFLO executable stored at:

- /Archive/pflotran_bragflo_comparison_20180928/executables/bragflo-santana

All PFLOTRAN results were produced on the Linux cluster head node (jt.sandia.gov) using the PFLOTRAN executable stored at:

- /Archive/pflotran_bragflo_comparison_20180928/executables/pflotran-071318

Input decks, plotting scripts, and results are located on the Linux cluster at /Archive/pflotran_bragflo_comparison_20180928/pfd_analysis/ in several folders:

- bragflo_decks/   (BRAGFLO input, standard tolerances)
- bragflo_output/   (BRAGFLO output, standard tolerances)
- bragflo_output_fluxes (post-processed BRAGFLO flux output, standard tolerances)
- bragflo_summary_orig_data/ (BRAGFLO scenario summary h5 files, standard tolerances)
- bragflo_decks_tt_04/ (BRAGFLO input, tight tolerances)
- bragflo_output_tt_04/ (BRAGFLO output, including post-processed flux, tight tolerances)
- bragflo_summary_tt_04/   (BRAGFLO scenario summary h5 files, tight tolerances)
- pflotran-bragflo-2d-flared-071318/   (PFLOTRAN input and output, standard tolerances)
- pflotran-bragflo-2d-flared-071818-tt04/   (PFLOTRAN input and output, tight tolerances)

PFLOTRAN input decks were generated using prePFLOTRAN, a collection of Python scripts that queries the parameter database at tgw.sandia.gov, creates the grid, and writes the PFLOTRAN input decks (Appendix A).

Table 8.2-1 shows the values of the solution control parameters used in the PFLOTRAN-BRAGFLO 2-D flared grid benchmark.

Table 8.2-1 Solution control parameters used in the PFLOTRAN-BRAGFLO 2-D benchmark.

BRAGFLO	PFLOTRAN KEYWORD	PFLOTRAN BLOCK	VALUE	UNIT
FTOLNORM(2)	LIQUID_RESIDUAL_INFINITY_TOL	OPTIONS	1.d-2/1.d-4	kg/m3
FTOLNORM(1)	GAS_RESIDUAL_INFINITY_TOL	OPTIONS	1.d-2/1.d-4	kg/m3
EPSNORM(2)	MAX_ALLOW_REL_LIQ_PRES_CHANG_NI	OPTIONS	1.d-2/1.d-4	-
EPSNORM(1)	MAX_ALLOW_REL_GAS_SAT_CHANGE_NI	OPTIONS	1.0d-3	-
DH(1)	REL_GAS_SATURATION_PERTURBATION	OPTIONS	1.0d-8	-
DH(2)	REL_LIQ_PRESSURE_PERTURBATION	OPTIONS	1.0d-8	-

HMIN(1)	MIN_GAS_SATURATION_PERTURBATION	OPTIONS	1.0d-10	-
HMIN(2)	MIN_LIQ_PRESSURE_PERTURBATION	OPTIONS	1.0d-2	Pa
SATLIMIT	GAS_SAT_THRESH_FORCE_EXTRA_NI	OPTIONS	1.0d-3	-
DEPLIMIT(1)	GAS_SAT_THRESH_FORCE_TS_CUT	OPTIONS	2.0d-1	-
DDEPMAX(1)	MAX_ALLOW_GAS_SAT_CHANGE_TS	OPTIONS	1.0d0	-
DELTADEPNORM(1)	GAS_SAT_CHANGE_TS_GOVERNOR	OPTIONS	3.0d-1	-
TSWITCH	GAS_SAT_GOV_SWITCH_ABS_TO_REL	OPTIONS	1.0d0	-
DEPLIMIT(2)	MIN_LIQ_PRES_FORCE_TS_CUT	OPTIONS	-1.0d8	Pa
DDEPMAX(2)	MAX_ALLOW_LIQ_PRES_CHANGE_TS	OPTIONS	1.0d7	Pa
DELTADEPNORM(2)	LIQ_PRES_CHANGE_TS_GOVERNOR	OPTIONS	5.0d5	Pa
P_SCALE	JACOBIAN_PRESSURE_DERIV_SCALE	OPTIONS	1.0d7	Pa
ITMAX	MAXIMUM_NUMBER_OF_ITERATIONS	NEWTON_SOLVER	8	-
IRESETMAX	MAXIMUM_CONSECUTIVE_TS_CUTS	TIMESTEPPER	40	-
DELTFACTOR	TIMESTEP_REDUCTION_FACTOR	TIMESTEPPER	5.0d-1	-
DTIMEMAX	TIMESTEP_MAXIMUM_GROWTH_FACTOR	TIMESTEPPER	1.25d0	-
MAXSTEPS	MAXIMUM_NUMBER_OF_TIMESTEPS	TIMESTEPPER	20,000	-
N/A	TIMESTEP_OVERSTEP_REL_TOLERANCE	TIMESTEPPER	1.0d-6	-
N/A	MAX_NUM_CONTIGUOUS_REVERTS	TIMESTEPPER	99	-
DELTMAX	MAXIMUM_TIMESTEP_SIZE	TIME	1.728d9	sec
DELTMIN	MINIMUM_TIMESTEP_SIZE	OPTIONS	8.64d-4	sec
YRSEC	(Seconds per year)	(hardwired)	3.1536d7	sec/yr

8.3   Description of Model and Scenarios

BRAGFLO and PFLOTRAN simulations for the PFD analysis use identical 2-D flared grids that extend approximately 46624 m from south to north (left to right) and are 1039.05 m in height. Values of alpha (the length of the third dimension) vary from 0.27575 at the borehole to 77095.8 m at the northern most column of grid cells (Figure 4.4-1). The repository is located approximately 642 m below the top of the model domain (Figure 8.3-1). A one degree dip in the Salado formation, marker beds, and repository regions (including the shaft to the top of the domain) is simulated using grid cell ELEVATION terms (Section 4.4.2) to account for the hydrostatic component of pressure. At time = −5 yr, hydrostatic initial conditions are applied throughout the model domain, except in repository regions, which are initially unsaturated and at atmospheric pressure. No-flow boundary conditions are applied at all faces except at the north and south ends of the Culebra and the Magenta, and at the top of the model domain. At these locations Dirichlet pressure boundary conditions are applied at cell centers. See Appendix A for additional discussion of how initial conditions are calculated for PFLOTRAN simulations and of the pressure and saturation reset that occurs at 0 years.
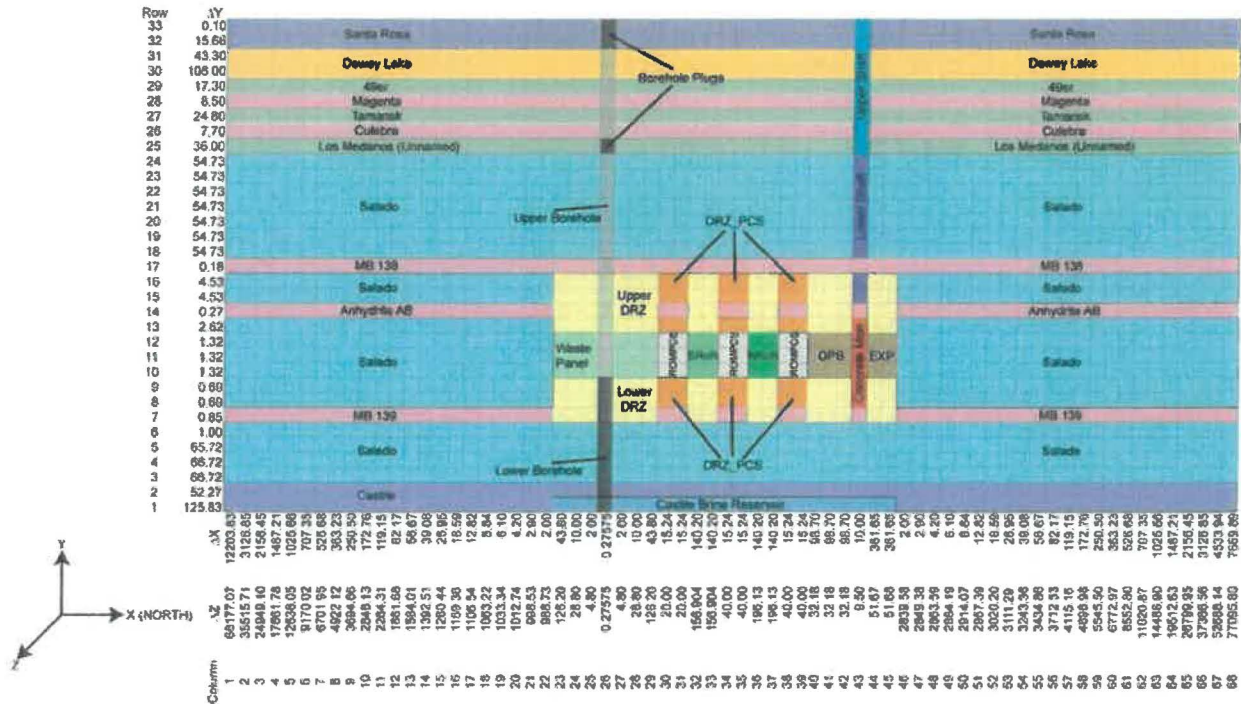
Figure is annotated with BRAGFLO coordinate axes (PA Appendix, DOE 2014). Grid cells are drawn as equal area squares with dimensions in meters indicated in the margins. The grid used in the PFD analysis differs in the width of the North (right) panel closure.

Figure 8.3-1 The 2-D flared grid model domain used in the 2014 CRA.

For WIPP PA flow calculations, six scenarios are simulated: a scenario in which the repository is undisturbed, and five scenarios in which the repository is disturbed by one or more borehole intrusions into the waste area. The 2014 CRA PA Appendix (DOE 2014) describes the conceptual pathways for release in the undisturbed and disturbed scenarios. In the undisturbed case:

> "Conceptually there are several pathways for radionuclide transport within the undisturbed disposal system that may result in releases to the accessible environment. Contaminated brine may migrate away from the waste-disposal panels if pressure within the panels is elevated by gas generated from corrosion or microbial consumption. Radionuclide transport may occur laterally, through the anhydrite interbeds toward the subsurface boundary of the accessible environment in the Salado, or through access drifts or anhudrite interbeds to the base of the shafts. In the latter case, if the pressure gradient between the panels and overlying strata is sufficient, contaminated brine may migrate up the shafts. As a result, radionuclides may be transported directly to the ground surface, or laterally away from the shafts through permeable strata such as the Culebra, toward the subsurface boundary of the accessible environment." (PA Appendix, DOE 2014)

In the disturbed case additional conceptual pathways exist. Flow simulations do not address some of these pathways (i.e., cuttings, cavings, spallings, and flow of contaminated brine up the open

borehole (DOE 2014)). Flow simulations do address the possibility of releases that occur through a plugged and abandoned borehole:

> *"An abandoned intrusion borehole with degraded casing and/or plugs may provide a pathway for fluid flow and contaminant transport from the intersected waste panel to the ground surface if the fluid pressure within the panel is sufficiently greater than hydrostatic. Additionally, if brine flows through the borehole to overlying units, such as the Culebra, it may carry dissolved and colloidal actinides that can be transported laterally th the accessible environment by natural groundwater flow in the overlying units." (PA Appendix, DOE 2014)*

Appendix PA (DOE 2014) additionally notes that "…units intersected by an intrusion borehole may provide sources for brine flow to a waste panel during or after drilling." Pockets of brine with liquid pressures greater than hydrostatic occur in the Castile Formation, which underlies the Salado. An intrusion borehole that penetrated an overpressured brine pocket "could provide a connection for brine flow from the Castile to the waste panel, thus increasing fluid pressure and brine volume in the waste panel."

The six scenarios for which flow calculations are made are:

- Scenario 1 – The undisturbed scenario (no borehole intrusion)

- Scenario 2 – Borehole intrusion penetrating a Castile brine pocket occurs at 350 yr. The borehole is initially simulated as an open borehole with concrete plugs in the Los Medanos and the Santa Rosa. At 550 yr, plugs and borehole are assigned properties representing a degraded borehole. At 1550 yr, the lower borehole (below the repository) is assigned properties representing closure due to salt creep.

- Scenario 3 – Borehole intrusion penetrating a Castile brine pocket occurs at 1000 yr. At 1200 yr, the borehole degrades. At 2200 yr, the lower borehole closes due to salt creep.

- Scenario 4 – Borehole intrusion (that does not penetrate the Castile) occurs at 350 yr. At 550 yr, the borehole degrades.

- Scenario 5 – Borehole intrusion (that does not penetrate the Castile) occurs at 1000 yr. At 1200 yr, the borehole degrades.

- Scenario 6 – Borehole intrusion (that does not penetrate the Castile) occurs at 1000 yr. At 1200 yr, the borehole degrades. At 2000 yr, a second borehole intrusion penetrates a Castile brine pocket, potentially causing flow up the first, degraded borehole. At 2200 yr, the second borehole degrades. At 3200 yr, the lower borehole closes due to salt creep. (Because the grid has explicit representation of a single borehole, the material changes corresponding to evolution of the second borehole occur only in the lower portion of the gridded borehole.)

For each of the six scenarios, 300 sample vectors are simulated. The 300 sample vectors are divided into three replicates of 100 vectors each, and the same replicates (sample vectors) are simulated for each scenario.

8.4   Outputs for Comparison

A comparison was made of liquid pressures, liquid saturations, and liquid mass flows.

Liquid pressures and liquid saturations were calculated as volume-weighted averages for each region of the domain included in the typical post-BRAGFLO ALGEBRA step, including the waste area, the south rest of repository, the north rest of repository, the south panel closure, the middle panel closure, the north panel closure, the operations area, and the experimental area. In addition, volume-weighted average liquid pressure and liquid saturation were calculated for the three cells of the shaft (part of the concrete monolith) that intersect the operations and experimental areas. These regions are referred to throughout this report as WAS_AREA, SROR, NROR, SPCS, MPCS, NPCS, OPS, EXP, and SHAFT, respectively. In this section, the terms "liquid pressure" and "liquid saturation" are occasionally substituted for "volume-weighted average liquid pressure" and "volume-weighted average liquid saturation".

The post-BRAGFLO ALGEBRA step also calculates total brine volume, volume-weighted average gas saturation, and volume-weighted average porosity for each of these regions (except SHAFT). These quantities are not discussed in this report for the following reasons: (1) Gas pressure (equal to brine pressure in all the regions listed above except the panel closures) and gas saturation (1 minus the brine saturation) would add little to no information to the comparison. (2) Differences in volume-weighted average porosity did not exceed thresholds similar to those described below for liquid saturation in any simulation. Therefore, neither porosity nor brine volume (a function of porosity and saturation) warrant discussion.

Liquid mass flow integrated over time was compared across the eight planes corresponding to the conceptual pathways for potential radionuclide release: across the south and north land withdrawal boundaries in Marker Bed 138, Anhydrite AB, and Marker Bed 139 (horizontal flow at 6 locations), and across the base of the Culebra in the borehole and the shaft (vertical flow at 2 locations). Throughout the text, the locations in the borehole and shaft are referred to as the "borehole/Culebra interface" and the "shaft/Culebra interface," respectively.

Regions for which average pressure and saturation were calculated and locations at which flow was compared are shown in Figure 8.4-1.

Domain is colored by material. Regions in which volume-weighted average liquid pressure and saturation were compared are labeled, as are planes across which liquid mass flow was compared.

Figure 8.4-1 2-D flared grid model domain with grid cells drawn as equal area squares.

8.5   Aggregate Results (Uncertainty Distributions)

8.5.1 *Cumulative liquid flow along pathways of potential radionuclide release*

Cumulative liquid mass flow over the 10,000-year regulatory period varies in direction and magnitude among the eight conceptual pathways of potential radionuclide release. Mass flow in the shaft and across the land withdrawal boundary has little dependence on scenario, while mass flow in the borehole varies in direction and magnitude depending on scenario.

At the marker bed intersections with the south and north land withdrawal boundaries, nearly all of the 1800 simulations predict flow toward the repository. Mass flow in Anhydrite AB is shown for illustration in Figure 8.5-1 and Figure 8.5-2. These box plots show the uncertainty distribution in cumulative liquid mass flow for each replicate/scenario pair. PFLOTRAN boxes (red) are narrower than BRAGFLO boxes (blue) so that both can be seen. In these plots, the boxes (with top and bottom drawn at the 0.25 and 0.75 quartiles) are too close to zero to see that the uncertainty distributions resulting from PFLOTRAN and BRAGFLO simulations fall on top of each other. However, the agreement between the two codes is apparent in the agreement between the outliers (and in subsequent plots of shaft and borehole mass flow).

Flow direction (sign) is relative to the X coordinates of the grid, so that positive flow at the south land withdrawal boundary and negative flow at the north land withdrawal boundary are toward the repository. In the set of 300 simulations performed for each scenario except Scenario 1, only one simulation (in Replicate 1) predicts cumulative flow away from the repository (at the south land withdrawal boundary). Two of the 300 simulations for Scenario 1 predict cumulative flow away from the repository (one in Replicate 1 and one in Replicate 2). The magnitude of the cumulative flow away from the repository (<150,000 kg over 10,000 yr) is less than 1% of the mass of brine

that would exist between the repository and the land withdrawal boundary in the liquid saturated Anhydrite AB (Table 8.5-1), and therefore represents insufficient movement of liquid to advect radionuclides across the land withdrawal boundary. The same analysis holds for Marker Beds 138 and 139 (See Appendix B for cumulative flow box plots).
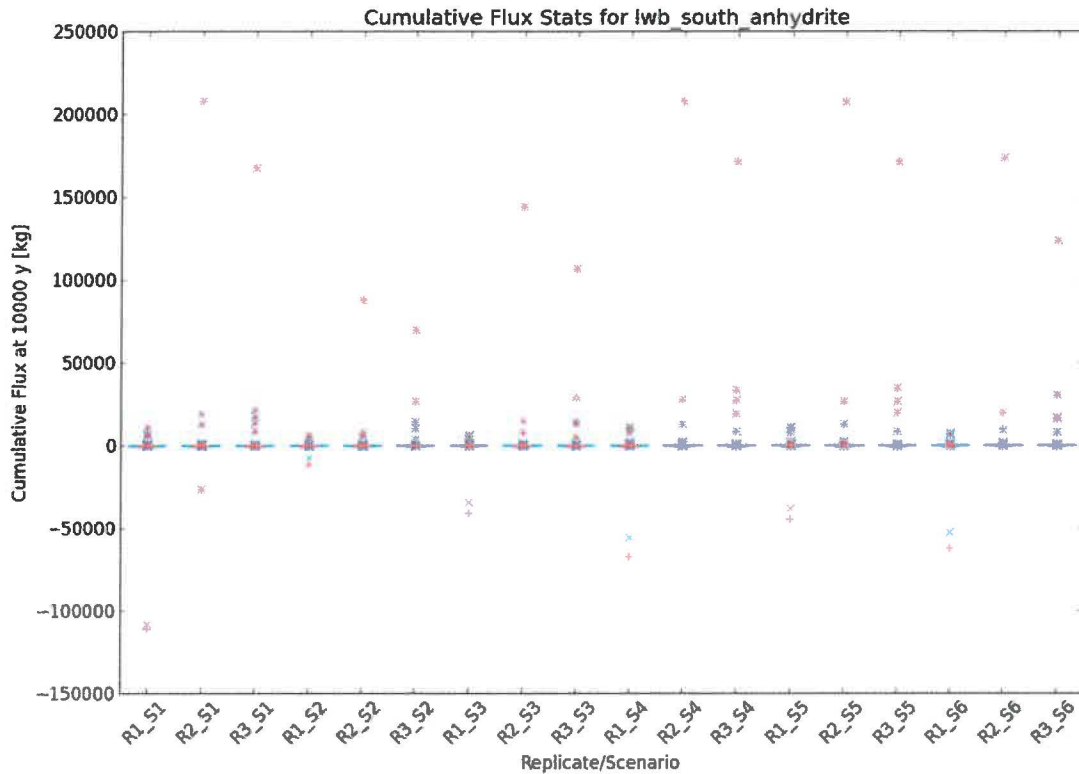
All replicate/scenario pairs (standard tolerances). PFLOTRAN boxes (red) are narrower than BRAGFLO boxes (blue) so that both can be seen. Boxes extend from the 1st to the 3rd quartile. The line dissecting the box is the median. Whiskers extend $1.5 \times IQR$, where IQR is the interquartile range $= Value_{3rd} - Value_{1st}$, or to the extent of the data range, whichever is less. Outliers are plotted with '+' for PFLOTRAN and 'x' for BRAGFLO. Flow direction (sign) is relative to the X coordinates of the grid, so that positive flow is toward the repository.

Figure 8.5-1 Uncertainty in cumulative liquid mass flow across the south land withdrawal boundary in Anhydrite AB.
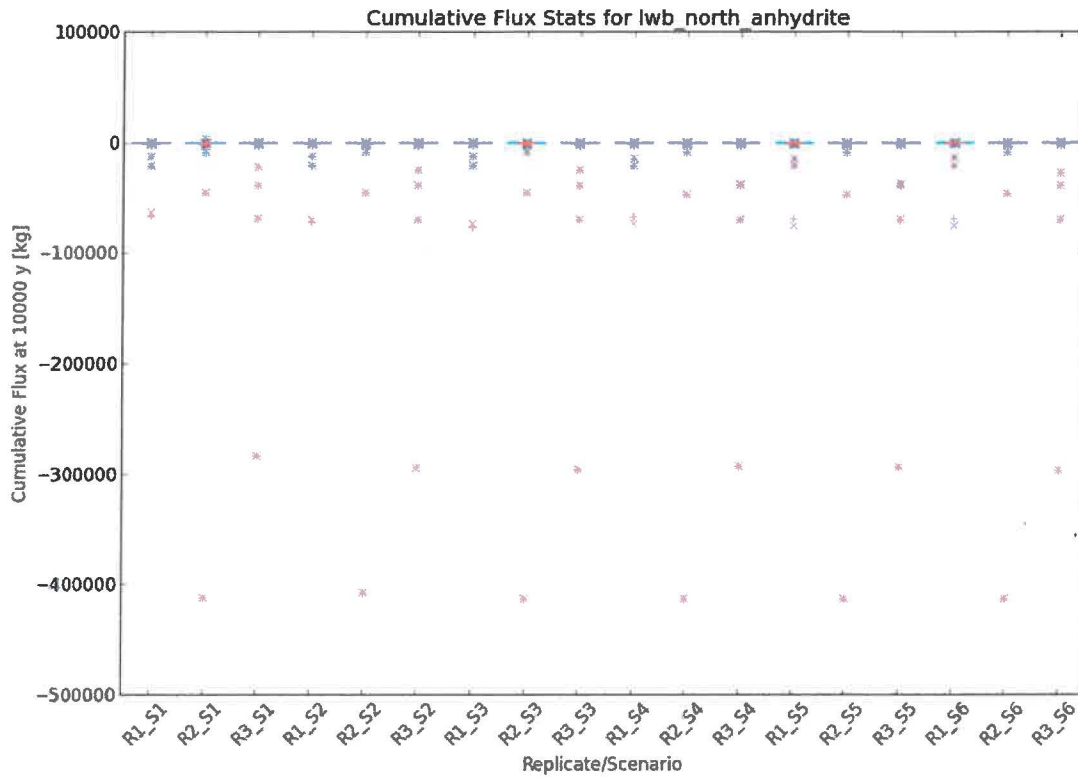
All replicate/scenario pairs (standard tolerances). PFLOTRAN boxes (red) are narrower than BRAGFLO boxes (blue) so that both can be seen. Boxes extend from the 1st to the 3rd quartile. The line dissecting the box is the median. Whiskers extend $1.5 \times IQR$, where IQR is the interquartile range $= \mathrm{Value_{3rd}} - \mathrm{Value_{1st}}$, or to the extent of the data range, whichever is less. Outliers are plotted with '+' for PFLOTRAN and 'x' for BRAGFLO. Flow direction (sign) is relative to the X coordinates of the grid, so that negative flow is toward the repository.

Figure 8.5-2 Uncertainty in cumulative liquid flow across the north land withdrawal boundary in Anhydrite AB.

Table 8.5-1 Potential Brine Mass between Repository and Flow Comparison Locations

	Total Volume (m³)	Porosity	Pore Volume (m³)	Equivalent Mass of Brine[c] (kg)	100 kg Threshold as Fraction of Mass
MB138 to south lwb	2.50E+06	0.011	2.75E+04	3.36E+07	2.98E-06
ANH_AB to south lwb	3.75E+06	0.011	4.13E+04	5.03E+07	1.99E-06
MB139 to south lwb	1.18E+07	0.011	1.30E+05	1.58E+08	6.31E-07
MB138 to north lwb	3.30E+06	0.011	3.63E+04	4.43E+07	2.26E-06
ANH_AB to north lwb	4.95E+06	0.011	5.45E+04	6.64E+07	1.51E-06
MB139 to north lwb	1.56E+07	0.011	1.72E+05	2.09E+08	4.78E-07
Shaft to Culebra	4.10E+04	Varies[a]	5.22E+03	6.37E+06	1.57E-05
Borehole to Culebra	3.28E+01	0.32[b]	1.05E+01	1.28E+04	7.81E-03

All 1800 simulations predict downward cumulative liquid mass flow at the shaft/Culebra intersection (Figure 8.5-3). PFLOTRAN (red) and BRAGFLO (blue) uncertainty distributions for each replicate/scenario pair plot on top of each other, as do the outliers. Distributions differ among the three replicates, but the cumulative flow distribution resulting from a single replicate is nearly constant across scenarios. This behavior indicates that flow in the shaft is not influenced by the occurrence of borehole intrusion, by the timing of intrusion, or by penetration of an overpressured brine pocket, and suggests that processes occurring in the shaft are largely decoupled from processes occurring in the waste area (the location of borehole intrusion). The largest cumulative flows (<200,000 kg) are less than 10% of the liquid mass that would be contained in a saturated shaft between the repository and the Culebra (Table 8.5-1). The small downward liquid mass flows predicted in the shaft are not likely to influence radionuclide release.
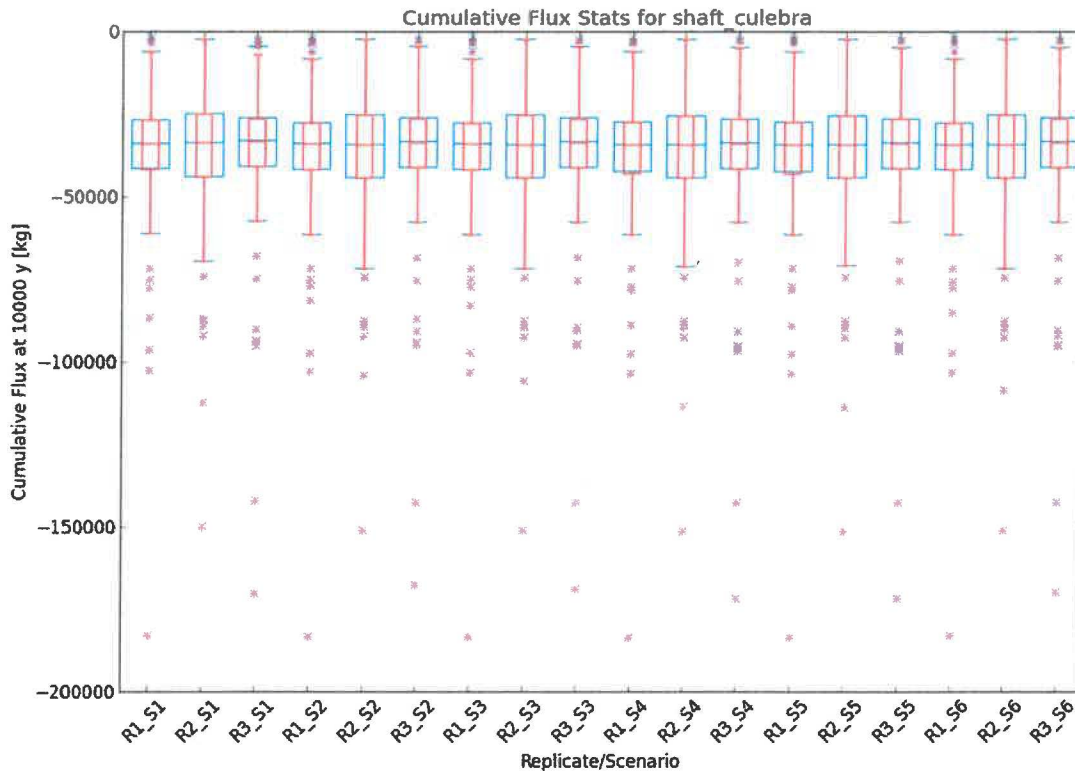
All replicate/scenario pairs (standard tolerances). PFLOTRAN boxes (red) are narrower than BRAGFLO boxes (blue) so that both can be seen. Boxes extend from the 1st to the 3rd quartile. The line dissecting the box is the median. Whiskers extend $1.5 \times$ IQR, where IQR is the interquartile range $=$ Value$_{3rd}$ $-$ Value$_{1st}$, or to the extent of the data range, whichever is less. Outliers are plotted with '+' for PFLOTRAN and 'x' for BRAGFLO. Flow direction (sign) is relative to the vertical coordinates of the grid, so that negative flow is downward

Figure 8.5-3 Uncertainty in cumulative liquid flow across the shaft/Culebra interface. .

Cumulative liquid flow at the borehole/Culebra interface varies in direction and magnitude as a function of scenario (Figure 8.5-4). Cumulative borehole flows are upward in Scenarios 2, 3, and 6. Most simulations of Scenarios 4 and 5 predict downward flows; a few predict small upward flows. In Scenarios 2, 3, and 6, the largest cumulative flows exceed 10^8 kg, more than 10,000× the mass of brine that could be contained in a fully saturated borehole.
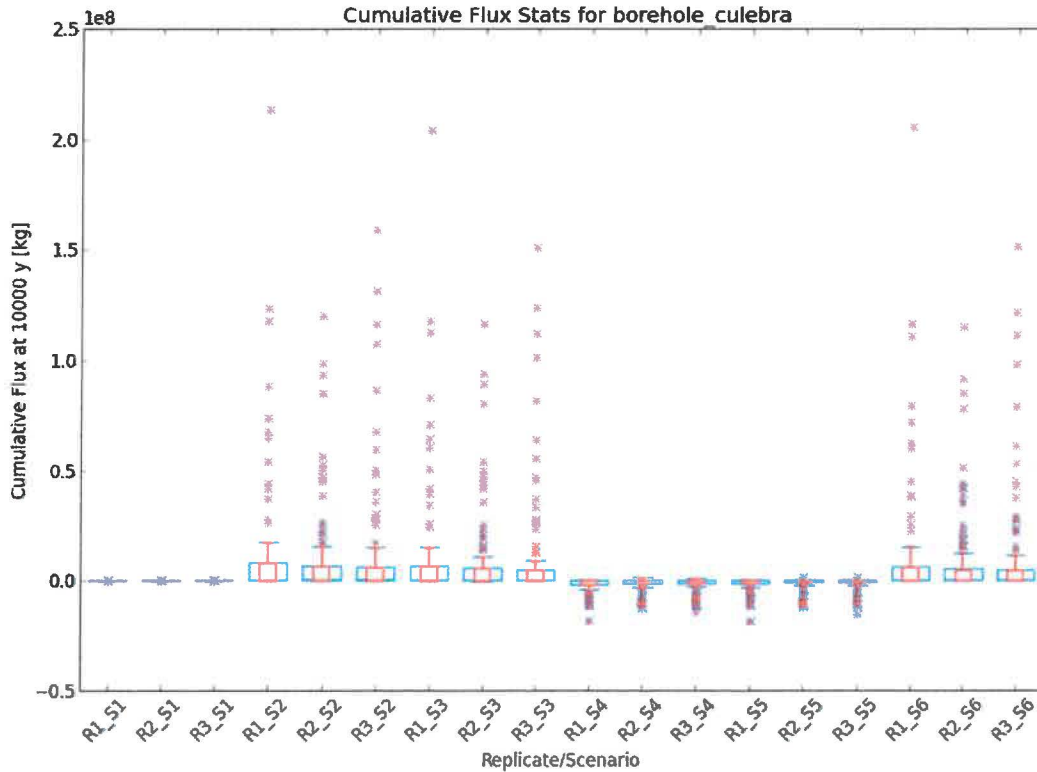
All replicate/scenario pairs (standard tolerances). Scenario 1 is plotted although no borehole intrusion occurs. PFLOTRAN boxes (red) are narrower than BRAGFLO boxes (blue) so that both can be seen. Boxes extend from the 1st to the 3rd quartile. The line dissecting the box is the median. Whiskers extend $1.5 \times$ IQR, where IQR is the interquartile range $= \text{Value}_{3rd} - \text{Value}_{1st}$, or to the extent of the data range, whichever is less. Outliers are plotted with '+' for PFLOTRAN and 'x' for BRAGFLO. Flow direction (sign) is relative to the vertical coordinates of the grid, so that negative flow is downward.

Figure 8.5-4 Uncertainty in cumulative liquid flow across the borehole/Culebra interface.

The results presented above identify one pathway (the borehole) and three scenarios (2, 3, and 6) in which fluid flow could be large enough to advect radionuclides from the repository to the accessible environment (via the Culebra). PFLOTRAN and BRAGFLO simulations predict nearly identical uncertainty distributions (including values of outliers) for borehole flow in these (and other) scenarios. Therefore, it should be possible to propagate PFLOTRAN results through the WIPP PA with negligible effect on the outcome of the PA. Section 8.7 provides a quantitative

analysis of differences between the PFLOTRAN and BRAGFLO solutions on a simulation by simulation basis that supports this conclusion.

8.5.2 Liquid Pressure and Saturation in the Waste Area

Because borehole intrusion occurs in the waste area (WAS_AREA), differences in liquid pressure and saturation in WAS_AREA have greater potential than differences in other regions of the repository to impact predictions of radionuclide release. For each replicate/scenario pair (100 simulations), uncertainties in volume-weighted average liquid pressure and saturation in WAS_AREA were quantified at 17 times, including the nine direct brine release times plus additional times chosen to provide coverage of the entire 10,000 y simulation period. These distributions are shown in Figure 8.5-5 and Figure 8.5-6 for Replicate 1, Scenario 2, one of the replicate/scenario pairs in which large upward mass flow in the borehole has the potential to cause radionuclide release. Distributions resulting from PFLOTRAN and BRAGFLO simulations are nearly identical, as are values of outliers. Appendix B contains additional plots of WAS_AREA pressure and saturation distributions for Scenarios 2, 3, and 6. All show similarly good agreement between the PFLOTRAN and BRAGFLO predictions. Section 8.7 provides a quantitative comparison of pressures and saturations in all repository regions on a simulation by simulation basis.
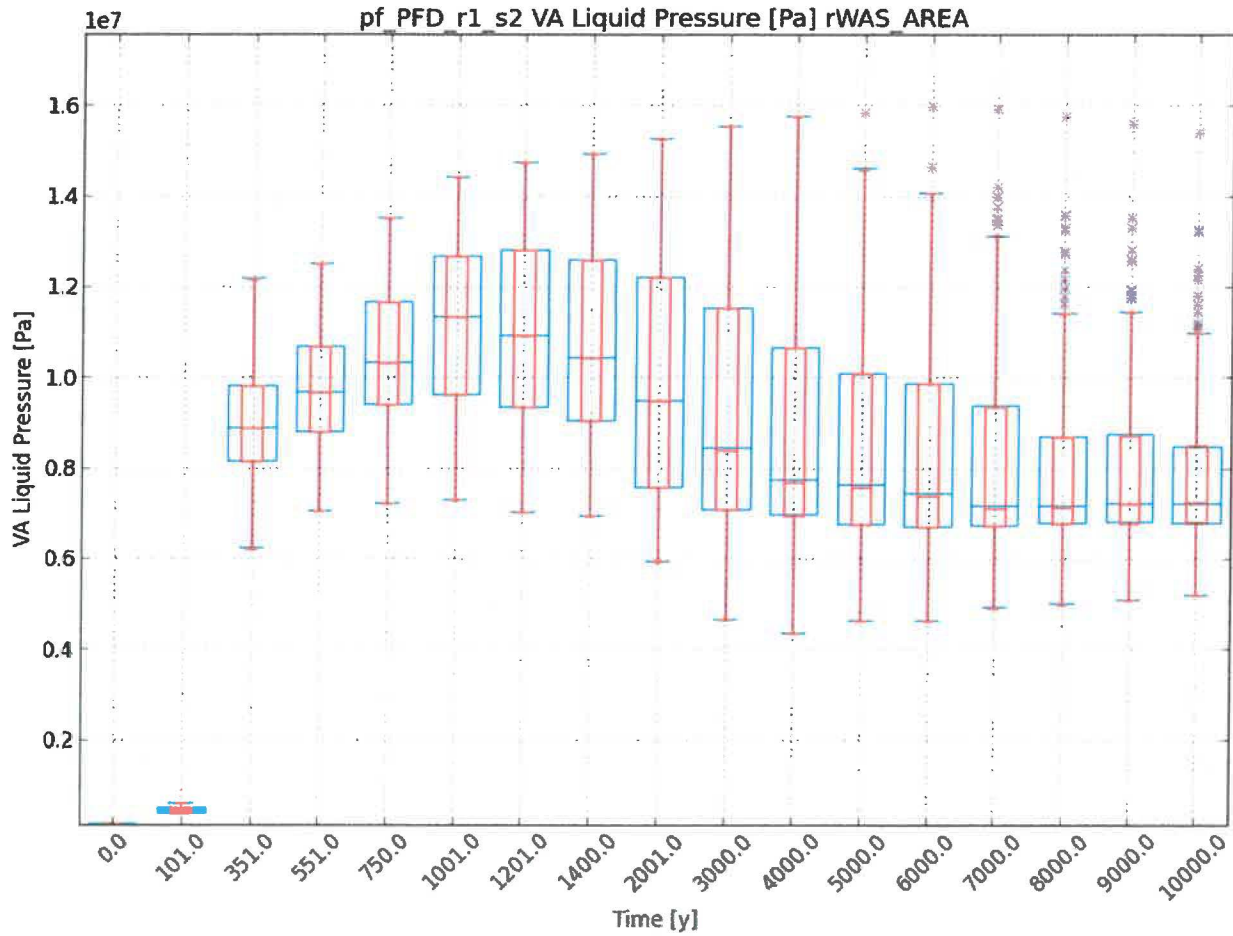
PFLOTRAN boxes (red) are narrower than BRAGFLO boxes (blue) so that both can be seen. Boxes extend from the 1st to the 3rd quartile. The line dissecting the box is the median. Whiskers extend $1.5 \times$ IQR, where IQR is the interquartile range $=$ Value$_{3rd}$ $-$ Value$_{1st}$, or to the extent of the data range, whichever is less. Outliers are plotted with '+' for PFLOTRAN and 'x' for BRAGFLO.

Figure 8.5-5 Uncertainty in volume-weighted average liquid pressure in the waste area in Replicate 1, Scenario 2 (standard tolerances).
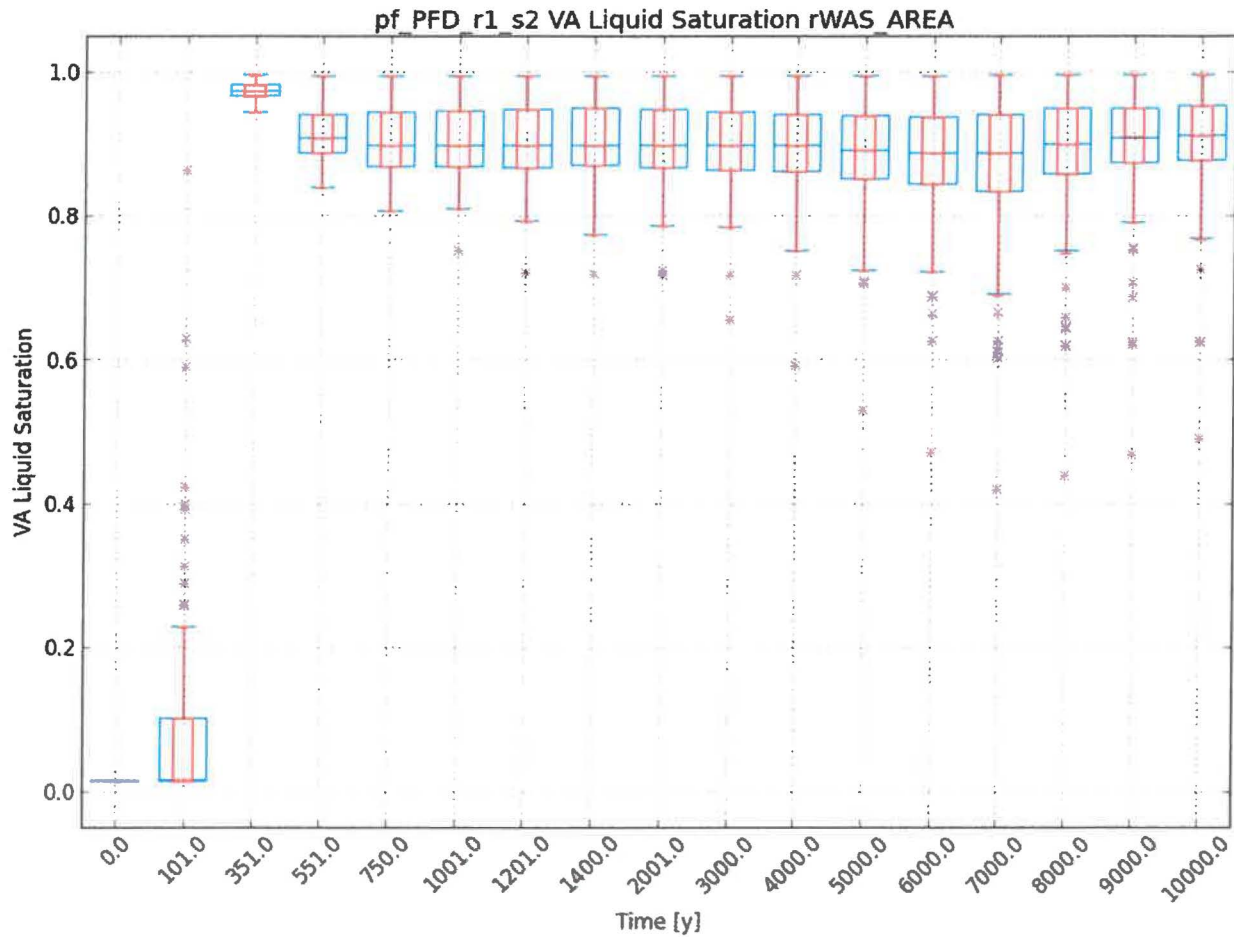
PFLOTRAN boxes (red) are narrower than BRAGFLO boxes (blue) so that both can be seen. Boxes extend from the 1ˢᵗ to the 3ʳᵈ quartile. The line dissecting the box is the median. Whiskers extend $1.5 \times$ IQR, where IQR is the interquartile range $= \text{Value}_{3rd} - \text{Value}_{1st}$, or to the extent of the data range, whichever is less. Outliers are plotted with '+' for PFLOTRAN and 'x' for BRAGFLO.

Figure 8.5-6 Uncertainty in volume-weighted average liquid saturation in the waste area in Replicate 1, Scenario 2 (standard tolerances).

8.6   Comparison of a Typical Simulation (R1S2V001)

Replicate 1, Scenario 2, Vector 001 (R1S2V001) did not exceed any of the difference thresholds used in the quantitative comparison of simulations (Section 8.7, below), and the excellent agreement between solutions seen in R1S2V001 represents the level of agreement typical of the vast majority of the 1800 simulations.

Absolute and relative differences shown in color contour plots were calculated at specific times for each cell in the model domain. Absolute difference on a cell-by-cell basis is defined as:

$$Abs.\,Diff = abs(BRAGFLO_{cell} - PFLOTRAN_{cell})$$

Relative difference on a cell-by-cell basis is defined as:

$$Rel.Diff = \frac{abs(BRAGFLO_{cell} - PFLOTRAN_{cell})}{abs(BRAGFLO_{cell})}$$

Note that, unlike the relative differences reported for the test cases (Sections 5, 6, and 7), this relative difference is not converted to percent difference.

At 349 y, one year prior to borehole intrusion, liquid pressures everywhere in the model domain agree to within a relative difference of 0.0006 with the largest differences in the marker beds down dip (left) of the repository (Figure 8.6-1). Liquid saturations agree equally well; the largest relative difference is approximately 0.0007 in the DRZ above the waste area (Figure 8.6-2).

At 350 y, one year after borehole intrusion, differences in pressure and saturation throughout the model domain remain small: less than 0.004 relative difference in both pressure and saturation with the largest differences in the anhydrite marker bed on either side of the waste area (Figure 8.6-3 and Figure 8.6-4).

Over most of the 10,000-year simulation, relative difference in saturation is less than < 0.01 everywhere in the model domain, although it climbs as high as 0.03 at 650 y in the DRZ down dip of the borehole (Figure 8.6-5). The maximum relative difference in pressure anywhere in the model domain remains < 0.01 throughout the simulation; at 10,000 y it is 0.005 (Figure 8.6-6).
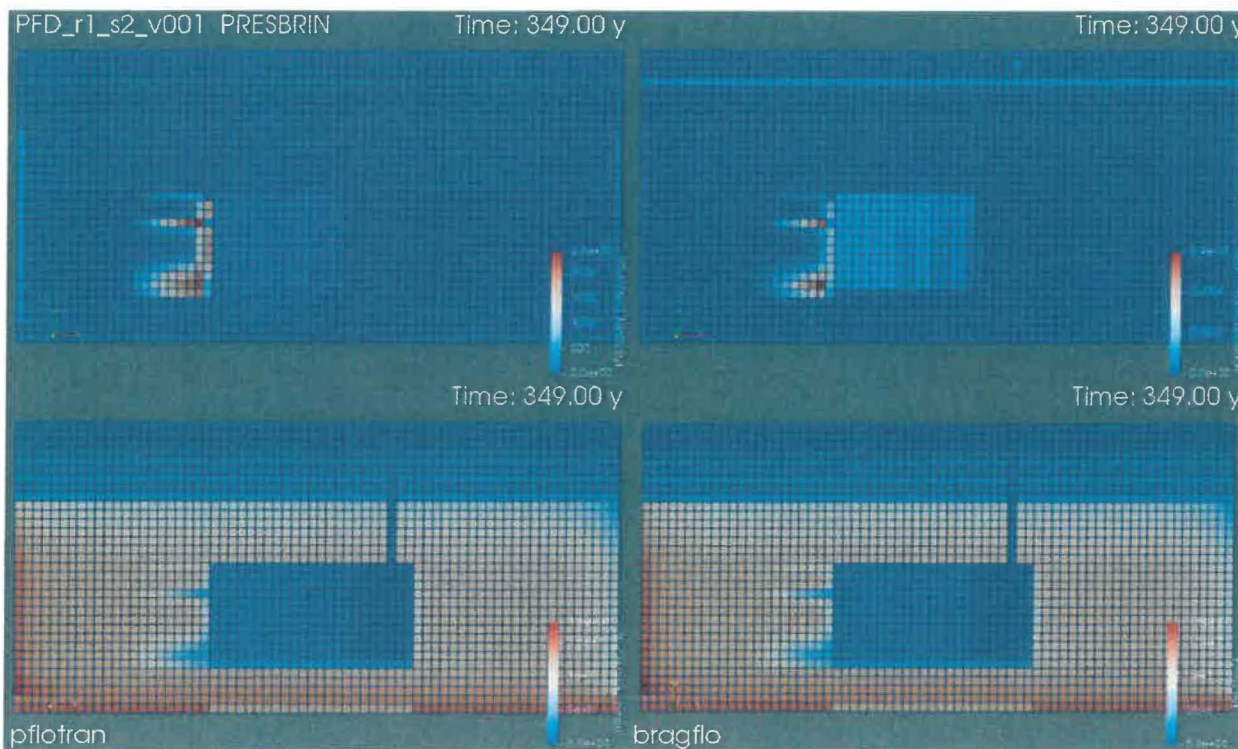
At top: Absolute difference (left) and relative difference (right). At bottom: PFLOTRAN solution (left) and BRAGFLO solution (right).

Figure 8.6-1 Liquid pressure in R1S2V001 at 349 y (one year prior to borehole intrusion).
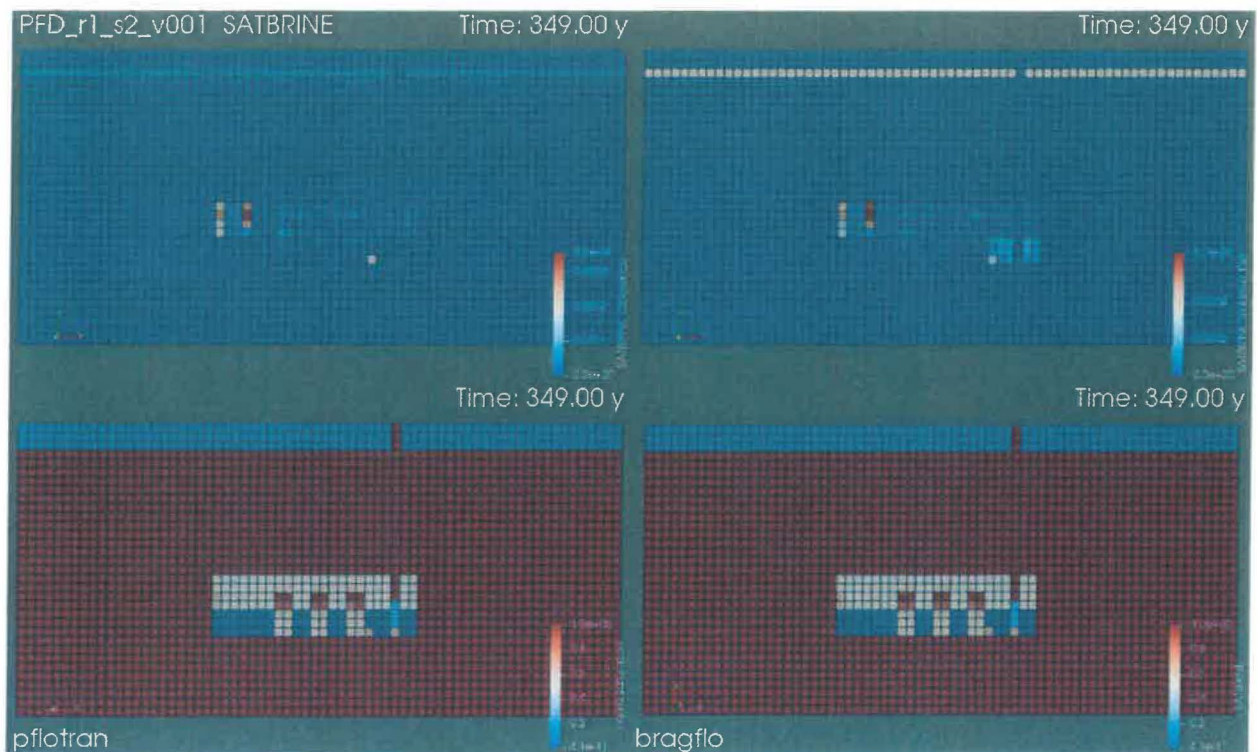
At top: Absolute difference (left) and relative difference (right). At bottom: PFLOTRAN solution (left) and BRAGFLO solution (right).

Figure 8.6-2 Liquid saturation in R1S2V001 at 349 y.
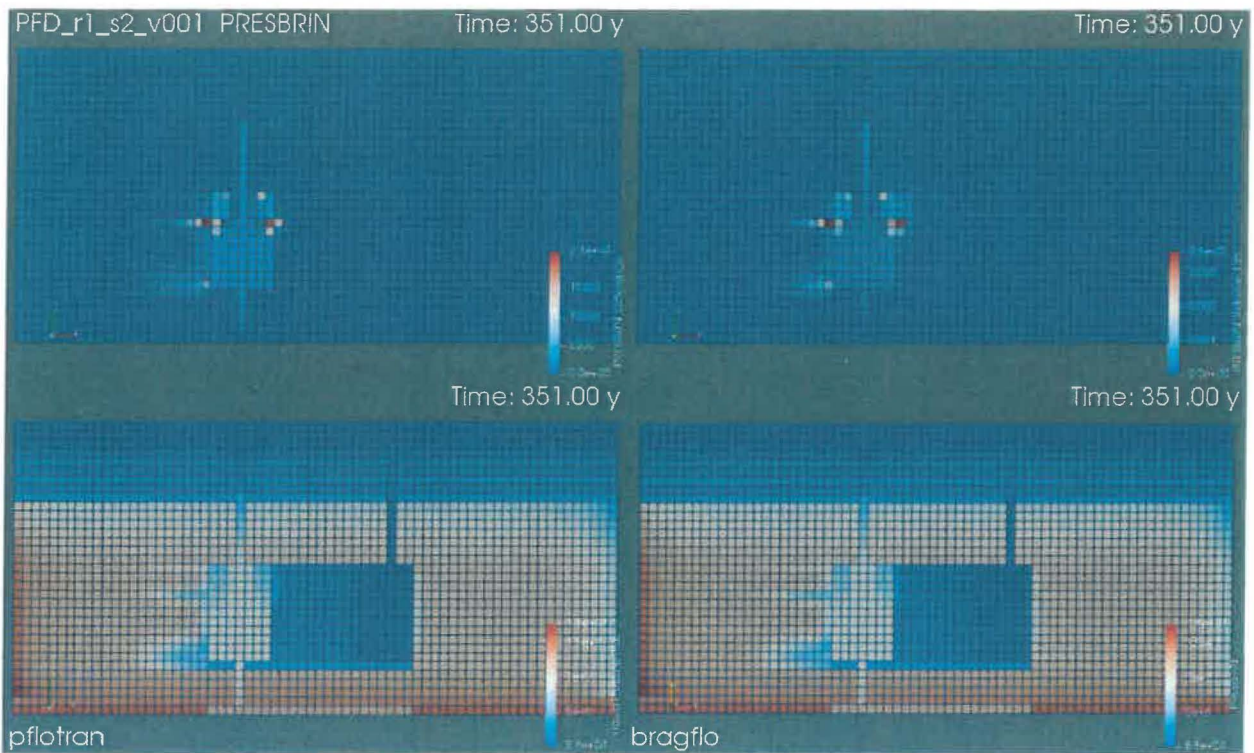
At top: absolute difference (left) and relative difference (right). At bottom: PFLOTRAN solution (left) and BRAGFLO solution (right).

Figure 8.6-3 Liquid pressure in R1S2V001 at 351 y (one year after borehole intrusion).
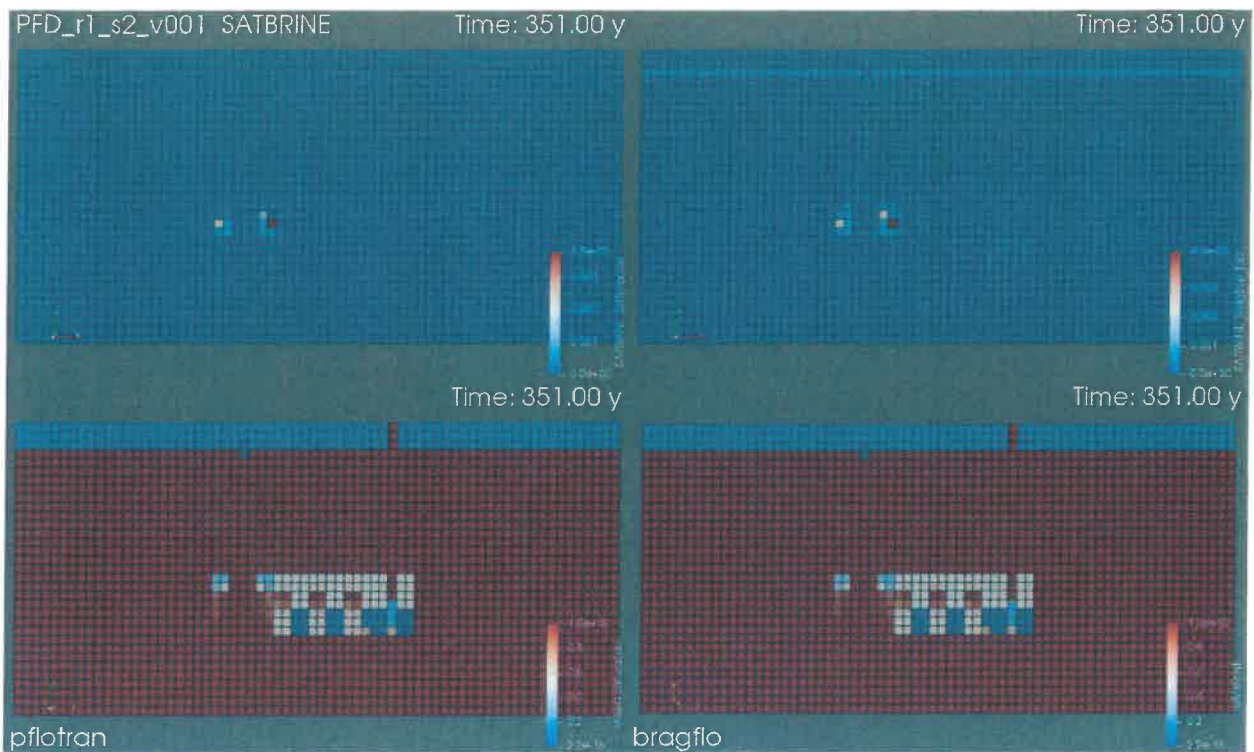
At top: absolute difference (left) and relative difference (right). At bottom: PFLOTRAN solution (left) and BRAGFLO solution (right).

Figure 8.6-4 Liquid saturation in R1S2V001 at 351 y.

Information Only
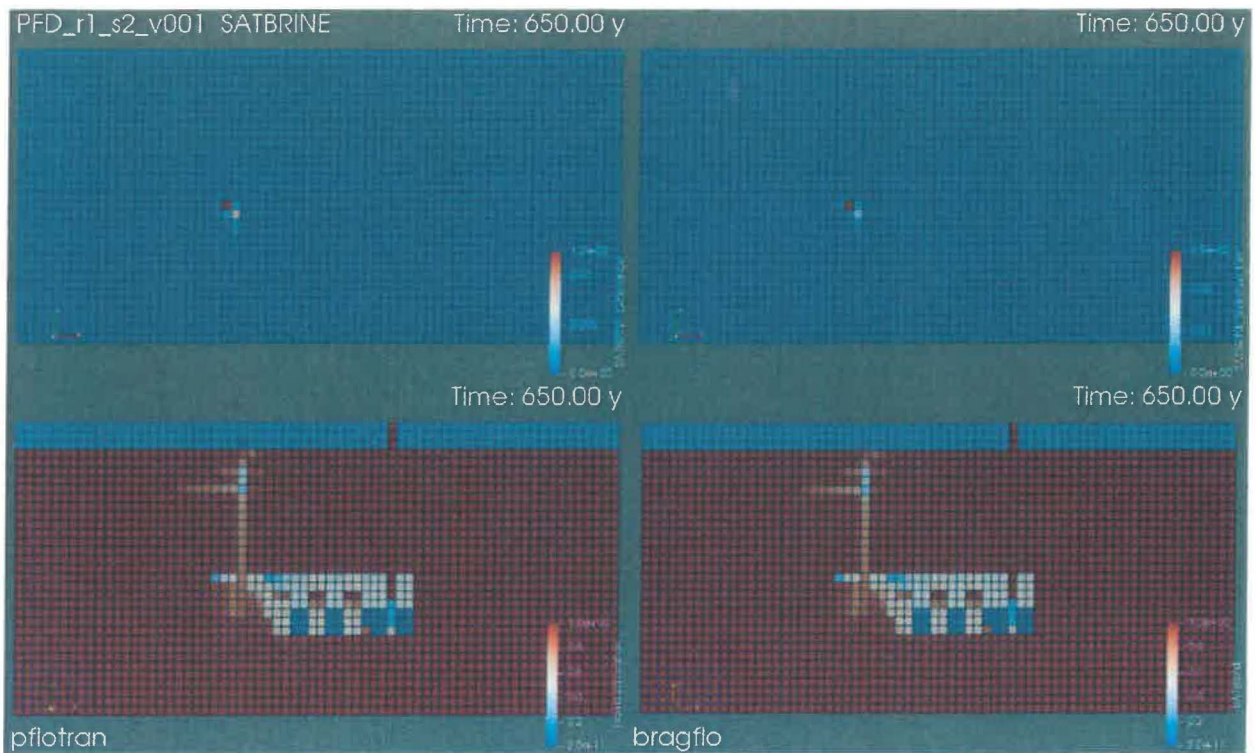
The largest relative difference in saturation at any time in the simulation occurs in the DRZ down dip of the borehole at 650 y. At top: absolute difference (left) and relative difference (right). At bottom: PFLOTRAN solution (left) and BRAGFLO solution (right).

Figure 8.6-5 Liquid saturation in R1S2V001 at 650 y.
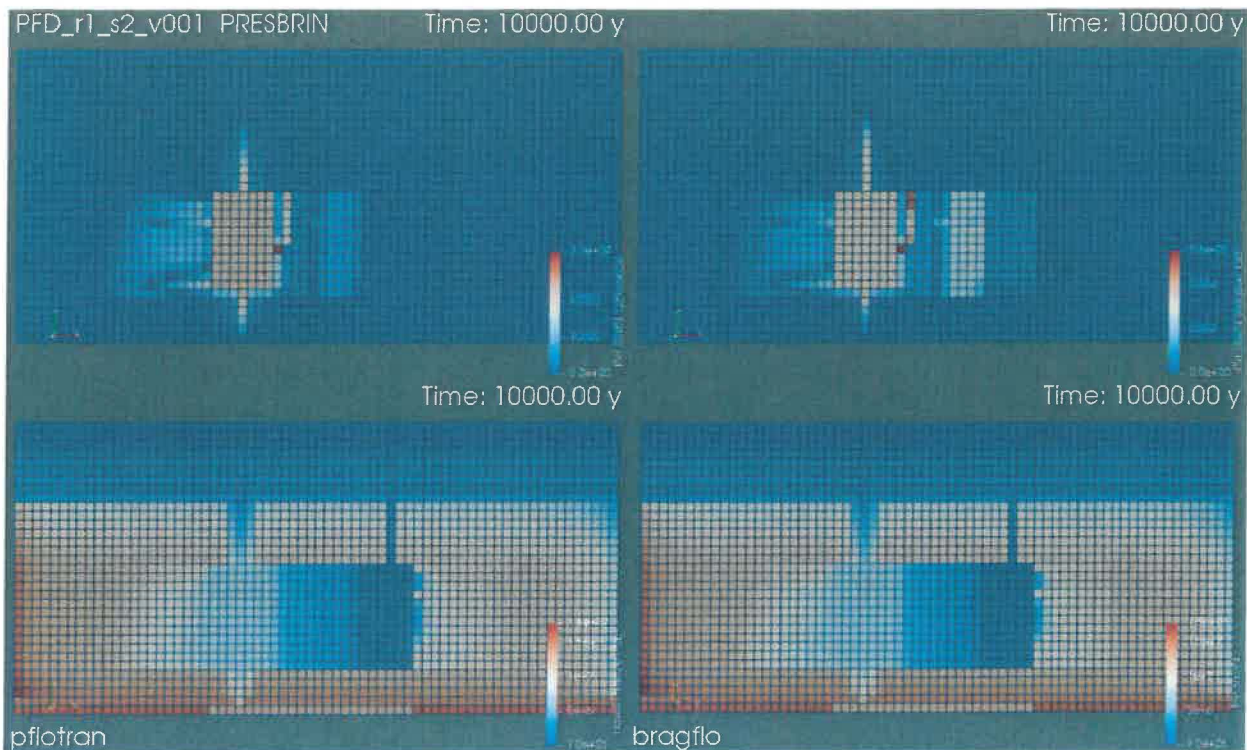
At top: absolute difference (left) and relative difference (right). At bottom: PFLOTRAN solution (left) and BRAGFLO solution (right).

Figure 8.6-6 Liquid pressure in R1S2V001 at 10,000 y.

Line plots of average liquid pressure and average liquid saturation versus time confirm that the PFLOTRAN and BRAGFLO solutions are nearly identical through time in all nine regions of the repository (Figure 8.6-7–Figure 8.6-9). Relative differences in these quantities (calculated using the metrics defined in Section 8.7.1.1) are similar in size to relative differences calculated for each cell, and are < 0.004 (Table 8.6-1).
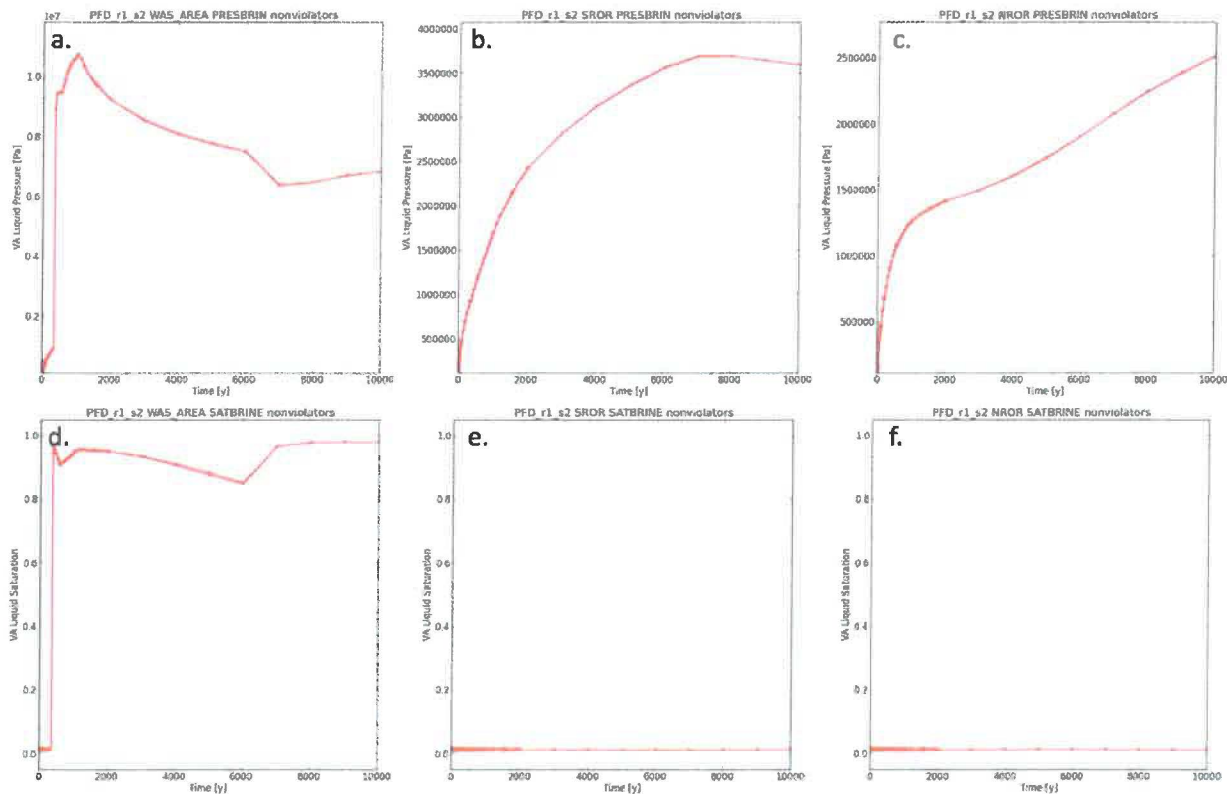
PFLOTRAN and BRAGFLO curves plot on top of each other. Symbols (PFLOTRAN '+' and BRAGFLO 'x') indicate 65 output times.

Figure 8.6-7 Volume-weighted average liquid pressure (top) and saturation (bottom) versus time in R1S2V001 WAS_AREA (left), SROR (middle), and NROR (right).
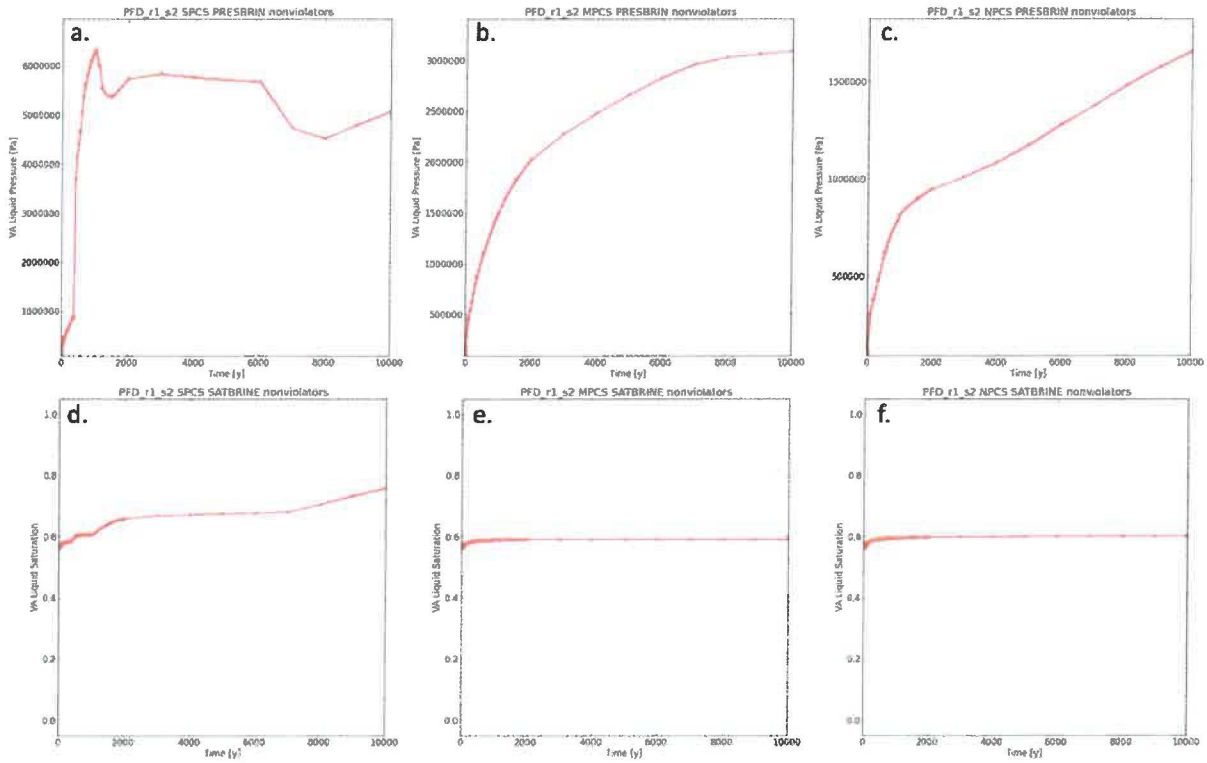
PFLOTRAN and BRAGFLO curves plot on top of each other. Symbols (PFLOTRAN '+' and BRAGFLO 'x') indicate 65 output times

Figure 8.6-8 Volume-weighted average liquid pressure (top) and saturation (bottom) versus time in R1S2V001 SPCS (left), MPCS (middle), and NPCS (right)..
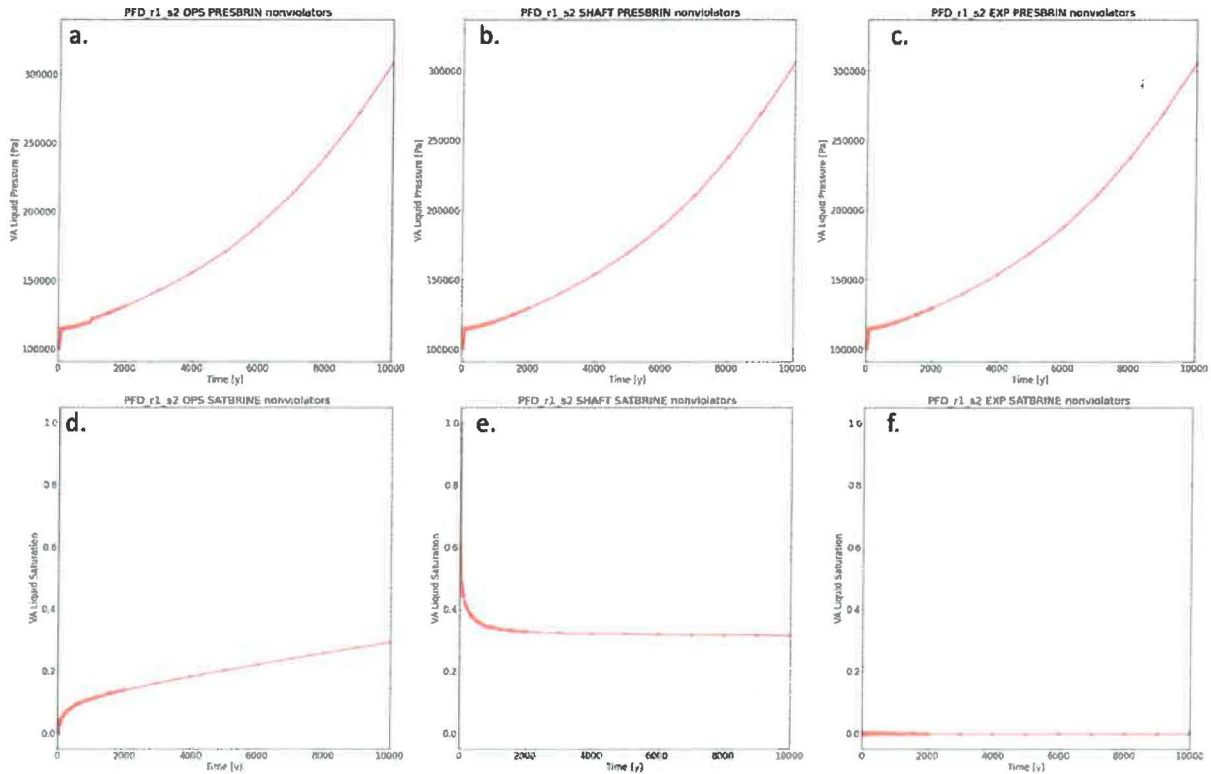
PFLOTRAN and BRAGFLO curves plot on top of each other. Symbols (PFLOTRAN '+' and BRAGFLO 'x') indicate 65 output times.

Figure 8.6-9 Volume-weighted average liquid pressure (top) and saturation (bottom) versus time in R1S2V001 OPS (left), SHAFT (middle), and EXP (right).

Table 8.6-1 Absolute and Relative Differences in Volume-Weighted Average Liquid Pressure and Saturation for R1S2V001.

Region	Liquid Pressure		Liquid Saturation	
	Abs Diff (Pa)	Rel Diff	Abs Diff	Rel Diff
WAS_AREA	29240	3.83E-03	2.1E-03	2.37E-03
SROR	5173	1.71E-03	4.8E-06	3.23E-04
NROR	3928	2.21E-03	7.2E-09	4.83E-07
SPCS	14604	2.82E-03	6.1E-04	9.02E-04
MPCS	2191	8.86E-04	1.9E-05	3.14E-05
NPCS	3319	2.82E-03	6.0E-06	9.96E-06
OPS	122	6.56E-04	1.9E-05	9.70E-05
SHAFT	122	6.63E-04	1.8E-06	5.42E-06
EXP	122	6.63E-04	2.2E-09	1.05E-04

Line plots of cumulative liquid flow versus time demonstrate good agreement between the PFLOTRAN and BRAGFLO solutions at the borehole/Culebra interface and the shaft/Culebra interface (Figure 8.6-10). Relative differences in flow at these location are less than 0.03

(calculated using the metric defined in Section 8.7.1.2). At the marker bed locations, relative differences are larger (Table 8.6-2), but the cumulative flow at 10,000 y is nearly zero (<0.5 kg) (Figure 8.6-11).
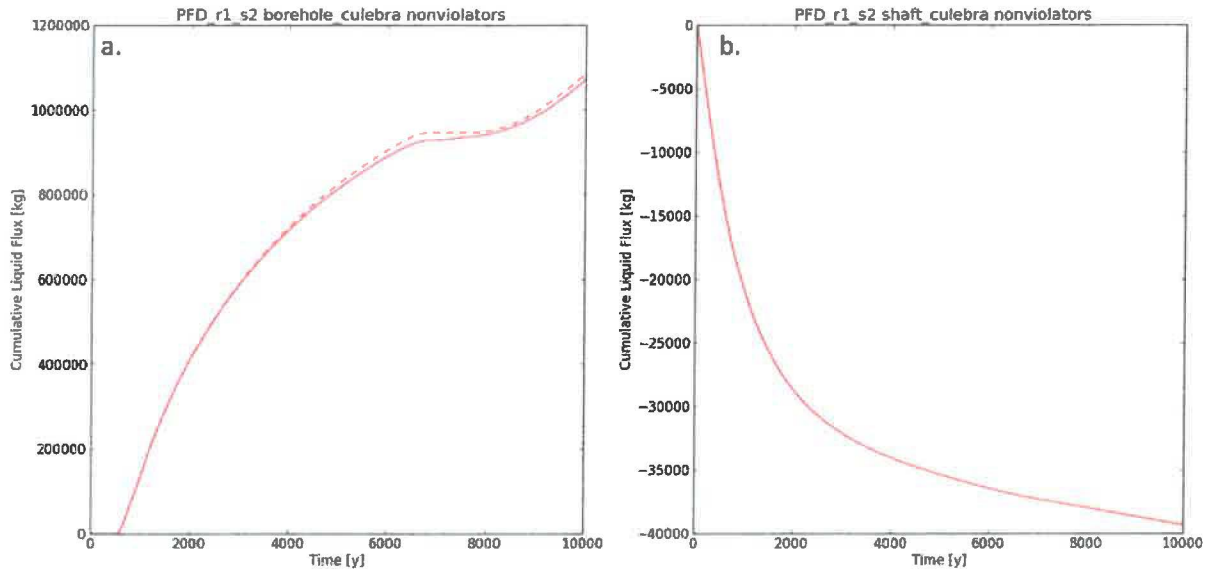
Values are plotted at every time step (PFLOTRAN solid line and BRAGFLO dashed line). Positive flow is upward.

Figure 8.6-10 Cumulative liquid flow versus time in R1S2V001 at the borehole/Culebra intersection (a) and the shaft/Culebra intersection (b).
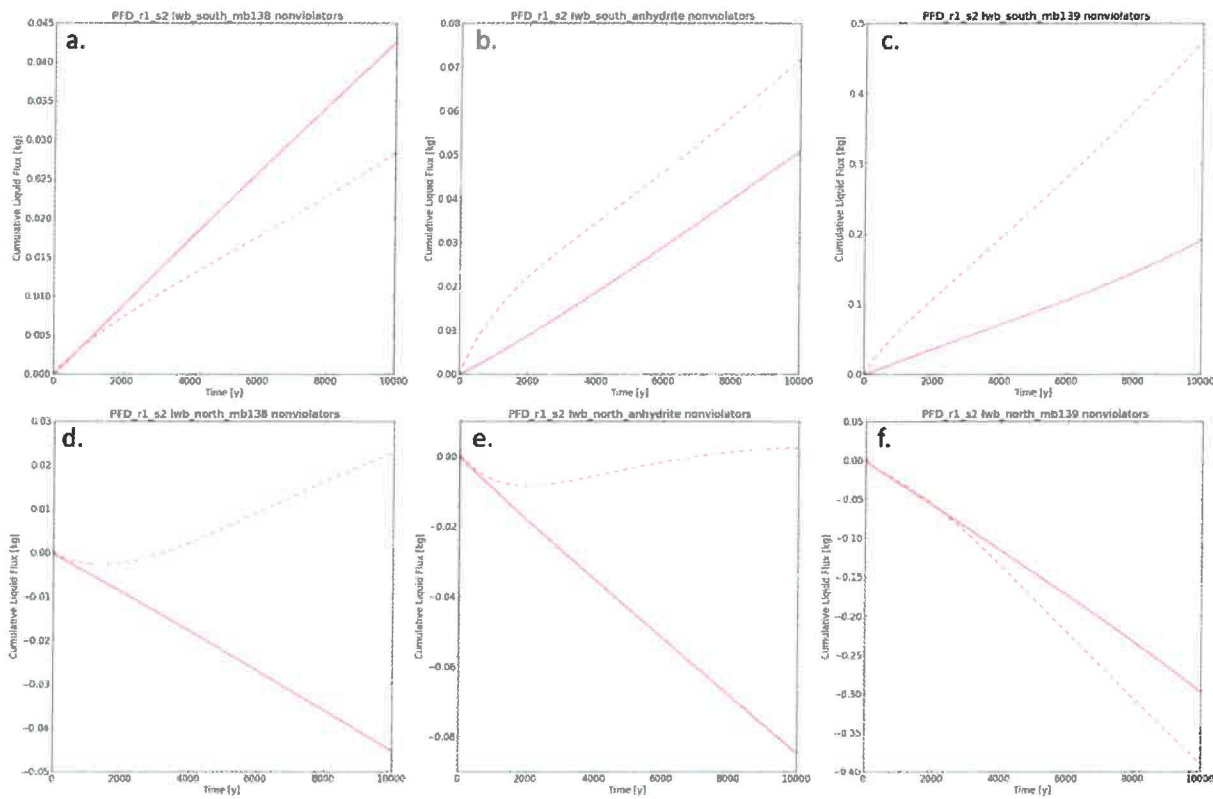
At top: south land withdrawal boundary (a. MB138; b. Anhydrite AB; c. MB139). At bottom: north land withdrawal boundary (d. MB138; e. Anhydrite AB; f. MB139). Values are plotted at every time step (PFLOTRAN solid line and BRAGFLO dashed line). Positive flow at the south land withdrawal boundary and negative flow at the north land withdrawal boundary are toward the repository. Note that all of these cumulative flows are essentially zero, < 0.5 kg over 10,000 yr.

Figure 8.6-11 Cumulative liquid flow versus time in R1S2V001 in the marker beds across the land withdrawal boundaries.

Table 8.6-2 Absolute and Relative Differences in Liquid Flow for R1S2V001.

Location	Liquid Flow	
	Abs Diff (kg)	Rel Diff
slwb MB138	1.47E-02	5.15E-01
slwb ANH_AB	2.12E-02	2.94E-01
slwb MB139	2.83E-01	5.96E-01
nlwb MB138	6.82E-02	2.42
nlwb ANH_AB	8.72E-02	4.44
nlwb MB139	9.70E-02	2.49E-01
Borehole/Culebra	3.59E+04	3.29E-02
Shaft/Culebra	1.71E+01	4.31E-04

8.7 Quantifying Differences for 1800 Simulations

8.7.1 Quantification of Differences

8.7.1.1 Liquid Pressure and Liquid Saturation

Outputs of liquid pressure and liquid saturation were saved at 65 user-specified times. The absolute difference between the PFLOTRAN and BRAGFLO solutions for a given region of the model domain is calculated by integrating the area between the curves (liquid pressure or liquid saturation versus time) and normalizing by the duration of the simulation (10000 y):

$$Abs.Diff. = \frac{\int_0^{10000} abs(BRAGFLO - PFLOTRAN)dt}{10000}$$

The absolute value of the difference (BRAGFLO-PFLOTRAN) is used in the integration so that positive and negative differences do not cancel each other out (Figure 8.7-1). The resulting value is normalized by the duration of the simulation so that the "absolute difference" is comparable to (having the same units and meaningful magnitude) individual values of pressure or saturation.
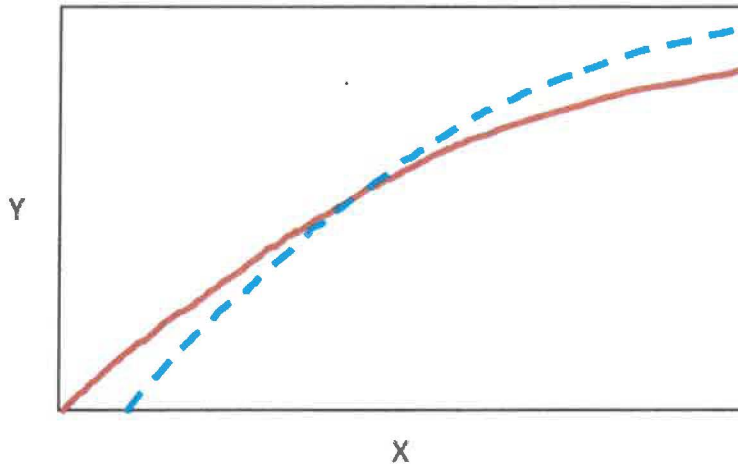
At small values of X the difference (Solid – Dashed) is positive and at large values of X it is negative. The absolute value of the difference between BRAGFLO and PFLOTRAN solutions is used in the integration of the area between the curves so that all differences are counted regardless of sign and none are cancelled due to occurrence of differences with the opposite sign.

Figure 8.7-1 Differencing schematic.

The relative difference between the two solutions is calculated by dividing the area between the curves by the area under the BRAGFLO curve:

$$Rel.Diff. = \frac{\int_0^{10000} abs(BRAGFLO - PFLOTRAN)dt}{\int_0^{10000} BRAGFLO\, dt}$$

Use of absolute values in the integration of the area under the BRAGFLO curve is not necessary because the volume-weighted averages of liquid pressure and liquid saturation are always greater than zero.

8.7.1.2 Liquid Flow

Liquid mass flow output was saved at every time step. The absolute difference between the PFLOTRAN and BRAGFLO solutions across a given plane is calculated by integrating the area between the curves (flow rate (kg/y) versus time):

$$Abs.Diff. = \int_0^{10000} abs(BRAGFLO - PFLOTRAN)dt$$

The absolute value of the difference (BRAGFLO-PFLOTRAN) is used in the integration so that positive and negative differences do not cancel each other out. Because absolute difference in flow is not divided by 10,000 (normalized by the duration of simulation), it has the same units as cumulative flow. In the case where liquid flow in both simulations (BRAGFLO and PFLOTRAN) is always positive (or always negative) and the two curves do not cross each other, use of the above equation is identical to taking the absolute value of the difference in cumulative flow at the end of the simulation.

The relative difference between the two flow solutions is calculated by dividing the area between the curves by the area under the BRAGFLO curve:

$$Rel.Diff. = \frac{\int_0^{10000} abs(BRAGFLO - PFLOTRAN)dt}{\int_0^{10000} abs(BRAGFLO)dt}$$

Use of the absolute value in the denominator assures that all contributions to the cumulative relative error are positive—given that liquid flow rate can be either negative or positive.

8.7.2 Difference Thresholds

Individual simulations (of the 1800 compared) were flagged for investigation and explanation of differences by comparing the relative and absolute differences in outputs to predetermined threshold values. For liquid pressure and liquid saturation, a small value (0.02) is used for the threshold in relative difference. The relative difference threshold for liquid flow (0.1) is derived from the threshold for liquid saturation as explained below. Because small absolute differences can cause large relative differences when parameter values are small, threshold values for absolute difference in liquid saturation and absolute difference in liquid flow are used to avoid flagging simulations in which saturation or flow is close to zero. Threshold values are summarized in Table 8.7-1 and choices are explained below.

Table 8.7-1 Threshold values for absolute and relative difference.

	Abs. Diff.	Rel. Diff.
Liquid Pressure	none	0.02
Liquid Saturation	0.01	0.02
Cumulative Liquid Flow	100 kg	0.1

8.7.2.1 Liquid Pressure

Simulations exceeding the relative difference threshold of 0.02 for volume-weighted average liquid pressure in any region of the repository were flagged for further analysis. An absolute

difference threshold is not used in the comparison of liquid pressures. Figure 8.7-2 provides a visual comparison of the differences in liquid pressure in the operations area (OPS) in Replicate 1, Scenario 2 (10^{-2} tolerances) flagged using the 0.02 relative difference threshold with those flagged using a relative difference threshold of 0.01. In this case, using the larger threshold eliminates 2 of 7 vectors from the list of violators: vector 63 (yellow) and vector 85 (green). In general, using the larger threshold avoids flagging vectors with nearly indiscernible gaps between the curves.
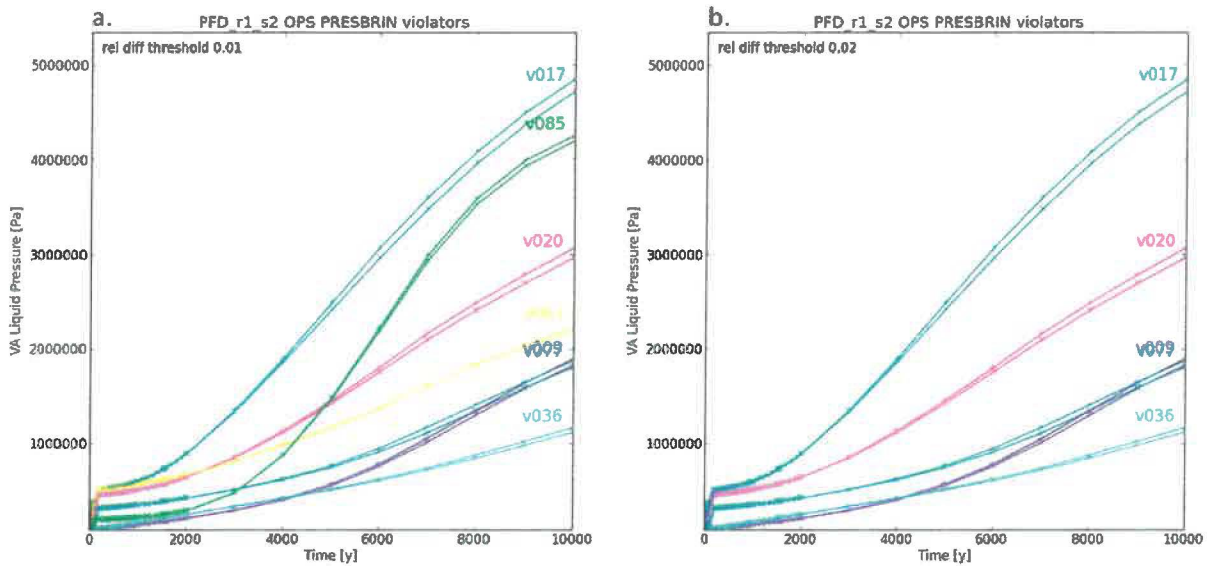
R1S2 OPS. Symbols for PFLOTRAN and BRAGFLO are '+' and 'x', respectively, shown at 65 output times.

Figure 8.7-2 Volume-weighted average liquid pressure versus time in vectors flagged using a relative difference threshold of 0.01 (a) or a relative difference threshold of 0.02 (b).

8.7.2.2 Liquid Saturation

Simulations exceeding the relative difference threshold of 0.02 and an absolute difference threshold of 0.01 for volume-weighted average liquid saturation in any region of the repository were flagged for further analysis. Figure 8.7-3a shows those vectors that exceed the relative difference threshold in the experimental area (EXP) in Replicate 1, Scenario 2 (10^{-2} tolerances), and Figure 8.7-3b shows the vectors that exceed both the relative difference and absolute difference thresholds. Application of both thresholds tends to eliminate vectors with liquid saturations near zero, which have little potential to contribute to radionuclide release.
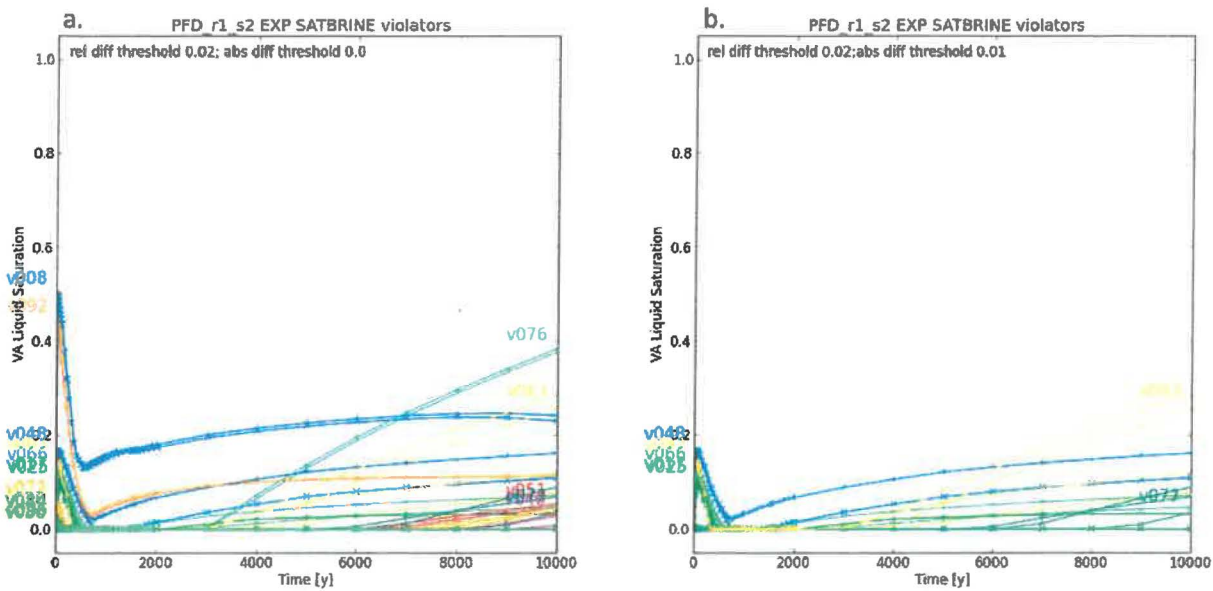
R1S2 EXP. Symbols for PFLOTRAN and BRAGFLO are '+' and 'x', respectively, shown at 65 output times.

Figure 8.7-3 Volume-weighted average liquid saturation versus time in vectors flagged using a relative difference threshold of 0.02 and an absolute difference threshold of 0 (a) or 0.01 (b).

8.7.2.3 Liquid Flow

Simulations exceeding the relative difference threshold of 0.1 and an absolute difference threshold of 100 kg at any of the flow comparison locations were flagged for further analysis. Both choices are explained below.

The 100 kg absolute difference threshold is used to avoid flagging simulations with high relative differences but near zero flow at the land withdrawal boundaries (such as R1S2V001 in Section 8.6). Given the large brine mass contained between the repository and any of the marker bed/land withdrawal boundary locations (Table 8.5-1), a 100 kg cumulative flow is insufficient to transport brine from the repository to the land withdrawal boundary. Use of the 100 kg absolute difference threshold does not prevent flagging any simulations that exceed the relative difference threshold for flow in either the shaft or borehole.

The 0.1 relative difference threshold accounts for the propagation of differences in pressure and saturation through the flux calculation. Liquid flux has a linear dependence on the gradient in liquid pressure and on the liquid density (function of pressure), and a nonlinear dependence on liquid saturation, which propagates through relative permeability. Small differences in liquid saturation (S_l) result in much larger differences in relative permeability (k_l^r) and therefore in flux. Specifically, for material BH_SAND, the material present in the borehole when liquid flow is largest, liquid relative permeability is calculated using KRP4:

$$k_l^r = S_{e1}^{3+2/\lambda}; \; S_l > S_{rl}$$

where effective saturation (S_{e1}) is:

$$S_{e1} = \frac{S_l - S_{rl}}{1 - S_{rl}}$$

The constant $\lambda = 0.94$, and residual liquid saturation $S_{rl} = 0$. Substitution of these parameter values into the above equations results in $k_l^r = S_l^{5.13}$. Given a 0.01 relative difference in S_l, the resulting relative difference in k_l^r is approximately 0.05, and given a 0.02 relative difference in S_l, the relative difference in k_l^r is approximately 0.1[20]. Figure 8.7-4 compares the differences in liquid flux at the borehole/Culebra intersection (for Replicate 2, Scenario 4, 10^{-2} tolerances) flagged using relative difference thresholds of 0.05 and 0.1. Simulations in which differences exceed the larger threshold were chosen for additional analysis and explanation of differences.
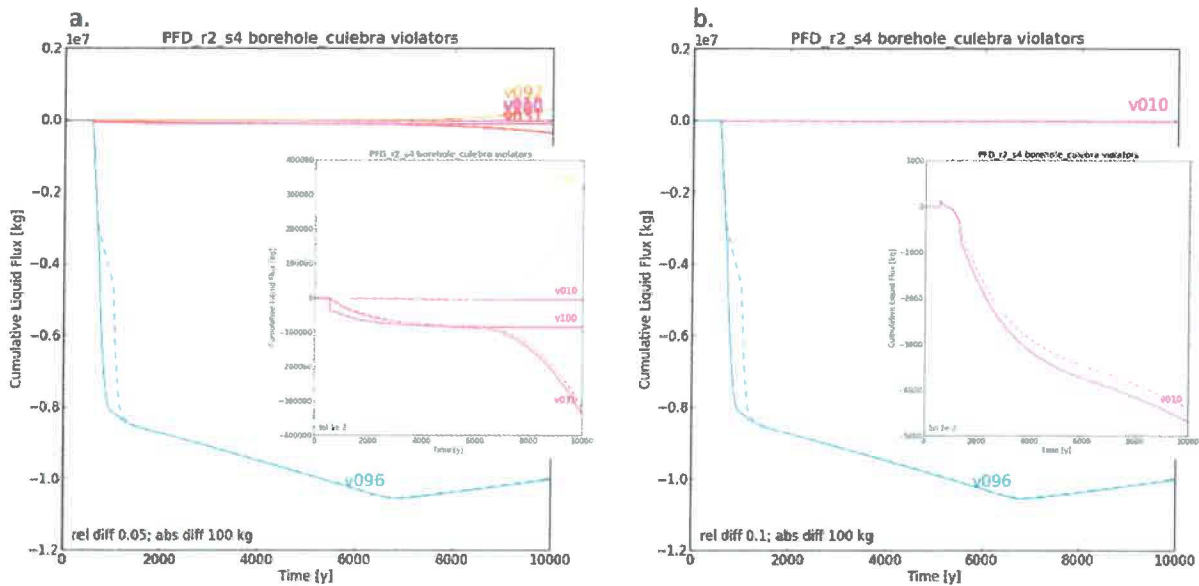
R2S4, borehole/Culebra interface. Values are plotted at every time step (PFLOTRAN solid line and BRAGFLO dashed line).

Figure 8.7-4 Cumulative liquid flow versus time for vectors flagged using a relative difference threshold of 0.05 (a) or a relative difference threshold of 0.1 (b).

8.7.3 *Visualization*

Visualization of differences on a simulation by simulation basis relied upon scatter plots and horsetail (line) plots (Appendices $E - K$). For each replicate/scenario/output combination, a scatter plot of relative difference versus absolute difference provided an at-a-glance summary of how differences in individual simulations compare to absolute and relative difference thresholds. After vectors exceeding the thresholds were identified, horsetail plots of output versus time were generated for each replicate/scenario/output combination. A single horsetail plot was generated if no vectors exceeded the thresholds. Otherwise, two plots were generated, one of violators and one

---

[20] These values result from combining the expressions for relative difference in k_l^r and S_l: $Rel.Diff(k_l^r) = 1 - (1 - Rel.Diff(S_l))^{5.13}$.

of non-violators. Line plots of violators were used to choose representative vectors for detailed analysis, so that factors contributing to differences could be identified. Line plots of non-violators were used to verify that the method of quantifying differences adequately identified simulations in which PFLOTRAN and BRAGFLO results significantly differed.

A complete set of scatter plots and horsetail plots was generated for the comparison with 10^{-2} tolerances and for the comparison with 10^{-4} tolerances. The sheer number of plots generated prohibits inclusion of all of them in the report. Because 10^{-2} tolerances are the standard tolerances used in PA, the plots included in the body of the report and in the appendices focus on the results of the 10^{-2} tolerance comparison.

The 10^{-4} tolerance comparison allowed the creation of a third set of line plots – simulations that violated difference criteria with 10^{-2} tolerances replotted with 10^{-4} tolerances. Plots of this type are included in both the body of the report and in select appendices.

8.7.4 Counts of Differences Across 1800 Simulations

This section identifies specific simulations that exceed threshold values for volume-weighted average liquid pressure or saturation in any of the nine repository regions, and for liquid flow at any of the eight flow comparison locations.

8.7.4.1 Liquid Pressure with Standard Tolerances (10^{-2})

Using 10^{-2} tolerances, 18 of 1800 simulations exceed the 0.02 relative difference threshold for volume-weighted average liquid pressure in one or more regions of the repository. Table 8.7-2 provides a count of "violators" (simulations in which the threshold is exceeded) for each region of the repository by replicate and scenario. The totals listed in Table 8.7-2 sum to greater than 18, because all simulations that exceed the relative difference threshold in SHAFT and EXP also exceed the relative difference threshold in OPS. Scatter plots of relative difference versus absolute difference in average liquid pressure for WAS_AREA and OPS are presented in Appendix E and Appendix F, respectively. Line plots of average liquid pressure versus time (horsetail plots) of violators and non-violators for these regions are also in these appendices.

Only two simulations (R2S4V096 and R2S5V096) exceed the threshold in the WAS_AREA, the region of the repository in which differences in pressure have the greatest potential to contribute to differences in radionuclide transport (Section 8.5).

Table 8.7-2 Liquid Pressure: Number of simulations that exceed the difference threshold in each region when run with standard (10^{-2}) tolerances.

	WAS_AREA	SROR	NROR	SPCS	MPCS	NPCS	OPS	SHAFT	EXP
Scenario 1									
r1	0	0	0	0	0	0	0	0	0
r2	0	0	0	0	0	0	0	0	0
r3	0	0	0	0	0	0	0	0	0
Scenario 2									
r1	0	0	0	0	0	0	5	4	2
r2	0	0	0	0	0	0	1	1	0
r3	0	0	0	0	0	0	0	0	0

Scenario 3									
r1	0		0	0	0	0	0	0	0	0
r2	0		0	0	0	0	0	2	0	0
r3	0		0	0	0	0	0	1	0	0
Scenario 4									
r1	0		0	0	0	0	0	2	1	1
r2	1		0	0	0	0	0	2	1	0
r3	0		0	0	0	0	0	1	1	1
Scenario 5									
r1	0		0	0	0	0	0	1	1	0
r2	1		0	0	0	0	0	0	0	0
r3	0		0	0	0	0	0	0	0	0
Scenario 6									
r1	0		0	0	0	0	0	0	0	0
r2	0·		0	0	0	0	0	1	1	1
r3	0		0	0	0	0	0	0	0	0
Totals									
	2		0	0	0	0	0	16	10	5

Tightening tolerances to 10^{-4} decreases the number of simulations exceeding the liquid pressure relative difference threshold to three (Appendix C). A single simulation, R2S5V096, violates liquid pressure criteria when run with both standard and tight tolerances. This simulation, which violates liquid pressure criteria in WAS_AREA, was chosen for additional analysis and explanation of differences (Appendix D).

8.7.4.2   Liquid Saturation with Standard Tolerances (10^{-2})

Using 10^{-2} tolerances, 325 of 1800 simulations exceed the absolute and relative difference thresholds for volume-weighted average liquid saturation in one or more regions of the repository. Table 8.7-3 provides a count of violators for each region of the repository by replicate and scenario. The totals listed in Table 8.7-3 sum to greater than 325, because some simulations exceed the relative and absolute difference thresholds in more than one region. Scatter plots of relative difference versus absolute difference in average liquid saturation for WAS_AREA and OPS are presented in Appendix G and Appendix H, respectively. Horsetail plots of violators and non-violators for these regions are also in these appendices.

Only three simulations exceed the liquid saturation relative difference threshold in WAS_AREA – these are R2S1V083, R2S4V083, and R2S5V083. That the large number of violations in SHAFT, OPS, and EXP is distributed across all scenarios indicates that model behavior in these regions (like cumulative flow in the shaft – Section 8.5.1) is independent of borehole intrusion. Differences in these regions are likely due to local differences in solution that would not affect flow up the borehole (and thus radionuclide releases). This idea is supported by the discussion in Appendix D, Analysis of Differences.

Table 8.7-3 Liquid Saturation: Number of simulations that exceed the difference thresholds in each region when run with standard (10^{-2}) tolerances.

	WAS_AREA	SROR	NROR	SPCS	MPCS	NPCS	OPS	SHAFT	EXP
Scenario 1									
r1	0	0	0	0	0	1	4	10	2
r2	1	0	0	2	0	1	5	11	4
r3	0	0	0	0	0	0	7	10	1
Scenario 2									
r1	0	0	0	0	0	1	12	18	7
r2	0	0	0	0	0	1	15	15	5
r3	0	0	0	0	0	0	16	9	4
Scenario 3									
r1	0	0	0	0	0	1	9	15	3
r2	0	1	0	0	1	1	14	19	6
r3	0	0	0	0	0	0	10	11	0
Scenario 4									
r1	0	0	0	0	0	1	10	17	4
r2	1	1	0	3	0	2	12	14	5
r3	0	0	0	0	0	0	13	12	3
Scenario 5									
r1	0	0	0	0	0	1	12	19	4
r2	1	0	0	2	0	2	7	15	4
r3	0	0	0	1	0	0	6	8	0
Scenario 6									
r1	0	0	0	0	0	1	6	12	2
r2	0	1	0	0	1	1	12	19	5
r3	0	0	0	1	0	0	11	13	1
Totals									
	3	3	0	9	2	14	181	247	60

Reducing tolerances to 10^{-4} decreases the total number of simulations exceeding the liquid saturation difference thresholds to 84 (Appendix I) – 80 violations occur in SHAFT, OPS, or EXP and one in WAS_AREA. Further analysis of differences in liquid saturation (Appendix D) focuses on R2S4V031, the simulation that violates liquid saturation criteria in SROR with both standard and tight tolerances.

8.7.4.3 Liquid Flow with Standard Tolerances (10^{-2})

Using 10^{-2} tolerances, 18 of 1800 simulations exceed the liquid flow absolute and relative difference thresholds at the borehole/Culebra intersection, and 32 at the shaft/Culebra intersection (Table 8.7-4). No simulations exceed both thresholds at any of the marker bed locations. Scatter plots of relative difference versus absolute difference in liquid flow at the borehole, the shaft, and one land withdrawal boundary location (Anhydrite AB at the south land withdrawal boundary) are

presented in Appendices I, J, and K, respectively, together with horsetail plots for violators and non-violators at the same locations.

Table 8.7-4 Liquid Flow: Number of simulations that exceed the difference thresholds when run with standard (10^{-2}) tolerances.

	Number of Violators			Vector IDs	
	Marker Beds	Borehole	Shaft	Borehole	Shaft
Scenario 1					
r1	0	NA	2	NA	27, 91
r2	0	NA	1	NA	27
r3	0	NA	2	NA	27, 84
Scenario 2					
r1	0	1	2	37	27, 91
r2	0	0	0		
r3	0	0	3		27, 46, 84
Scenario 3					
r1	0	0	2		27, 91
r2	0	0	0		
r3	0	0	4		27, 46, 80, 84
Scenario 4					
r1	0	3	2	6, 17, 78	27, 91
r2	0	2	1	10, 96	27
r3	0	2	2	67, 73	27, 84
Scenario 5					
r1	0	1	2	12	27, 91
r2	0	5	1	28, 95, 96, 99, 100	27
r3	0	3	2	49, 69, 73	27, 84
Scenario 6					
r1	0	0	2		27, 91
r2	0	0	0		
r3	0	1	4	69	27, 46, 80, 84
Totals					
	0	18	32		

Reducing tolerances to 10^{-4} does not change the number of flow violators at the borehole/Culebra intersection, although the list of violators is not identical to that generated using 10^{-2} tolerances (Appendix C). Tightening tolerances does improve the comparison of flow at the shaft/Culebra intersection, reducing the number of violators to 26 (Appendix C). Further analysis of differences in liquid flow provided in Appendix D focuses on the nine simulations that caused flow violations at the borehole/Culebra intersection with both 10^{-2} and 10^{-4} tolerances.

8.8   PFLOTRAN-BRAGFLO Benchmark Conclusion

PFLOTRAN and BRAGFLO outputs were compared for 1800 simulations whose input parameters duplicated those used for the three replicates of sampled parameters and six scenarios in the 2014 CRA WIPP PA calculations. A comparison was made of volume-weighted averages of liquid pressure and liquid saturation for each of nine regions in the excavated volume (waste area, operations area, etc.), and of liquid mass flow at eight locations: the intersections of the marker beds with the north and south land withdrawal boundaries and at the intersections of the borehole and the shaft with the Culebra.

A comparison of aggregate results in the form of uncertainty distributions (Section 8.5) provides insight into model behavior and demonstrates good agreement between the codes. A quantative comparison of each of the 1800 simulations (Section 8.7) allows the number of simulations exceeding predetermined difference thresholds to be counted. The greatest number of differences that exceed thresholds occur in the shaft, where 247 simulations differ in liquid saturation and 32 simulations differ in liquid flow (using standard tolerances). However, because simulation results in the shaft appear to be largely decoupled from the waste area and the effects of borehole intrusion, and cumulative flow in the shaft is always downward, differences in the shaft are unlikely to affect radionuclide releases or propagate through PA. Agreement between PFLOTRAN and BRAGFLO is excellent in other regions of the repository, including the in the waste area, the region of the repository where differences in liquid pressure and saturation have the greatest potential to propagate through PA – in the waste area where only two simulations exceed liquid pressure difference thresholds and only three simulations exceed liquid saturation difference thresholds (using standard tolerances). The two codes also agree well in predictions of borehole flow with only 18 of 1800 simulations exceeding the relative difference threshold.

Given the success of the comparison, the PFLOTRAN-BRAGFLO 2D flared grid benchmark provides a new (PFLOTRAN) baseline for WIPP PA two-phase flow calculations, against which further changes to conceptual and numerical models accrued in the transition to a 3-D WIPP PA may be compared.

9 Summary

The proposed addition of new waste panels to the Waste Isolation Pilot Plant (WIPP) challenges the modeling assumptions inherent in the two-dimensional (2-D) flared grid used in performance assessment (PA) calculations of brine and gas flow in and around the repository, and requires development of a new 3-D model for use in PA. Because a 3-D grid that adequately represents the WIPP repository and its surroundings is expected to be considerably larger than the current 2-D flared grid, replacement of BRAGFLO with a two-phase flow simulator capable of running in a high-performance computing environment is essential. PFLOTRAN, a massively-parallel simulator of subsurface multiphase flow and reactive transport sponsored by the Department of Energy (DOE), has been adopted and its capabilities have been extended to include simulation of two-phase, immiscible flow (as in the current WIPP PA) and associated WIPP-specific process models such as gas generation, creep closure, and fracture.

PFLOTRAN development and testing has been ongoing since 2014 (Zeitler et al. 2017). In FY 2018, the focus has been on ensuring and demonstrating that implementations of two-phase immiscible flow and all WIPP-specific process models in PFLOTRAN are consistent with implementations in BRAGFLO, and that flow simulations run with PFLOTRAN mimic the results obtained with BRAGFLO for the WIPP PA. Previously existing and newly developed zero-, one-, and two-dimensional test cases were used to verify correct implementation of two-phase flow and WIPP-specific process models in PFLOTRAN by comparing PFLOTRAN results to BRAGFLO results. A PA-scale benchmark comparison of the two codes was executed using the 2-D flared grid and inputs from the 1800 simulations performed for the 2014 Compliance Recertification Application (CRA). The PFLOTRAN-BRAGFLO benchmark was used to verify that PFLOTRAN performs robustly across the full input parameter space sampled in PA and to quantify the effect, if any, of transitioning to PFLOTRAN on the results of WIPP PA flow calculations.

The WIPP-specific process models incorporated in PFLOTRAN are gas generation and brine consumption/generation; creep closure in portions of the underground excavation that contain waste; fracturing in the disturbed rock zone (DRZ) and marker beds; pore compressibility; the Klinkenberg correction for gas permeability; characteristic curves (relative permeability and capillary pressure as functions of saturation); the Redlich-Kwong-Soave equation of state for gas; and material changes associated with borehole intrusion and with evolution of the DRZ, panel closures, and the borehole. Initially, these process models were coupled to PFLOTRAN's GENERAL mode, which simulates two-phase, miscible flow plus energy conservation (heat transport).

Testing in FY 2017 made clear that (1) calculations on the 2-D flared grid (particularly those involving borehole intrusion) challenged Newton solver convergence in PFLOTRAN's GENERAL mode, and that (2) PFLOTRAN and BRAGFLO solutions on the 2-D flared grid were not yet sufficiently close to demonstrate with confidence that WIPP-specific process models were correctly implemented and coupled in PFLOTRAN. Both of these problems were addressed over the course of FY 2018 by more precisely implementing BRAGFLO's solver tolerances, time step and iteration controls, and method of discretizing the governing equations in PFLOTRAN's two-phase, immiscible flow mode; by tightly coupling the constitutive relationships described by

process models into the system of flow equations; and by refactoring individual process models to ensure numerical implementation consistent with numerical implementation in BRAGFLO.

FY 2018 test case results demonstrate uniformly good agreement between PFLOTRAN and BRAGFLO solutions with relative differences in porosity, liquid and gas pressure, liquid and gas saturation, and liquid and gas density generally less than 1%. Rates of MgO hydration and gas generation calculated when using the gas and brine source/sink model agree to within 1% as well. The comparison is improved relative to results of the same test cases in FY 2017, when calculated brine pressures in test cases including creep closure differed by up to 20%, and MgO hydration rates differed by > 25%.

PFLOTRAN and BRAGFLO outputs were compared for 1800 simulations whose input parameters duplicated those used for the three replicates of sampled parameters and six scenarios in the 2014 CRA WIPP PA calculations. A comparison was made of volume-weighted averages of liquid pressure and liquid saturation for each of nine regions in the excavated volume (waste area, operations area, etc.), and of liquid mass flow at eight locations, including the intersection of the borehole and the Culebra. Comparison of standard uncertainty analysis metrics, e.g., mean, median, etc., displayed in the form of box plots, showed no statistically meaningful differences between PFLOTRAN results and BRAGFLO results. The uncertainty metrics and quantiles effectively overlie each other.

The good agreement on both small test problems and on the full set of PA flow simulations indicates correct implementation of two-phase, immiscible flow and associated WIPP-specific process models in PFLOTRAN. Additionally, robust simulation over the full input parameter space sampled in PA has been demonstrated. In the future, these simulations can support formal verification of PFLOTRAN for quality assurance, and the PFLOTRAN-BRAGFLO 2-D flared grid benchmark will provide a new (PFLOTRAN) baseline for WIPP PA flow calculations, against which further changes to conceptual and numerical models may be compared during the transition to a 3-D WIPP PA.

10 References

Camphouse, C. 2012a. *User's Manual for BRAGFLO Version 6.02*. ERMS #558663. Sandia National Laboratories, Carlsbad, NM.

Camphouse, C. 2012b. *Design Document for BRAGFLO Version 6.02*. Sandia National Laboratories, Carlsbad, NM.

Camphouse, C. 2012c. *Requirements Document & Verification and Validation Plan for BRAGFLO Version 6.02*. ERMS #558659. Sandia National Laboratories, Carlsbad, NM.

DOE 1996. *Title 40 CFR Part 191 Compliance Certification Application for the Waste Isolation Pilot Plant*. DOE/CAO-1996-2184. U.S. Department of Energy, Carlsbad Area Offfice, Carlsbad, NM.

DOE 2014. *Title 40 CFR Part 191 Subparts B and C Compliance Recertification Application 2014 for the Waste Isolation Pilot Plant*. U.S. Department of Energy, Carlsbad Field Office, Carlsbad, NM.

Hammond, G.E. and J.M. Frederick 2017. "Minimizing the Impact of Software Evolution on Radioactive Waste Management," in Proceedings of the International High-Level Radioactive Waste Management (IHLRWM 2017) Conference, April 9 – 13, 2017, Charlotte, NC, SAND2016-12458C.

Hammond, G.E., P.C. Lichtner, C. Lu, and R.T. Mills. 2011. "PFLOTRAN: Reactive Flow and Transport Code for Use on Laptops to Leadership-Class Supercomputers", in F. Zhang, G.T. Yeh, and J. Parker (ed.) Groundwater Reactive Transport Models, Bentham Science Publishers.

Hammond, G.E., P.C. Lichtner, and R.T. Mills 2014. "Evaluating the Performance of Parallel Subsurface Simulators: An Illustrative Example with PFLOTRAN", Water Resources Research, 50, 208-228, doi:10.1002/2012WR013483.

Lichtner, P. C., G. E. Hammond, C. Lu, S. Karra, G. Bisht, B. Andre, R. Mills, J. Kumar, and J.M. Frederick 2018. PFLOTRAN Documentation, Release 1.1, https://www.pflotran.org/documentation/index.html.

Peaceman, D. W. 1977. *Fundamentals of Numerical Reservoir Simulation* (Vol. 6). New York: Elsevier Scientific Publishing Company.

SNL 1992. Preliminary Performance Assessment for the Waste Isolation Pilot Plant Volume 5: Uncertainty and Sensitivity Analyses of Gas and Brine Migration for Undisturbed Performance. SAND92-0700/5. Sandia National Laboratories, Albuquerque, NM.

Voss, C. I. 1984. A Finite-Element Simulation Model for Saturated-Unsaturated, Fluid-Density-Dependent Groundwater Flow with Energy Transport or Chemically-Reactive Single-Species Solute Transport. Water-Resources Investigations Report 84-4369. U.S. Geological Survey, Reston, VA.

Zeitler, T. R., B. A. Day, J. Bethune, J. M. Frederick, G. E. Hammond, R. Sarathi, and E. R. Stein 2017. *Assessment of 2-D Benchmark: BRAGFLO vs. PFLOTRAN for an Explicit Flared Grid*. Sandia National Laboratories, Carlsbad, NM.